International Committee for Future Accelerators
Sponsored by the Particles and Fields Commission of IUPAP

Beam Dynamics Newsletter

No. 32

Issue Editor:
J. Gao

Editors in Chief:
W. Chou and J.M. Jowett

December 2003

Contents

1. Foreword

1.1. From the Chairman

John Jowett, CERN
mail to: John.Jowett@cern.ch

1.1.1. A look back at the ICFA Beam Dynamics Newsletter

This newsletter is generally meant to be a forward looking document but, as this is the last time I shall write this introduction, I hope I can be forgiven the indulgence of a look backwards over its history. The permanent Web archive at Jefferson Lab provides access to newsletters going back to No. 7 published in early 1995 and edited by K. Hirata, S.Y. Lee and F. Willeke (my personal involvement started with issue No. 10 in 1996). Since 1995 the newsletter has been published at a rather constant rhythm of three issues per year. Some recent issues have been quite a bit thicker and contained more detailed material than the earlier ones. And, of course, the main distribution medium is now the Web.

Extrapolating backwards from the archive, a typical physicist would infer that issue No. 1 was published in late 1992 and he would be wrong. Although I do not have a complete set of copies of the early issues, there was a break in publication of about four years before the newsletter was revived by the editors of No. 7. I have copies of No. 5 from November 1990 and three issues predating it (January and September 1988, August 1989). All of these were edited by Eberhard Keil and Anton Piwinski.

Although they carry DESY-M report numbers, they are not numbered in the sequence of Beam Dynamics Newsletters so I cannot tell if the issue DESY M-88-01 of January 1988 was the first or second. If someone can provide enlightenment, preferably with dates and copies of the two missing issues, it would be of great interest. Similarly, it would be good to complete the Web archive by scanning these few early issues. Volunteers for this job would be welcome!

The editors of those early issues formulated the basic guideline that we still try to apply:

The Beam Dynamics Newsletter is not intended to be a substitute for journal articles, conference proceedings, etc. which usually describe completed work. It is rather intended as a channel for describing planned work and unsolved problems. The panel hopes that in this way international collaboration can be stimulated and unnecessary duplication of work can be avoided.

A glance through the January 1988 issue reminds us just how long are the time scales associated with the front-line high-energy accelerator projects. While many things have changed and much of what is going on now was not foreseen then, it is also remarkable how much continuity there is between what was past, present and future then and what is now.

Following the first article by Alex Chao on the activity at the SSC Central Design Group, other articles mention SSC-related activities in Fermilab and LBL. While we all regret this case of a great future becoming past without passing through the present, this is the perhaps the place to recall its invaluable legacy of work in beam dynamics.

On the linear collider side, N.S. Dikansky briefly mentioned ideas at the Novosibirsk Institute of Nuclear Physics for the VLEPP project for electron-positron colliding beams at 2 TeV in the centre-of-mass. He recalled that this project had first been reported at a

meeting in April of 1978! Ron Ruth gave news of progress at the SLC (then present, now past) and described work that was just beginning on a next generation linear collider. After many more years of R&D, intensive work and representations to politicians and funding agencies, ICFA is now taking steps towards securing the approval of a linear collider as an international project. After spending such a long time in the future, we hope to see such a machine show up in the present in just a few more years.

An article by David Johnson described beam dynamics investigations at the Tevatron, a case where the present then remains present now and will do so for some years to come. A. Piwinski discussed work at DESY where the imminent future, HERA, was being installed and is now in the present.

E. Keil's account of activities at CERN mentioned progress in machines from the past continuing in what was then the present. Among them, the CERN PS was then a venerable 30 years old but being prepared for a future as a lepton accelerator. Of course that part of the LEP project, then CERN's imminent future, is now the past. But the PS now has yet another future as a proton and heavy ion pre-injector for CERN's present principal future, the LHC.

T. Suzuki's description of beam dynamics work at KEK naturally highlighted the recently commissioned TRISTAN collider, now past. There was no mention yet of its future successor, the present KEKB collider.

Should we worry about all this? No, and yes. No, we should rather take pride in the fact that old particle accelerators can be judiciously upgraded and continue to serve high energy physics for decades longer than their builders might have envisaged. Yes, we should worry about the time it can take to get new major projects off the ground. This is not only an obvious matter of economics and politics. The long time scales give rise to well-known social problems for experimenters in particle physics when a single experiment can last most of a career. Analogous problems exist for the designers, builders and operators of the accelerators and colliders. It is essential for the individuals charged with sustaining the momentum of the field to maintain a grasp of the overall picture, even when they spend long years deeply imbedded in the details of a particular project. This is a major purpose of this newsletter and the other collaborative activities (working groups and ICFA Advanced Beam Dynamics Workshops) organised by the Beam Dynamics Panel.

1.1.2. Changes in the Panel

Helmut Mais who, like me, has served on the Panel since 1996 has asked to retire at the end of 2003. I would like to thank Helmut for his collaboration and work to the benefit our community.

I wish to retire myself after this three-year term as Chairman of the Panel. I have enjoyed the work enormously and appreciated the many contacts to which it has given rise. I have made a particular point of steadily renewing the membership of the Panel, which is most definitely not any kind of honorary long-term appointment. It is a "community-service" job, carrying significant demands on one's time and energy and it is difficult for any individual to do it conscientiously for too long.

I would like to thank ICFA for the opportunity and the many colleagues around the world who have helped sustain and expand the activities of the Beam Dynamics Panel. These include not only those who have served as Panel members, but many others who have volunteered to participate by organising workshops, collaborating in the working groups and contributing to the newsletter.

ICFA has appointed Weiren Chou as the new chairman of the Beam Dynamics Panel. Weiren has already contributed much to the Panel's activities, chairing the working group on High Intensity High Brightness Hadron Beams, organizing workshops and acting

as Chief Editor of this newsletter. I know that he will bring new ideas to the running of the Panel and wish him the best of luck.

The Panel's Web site will continue to be the main source of information on its activities. For technical reasons, it will unfortunately be necessary to change the address from

http://wwwslap.cern.ch/icfa/

to
http://www-bd.fnal.gov/icfabd/

Once the new Web site is ready, the old one will automatically re-direct you to it. However it would help the transition process if anyone who maintains links (public or personal) to the panel's home page would update them at the appropriate time.

1.2. From the Editor

J. Gao, LAL, Orsay, France
mail to: gao@lal.in2p3.fr

Accelerating structures of linacs for future electron-positron linear colliders, which is one of the main axes of research efforts of international particle accelerator community, have been chosen as the main subject of this issue. Reports from TESLA, GLC, NLC and CLIC reflect their state-of-the-art technological advances and challenges. As contra-balance, we have invited ICFA Panel on Advanced and Novel Accelerators headed by Dr. W. Leemans to provide us information on the progresses of advanced and novel accelerating possibilities, which are not the simple extrapolations from the well known particle accelerating technologies (in this issue we publish the first part of the contributions, and the second part will be appeared in the next issue). As a pivot, we have collected reports from the workshops focused mainly on the problems in storage ring colliders, which represent the main powerful operational facilities for the particle physics researches of our community nowadays. It is with the above mentioned global view that authors are invited, contributions are structured and presented. Finally, I hope, as editor, that readers of this issue benefit not only from the single contribution effect, but also from the global collective effect of this issue.

2. Accelerating Structures for Future Linear Colliders

2.1. Superconducting Cavities of Ultimate Gradient for the TESLA Electron-Positron Collider

Lutz Lilje
DESY, Notkestrasse 85, D-22607 Hamburg, Germany
mail to: lilje@desy.de
Matthias Liepe
Cornell University, Ithaca N.Y. 14853, USA
mail to: matthias.liepe@desy.de
Peter Schmüser
Universität Hamburg, Notkestrasse 85, D-22607 Hamburg, Germany
mail to: peter.schmueser@desy.de

2.1.1. Abstract

The Tera Electronvolt Superconducting Linear Accelerator TESLA is the only linear electron-positron collider project based on superconductor technology for particle acceleration. In the first stage with 500 GeV center-of-mass energy an accelerating field of 23.4 MV/m is needed in the superconducting niobium cavities which are operated at a temperature of 2 K and a quality factor Q_0 of 10^{10}. This performance has been reliably achieved in the cavities of the TESLA Test Facility (TTF) accelerator. The upgrade of TESLA to 800 GeV requires accelerating gradients of 35 MV/m. Using an improved cavity treatment by electrolytic polishing it has been possible to raise the gradient to 35 - 40 MV/m in single cell resonators and to more than 35 MV/m in nine-cell cavities.

2.1.2. Introduction

Electron-positron colliders have played a central role in the discovery of new quarks and leptons and the formulation and detailed verification of the Standard Model of elementary particle physics. In the energy range beyond LEP, circular colliders are ruled out by the huge synchrotron radiation losses, increasing with the fourth power of energy. Hence a linear collider is the only viable approach to centre-of-mass energies in the TeV regime. Such a linear lepton collider would be complementary to the Large Hadron Collider (LHC) and allow detailed studies of the properties of the Higgs particle(s). In the baseline design of the superconducting TESLA collider [1] the centre-of-mass energy is 500 GeV (TESLA-500), well above the threshold for the production of the Standard-Model Higgs particle. The possibility for a later upgrade to 800 GeV (TESLA-800) is considered an essential feature to increase the research potential of the facility for the study of supersymmetry and other physics beyond the Standard Model.

A detailed description of the superconducting TESLA cavities and their status as of February 2000 can be found in [2]. Here we report on the considerable increase in accelerating field that has been achieved in the past three years. This progress is largely due to an improved preparation technique of the inner cavity surface by electrolytic polishing instead of chemical etching. The chemical and electro-chemical preparation

methods are therefore addressed in some detail. For a thorough discussion of superconducting radio frequency (rf) cavities and of microwave superconductivity we refer to the book *RF Superconductivity for Accelerators* by H. Padamsee, J.Knobloch and T. Hays [3] and to the review article *Superconductivity in High Energy Particle Accelerators* by P. Schmüser [4].

2.1.3. Cavity Preparation

2.1.3.1. Status and properties of the cavities for the TESLA Test Facility linac

The 1.3 GHz nine-cell niobium cavities for the TESLA Test Facility (TTF) linac (Fig.2) are made from 2.8 mm thick niobium sheets by deep drawing and electron beam welding. A damage layer of about 100 μm thickness is removed from the inner surface to obtain optimum performance in the superconducting state. For the TTF cavities this has been done so far by chemical etching. Niobium metal has a natural Nb_2O_5 layer with a thickness of about 5 nm which is chemically rather inert and can be dissolved only with hydrofluoric acid (HF). Chemical etching of niobium consists of two alternating processes: dissolution of the Nb_2O_5 layer by HF and re-oxidation of the niobium by a strongly oxidizing acid such as nitric acid (HNO_3) [5,6]. To reduce the etching speed a buffer substance is added, for example phosphoric acid H_3PO_4 (concentration of 85%) [7], and the mixture is cooled below 15°C. The standard procedure with a removal rate of about 1 μm per minute is called *buffered chemical polishing* (BCP) with an acid mixture containing 1 part HF, 1 part HNO_3 and 2 parts H_3PO_4 in volume. At TTF, a closed-circuit chemistry system is used in which the acid is pumped from a storage tank through a cooling system and a filter into the cavity and then back to the storage.

In the most recent industrial production of 24 TTF cavities an average gradient 26.1± 2.3 MV/m at a quality factor $Q_0 \geq 1 \cdot 10^{10}$ was achieved. Typical excitation curves are shown in Fig. 1. The technology developed for TTF is hence adequate for TESLA-500 but considerable improvements are needed for an upgrade of the collider to 800 GeV. A detailed description of the present status of the nine-cell cavity layout, fabrication, preparation and tests can be found in [2].

After many years of intensive R&D there exists now compelling evidence that the BCP process limits the attainable field in multi-cell niobium cavities to about 30 MV/m. This is significantly below the physical limit of about 45 MV/m which is given by the condition that the rf magnetic field has to stay below the critical field of the superconductor. For the type II superconductor niobium the maximum tolerable rf field appears to be close to the thermodynamic critical field ($B_c \approx 190$ mT at 2 Kelvin).

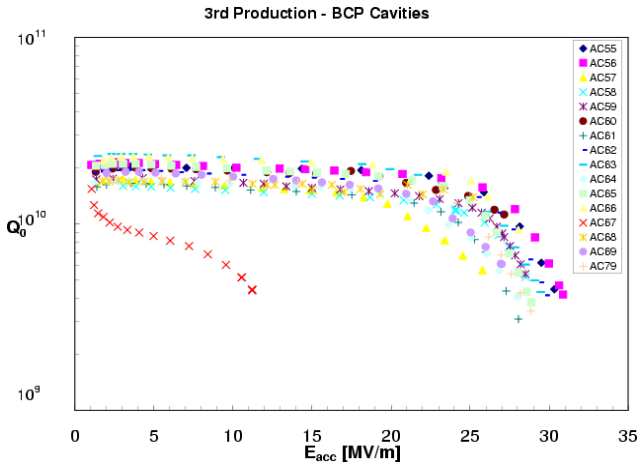

Figure 1: Excitation curves of several nine-cell TESLA cavities with surface preparation by chemical etching (BCP). The quality factor is plotted as a function of the accelerating field. The test temperature is 2 Kelvin. Cavity AC67, marked by crosses, developed a cold-leak during the test.

2.1.3.2. Electrolytic polishing

An alternative surface preparation method to etching is electrolytic polishing (EP). The material is removed in an acid mixture under the flow of an electric current. Sharp edges or tips are smoothed out and a very glossy surface can be obtained. The electric field is high at protrusions so these will be dissolved readily while the field is low in the boundaries between grains and little material will be removed here. This is an essential difference to the BCP process which tends to enhance the steps at grain boundaries. Using electrolytic polishing, scientists at the KEK laboratory in Tsukuba (Japan) achieved gradients of up to 40 MV/m in single-cell cavities [8]. This remarkable success motivated an R&D program on the electropolishing of single-cell cavities which was carried out in a collaboration between CERN, DESY and Saclay [9].

The electro-chemical reactions in the EP process are as follows [10, 11]:

$$2\mathrm{Nb} + 5\mathrm{SO_4^{--}} + 5\mathrm{H_2O} \rightarrow \mathrm{Nb_2O_5} + 10\mathrm{H^+} + 5\mathrm{SO_4^{--}} + 10\mathrm{e^-}$$

$$\mathrm{Nb_2O_5} + 6\mathrm{HF} \rightarrow \mathrm{H_2NbOF_5} + \mathrm{NbOF_2} \cdot 0.5\mathrm{H_2O} + 1.5\mathrm{H_2O}$$

$$\mathrm{NbOF_2} \cdot 0.5\mathrm{H_2O} + 4\mathrm{HF} \rightarrow \mathrm{H_2NbF_5} + 1.5\mathrm{H_2O}$$

Recently, the EP technique has been successfully transferred to nine-cell cavities within a joint KEK-DESY R&D program [12]. The cavity is installed horizontally together with the cathode. The lower half is filled with the electrolyte which attacks the niobium only very slowly when no voltage is applied (etch rate less than 1 nm per hour). After the equilibrium filling level has been reached, the cavity is put into rotation and the current-voltage characteristic is measured. At a voltage of 15 - 20 V the current starts an amplitude oscillation of 10 - 15% about the mean value which is an indication that two alternating processes are taking place: dissolution of Nb_2O_5 by HF and re-oxidation by H_2SO_4. The temperature of the acid is 30 - 35°C during the EP. When the desired amount of material has been removed, the current is switched off, the rotation is stopped and the cavity is turned into the vertical position to drain the acid mixture. After rinsing with pure water the electrode is dismounted while keeping the cavity filled with water, thus avoiding drying stains from acid residues. The cavity is then transported into a clean room for rinsing with ultrapure water at high pressure.

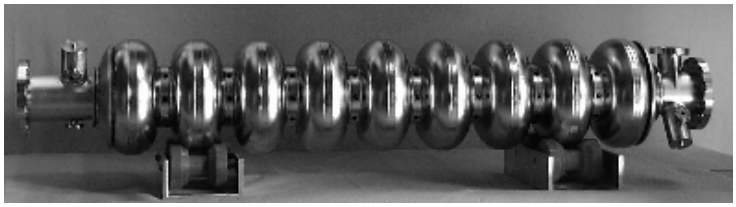

Figure 2: Superconducting 1.3 GHz 9-cell cavity for the TESLA Test Facility.

2.1.4. Comparison of etched and electropolished surfaces

Micrographs of BCP and EP treated niobium samples are compared in figure 3. One can see that EP smoothes out the grain boundaries far better than BCP. The average roughness of chemically etched niobium surfaces is in the order of 1 µm [13] while EP surfaces are at least an order of magnitude smoother. On etched surfaces the step height at grain boundaries can be a few µm. These steps may lead to a magnetic field enhancement and a premature breakdown of superconductivity [14].

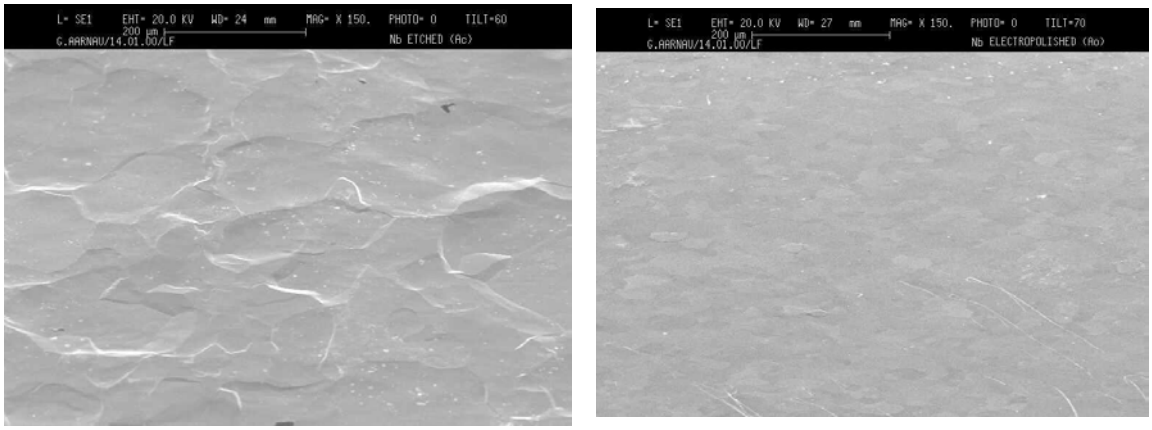

a) 400 ×800 µm b) 400 ×800 µm

Figure 3: Niobium surfaces after etching (left) and electropolishing (right). SEM micrographs are courtesy of G. Arnau, CERN.

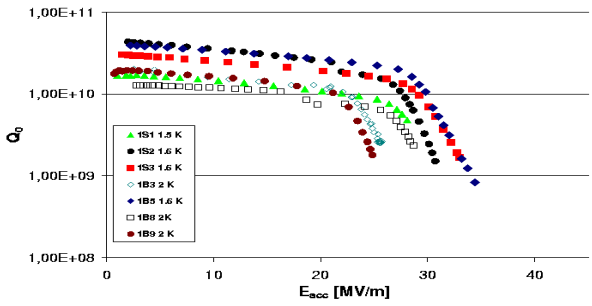

Figure 4: First tests of electropolished single-cell resonators. Note the strong degradation of the quality factor at accelerating fields $E_{acc} \geq 25$ - 30 MV/m.

2.1.5. Measurements on Electropolished Cavities

2.1.5.1. *Single-cell cavities*

A) First tests

In the first tests the electropolished cavities of the CERN-DESY-Saclay program faced an unexpected limitation: the excitation curves exhibited a strong degradation in quality factor at high field as can be seen in figure 4. Field emission of electrons could be excluded as an explanation for the performance degradation since neither X rays nor secondary electrons were observed.
It was discovered by Visentin et al. [15] that the performance of etched cavities could be considerably improved by applying a moderate thermal treatment to the finished cavity. This will be called *bakeout* in the following. The procedure at Saclay was as follows. After the last high-pressure water rinsing the cavities were evacuated and then heated up to 170°C for 70 hours. The remarkable observation was that this low-temperature baking improved the quality factor at maximum field by a nearly factor of 3.

B) Application of low-temperature bakeout to EP cavities

Building on the experience with BCP cavities at Saclay and with EP cavities at KEK (where a bakeout at 85-100°C had been part of the standard preparation) a 48 hour bakeout at 120°C was applied to the EP cavities of the CERN-DESY-Saclay collaboration. Figure 5 shows that a dramatic improvement is achieved: several single cell cavities reach now accelerating gradients of up to 40 MV/m with quality factors above $5 \cdot 10^9$. This behaviour is very similar to the observations made at KEK.

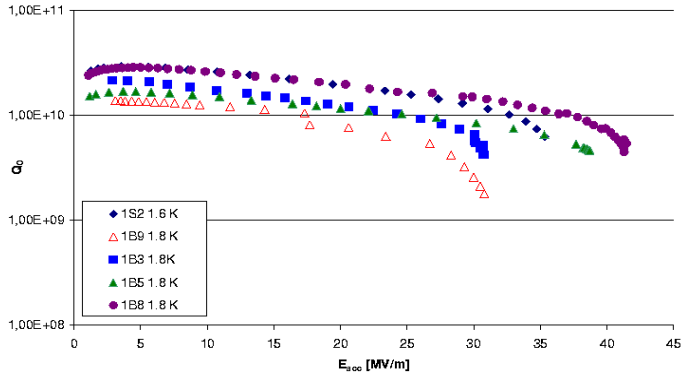

Figure 5: Excitation curves of electropolished one-cell cavities after the low-temperature bakeout. The tests have been performed at slightly different temperatures (1.8-2 K).

The high-temperature treatment of niobium cavities is a well-known method to improve the performance, see below. The surprising observation made with the bakeout effect is that a thermal treatment at 120-140°C, where the diffusion of gases dissolved in the niobium lattice is extremely slow, has a profound influence on the high-gradient performance. It it obvious that the bulk niobium cannot be affected by the bakeout but

only a thin surface layer which, however, is essential for the microwave superconductivity.

C) "Q-disease" and 800°C annealing

Electrolytic polishing generates hydrogen which can easily penetrate into the niobium lattice. The danger exists that niobium hydride compounds are formed if the material is exposed to temperatures around 100 K for an extended period. These Nb-H compounds have very high microwave losses and may reduce the quality factor by one or two orders of magnitude. This unfortunate effect has been named *Q-disease*. The hydride formation depends on the dwell time the cavity spends in the dangerous region around 100 K. With a fast cooldown from room temperature within 1 hour, the hydride formation is reduced to an acceptable level.

A dedicated experiment was carried out to this end, the results are shown in figure 6. An electropolished cavity with excellent performance after a fast cooldown was then exposed to a temperature of 100 K for 2 days. In the new test the quality factor was very low. Then the cavity was heated to 800°C in a UHV furnace to remove the hydrogen from the bulk material. The exposure of the cavity to the dangerous temperature of 100 K for 2 days was repeated. This time no Q degradation was observed, indicating that the "Q-disease" was completely cured by the furnace treatment.

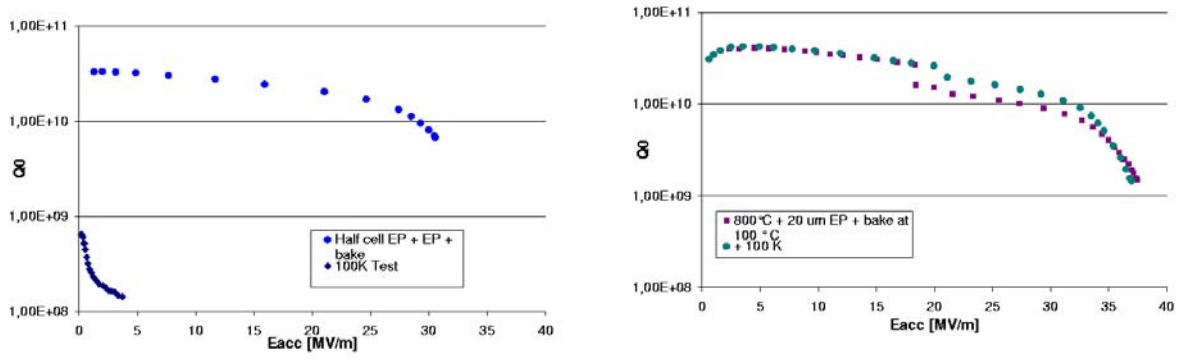

Figure 6: Demonstration of the "Q disease". Left: The excitation curve of an electropolished and baked cavity before and after a two-day exposure to a temperature of 100 K.
Right: The same cavity after an 800°C furnace treatment and a short EP of 20 μm. The "Q disease" is completely cured and does not reappear when the cavity is exposed to 100 K. Test temperature 1.6 K.

2.1.5.2.Nine-cell cavities

Within the KEK-DESY program 9 nine-cell cavities of the last production series were electropolished at the Japanese company Nomura Plating and sent back to DESY for the performance tests. Two cavities with strong field emission at 15-17 MV/m were sorted out for a second EP. The remaining seven cavities were evacuated to a pressure of 10^{-7} mbar and subjected to a 48-hour bakeout at 120°C. The excitation curves of the four best cavities are shown in figure 7. These results prove that the TESLA-800 gradient of 35 MV/m is indeed within reach.

Very recently, one of the field-emission loaded cavities has been electropolished for the second time in the new EP facility at DESY. The test results of this cavity at helium temperatures between 1.6 and 2.0 K are shown in figure 8. Accelerating fields of up to 40 MV/m have been reached which is a record for multicell niobium cavities. The maximum accelerating fields achieved in all eight TTF cavities are also shown in figure 7.

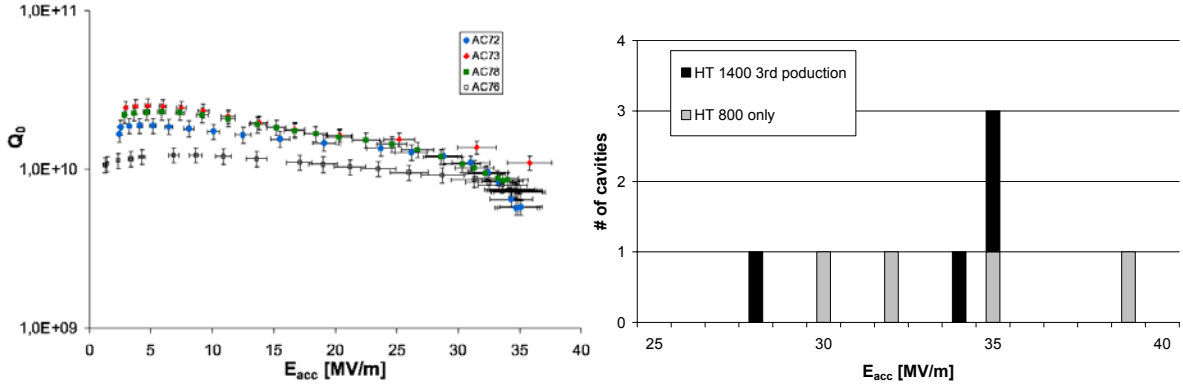

Figure 7: Left: Excitation curves of four excellent electropolished nine-cell cavities after EP at KEK. The tests have been performed at 2 K. Right: Maximum accelerating field achieved in eight electropolished nine-cell cavities. Gray bars: cavities with 800°C annealing, black bars: cavities with both 800°C and 1400°C annealings.

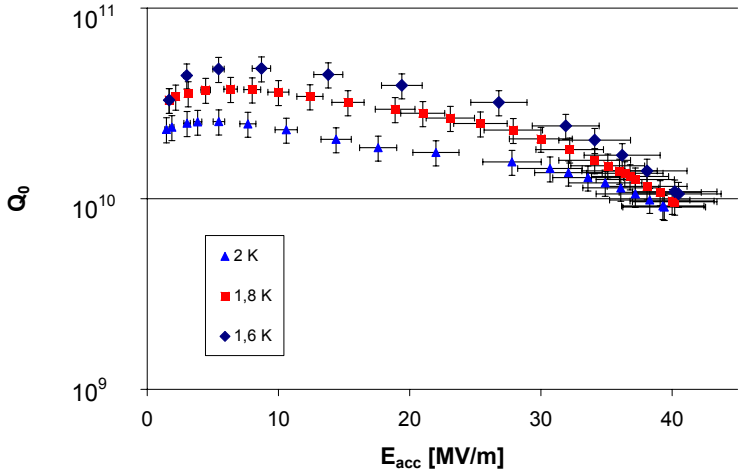

Figure 8: Performance of an initially field emission limited cavity after a second EP at DESY.

2.1.6. Microwave Surface Resistance

Superconducting magnets operated with direct current are free of energy dissipation, however, this is not the case in microwave cavities. The “normal” electrons, which are not bound in Cooper pairs, carry out forced oscillations in the time-varying magnetic field and dissipate power in the material. Although the resulting heat deposition is many orders of magnitude smaller than in copper cavities it still constitutes a significant heat load on the refrigeration system. As a rule of thumb, 1 W of heat deposited at 2 K requires almost 1 kW of primary ac power in the refrigerator. There is now a worldwide consensus that the overall efficiency for converting primary electric power into beam power is about a factor two higher for a superconducting than for a normal-conducting linear collider with

optimized parameters in either case [22]. Another definite advantage of a superconducting collider is the low resonance frequency of the cavities that can be chosen (1.3 GHz in TESLA). The longitudinal (transverse) wake fields generated by the ultrashort electron bunches upon passing the cavities scale with the second (third) power of the frequency and are hence much smaller in TESLA than in the "Next Linear Collider NLC" (f = 11 GHz). The wake fields may have a negative impact on the beam emittance.

According to the BCS (Bardeen-Cooper-Schrieffer) theory of superconductivity the microwave surface resistance of a superconductor is given by

$$R_{BCS}(T,f) = A\frac{f^2}{T}\exp\left(-\frac{\Delta}{k_B T}\right)$$

Here 2Δ is the energy gap of the superconductor and f the radio frequency. The most important prediction is the exponential temperature dependence which is experimentally verified (Fig. 9). The factor A depends on material parameters like the coherence length ξ, the electron mean free path l, the Fermi velocity v_F and the London penetration depth λ_L. The BCS resistance of niobium at 1.3 GHz is about 600 nΩ at 4.2 K and drops to 10 nΩ at 2 K. For this reason cooling with superfluid helium at 2 K is essential for ultimate cavity performance. Moreover, the quadratic frequency dependence favours low-frequency cavities, e.g. f = 1.3 GHz at TESLA. A refined expression for R_{BCS}, derived from the two-fluid model of superconductors, is [16]:

$$R_{BCS}(T,f) \propto \sigma_{nc}\cdot\lambda_{eff}^3\frac{f^2}{T}\exp\left(-\frac{\Delta}{k_B T}\right) \qquad \lambda_{eff} = \lambda_L\sqrt{1+\xi/\ell}$$

Here σ_n is the conductivity due to the normal-conducting component. As a consequence, the BCS resistance is does not assume its minimum if the niobium is extremely pure ($l >> \xi$) but only moderately pure, $l \approx \xi$. The surface resistance contains in addition a term called *residual resistance* which is caused mainly by impurities and amounts to a few nano-ohms for an excellent niobium surface.

The low-temperature bakeout has an interesting effect on the surface resistance: the residual resistance increases by a factor of about 1.5 whereas the BCS resistance decreases by the same factor, see Fig. 9. Both observations can be understood if one assumes that the baking creates a somewhat "dirty" surface layer with shorter mean free path l than in the bulk niobium. One conceivable explanation is a partial disintegration of the Nb_5O_5 oxide layer and the formation of niobium suboxides. For a detailed discussion we refer to the review talk by B. Visentin at the 2003 SRF workshop [17].

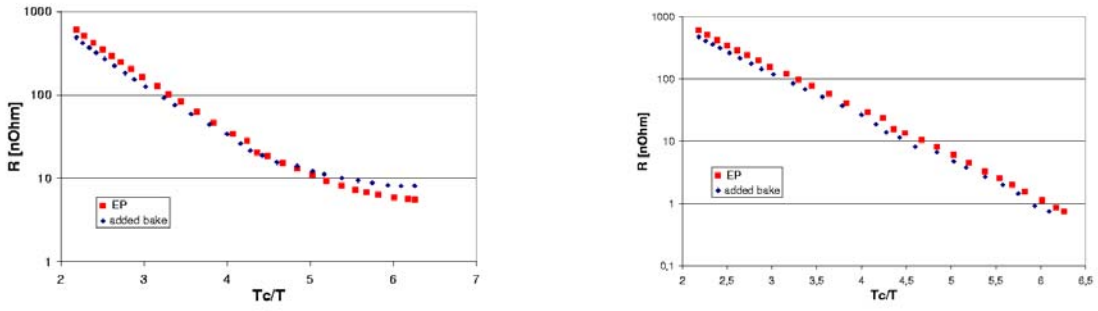

Figure 9: Left: Temperature dependence of the surface resistance before and after bakeout of an EP cavity. Right: The BCS surface resistance. The residual resistances of 4.7 nΩ for the unbaked cavity and of 7.4 nΩ for the baked cavity have been subtracted.

It should be noted that these surface resistance data are derived from measurements of the cavity quality factor at a few MV/m. The peculiar high-field behaviour of unbaked EP-cavities, namely the strong Q degradation, cannot be explained in terms of the surface resistance since this quantity is independent of the magnitude of the electromagnetic field in the cavity. On the contrary, a strongly field-dependent resistance would be needed to account for the rapid decrease of Q_0 towards large gradients. This effect is not yet understood.

2.1.7. High-Power Pulsed Operation of Electropolished Cavities

2.1.7.1.Excitation curves

In the TESLA collider the cavities have to be operated in the pulsed mode to keep the heat load on the superfluid helium system within acceptable limits. The rf field in the cavity has a filling time of 500 μs and a „flat-top“ time of 800 μs during which the bunched beam is accelerated. The nominal pulse repetition rate is 5 Hz.
At an accelerating field of 23.4 MV/m and an average beam current of 9 mA (for TESLA-500) an rf power of 210 kW per nine-cell cavity is transmitted through a coaxial power coupler. Almost all of this power is transferred to the beam. The external quality factor amounts to $Q_{ext} = 2.5\ 10^6$.

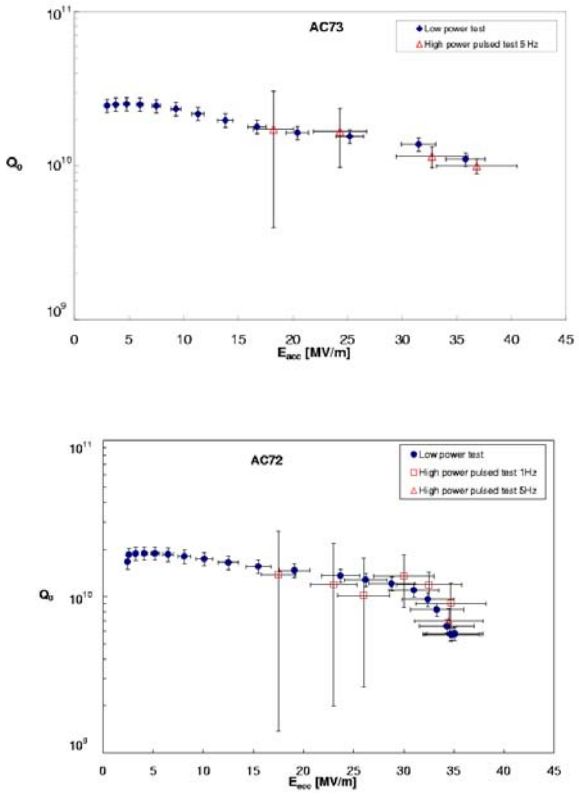

Figure 10: High power test of two electropolished nine-cell cavities: (a) Cavity AC73, this cavity was operated for more than 1100 hours at 35 MV/m. (b) Cavity AC72. The excitation curves obtained in the low power test in the vertical bath cryostat are shown for comparison and prove that the excellent performance is preserved after assembly of helium tank and high power coupler.

So far, two electropolished cavities (AC72, AC73) have been welded into a liquid helium tank and equipped with a high-power coupler and a frequency tuning mechanism. High power tests without beam have been carried out in a horizontal cryostat at the TESLA Test Facility. Figure 10 shows the results at a repetition rate of 5 Hz for AC73 and of 1 Hz for AC72 in comparison with the excitation curves measured in the low-power tests. It is very encouraging that both cavities achieve the same maximum gradient as in the low-power test. Within the large errors also the quality factors are in agreement. Another very important result is that cavity AC73 could be operated at maximum gradient for more than 1100 hours without any degradation.

2.1.7.2. Frequency stabilization in pulsed operation

The Lorentz force between the rf magnetic field and the induced currents in a thin surface layer causes a slight deformation of the cells in the order of micrometers and a shift in resonance frequency which is proportional to the square of the magnetic field. In the pulsed operation of the 9-cell cavities this leads to a time-dependent frequency shift during the rf pulse. The TESLA cavities are reinforced by stiffening rings which are welded between neighbouring cells and reduce the detuning by a factor of two. Experimental data on the detuning are shown in Fig. 11. The rf control system changes the klystron frequency and phase dynamically to accomodate for the cavity detuning. This method works properly up to the nominal TESLA-500 gradient of 23.4 MV/m.

To allow for higher gradients the cavity detuning must be compensated. This can be done with a piezoelectric tuner, see Fig. 12. The piezo-actuator changes the cavity length dynamically by a few µm and stabilizes the resonance frequency to better than 100 Hz during the beam acceleration time. The piezoelectric tuning system will permit cavity operation at fixed frequency up to the TESLA-800 gradient of 35 MV/m. In addition, the piezoelectric actuator may be used to cancel microphonic noise between the rf pulses.

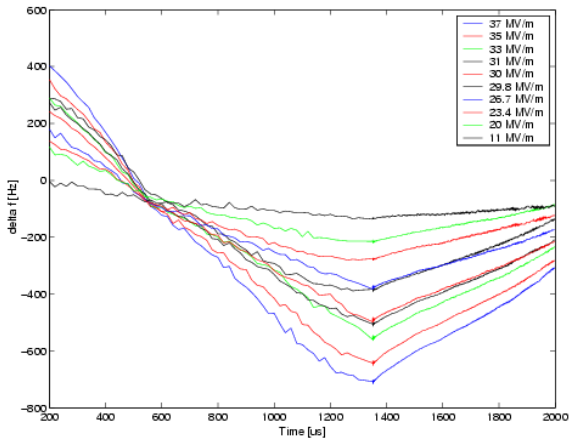

Figure 11: Lorentz-force detuning in pulsed mode operation at gradients from 11 to 37 MV/m.

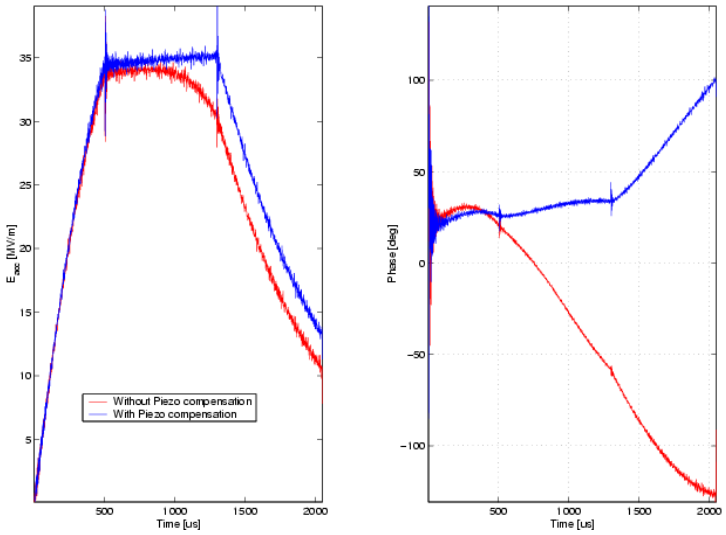

(a)

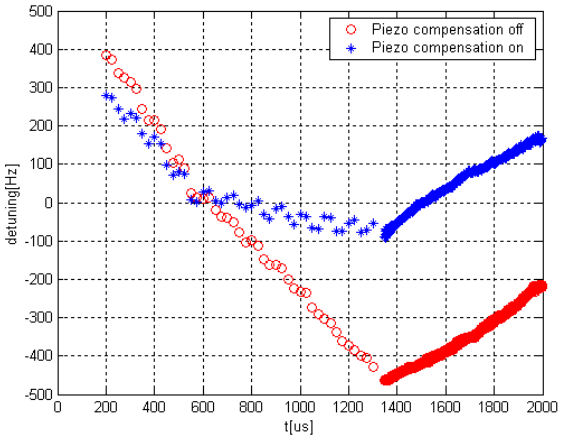

(b)

Figure 12: High-power pulsed test at 35 MV/m of an electropolished nine-cell cavity.
(a) Lorentz-force detuning causes a mismatch between klystron and cavity, associated with a time-dependent reduction of the accelerating field and a strong variation of the cavity phase with respect to the rf frequency. The compensation of the cavity detuning by a piezoelectric actuator leads to a nearly constant accelerating field and phase.
(b) The measured detuning during cavity filling and "flat top" at 35 MV/m with and without piezo-electric compensation.

2.1.8. The Superstructure Concept

In striving for highest collider energies not only the gradient in the cavities but also the active acceleration length have to be maximized. There are, however, two effects which limit the number of cells N_c per resonator. With increasing N_c it becomes more and more difficult to tune the resonator for equal field amplitude in every cell: the sensitivity of the field homogeneity to small perturbations grows with N_c^2. Secondly, in a very long multicell cavity 'trapped modes' may be excited by the short particle bunches. These are coupled oscillations at high frequency which are confined to the inner cells and have such a low amplitude in the beam pipe sections that they cannot be extracted by the higher-order mode (HOM) couplers mounted the beam pipe. Trapped modes may have a detrimental influence on the beam emittance and must be avoided. The number $N_c = 9$ chosen for TESLA appears a reasonable upper limit.

The limitation in the number of cells can be overcome by the *superstructure* concept proposed by J. Sekutowicz [23]. Several multicell cavities are joined by beam tubes of length λ/2 (λ = 230 mm is the wavelength of the accelerating mode). Within each cavity there is an rf phase advance of π from cell to cell, while the phase advance between adjacent multicell units is zero. This ensures that the particles experience the same accelerating field in all cells of the superstructure. The superstructure is supplied with rf power by a single input coupler at one end. The interconnecting pipes have a sufficiently large diameter to permit the flow of rf power from one cavity to the next.
For the TESLA electron and positron linacs a superstructure consisting of two 9-cell cavities is envisaged [1], see figure 13. Compared to the layout with separated 9-cell cavities, this superstructure improves the filling factor by 6 % and saves a factor of two in input couplers and waveguide components.

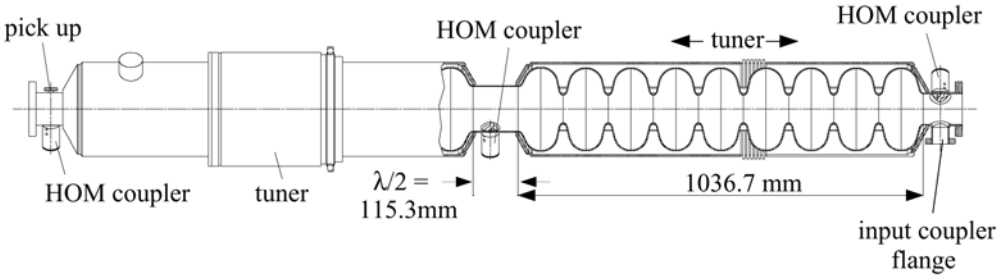

Figure 13: Layout of the 2x9-cell superstructure for TESLA-800 (the right 9-cell subunit is shown in cutaway view). One input coupler supplies the rf power for 18 cells.

The coupling between two adjacent cavities in a superstructure is about two orders of magnitude smaller than the cell-to-cell coupling within each subunit. To demonstrate that this small coupling is compatible with the requirement of a low beam energy spread a proof-of-principle experiment of two 2x7-cell superstructures was carried out at the TTF linac [23]. The rf power flow through the interconnecting pipe was found to be sufficient to replenish the stored energy in each cell between successive electron bunches. The measured bunch-to-bunch energy fluctuation was within the TESLA specification of $\sigma_E/E \leq 5 \cdot 10^{-4}$, see figure 14. Besides this, it was confirmed that a field homogeneity of better than 90% could be achieved in the superstructure. The excitation of beam-induced higher-order-modes was thoroughly studied and sufficient damping was verified.

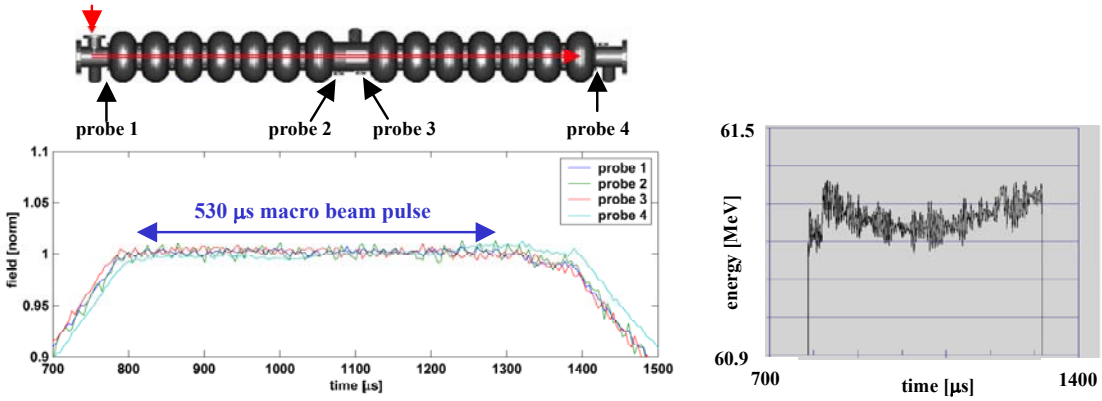

Figure 14: Energy gain along a 530 µs macro beam pulse (4 nC bunch charge, 1 µs bunch separation). Left: Measured signals of field probes near the end-cells of a 2x7-cell superstructure. Right: Measured beam energy at the end of the TTF linac. The energy fluctuations are within the specified limits of $\sigma_E/E \leq 5 \cdot 10^{-4}$. (Courtesy J. Sekutowicz.)

2.1.9. Discussion of the Results and Conclusions

A comprehensive understanding why electropolishing is so much superior to chemical etching is still missing, however a few explanations exist. The sharp ridges at the grain boundaries of an etched niobium surface may lead to local enhancements of the rf magnetic field and cause a premature breakdown of superconductivity at these localized spots. A model based on this idea was developed by Knobloch et al. [14] and is able to explain the reduction of the quality factor Q_0 at high field. Magnetic field enhancements will not occur on the smooth EP surface. Another advantage of a mirror-like surface is that a surface barrier of the Bean-Livingston type [18] may exist. The surface barrier prevents the penetration of magnetic flux into the bulk niobium in a certain range above the lower critical field B_{c1} ($\approx$ 160 mT for niobium at 2 K). The "penetrating field" B_{pen} may exceed the lower critical field B_{c1} by a significant amount for a perfectly smooth surface. Only above this penetrating field magnetic fluxoids will enter and leave the material in a periodically varying field and cause power losses. The delayed flux penetration was experimentally verified in electropolished samples of the type II superconductors Pb-Tl and $Nb_{0.993}O_{0.007}$ [18,19]. The experiments showed also that roughening of the surface by scratching or chemical etching destroyed the barrier and reduced the penetrating field to $B_{pen} = B_{c1}$. From these results we may conclude that an EP-treated superconducting cavity is likely to remain in the Meissner phase up to an rf magnetic field exceeding B_{c1} by a significant amount. On the other hand, a BCP-treated cavity with rough surface will allow magnetic flux penetration at $B_{rf} \geq B_{c1}$ and then suffer from enhanced power dissipation.

In summary we can say that electropolished bulk niobium cavities offer the very high accelerating gradients which are required for the upgrade of the TESLA collider to 800 GeV. For the first time, accelerating fields of up to 39 MV/m have been achieved in nine-cell cavities. In high-power tests it could be verified that EP-cavities keep their excellent performance after assembly of the helium cryostat and the high power coupler [12]. One cavity was operated at the TESLA-800 gradient of 35 MV/m for 1100 hours without any degradation.

2.1.10. Acknowledgements

The results shown in this publication represent the work of many people. We want to thank all members of the TESLA collaboration for many interesting discussions. Special thanks go to Jacek Sekutowicz for discussions on the superstructure and to Kenji Saito and Eiji Kako from KEK for carrying out the electropolishing of nine-cell cavities together with Nomura Plating.

2.1.11. References

[1] R. Brinkmann, et al. (editors), *TESLA - Technical Design Report*, volume II. DESY, March 2001. ECFA 2001-209, TESLA Report 2001-23.
[2] B. Aune et al. The Superconducting TESLA Cavities. *Phys. Rev. ST-AB*, 3(9), September 2000. 092001.
[3] H. Padamsee and J. Knobloch and T. Hays, RF Superconductivity for Accelerators, John Wiley & Sons, 1998
[4] P. Schmüser, *Superconductivity in High Energy Particle Accelerators*
[5] B. Hillenbrand, N. Krause, K. Schmitzke, and Y. Uzel. Abschlussbericht - Supraleitende Resonatoren. Technical Report NT 2024 7, Siemens AG, Dezember 1982. BMBF Forschungsbericht.

[6] Gmelin, *Handbuch der anorganischen Chemie*, volume 49 (Nb). Springer Verlag Berlin, 1970.
[7] J. Guerin, *Etude du bain de polissage chimique de niobium*, Technical Report TE/LC/157/89, CERN, October 1989.
[8] K. Saito et al. Superiority of Electropolishing over Chemical Polishing on High Gradients. In V. Palmieri, editor, *Proceedings of the 8th Workshop on RF Superconductivity*, volume I+II, pages 759 - 813, Abano terme, October 1997. INFN.
[9] L. Lilje, D. Reschke, D. Proch, A. Matheisen, P. Schmüser, D. Trines, C. Benvenuti, D. Bloess, H. Preis, L. Ferreira, H. Wenninger, E. Chiaveri, R. Losito, C. Antoine, J.-P. Charrier, and H. Safa. Improved surface treatment of the superconducting TESLA cavities. 2003. Accepted for publication in NIM A.
[10] P. Kneisel. Surface preparations of niobium. In M. Kuntze, editor, *Proceedings of the Workshop on RF Superconductivity*, volume I+II, page 27, Karlsruhe, 1980. KFK. KFK-3019.
[11] L. Ponto and M. Hein. Elektropolitur von Niob. Technical Report WUP 86-17, Bergische Universität Wuppertal, 1986.
[12] L. Lilje, Peter Schmüser et al., Achievement of 35 MV/m in the Superconducting Nine-Cell Cavities for TESLA, to be published.
[13] C. Z. Antoine et al. Alternative approaches for surface treatment of Nb superconducting cavities. In Krawcyk [21], pages 109-117.
[14] J. Knobloch, M. Liepe, R.L. Geng, and H. Padamsee. High-Field Q slope in Superconducting Cavities Due to Magnetic Field Enhancement at Grain Boundaries. In Krawcyk [21], pages 77-91.
[15] B. Visentin, J.P. Charrier, and B. Coadou. Improvements of superconducting cavity performances at high gradients. In *Proceedings of the 6th EPAC*, volume III, page 1885, 1998.
[16] B. Bonin. Materials for superconducting cavities. In S. Turner, editor, *Superconductivity in Particle Accelerators*, pages 191-200. CERN, May 1996. CERN 96-03.
[17] Bernard Visentin, Q-slope at high gradients: Review about experiments and explanations, TuO01, SRF Workshop 2003, Travemünde
[18] C.P. Bean and J. D. Livingston. Surface Barrier in Type-II Superconductors. *Phys. Rev. Lett.*, 12(1):14-16, January 1964.
[19] A.S. Joseph and W. J. Tomasch. Experimental Evidence for Delayed Entry of Flux into a Type-II Superconductor. *Phys. Rev. Lett*, 12(9):219-222, March 1964.
[20] R.W. De Blois and W. de Sorbo. Surface Barrier in Type-II Superconductors. *Phys. Rev. Lett.*, 12(18):499-501, May 1964.
[21] F. Krawcyk, editor. *Proceedings of the 9th Workshop on RF Superconductivity*, volume I+II, Santa Fe, November 1999. LANL.
[22] G. Loew et al; International Linear Collider Technical Review Committee. Second report; 2003; SLAC-R-606.
[23] J. Sekutowicz, M. Ferrario and Ch. Tang, Phys. Rev. ST Accel. Beams, vol. 2, No. 6 (1999)
[24] J. Sekutowicz et al., Cold- and Beam Test of the First Prototypes of the Superstructure for the TESLA Collider, ROAA003, PAC2003.

2.1.12. Power Couplers

T. Garvey, LAL, Orsay

mail to: garvey@lal.in2p3.fr

The impressive progress made in super-conducting (SC) cavity gradients in recent years can only be fully exploited if corresponding progress can be achieved in ancillary systems. The most important of these systems is the input power couplers which transmit the RF power from the klystrons to the cavities. In the context of a DESY/LAL collaboration, a program of development on power couplers is presently underway at LAL-Orsay with the aim of improving the performance, and reducing the cost, of couplers destined for the TESLA linear collider.

In general, one might not immediately think of beam dynamics considerations when specifying the design of power couplers. However, the influence of the coupler on the beam dynamics is far from negligible. In order to avoid perturbing the cavity fields, power couplers for SC cavities are mounted on the cut-off beam pipe. The presence of the coupler breaks the cylindrical symmetry of the cavity thus introducing a transverse component in the electric field. This transverse component induces an unwanted steering effect or "kick" on the beam. The magnitude of the kick imparted to a given electron is dependent upon the longitudinal position of the electron within the bunch. Thus the finite bunch length implies that different bunch 'slices' will suffer different radial kicks. The ultimate effect is a dilution in the effective emittance of the beam after traversing the large number of couplers (~ 10,000 per linac in the present TESLA design). The magnitude of the kick, and the resulting emittance dilution, will depend upon the chosen coupler geometry.

The TESLA Test Facility (TTF) linac at DESY (Hamburg) employs a co-axial coupler mounted in the horizontal plane, downstream of the nine-cell cavity. The present design calls for a coupler capable of transmitting 230 kW of travelling wave power during 1.3 ms pulses at a repetition frequency of 5 Hz. Higher powers (~ 1 MW) are needed for conditioning of the couplers, albeit with shorter pulse duration. As the effect of the kicks on the beam will diminish with energy, mounting the coupler in the downstream position is beneficial for the low energy part of the machine. As control of the vertical emittance is of great importance for the luminosity of all linear collider designs it is clearly advantageous to mount them in the horizontal plane. Exciting the cavities alternately from the right and then left hand side would reduce the cumulative effects of the kicks but would complicate the design of the wave-guide distribution. The radial kick, $\delta x'$, imparted to an electron is given by the following expression;

$$\delta x' = T_x [\Delta E/E_f] .\cos(\phi_{rf} + \phi_0),$$

where ΔE is the energy gain in the cavity, E_f is the exit energy, ϕ_{rf} is cavity phase and ϕ_0 is a phase constant related to the distance, d, between the coupler axis and the centre of the first cavity cell, $\phi_0 = 2\pi d/\lambda$, with λ the RF wavelength. The constant T_x is a measure of the strength of the steering effect.

The magnitude of the RF steering effect induced by these kicks in the first module of the TTF linac has been measured experimentally. The experimental set-up allowed one only to observe the average effect from the eight couplers of the module. Beam position measurements downstream of the module, taken as a function of the RF phase and with the

SC quadrupole inside the module turned off, allowed an estimate of the value of T_x. The value obtained, although larger than theoretical estimates, indicated that the magnitude of the steering effect of the present couplers would have little impact on the TESLA luminosity.

One of the main limitations in coupler performance, as observed at several laboratories using SC technology, is the time required to "condition" the coupler. By this we mean the time required to establish routine operation of the coupler at its nominal power level. When first exposed to RF fields those surfaces of the coupler under vacuum are normally prone to *multipactoring*, an electronic discharge which consumes the RF power and which can lead to severe local heating and increase of vacuum pressure in the coupler. The duration of the conditioning period is greatly extended if the coupler suffers severely from this effect. For co-axial couplers scaling laws show that the multipactor levels can be pushed to higher powers by increasing the outer diameter of the co-axial line (the multipactor levels scale with the fourth power of the diameter). The present TTF coupler employs a co-axial line of 40 mm outer diameter (o.d.) at the cavity flange. In the framework of the DESY/LAL collaboration we will test alternative coupler designs which could be used to power several cavities coupled together. Such a coupler would need to operate at higher power levels than those used for TTF (typically 2MW). In order to push the multipactor levels to higher values we have constructed an 80 mm o.d. co-axial coupler. The figure below shows the coupler attached to the RF test bench awaiting tests with high power pulsed RF.

Figure 1. Power Coupler mounted on the wave-guide test bench. The ceramic window which separates the coupler vacuum from the wave-guide is visible at the top of the coupler.

2.2. Accelerator Structure Development for NLC/GLC

Juwen Wang
Stanford Linear Accelerator Center
Menlo Park, California, 94025, USA
mail to: jywap@SLAC.Stanford.EDU

Toshiyasu Higo
KEK, High Energy Accelerator Research Organization
1-1 Oho, Tsukuba, Ibaraki, 305-0801, Japan
mail to: toshiyasu.higo@kek.jp

2.2.1. Abstract

The NLC (Next Linear Collider) and GLC (Global Linear Collider) [1,2] are e^+ e^- linear collider proposals based on room-temperature accelerator technology – so called "warm machines" in comparison with the TESLA "cold machine" that is based on superconducting accelerator technology. There have been two major challenges in developing X-band (11.4 GHz) accelerator structures for the GLC/NLC. The first is to demonstrate stable, long-term operation at the high gradient (65 MV/m) that is required to optimize the machine cost. The second is to strongly suppress the beam induced long-range wakefields, which is required to achieve high luminosity. The development of high gradient structures has been a high priority in recent years. Nearly thirty X-band structures with various rf parameters, cavity shapes and coupler types have been fabricated and tested since 2000. This program has been a successful collaborative effort among groups at SLAC, KEK, FNAL and other labs. A summary of the main achievements and experiences are presented in this paper as well as a status report on the structure design, high power performance, manufacturing techniques, and other structure related issues.

2.2.2. Introduction

With the advent of the SLAC electron-positron linear collider in the 100 GeV center-of-mass energy range, research and development on even higher energy machines of this type started at several laboratories around the world. This research is motivated by the fact that linear colliders are the only viable approach to study e^+ e^- physics at center-of-mass energies approaching 1 TeV. As part of this effort, R&D on advanced accelerator structures at SLAC and KEK started in the late 1980's. The flow chart below provides a brief summary of the accelerator structure design progression that followed[3].

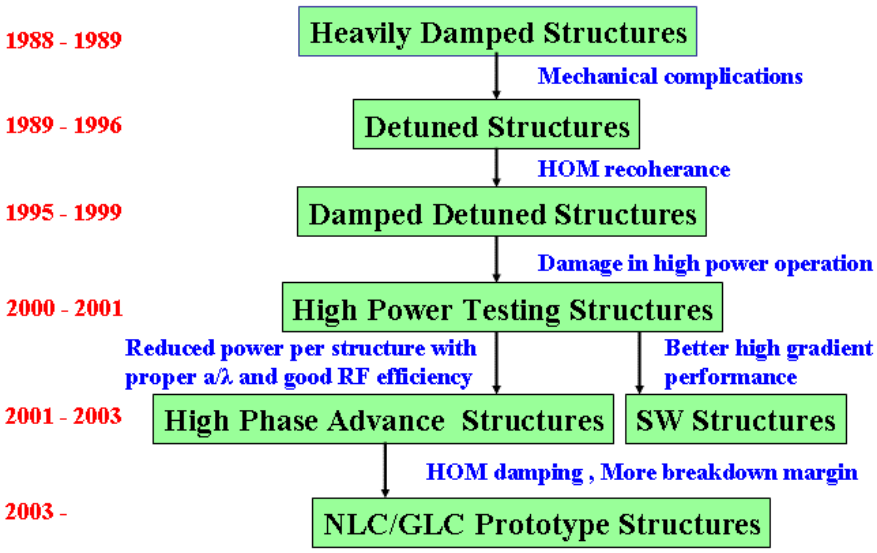

Figure 1. Brief history of accelerator structure R&D.

For X-Band (11.4 GHz) structures, the long-range transverse wakefield excited by the beam is relatively strong. These fields need to be reduced by about two-orders of magnitude within the 1.4ns bunch spacing. In the late 1980's, we developed two types of heavily damped structures: radial slots in the accelerator disks and circumferential slots in the side walls of the accelerator cavities. From computer simulations and cold tests of short cell stacks, dipole mode Q's as low as 10 seemed possible in both types of structures. However, due to the mechanical complications of making such structures, we instead switched to a detuning approach to suppress the wakefields. Detuning requires that each cell of the structure have a slightly different dipole frequency such that the net wakefield from the different modes decreases rapidly and smoothly during the period between bunches. Specifically, the dipole frequency is varied along the structure to produce a Gaussian distribution in the product of the mode density and the mode coupling strength to the beam.

Two 1.8m long Detuned Structures (DS1, DS2) with 10% Gaussian frequency detuning were produced initially. The prediction and measurement of the DS1 wakefield showed that the detuning produces an approximately Gaussian falloff in the net wakefield generated by each bunch, and works well to suppress the wakefield for about 30 ns, after which the amplitude increases due to a partial recoherence of the mode excitations. To offset this rise in the next generation of structures, weak mode damping was introduced by coupling each cell through longitudinal slots to four TE11 circular waveguides (manifolds) that run parallel to the structure. This reduces the dipole mode quality factors from about 6000 to 1000. By the late 1990's, several 1.8m Damped Detuned Structures (DDS1, DDS2 and DDS3) were fabricated and good agreement was achieved between the measured and predicted wakefields. This success had required advances in several areas including precision field calculations, machining and assembly procedures.

The final step in the design evolution was to optimize the cell shape to decrease the required power for a given gradient. This resulted in a rounded cell shape and the first

prototype Rounded Damped Detuned Structure (RDDS1) was fabricated to evaluate its performance. The design proved successful in improving efficiency. However, the high gradient studies that were ongoing at this time began to show serious gradient limitations with the basic 1.8m structure design, independent of the wakefield suppression features.

The high gradient testing has been done at the Next Linear Collider Test Accelerator (NLCTA), which was designed for RF system integration studies. Improvements to the power sources and operational capabilities in the late 1990's allowed more systematic studies at higher gradients. After high power operation, both RF measurements and visual inspections by boroscope revealed that the 1.8m structures were being damaged by rf breakdown. The net RF phase advance through the structures had increased by roughly 20 degrees per 1000 hours of operation at gradients as low as 50MV/m[4,5]. In 2000, we started an aggressive program to improve the high gradient performance of the structures. A large design parameter space was explored including different accelerator lengths, aperture sizes, group velocities, phase advances, and cavity types (standing-wave and traveling-wave). Also, improvements were made in the techniques used to clean and bake the structures before testing. Based on the experience gained from having tested nearly thirty structures, an optimal design has been selected that includes the wakefield suppression features originally developed for the 1.8m structures.

2.2.3. Structure Design

2.2.3.1. RF system configuration

The layout of an rf unit in the NLC/GLC linac is shown in Figure 2. Two 75 MW PPM klystrons with 1.6 μs pulses drive a dual-moded SLED-II pulse compression system to obtain 450 MW, 400 ns rf pulses. This power is then divided to feed eight, 60-cm long accelerator structures. The 56 MW of rf input power per structure produces an unloaded gradient of 65 MV/m.

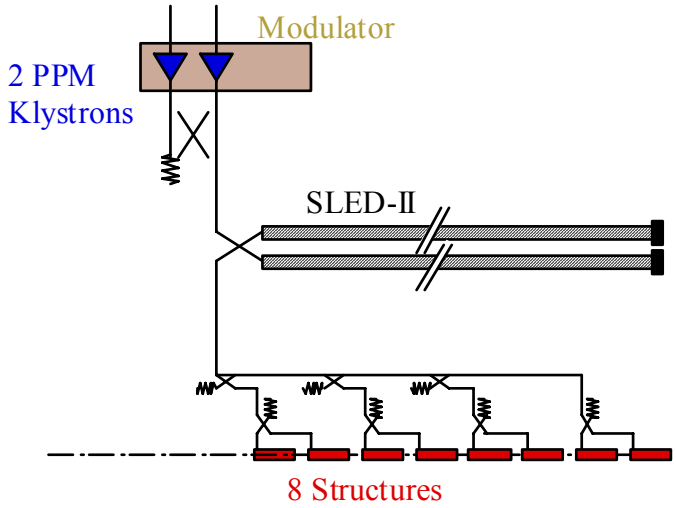

Figure 2. RF system configuration in the GLC/NLC main linac.

2.2.3.2. Basic RF parameters of the accelerator structures

The choice of operating frequency has a major influence on almost every aspect of linear collider design. The X-Band operating frequency (11.4 GHz) is believed to provide the major cost benefits of a high frequency RF system (high gradient with good efficiency and low RF energy per pulse) while still having achievable wakefield related alignment tolerances.

The choice of the average accelerator iris aperture, a, is a tradeoff between efficiency, where a small size is desired, and limits on the allowed short-range wakefield strength, which scales as $1/a^{3.5}$. As a compromise, values of a/λ of 0.17~0.18 have been chosen (λ is the rf wavelength). Also, a quasi-constant gradient traveling-wave structure design is used. Considering the multi-bunch beam loading, the accelerator attenuation factor, $\tau = 0.5\ln(P_{in}/P_{out})$, for optimal rf efficiency is 0.5 ~ 0.6, which corresponds to an rf filling time of 100 ~ 120 ns[6].

2.2.3.3. High phase advance accelerator structures

The first set of structures tested as part the high gradient program were low group velocity (0.03c ~ 0.05c) since the low-group velocity (downstream) portion of the 1.8m structures showed little damage. Although these structures proved much more robust, they have a smaller iris size ($a/\lambda = 0.13$) than required. Designing a low group velocity structure with $a/\lambda = 0.17 \sim 0.18$ is difficult since the simple solutions significantly lower the rf efficiency. The design that was adopted required increasing the phase advance per cell ($5\pi/6$ instead of $2\pi/3$) and using thicker irises to maintain a relatively high shunt impedance with the larger iris size. In order to maintain an optimal filling time, the structure length was scaled from the earlier 1.8m structures, which had group velocities of 0.12 c ~ 0.03 c, to a 0.6 m length with group velocities of 0.04 c ~ 0.01 c.

Table 1 lists the parameters for the most recent structure design. Note that this structure has pillbox-shaped cells. By optimally shaping the cell, as was done for RDDS1, the Q value and shunt impedance can be increased by about 10%.

Table 1. Basic structure parameters.

Structure name	HDDS (H60VG4SL17)
Structure length	62 cm (including couplers)
Number of acceleration cells	53 cells + 2 matching cells
Average cell iris radius	$< a/\lambda > = 0.17$
Phase advance / cell	$5\pi/6$
Group velocity	4.0 ~ 0.9 % speed of light
Attenuation parameter τ	0.64
Filling time	118 ns
Q value	7000 ~ 6500
Shunt impedance	51 ~ 68 MΩ/m
Coupler	Wave Guide type
1st Band dipole mode distribution	$Sech^{1.5}$ distribution with Δf~ 11% (4σ)
Es/Ea	2.22 – 2.05
Required input power	59 MW
Gradient without beam $<E_0>$	65 MV/m
Beam loaded gradient $<E_L>$	52 MV/m

2.2.3.4. Cavity dimension calculation

The parallel computing code Omega3P has been used to compute the cell dimensions for various accelerator structures[7]. The left half of Figure 3 shows the domain composition by color-coded meshes for a 16-parallel-processor simulation of one-eighth of an accelerator cavity with damping manifolds. The cavity frequency convergences as the fourth power of the mesh size. The Omega3P results agree with cold test measurements to within half a MHz for the 11424 MHz cavities, which is an accuracy well within the fabrication tolerances. The right half of Figure 3 shows the temperature increase due to rf pulse heating.

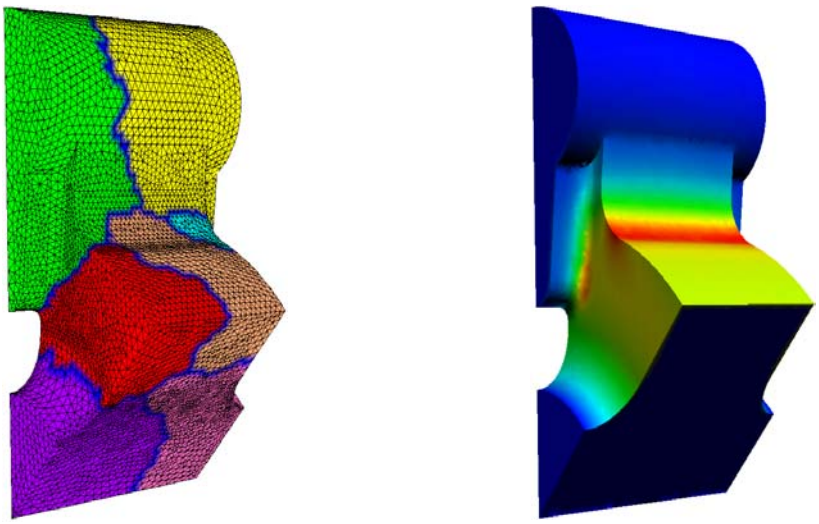

Figure 3. Meshes for parallel modeling (left) and illustration of pulse heating (right).

2.2.4. Wakefield Suppression

The manifold dipole mode damping scheme discussed above requires careful design to ensure the extracted energy flows out of the structure. At the ends of the structure, each manifold is connected to a rectangular waveguide through a coupling region followed by a 90 degree circular H bend, a taper to WR62 waveguide, and finally a manifold load with a coaxial probe for HOM signal monitoring. The matching quality for the propagating HOM frequencies of this assembly has a significant affect on the long-range wake. Figure 4 shows the HOM coupler layout used in computer simulations.

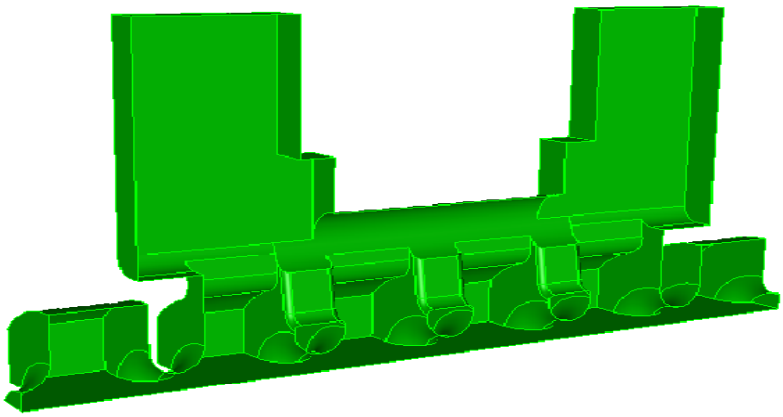

Figure 4. HOM coupler layout used in computer simulations.

The wakefield calculations are based on an equivalent circuit model that consists of a sequence of elements corresponding to the accelerator cells. Each cell is coupled to a transmission line representation of the HOM manifolds. All damped mode frequencies can be determined with this model. For moderate coupling to a manifold in our DDS structures, the modes are perturbed significantly and it becomes difficult and time consuming to calculate the wakefield from a modal summation. For this reason we

developed a Spectral Function Method.[8] The wakefield is expressed as a Fourier-like integral of a spectral function over the propagation band of the manifolds.

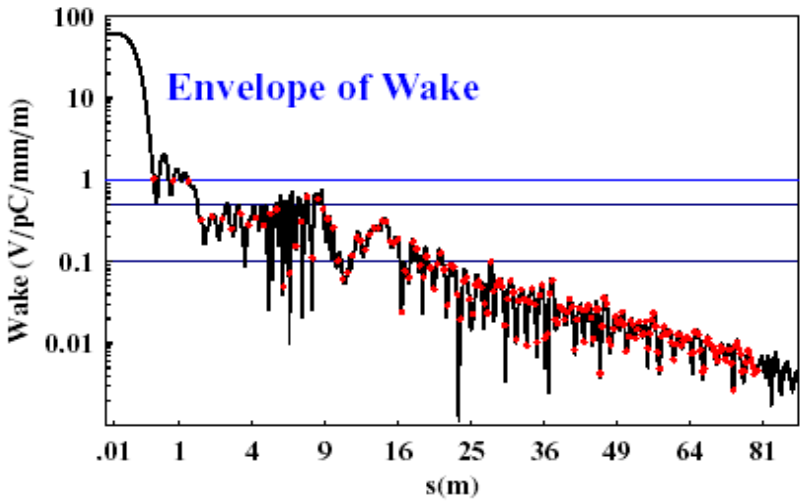

Figure 5. Calculated wakefield for recently designed HDDS structure. The dots indicate the locations of the bunches, which have a 1.4 ns spacing.

The wakefields for three of the damped and detuned structures have been measured at the ASSET facility in Sector 2 of the SLAC Linac[9]. Here, positrons extracted from the South Damping Ring serve as the drive bunch and electrons extracted from the North Damping Ring serve as the witness bunch. Figure 6 shows that a good agreement was achieved between the measurement and prediction for the RDDS1 structure. This structure has frequency errors in a few cavities near its center due to fabrication problems. These errors were estimated from bead-pull measurements of the fundamental mode. The wakefield is likely dominated by a few modes in the region of the cell errors, which can be corrected in the future. To realize the wakefield suppression afforded by the detuning also requires that the structure straightness be maintained (up to 100 micron peak-to-peak excursions are allowed). Such straightness has been routinely achieved in prototype structures.

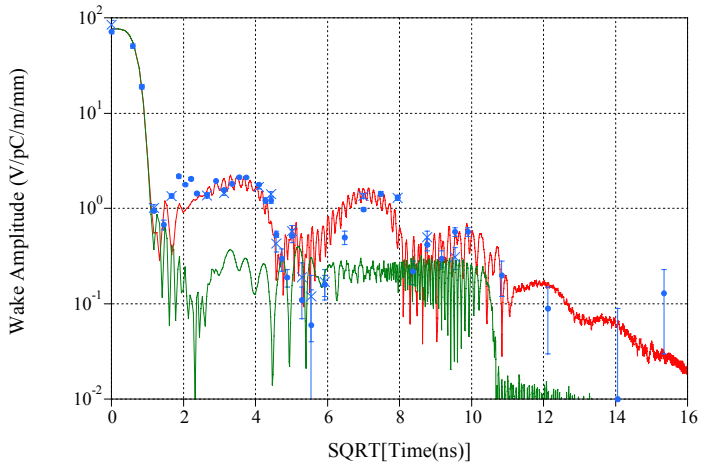

Figure 6. RDDS1 ASSET wakefield data (vertical = dots, horizontal = crosses) and prediction with (red) and without (green) known frequency errors.

Besides damping the dipole modes, the manifolds serve another useful function. Their signals provide a measure of the transverse position of the beam in the structure. Moreover, the beam coupling to the modes is fairly localized (2 to 10 cells) so filtering the signals by frequency yields beam offset information at different regions along the structure. As part of the wakefield measurement program, beam centering tests were done using dipole signals at two frequencies as a guide to position the drive beam. Measurements of the resulting short-range wakefield (< 300 ps) indicated that the drive beam had been centered to the 11 micron rms measurement accuracy, which was limited by the position jitter in the incoming beam. For comparison, the NLC/GLC goal is < 5 microns rms.

2.2.5. High Gradient Operation

Since the start of the linear collider program, much attention has been paid to the issue of high gradient performance. We were encouraged by tests in the early 1990's showing that unloaded gradients greater than 100 MV/m are possible and that the gradient limit increased with RF frequency. However, these tests were done with standing wave or low group velocity structures because high gradients were possible with the limited peak power available at that time. Later, higher group velocity structures (12% c in the first cell) were chosen for their lower cost and lower wakefields. However, these 1.8m structures failed to reach these high gradients and incurred significant breakdown related damage near their upstream ends at unloaded gradients of 45~50 MV/m with 240 ns pulses.

Stable high-field operation is very important since it affects the up-time of a linear colldier. For a 0.6 m structure, less than 1 breakdown per 2 million pulses is tolerable so as to rarely deplete the planned 2% overhead of rf units (this assumes a 10 second recovery time from a fault, which has been tested). In addition to the trip rate, there are limits on the copper erosion due to these breakdowns, which cause beam-to-rf-phase slip and reduce the energy gain. A rough guideline (less than 5% gradient reduction in 20 years of operation) imposes a criterion that the net phase advance change be less than 0.1 degrees per month of operation. From the small phase changes (typically 1 degree or less) that occur during the processing of the structures when there are thousands of breakdowns, we expect to meet this criterion if we extrapolate using the acceptable breakdown rate limit defined above.

2.2.5.1. Structure design optimization for efficiency and high gradient performance

After careful examination of GLC/NLC linac beam dynamics issues, we recently reduced the a/λ parameter for the structure design from 0.18 to 0.17. This change increases the structure efficiency by 10%, which reduces the required input power proportionally, and hence lowers the cost. Earlier studies also indicated that breakdown rates were lower with reduced input power, presumably because less 'collateral' damage is produced during breakdown. While this change increases the short-range wakefield by 20%, the increase is manageable. Another change that was made involves tailoring the gradient profile along the structures. We have seen that the breakdowns that occur after processing tend to be near the input end of the structure. Therefore, we have lowered the gradient at this end and increased it in output end while maintaining $a/\lambda = 0.17$ and a similar efficiency. Figure 7 shows the peak electric field profiles for different structure designs.

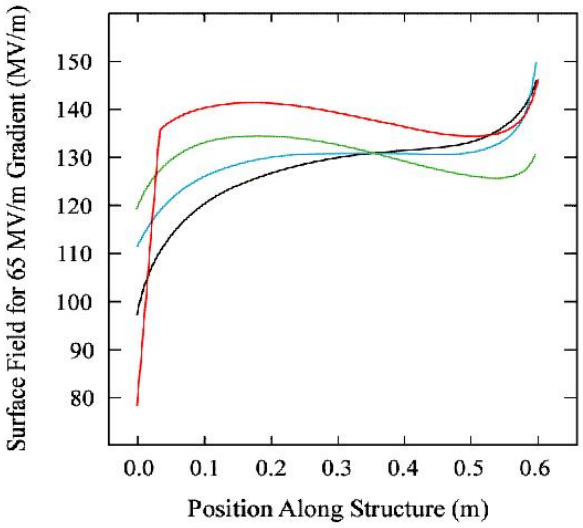

Figure 7. Comparison of maximum iris surface field for different structure designs at an unloaded gradient of 65 MV/m. The red curve is for H60VG3N (a/λ=0.18), which has rounded shaped irises – the others have elliptical shaped irises, which lowers the peak field. This structure also has a reduced field in the first several cells. The green curve is for H60VG3S18 (a/λ=0.18), which shows the effect of the elliptical shaped irises. The light blue curve is for H60VG3S17 (a/λ=0.17) and black curve is for the optimized H60VG4S17 (a/λ=0.17).

2.2.5.2. Structure input, output couplers and rounded coupling slots

During the early tests of low group velocity structures, the breakdown rate at high gradient was dominated by events in the input and output couplers. The rf signature of these events was different from those in the body and was similar from one structure to another. An autopsy of the input coupler of one of the structures revealed severe damage and some melting on the edges of the waveguide openings to the cell, and extensive pitting near these edges. The waveguide edges see large rf currents that are a strong function of their sharpness, and the associated pulse heating can be significant. By design, the edges in these structures were sharper (76μm radius) than those in the 1.8m structures (500μm radius), where this problem did not occur. The predicted pulse heating for the low group velocity structures was 130~170 °C, well below the copper melting point, but high enough to produce stress-induced cracking, which can enhance heating.

Several coupler designs that produce much lower pulse heating have been proposed[10]. Those shown in Figures 8(a) and 8(b) use rectangular-TE to circular-TM mode converters with different matching designs. Design (a) is referred to as a mode converter type and design (b) as a waveguide type. The pulse heating for both types of couplers is negligible.

Figure 8(c) shows an HDDS cell with pie-shaped slots to couple the dipole modes to the circular manifolds. The temperature rise due to rf pulse heating is reduced from 70^0C to about 25^0C by rounding the four slot edges with a 0.5mm radius and rounding the manifold openings to the accelerator cavities with a 2mm radius.

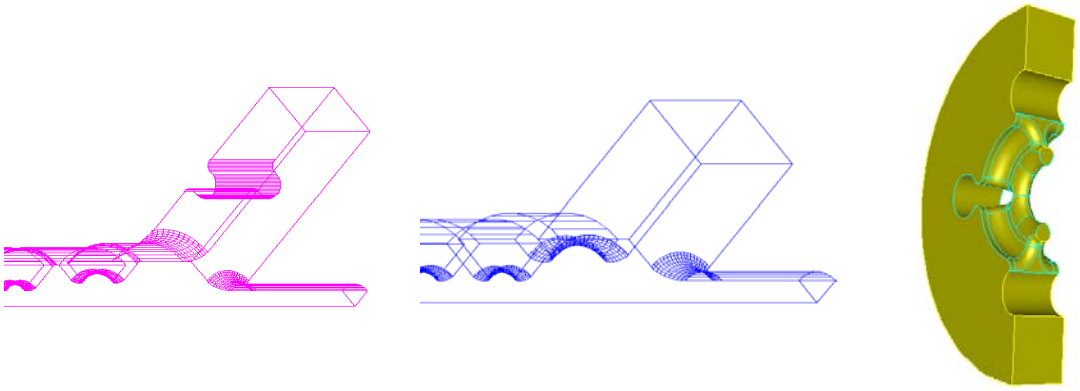

(a) (b) (c)

Figure 8. (a) and (b): Two types of rf couplers. (c): Rounded HOM coupling slots with low pulse heating.

2.2.5.3. High power test results

Since 2000, nearly thirty structures have been tested at the NLCTA shown in Figure 10(a) with over 15,000 hours of high power operation logged. The figure below summarizes the performance of the candidate structures tested in 2003. It shows the breakdown rate versus unloaded gradient during operation at the nominal 400 ns pulse width at a repetition rate of 60Hz. All of these structures have an acceptable average iris radius and dipole mode detuning. In addition, three of the structures (H60VG3-6C, H60VG3S18 and H60VG4S17-1) have slots (manifolds) in all or some of the cells to damp the long-range wakefield, consistent with GLC/NLC specifications. The observed variation in performance is due in part to variations in the design parameters as well as variations in the structure preparation methods, which are currently being refined. Some structures are also known to have problems that occurred during assembly and installation.

Although none of the structures meet the breakdown rate requirement of < 0.1 per hour at 65 MV/m, several do at 60 MV/m, and the average rate for all of these structures is acceptable at this gradient. While better performance is expected in future structures, these results already demonstrate the feasibility of a collider based on operation with an unloaded gradient of 60 MV/m. It should also be noted that, because of the field reduction from beam loading and the effective shortening of the pulse from the shaping required for beam loading compensation, the actual breakdown rates during beam operation at GLC/NLC will be smaller than those currently measured in tests with square pulses. The effect of the pulse shaping is shown by the two data points for the H60VG4S17-1 structure at 65MV/m.

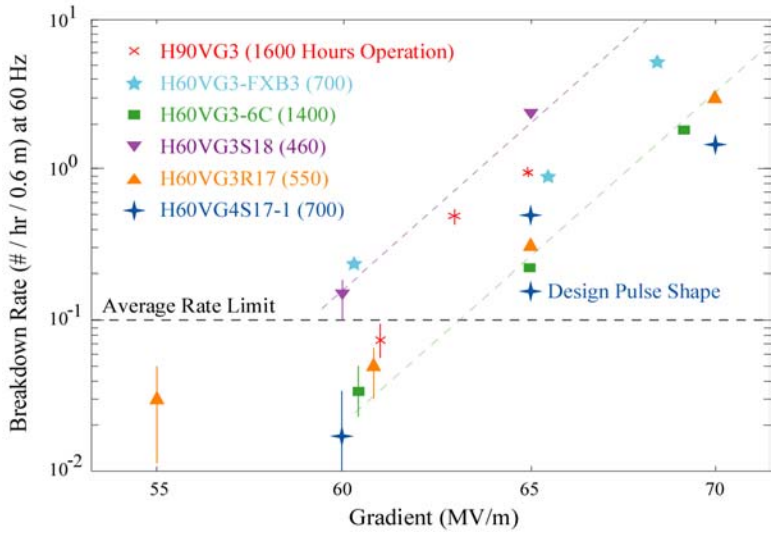

Figure 9. Breakdown rate as a function of unloaded gradient for several recently tested structures. The 'Design Pulse Shape' data point was taking with the ramped pulse that would be used in the NLC/GLC for beam loading compensation (square shaped pulses are normally used for testing as a worst case).

2.2.5.4. High power testing at KEK

A high power X-band rf system was recently re-established at KEK as shown in Figure 10(b). Structures having some of the designs listed in Figure 9 will be tested there starting in 2004. This program will help provide additional experience with high power operation of X-band accelerator structures. Eventually the facility will also allow us to conduct beam-related studies since its location was chosen to accept the ultra-low emittance beam that is extracted from the ATF (Accelerator Test Facility).

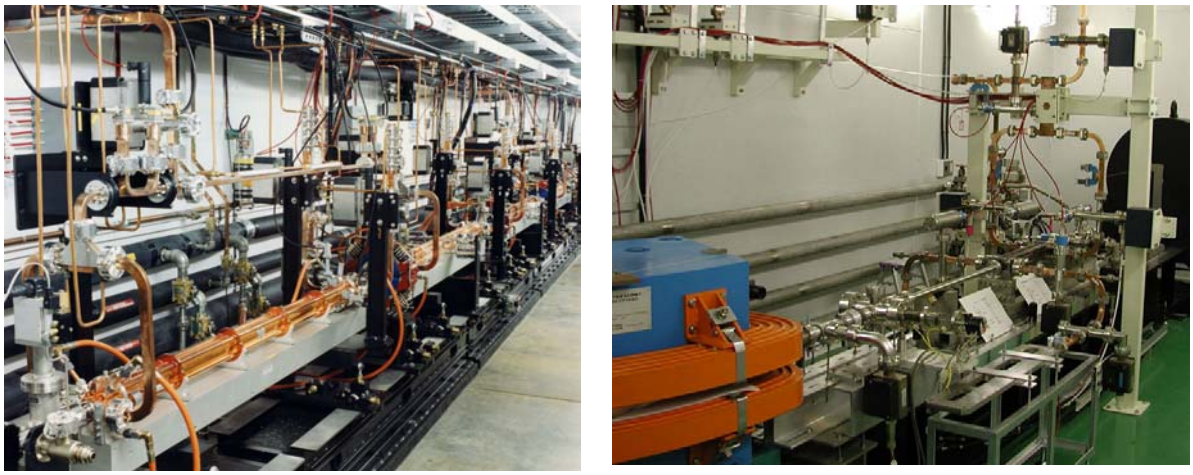

Figure 10: X-band high power test setup at SLAC and KEK.

2.2.6. Standing Wave Option

Standing-wave (SW) structures were considered for the NLC/GLC linacs because previous tests indicated they can operate at high gradients and they have the added benefit that they need only run at the loaded gradient. To explore this possibility, we built several 15-cell π-mode structures for evaluation. In all, four pairs of SW structures were tested[11]: two pairs of $a/\lambda = 0.18$ structures, one pair of higher a/λ structures and one pair of lower a/λ structures; these different a/λ designs would be used to produce piece-wise detuning of the dipole modes. Each pair of structures is fed from a high power 3db hybrid with a 90-degree phase difference in order to cancel the transient reflection back to the power source. After processing, the structures were operated at 55 MV/m, the GLC/NLC loaded gradient at the time (it is now 52 MV/m).

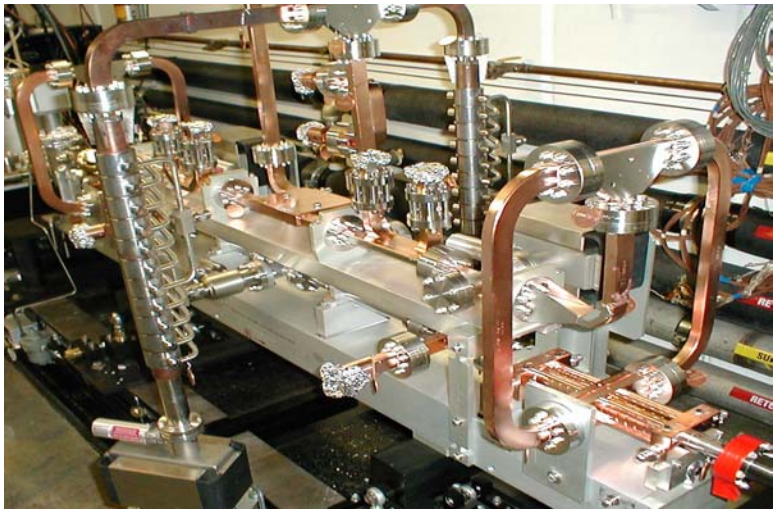

Figure 11. A pair of SW structures installed in the NLCTA beamline.

For two pairs of structures, the average breakdown rate at 55 MV/m was acceptable and no discernible shift in frequency was observed. However, at 60 MV/m the breakdown rate exceeded the acceptable limit, so they do not offer much more operating overhead than the present traveling wave structures. Also, damping the dipole modes in these structures is non-trivial and has not been tried. Currently, the development of these structures is on hold.

2.2.7. Other R&D

Besides the high gradient program, progress is also being made in improving the methods to suppress the long-range wakefield and in better understanding the various alignment and frequency tolerances. In addition, a wire-based method for measuring the wakefields is being developed so the time-consuming beam-based approach does not need to be used as often.

The long-range wakefield calculation program has been rewritten to automatically minimize the RMS and standard deviation of the sum wakefield (i.e. the net wakefield that would be seen by the 192 bunches). Another improvement involves the way detuning is applied to groups of structures, which is referred to as interleaving since the dipole frequencies are systematically offset structure to structure. This interleaving is necessary given that there are fewer modes in the shorter (60cm) structures to 'beat' against: the NLC/GLC linacs will probably use four-fold interleaving so there would be four unique

structure electrical designs. The improvement in this method has to do with making sure the actual modes are uniformly interleaved in frequency, not just the simple estimate of the mode frequencies that have been used in the past for design purposes. Finally, work is progressing to better define frequency and alignment tolerances. By simulating the emittance dilution of GLC/NLC bunch trains as they traverse the main linac, the cell-to-cell and the structure-to-structure frequency tolerances and alignment tolerances have been specified for both random and systematic errors. [12] Also, the structure bow tolerances and angle-offset tolerances are being carefully analyzed, and the contribution of higher frequency dipole bands to the wakefield are being evaluated.

A wire-based structure analysis method is being developed to quickly and inexpensively analyze the wakefield suppression properties of accelerator structures[13]. Using a 300-micron thick brass wire, measurements of the structure S-parameters are made to compute the impedances for the monopole band and higher dipole mode bands. The test results for a standing-wave structure, a short traveling-wave structure, and the RDDS1 structure show a reasonable agreement with computer simulations.

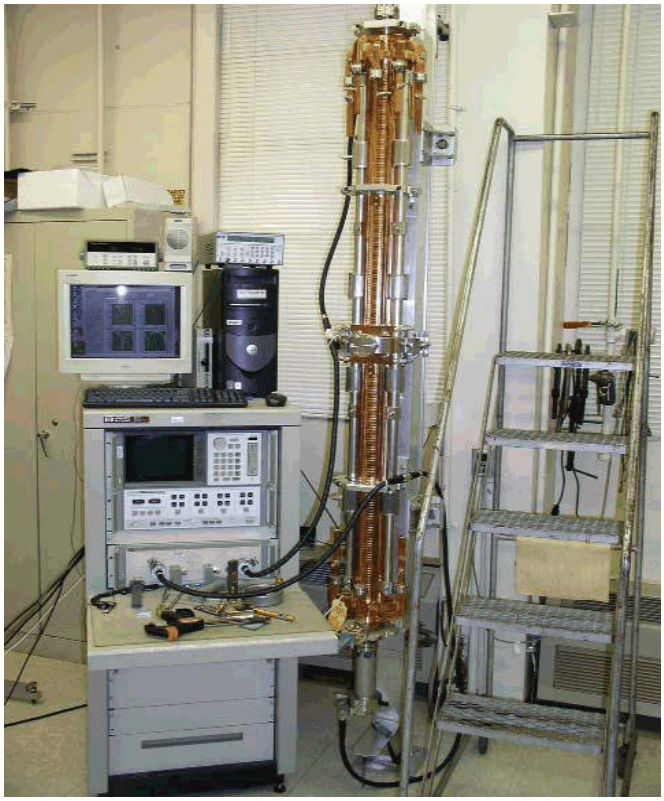

Figure 12. Wire measurement set-up with the RDDS1 Structure.

2.2.8. Structure Fabrication

Since early 1990's KEK has been a pioneering center for high-precision fabrication of structure cells using the diamond turning technique, which KEK originally introduced for fabrication of mirrors for use at SR light sources [14]. This high precision machining

technology, together with a variety of RF measurement techniques, allowed the NLC/GLC team to conduct a very precise validation of design calculations of the structure cells that involved complex 3-dimensional modeling. This program has been highly instrumental in advancing the designs of X-band accelerator structures.

2.2.8.1. Cell fabrication

Figure 13 shows a cell for the latest GLC/NLC accelerator structure. The material chosen is oxygen-free copper of grade-1, class-1, from which the cells are fabricated through a combination of precise milling and diamond turning.

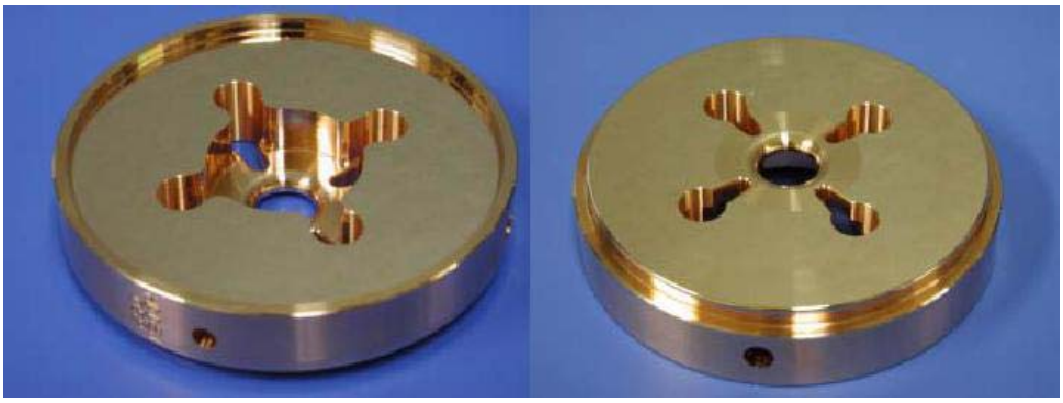

Figure 13. Photos of a HDDS cell.

Milling is required to create the slots and manifolds. Position control of about 10μm is required during milling to ensure proper mode frequencies as well as a smooth connection between the milled surfaces and the turned surfaces. The latter is required to avoid excessive surface heating during operation, which may lead to rf breakdown. Since a precision of this magnitude is readily available in industry, initial machining (so called "rough machining") of the cells, including milling, is done typically by outside contractors. The final cutting is done by using a diamond tool with a precision turning lathe which is placed in a temperature-controlled environment. The typical precision of 2μm in both the diameter and thickness can easily be obtained by using the following two procedures. The first is to measure the diameter of a cell after cutting, and apply corrections to the lathe set-up for the cutting of the later cells. This allows continual initialization of the radial position of the cutting tool. The second is the periodic cutting of the vacuum chuck surface with the diamond tool. This properly initializes the longitudinal position of the cutting tool. In addition, a few precautions specific to the accelerator cells need to be taken. For instance, since the material is very soft, excessive mechanical stress due to inadequate chucking and other forces must be avoided. While the dimensions inside the cavities are of critical importance in the light of precision control of the resonant rf frequencies, the outer features of the cell (for example, the surface flatness and outer diameter) also require attention since they determine the relative cell-to-cell alignment and bonding quality. These techniques, which were developed in the laboratory environment at KEK, are currently being transferred to industry. Typical specifications for the recent HDDS cells are summarized in the Table 2.

Table 2. Typical mechanical tolerances of a structure.

Item	Unit	Specification
Milling positioning	μm	10
Turning diameter	μm	2
Turning depth	μm	2
Tangential discontinuity	degree	5 or 8
Concentricity between milling and turning	μm	10
Concentricity of 2a, 2b and outer diameter	μm	1
Cell-to-cell alignment	μm	5 ~ 10

2.2.8.2.Frequency requirements

Many aspects of the electrical performance of accelerator structures are characterized by the resonant frequencies of individual cells. Of critical importance at GLC/NLC are the control of the fundamental mode (accelerating mode) resonance frequency f_0 and the lowest band dipole mode frequency f_1 in each cell. For adequate performance of accelerator structures at GLC/NLC in terms of wakefield detuning, the tolerance on f_1 is such that its rms random error stays below 3 MHz. As for f_0, the requirement of keeping the total phase slip of the fundamental mode along a structure within several degrees translates to a tolerance of ~0.1MHz for each cell. It is, however, not feasible to achieve this latter tolerance on f_0, unless one uses a feed-forward machining technique (to be discussed later) or resorts to post-assembly tuning. Thus, we impose an f_0 tolerance of ±1 MHz to dictate the machining tolerances, which can reasonably be realized by the present fabrication technology. This allows the issues of the total phase slip to be addressed in combination with suitable rf measurements as described later. If this is done, because of the known correlation between errors of f_0 and f_1 which arise from a variety of cell dimension errors, the associated errors of f_1 are expected to be within 2 ~ 3 MHz, which automatically satisfies the detuning requirement.

Extensive single and multi-disk rf measurements were made to verify the fundamental and dipole mode frequencies in the process of preparing RDDS1[15]. For single disk QC, each disk was sandwiched between two flat plates. The frequency deviation of four modes (fundamental zero and π mode, π mode of first dipole band and zero mode of second dipole band) were measured as shown in Figure 14. The rms deviations of the four sets of frequencies from smoothly varying curves is within 0.6 MHz.

Systematic errors in the fundamental frequency f_0 can be addressed in the following manner. First, it is known that an “average” f_0 of a “short stack” of disks (typically 6 disks in our experience), which correspond to a part of a completed accelerator structure, can be measured within ~ 0.2MHz. This allows us to estimate the average errors of f_0 with an adequate precision, so that if the accumulated phase error of the fundamental mode is predicted to exceed the desired value, 5 degrees for instance, one could perturb the cavity dimensions of subsequent cells to offset the systemic errors of previous cells. The most straightforward way of achieving this is to apply a correction in "b" (cavity radius) to the disks in later fabrication. A total integrated phase shift less than 3° for 2π/3 mode frequency was obtained for the RDDS1 structure.

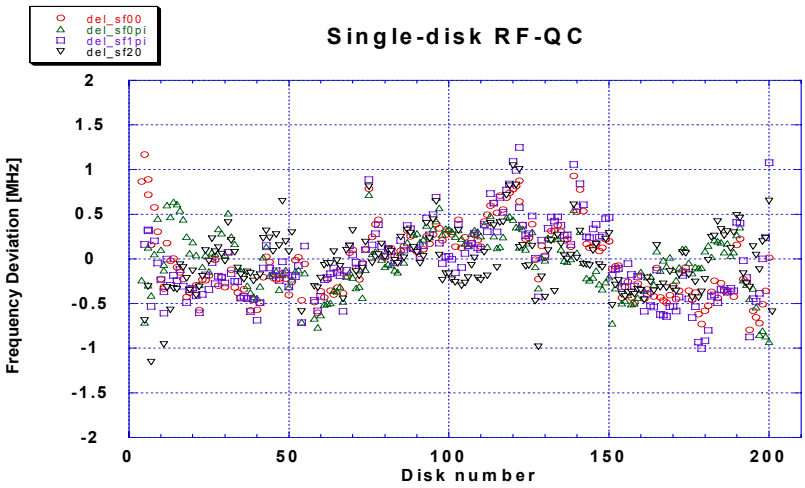

Figure 14. Four frequencies measured in a single-cell QC setup versus cell number.

In mass production environment this or other techniques may be employed to satisfy the tolerance on f_0 in addition to f_1. One may consider preparing a multiple set of cells with suitable rf measurements first, and select adequate ensembles of cells to build accelerator structures with the desired frequency distributions. One may also introduce "tuners" on the cells to do post-assembly frequency tuning. The exact choice of actions during cell fabrication, cell selection, structure assembly and rf measurements would depend on cost optimization in conjunction with the desired construction period and available mass production technology at the time of construction.

Of all these possibilities, a critical technological prerequisite is to fabricate the structure cells with a precision of ±1 MHz. However, it should be noted that this does not necessarily mean absolute control of all relevant dimensions. Rather, it requires the ability to make a contiguous set of cells with machining accuracy stable enough that the absolute frequency of a structure is maintained as a whole. The technology we have now is at the level listed in Table 2 and so is adequate. We know that the effect of a systematic error on higher mode frequencies from structure to structure in a linac is more severe than a random one. So we think that it is better to randomize the dipole frequencies among the structures in a linac by adding sub-micron offsets in the numerically controlled machining program.

2.2.8.3. Assembly through diffusion bonding

After fabrication, the cells are rinsed in an acid bath to remove the damaged layer from machining. The thickness of the layer removed is a few microns. These cells are subsequently stacked, guided by their outer diameter on a V-block, and are bonded in a copper-to-copper mutual diffusion process in a high-temperature (> 900°C) furnace. Here, a diffusion bonding technology was employed to assemble the structure body[16], while realizing the required alignment precision. The feasibility of this technology choice has been proven for the 1.8m RDDS1 structure. Stacking of cells on a V-block was good enough to obtain a cell-to-cell alignment at the micron rms level. After assembly, the bow of RDDS1 was about 200μm. Therefore, the bow of the present 60-cm-long structures should be an order of magnitude better, resulting in a much smaller bow than required.

2.2.8.4. Complete structure

All recent structure cells made by KEK were assembled and bonded at SLAC. In order to acquire the assembly and tuning experience at KEK, a program to complete full-size structures has been started. Recently KEK made a 60-cm-long structure, which is shown in Figure 15. The cells for this structure were machined and electrically inspected by a manufacturing company as a first step toward industrialization. The cells were chemically etched at KEK following the SLAC procedure. They were then bonded in a hydrogen furnace at 1020 °C for an hour at a local company. The bonding showed vacuum tightness, indicating that is possible to skip any brazing process for the main body. The couplers and some peripheral parts were integrated by brazing them in a hydrogen furnace. Finally, the structure at KEK was vacuum baked at 500 °C for a week in a double evacuation system. The structures at SLAC are wet and dry hydrogen fired, then vacuum baked at 650 °C for 2-3 weeks in a double evacuation system.

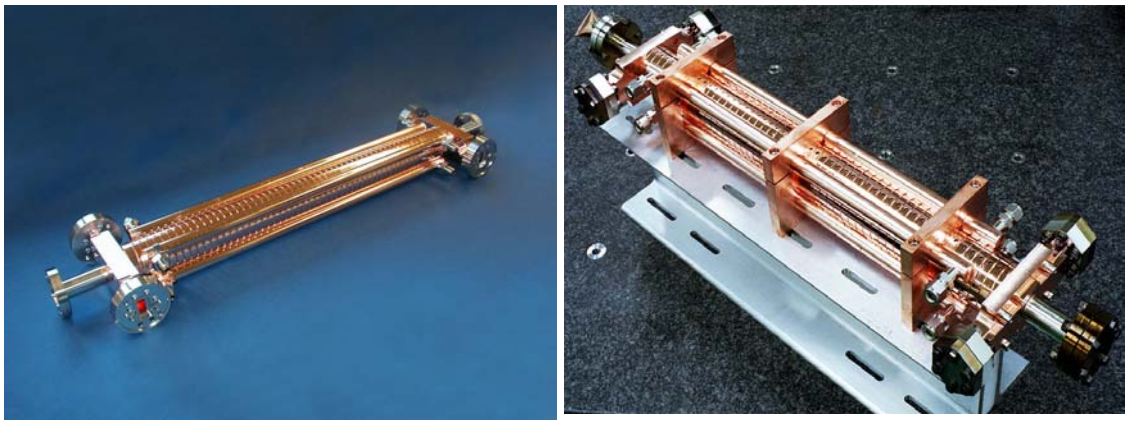

Figure 15. Recent 60 cm-long structure made by SLAC (left) and KEK (right).

2.2.9. Structure Fabrication at FNAL

The first structures built at Fermilab were proposed and designed by SLAC RF group. The initial goal of the Fermilab group was industrialization of NLC/GLC type structures. Subsequently, the RF group was formed and we developed extensive infrastructure (clean room, rf lab, vacuum furnaces, chemistry, tooling etc), and we have started to participate more extensively in structure development. We developed initial production techniques by making short 20cm long FXA structures, and we further honed the technology by building numerous 60cm long detuned structures (FXB series, or H60VG3R18) for high gradient testing. Five FXB's have been successfully tested at NLCTA. We have just completed development of the FXC structures (H60VG3S17), which incorporates damping and thus has all the features needed for the NLC/GLC. Our goals include: verification of SLAC's cell dimension table, design of input/output couplers, development of mechanical quality assurance, and rf quality control on each step of production including final tuning. Also, some effort will be spent on R&D on movable supports (girders), which constitute the basic cell in the main linac.

Recent FNAL structures differ in two basic ways from those produced by SLAC/KEK. One difference is that waveguide style couplers (Figure 8b) are used instead

of the mode converter style (Figure 8a). We designed the waveguide couplers to be more compact, and like the mode converter coupler, they have not been a problem during high gradient operation. Another difference is in the assembly and baking techniques used for the structures. We braze the cells together in a hydrogen-free environment at 780 degC while SLAC diffusion bonds the cells at 1020 degC in a hydrogen atmosphere. The idea is to avoid a high temperature exposure to hydrogen so a long vacuum bake is not required to remove it. Recent structures have also included a 1000 degC pre-bake of the cells to increase the grain sizes (we see some breakdown enhancement near grain boundaries), and to benefit from the surface conditioning that occurs when heating copper to a temperature near melting. All high temperature furnace heat treatments are done in a 500 mTorr partial pressure of argon to prevent copper sublimation. These changes have improved the high gradient performance of recent structures. For the FXC structures, a 3% hydrogen firing at 500 degC (in 500 mTorr Ar), followed by a three day full vacuum bake at 500 deg C is being performed to remove any copper oxide that may be present.

2.2.10. C-Band Development

The GLC team maintains a C-band main linac scheme (GLC-C) [2] as a possible backup option in addition to the X-band design. GLC-C features heavily damped, choke-mode structures[17] whose damping performance of the wakefield has been demonstrated in the past. The high-power operation of a GLC-C pulse compression was successfully tested at KEK in 2003. Since the SPring-8 Compact SASE Source (SCSS) program at RIKEN has adopted a C-band rf system which is basically identical to that of GLC-C, including the accelerator structure, it has been decided that many other aspects of the high-power feasibility studies concerning GLC-C would be studied in the course of the system development of SCSS. Figure 16 shows a setup at SPring-8 currently under preparation. A high field testing of a GLC-C accelerator structure is scheduled to take place in 2004.

Figure 16. High-power setup for C-band accelerator structure testing at SPring8.

2.2.11. Conclusions

An overview of the accelerator structure development efforts for the NLC/GLC have been presented. In summary:

- Computational techniques related to electrical designs are very mature. Likewise, practical design procedures for travelling wave structures are well advanced.

- Basic techniques for fabricating the cells within required precision are well established and are considered reasonable. In addition, a large amount of assembly experience has been accumulated. These techniques yield acceptable wakefield suppression as has been demonstrated.

- Full transfer of fabrication and assembly technologies to industry is believed doable and is in progress.

- Recent high-field testing shows the feasibility of a NLC/GLC with a 60 MV/m unloaded gradient. With additional improvements, the structure performance at 65 MV/m should also meet specifications. There is little cost difference (3 %) between machines based on either of these gradients.

2.2.12. Acknowledgements

We thank the present and former directors of SLAC and KEK for establishing and maintaining a formal R&D collaboration agreement on structure development. During the past 15 years, many people have contributed to the X-band structure program: they include C. Adolphsen, N. Baboi, K. Bane, G. Bowden, D.L. Burke, J. Cornuelle, V. Dolgashev, Z. Farkas, J. Frisch, E. Garwin, S. Harvey, H. Hoag, K. Jobe, R.M. Jones, R. Kirby, N. Kroll, F. Le Pimpec, Z. Li, G.A. Loew, J. Lewandowski, R.J. Loewen, D. McCormick, R.H. Miller, C. Nantista, J. Nelson, C.K. Ng, R. Palmer, E. Paterson, C. Pearson, N. Phinny, T. Raubenheimer, M. Ross, R.D. Ruth, T. Smith, S. Tantawi, K. Thompson, P.B. Wilson, **SLAC**. H. Baba, Y. Funahashi, N. Higashi, Y. Higashi, N. Hitomi, H. Kawamata, N. Kudo, T. Kume, H. Matsumoto, Y. Morozumi, J.S. Oh, T. Shintake, K. Takata, T. Takatomi, N. Toge, K. Ueno, Y. Watanabe, **KEK**. T. Arkan, C. Boffo, H. Carter, D. Finley, I. Gonin, T. Khabiboulline, S. Mishra, G. Romanov, N. Solyak, **FNAL**. J. Klingmann, K. van Bibber, **LLNL**. Finally, a special thanks to Chris Adolphsen and Nobu Toge for helping to edit this report.

2.2.13. References

[1] ISG Study Report, KEK-Report 2000-7 and SLAC R-559.

[2] GLC Project Report, KEK-Report-2003-7, also available from http://lcdev.kek.jp/ProjReport/.

[3] J. Wang, et al., Accelerator Structure R&D for Linear Colliders, PAC99, SLAC-REPRINT-1999-155.

[4] C. Adolphsen, et al. Processing studies of X-band accelerator Structures at NLCTA, PAC01, SLAC-PUB-8901.

[5] C. Adolphsen, Normal Conducting RF Structure Test Facilities and Results, PAC03, SLAC-PUB-9906.

[6] Z. Li, et al. Traveling Wave Structure Optimization for the NLC, PAC2001, SLAC-PUB-9049.

[7] Z. Li et al. RDDS Cell Design and Optimization for the Linear Collider Linacs, PAC99, SLAC REPRINT-1999-150.

[8] R. Jones, et al. A Spectral Function Method Applied to the Calculation of the Wake Function for the NLCTA, LINAC96, SLAC-PUB-7287.

[9] C. Adolphsen, et al. Measurement of Wake Field Suppression in a Damped Detuned Accelerator Structure, SLAC-PUB-7519, Phys. Rev. Lett. Vol 27, p2475, 1995.

[10] C. Nantista, et al. Novel Accelerator Structure Couplers, PAC2003, SLAC-PUB-10219.

[11] V. Dolgashev, et al. Status of X-Band Standing Wave Structure Studies at SLAC, PAC03, SLAC-PUB-10124.

[12] R. M. Jones, et al. Optimized Wakefield Suppression and Emittance Dilution Imposed Alignment Tolerances for the JLC/NLC, PAC03, SLAC-PUB-9868.

[13] N. Baboi, et al. Impedance Measurement Setup for Higher Order Mode Studies in NLC Accelerator Structures with Wire Method, LINAC 2002, SLAC-PUB-9472.

[14] Y. Higashi et al., Studies on High-precision Machining of Accelerator Disks of X-band Structure for a Linear Collider, KEK-Report 2000-1, 2000.

[15] T. Higo, et al. “Meeting Tight Frequency Requirement of Rounded Damped Detuned Structure”, Proceedings of the XX International Linac Conference, Monterey, USA, Aug., 2000.

[16] Y. Higashi et al, “Study on High-precision Diffusion Bonding for X-band Accelerator Structure”, KEK-Report 2000-2, 2000.

[17] C-band R&D, http://www-xfel.spring8.or.jp/.

2.3. The Major Issues for CLIC Accelerating and Transfer Structure Development

Walter Wuensch, CERN, Geneva, Switzerland
mail to: walter.wuensch@cern.ch

2.3.1. Introduction

Both main-linac accelerating structures and drive-linac decelerating structures, the latter referred to as 'transfer structures', are being developed by the CLIC study. In order to introduce the transfer structure, which is unique to CLIC, and to motivate the design requirements of both structures, this article begins with a short summary of the ideas that underlie the CLIC machine from the perspective of its two-beam power source and rf structures.

The goal of CLIC is to produce multi-TeV e^+e^- collisions [1] which leads to the three main features which define its accelerators: a very high accelerating gradient, a high rf frequency and a two beam power source. The three features are linked through rf power. The rf power needed to establish an accelerating gradient in a structure of a fixed geometry is proportional to the square of the gradient and inversely proportional the square of the frequency. The optimum parameters found by the CLIC study for a 3 TeV collision energy are a frequency of 30 GHz and an accelerating gradient of 150 MV/m, which results in the requirement of about 150 MW of structure input power. Such a combination of power and frequency is well beyond the performance of any discrete power source, such as a klystron, which has lead to the idea of the two-beam rf power source [2,3].

The two-beam power source can be thought of as an impedance transformer where power is transferred from a low-energy high-current drive beam to the high-energy low-current main, i.e. used for the physics experiment, beam. The power is transferred via 30 GHz rf power which is generated in low-impedance transfer structures by the drive beam and is piped over to high-impedance accelerating structures to accelerate the main beam.

Both types of structures have extremely demanding high-gradient, high-power and wakefield performance requirements. Extensive theoretical, computational and experimental studies and developments have been necessary to progress towards the realization of these structures. The main challenges, their interplay and progress in developing the two structures are summarized in this article.

2.3.2. Accelerating Structures

The accelerating structures are considered first, as most readers will be more familiar with this type of structure. The most striking performance requirement for the accelerating structures is of course the 150 MV/m accelerating gradient – in contrast to 65 MV/m for NLC/GLC and up to 35 MV/m for TESLA. Accelerating gradient in CLIC structures is limited by two physical effects: rf breakdown and pulsed surface heating. Stable electron emission, a.k.a. dark current, does not appear to be a limiting effect.

Two early rf-breakdown tests of structures made by the CLIC study team gave apparently contradictory results, a peak accelerating gradient of 153 MV/m at 11 GHz with a 150 ns pulse was achieved successfully [4] and a peak accelerating gradient of 66 MV/m at 30 GHz with a 15 ns pulse caused spectacular, and unacceptable, damage to the structure [5].

Through extensive experimentation in the CTFII (CLIC Test Facility) and the NLCTA (Next Linear Collider Test Facility), and some thought, the essential difference between the tests has apparently emerged: the 11 GHz structure achieved a much higher

accelerating gradient because it had a much lower a/λ (a is the beam aperture radius and λ is the rf wavelength) than the 30 GHz structure. An explanation, which is neither rigorously proven nor complete, of why a/λ is so important for rf breakdown appears to be a combination of the increased power flow and peak surface electric field that result from increasing a/λ for a fixed accelerating gradient [6,7].

The consequences for linac design are dramatic, however, because of the increase in short-range wakefields caused by a small beam aperture. Short range-wakefields are proportional to a cubed and the geometry of the 11 GHz structure with an a/λ of 0.11, for example, is not usable in a linear collider [8]. Faced with such a stark design compromise between emittance growth and high gradient performance, a major effort is being carried out to find a way to make 150 MV/m feasible for structures with acceptable wakefield characteristics.

The main thrust to raise achievable gradient for a given rf geometry has been to investigate materials other than copper to see if there are any alternatives that support higher gradients and better survive the effects rf breakdowns [9]. The first materials being investigated are tungsten and molybdenum. The motivations behind the choice of these two refractory metals are that extensive melting is observed in the damaged copper structures, so a material with a high melting point and a low vapor pressure is expected to be more resistant to damage. Additionally tungsten and molybdenum are used in a variety of high electric field and high power applications and have a DC conductivity only three time worse than copper.

An experimental investigation of the relative high gradient performances of copper, tungsten and molybdenum has been made in CTFII using three identical geometry, thirty cell, 30 GHz accelerating structures, shown in Fig. 1 [9]. One was made entirely from copper, the second was made from copper cavity walls and tungsten irises and the third was made from copper cavity walls and molybdenum irises. After conditioning with 15 ns pulses (the maximum for CTFII), the copper, tungsten-iris and molybdenum-iris structures achieved peak accelerating gradients of 110, 150 and 193 MV/m respectively, clearly demonstrating the potential of these refractory metals.

Figure 1: Copper, tungsten iris and molybdenum iris 30 GHz accelerating structures.

It bears emphasizing that the CTFII tests were limited, due to the capabilities of the test facility, to an rf pulse length shorter than that required for CLIC. Extension of the CTFII, 30 GHz, 15 ns results out to CLIC-length pulses, 50 ns and above, will begin when CTF3 [10] starts power production in 2004. In order to investigate long pulse behavior sooner, a CLIC-built 11 GHz molybdenum-iris structure has recently been tested in the

NLCTA. The results are still under analysis, however the structure conditioned very slowly and started from a very low value. A limiting gradient was not reached in the testing time available for pulses longer than 30 ns. For shorter pulses the klystron plus pulse compressor ran to its power limit. The slow conditioning speed has inspired a renewed vigor in the investigation of improved material and surface preparation techniques. A dc-spark test stand is being commissioned in order to guide the development of new preparation procedures and materials before making full-blown rf tests, which are expensive, infrequent and often limited in time.

The second major physical effect which limits accelerating gradient is pulsed surface heating [11,12]. Rf induced currents cause a temperature rise, of the order of a few tens of degrees in the case of CLIC, in the structure surface on each pulse of a machine. This temperature rise induces mechanical stresses which, a linear collider is expected to run for decades with a repetition rate of around 100 Hz, if large enough can lead to cracking. Pulsed surface heating is being addressed in two ways: through rf design and the investigation of copper alloys. The effect of rf design on pulsed surface heating is heavily influenced by the features needed for higher-order mode suppression, so this discussion is left until damping has been introduced.

Copper alloys are being investigated to try to find an optimum compromise between reduced electrical and thermal conductivities and increased fatigue strength (the stress level a material can support for a given number of stress-relaxation cycles) [13]. For example, copper zirconium appears to be an excellent candidate for accelerating structures with electrical and thermal conductivities better than 92% of copper and a fatigue strength twice as high as copper.

Tabulated data of fatigue strengths provides a basis for predicting the relative performances of different alloys, but the actual fatigue behavior in an rf structure may be affected by the one-hundred-nanosecond time and ten-micron-distance scales of pulsed surface heating in a CLIC structure. In order to investigate fatigue in such conditions, tests are being made using a pulsed excimer laser, which is an inexpensive and high repetition rate alternative heat source to high-power high-frequency rf. An ultra-sonic fatigue measurement set-up is also being commissioned to make the comparison between short-pulse laser and low-frequency bulk fatigue properties, to extend fatigue data beyond the expected lifetime of a linear collider and to give quick and inexpensive comparisons between materials.

In order to maintain stability of the main-beam bunch train, long-range transverse wakefields in the accelerating structures must be suppressed by a factor of about 100, to a level below 20 V/(pC mm m), in the interval between bunches. It is crucial to minimize this interval, in order to allow a higher current and consequently a higher rf-to-beam efficiency. A combination of strong damping and detuning are used for the higher order mode suppression in CLIC accelerating structures. A successful experimental demonstration of an early design of a heavily damped and detuned accelerating structure and a verification of the tools developed to compute the wakes was made in ASSET [14]. Damping features however generally result in localized concentrations of magnetic fields which increase pulsed surface heating and thus reduce achievable accelerating gradient [15]. Providing maximum damping for minimum field concentration is a central design challenge for the CLIC accelerating structures.

The damping topology that has been adopted for the most recent evolution of the structure uses both iris slots and radial damping waveguides to reduce dipole mode Q's to the order of 10. Surface electric and surface magnetic field increases caused by the damping features are limited to below 10% by profiling the transverse cross-sections of the iris and the outer cell wall. The resulting geometry, dubbed the HDS (Hybrid Damped

Structure) is shown in Fig. 2 [16]. The structure must be milled but consists of (basically) only four parts which have no current carrying contacts when assembled. Detailed designs of power couplers and damping loads must still be made, but are not expected to produce any fundamental challenges.

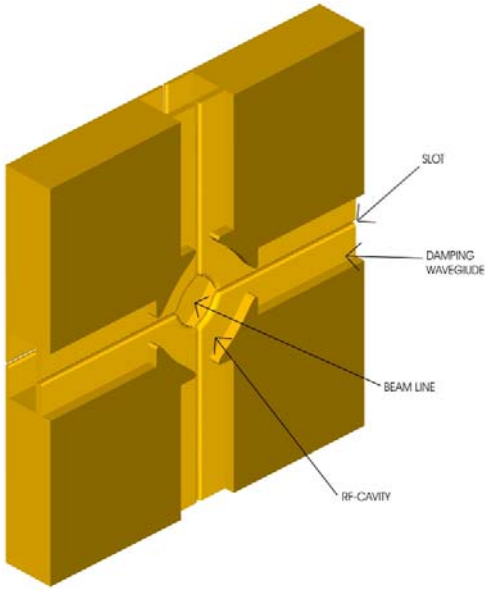

Figure 2: The HDS geometry.

When high-gradient and efficiency effects are all considered together, the full structure design can be optimized. In this step damping, detuning, time dependencies of rf breakdown and pulsed surface heating (both of which appear to have a square root of time dependence [7,11]), rf to beam efficiency and a/λ dependencies of rf breakdown and single bunch emittance growth are balanced. This optimization procedure [16] is now being refined and a new reference structure design is being produced to be used in the ongoing evolution of the CLIC machine design.

2.3.3. Transfer Structures

Each transfer structure must extract an rf power of the order of 560 MW from the 300 GW, 150 A drive beam [17]. The structure must extract power efficiently, survive the effects of very high powers and have wakefield characteristics consistent with stably transporting the high current drive beam through 600 m of decelerating linac. The beam dynamics of the drive linac is complicated by adiabatic damping that is working in the difficult direction as the beam energy drops from 2 GeV down to about 250 MeV. Very generally, these requirements result in periodically loaded traveling wave structures with a very large beam aperture and with strong long-range transverse wakefield damping. The transfer and accelerating structure share many features but the large aperture of the former is the main source of its specific design challenges.

The transfer structure must have fundamental mode R/Q of about 240 Ω and a short-range transverse wakefield of less than 1.5 V/(pC mm m). Such parameters can be achieved with a structure that is best viewed as an over-moded circular waveguide with just enough periodic loading to give a weak coupling to the drive beam. The a/λ is 1.25 and the periodic loading is sinusoidal with a depth of 1.2 mm, which results in a v_g/c of 85% and a length of 1 m [18].

Despite the very low transverse impedance of the large aperture structure, the long range transverse wakefield must be damped with a Q below 50. The large aperture introduces two main challenges to achieving such a low Q. Firstly, both fundamental and dipole mode group velocities are near c, which means that both modes have nearly the same synchronous frequencies. Consequently cut-off waveguide damping and detuning are not possible - slot type damping alone is used. Secondly, the large aperture makes the coupling of the dipole mode to the damping slots weak because surface currents are low. Eight damping slots are needed to achieve a low enough Q. The slots are terminated with long slabs of a lossy dielectric such as silicon carbide. Surface electric field enhancement at the edge of the slots is limited by profiling the iris's transverse cross section, analogously to the accelerating structure. However, since surface fields are lower in the transfer structure than in the accelerating structure, a simple straight line cross-section with circularly rounded edges is sufficient. The optimized rf geometry is shown in Fig. 3.

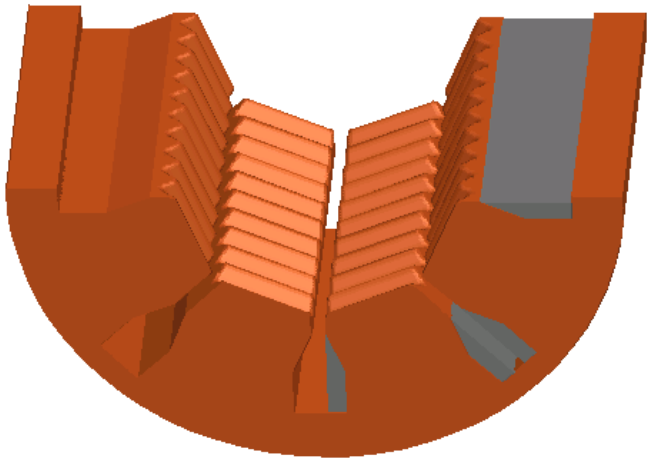

Figure 3: The transfer structure geometry (half).

The output power coupler is another rf design challenge caused by the large aperture - power must be extracted with high efficiency, of the order of 99%, from an over-moded waveguide 2.5 wavelengths in diameter. The challenge is elevated because the coupler must also be short, not create any significant longitudinal or transverse impedances and not have any significant surface field enhancements. The current power-coupler design [19] uses quasi-optical design principles and is shown in Fig. 4.

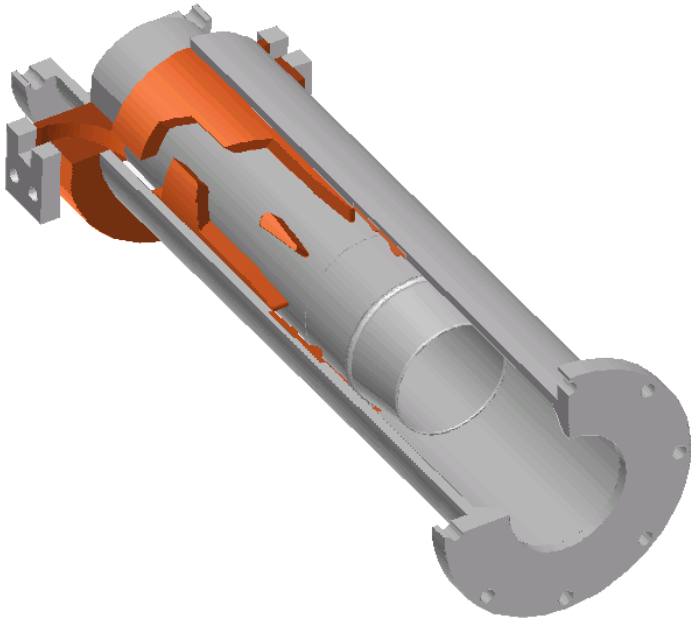

Figure 4: Segmented view of the output power coupler of the transfer structure.

Test transfer structures have been constructed and successfully tested to an output power of over 200 MW (15 ns pulse length) in CTFII. However, these structures had small, 15 mm, beam apertures to give an increased coupling to the available beam, and consequently did not address some of the most critical issues. Thus the high-power performance of the CLIC transfer structure is not yet known, but will be directly tested in the later stages of CTF3 operation when a sufficiently high current drive beam becomes available. In the mean time, the expected high power behavior of the transfer structure is being based on extrapolation of small aperture transfer structure and accelerating structure data. Because of its high group velocity, the transfer structure naturally has low surface fields with peak surface electric field of 96 MV/m and a peak surface magnetic field of 0.15 MA/m for 560 MW power. The surface fields are low compared to accelerating structures, and are well within the currently understood physical limits. On the other hand, the total power flow in the structure is extremely high, four accelerating structures designed to be at the power limit are fed with each transfer structure [17]. The power flow in the transfer structure is however split into eight distinct regions and consequently breakdown arcs will probably be fed by only a fraction of the total power flowing in the structure. This should reduce the potential for damage, but the supposition must be experimentally verified.

Also unknown are the extent to which the transfer structures will need to be conditioned, if they can be pre-conditioned, how hundreds can be simultaneously conditioned with a single drive beam and the probability of structure failure during extended operation. Although the tests of these issues are some years away, the large fraction of the technological developments being made for the accelerating structures will be relevant for solving these issues if they turn out to be problems. The predicament encountered by the failure of a single transfer structure, because of uncontrollable breakdown for example, when hundreds of structures are driven by a single beam, is unique to the two-beam scheme. A system to interrupt power production in an individual structure, ‘on/off capability’, by detuning with ‘knives’ inserted into a transfer structure through four of the damping slots is now being developed [21].

2.3.4. References

[1] J. Ellis, I. Wilson, “Physics With the Compact Linear Collider”, Nature, Volume 409, 18 January 2001.
[1] A. M. Sessler, LBL-25760 (1988).
[3] W. Schnell, “Consideration of a Two-Beam Twin RF Scheme for Powering an Rf Linear Collider”, CLIC Note 7 (1985).
[4] J.W. Wang, G.A. Loew, R.J. Loewen, R.S. Ruth, A.E. Vlieks, I. Wilson, W. Wuensch, “SLAC/CERN High Gradient Tests of an X-Band Accelerating Section”, CERN/SL 95-27, Proc. PAC95.
[5] H. H. Braun, S. Döbert, L. Groening, I. Wilson, W. Wuensch, “Status of CLIC High Gradient Studies”, CERN/PS 2001-045 (RF), Proc. PAC2001.
[6] W. Wuensch, “High-Gradient Breakdown in Normal-Conducting Cavities”, CERN/PS 2002-28, Proc. EPAC2002.
[7] V. Dolgashev, “Particle-in-Cell Modeling of Rf Breakdown in Accelerating Structures and Waveguides”, http://www.mice.iit.edu/rfworkshop/.
[8] D. Schulte, “Luminosity Limitations at the Multi-TeV Linear Collider Energy Frontier”,
CERN/PS 2002-054 (AE), Proc. EPAC2002.
[9] W. Wuensch, C. Achard, S. Döbert, H. H. Braun, I. Syratchev, M. Taborelli, I. Wilson, "A Demonstration of High Gradient Acceleration", CERN-AB-2003-048-RF; CLIC-Note-569, Proc. PAC2003.
[10] R. Corsini, “An Overview of the New CLIC Test Facility (CTF3)”, CERN/PS 2001-030 (AE), Proc. PAC 2001.
[11] I. Wilson, “Surface Heating of the CLIC Main Linac Structure”, CLIC note 52, 1987.
[12] D. P. Pritzkau and R. H. Seimann, “Experimental Study of rf Pulsed Heating on Oxygen Free Electronic Copper”, Phys. Rev. ST Accel. Beams, vol. 5, 112002, 2002.
[13] S. Heikkinen, http://clic-meeting.web.cern.ch/clic-meeting/2003/06_26sh.pdf.
[14] I. Wilson, W. Wuensch, C. Achard, M. Dehler, E. Jensen, M. Luong, C. Adolphsen, M. Ross, T. Slaton, D. McCormick, “An ASSET Test of the CLIC Accelerating Structure”, CERN/PS2000-044, Proc. EPAC2002.
[15] J.-Y. Raguin, I. Wilson, W. Wuensch, "Progress in the Design of a Damped and Tapered Accelerating Structure for CLIC", CERN-AB-2003-045-RF, CLIC-Note-567, Proc. PAC2003.
[16] A. Grudiev, http://clic-meeting.web.cern.ch/clic-meeting/2003/10_03ag.pdf
[17] G. Guignard editor, “A 3 TeV e+e- Linear Collider Based on CLIC Technology”, CERN 2000-008.
[18] I. Syratchev, “Circularly Symmetric PETS Status”, 9th International Workshop on Linear Colliders (LC-2002), Stanford, CA, USA, 2002.
[19] I. Syratchev, “Efficient RF Power Extraction from the CLIC Power Extraction and Transfer Structure (PETS)”, CLIC note 571, 2003.
[20] I. Syratchev, private communication.

3. Reports from ICFA Panel on Advanced and Novel Accelerators

3.1. Optical-Accelerator Experiments at Berkeley Lab

Wim Leemans
l'OASIS Group
Lawrence Berkeley National Labs
mail to: wpleemans@lbl.gov

3.1.1. Introduction

Laser-driven, plasma-based accelerators [1] hold the potential of becoming compact alternatives to conventional radio-frequency-based linear accelerators (linacs). Accelerating gradients in the 10's to 100's GV/m have been measured in many laser wakefield accelerator (LWFA) experiments around the world, [2-4] which is three orders of magnitude higher than in conventional linacs. Acceleration of electron bunches containing several nC of charge and energy spectra characterized by a Boltzmann-like distribution with an equivalent temperature ranging from the few MeV to tens of MeV has been demonstrated in the self-modulated regime of the LWFA. Recently, experiments have measured electrons with energies above 200 MeV. [4] Through measurement of the coherent radiation emitted by the laser accelerated beams, indications have been obtained that the bunches are shorter than 50 fs in duration. [5] The next steps in the development of a laser based accelerator are aimed at increasing the quality of the beams. Although electron beams originating from micron sized spots have been observed with divergences that are substantially less than 1˚, the energy spread has been 100 %. Methods are being explored by several groups around the world to enhance the level of control over the injection or trapping process of electrons in the plasma wakes. Recent progress towards the development of a laser accelerator at LBNL are discussed next.

Optical accelerator experiments are ongoing within the l'OASIS Group (Laser Optics and Accelerator Systems Integrated Studies) of LBNL's Center for Beam Physics centered around the development of a 1 GeV laser driven accelerator. The current experimental and theoretical program consists of three parts: (i) guiding of high intensity laser beams (10^{18} W/cm^2) over macroscopic distances (1- 10 cm scale length) in a plasma channel, (ii) study of an all-optical injector via laser triggered injection of electrons in a plasma structure, and (iii) development of beam diagnostics with femtosecond resolution for measurement of the beam's phase space properties.

The experiments are done at the l'OASIS facility which houses a multi-terawatt Ti:sapphire laser system that can deliver five different beams to the target. One beam has peak power up to 10 TW in 50 fs, two of the beams have peak power at the 3 TW level, one beam contains up to 250 mJ in 200 ps and the fifth beam is a frequency doubled (blue, 400 nm) probe beam. A sixth beam is under construction and will deliver up to 100 TW peak power in a 40 fs duration pulse. All pulses are derived from a single oscillator pulse and hence are intrinsically synchronized, limited by path length variations. The facility has been equipped with a radiation shielded experimental cave and radiation interlock system, as well as a remote control room, allowing operation at high repetition rates while producing significant radiation doses.

The current target chamber allows the use of up to five laser beams: a nominally 50 fs pre-ionizing laser beam, a nominally 250 ps plasma heating beam, (3) a nominally 50 fs

main drive beam, a nominally 50 fs colliding laser beam and 70 fs frequency doubled probe beam. The lay-out is shown in Fig. 1.

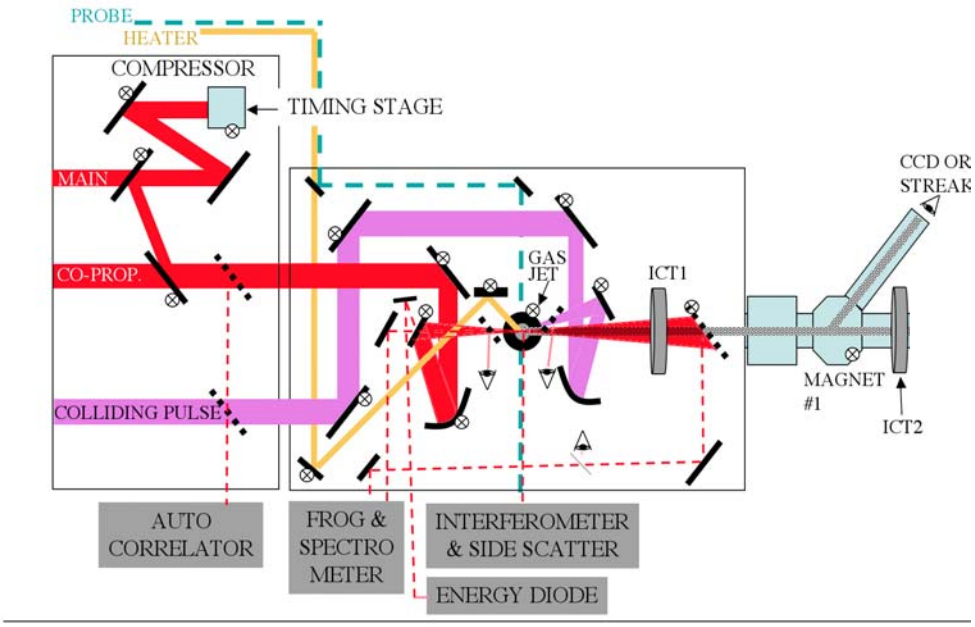

Figure1: Lay-out of the multi-beam experiments. The pre-ionizing and drive beam (10 TW, 50 fs, 10 Hz) are in red. The colliding pulse beam path is shown in purple and the heater beam for channel production and blue probe beam are shown in orange and dashed blue, respectively.

The theory and computational efforts of the Group are focused on new concepts and analysis of ongoing experiments at the l'OASIS Laboratory and significant progress has been made in developing analytic and computational tools (e.g. fluid codes) for prediction and analysis. To further extend our capabilities, a collaborative effort (part of a SciDAC program, between CBP researchers, the University of Colorado, Tech-X Corporation and our group) has continued on the use of particle-in-cell (PIC) codes for self-consistent modeling of the laser-plasma interactions, including particle trapping and acceleration.

Recent results on controlling the electron yield in a laser driven accelerator, generation of coherent infrared radiation from laser accelerated electron bunches and radio-isotope production are discussed next as well as a brief overview of the current status of laser guiding and injection experiments.

3.1.2. Electron yield control via the use of shaped laser pulses

Controlling and optimizing the coupling of laser light to plasma waves is important in numerous applications. The first experimental demonstration of laser pulse shape effects on the electron yield in a laser driven accelerator was recently shown. [3] The experiments were carried out using the l'OASIS laser system with non-linearly chirped laser pulses. Laser pulses from the l'OASIS amplifier chain were compressed in a vacuum compressor by changing the distance between the gratings. On one side of the compressor zero (distance for which the minimum pulse duration is achieved), pulses were generated having positive chirp (red color in front) and on the other side they had negative chirp (blue in front). By tuning the angle of the gratings, non-linear chirp was present in the

compressed pulses. The dominant effect of non-linear chirp is to cause pulse shape asymmetries with fast rises and slow fall times on one side of the compressor zero position and vice versa on the other side. [6] For the same sign of the chirp, pulses with fast or slow rise times can be generated through careful angle tuning of the gratings. If the rise time of the pulse is close to the plasma period, and the pulse duration is several plasma periods long, plasma density waves can be excited underneath the main pulse. Pulses with a slow rise time and sharp fall time will not generate a significant wake underneath but only behind the laser pulse. In the former case, as this pulse propagates through the plasma, the Raman forward instability can grow from this seeded wave and reach amplitudes earlier than for the latter case that are sufficiently large for particle trapping. [7] This in turn can then result in larger electron yield as was observed in the experiments. Figure 2 shows the electron yield vs compressor setting, indicating that for the experimental settings, the shortest pulse did not result in the highest electron yield.

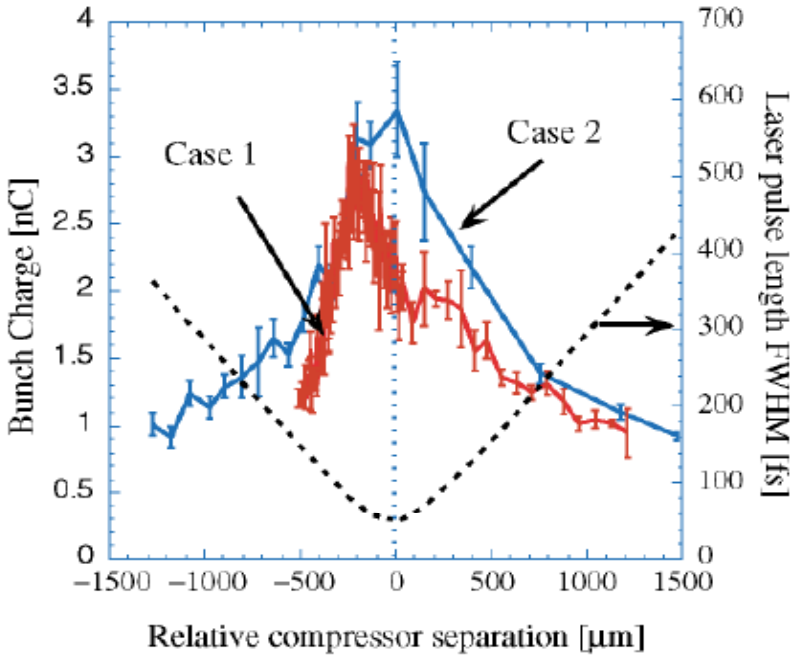

Figure 2: Electron yield (color) for two cases and pulse duration (dashed) vs. compressor separation. In Case 1, the laser pulses were focused on the low density edge of the gas jet. In case 2, the laser pulses were focused on the high density edge. The laser pulse shape had a fast (slow) rise time on the left (right) hand side of the compressor zero. When focusing on the low density edge, a clear asymmetry in electron yield was observed: fast rise time pulses showed a larger electron yield than slow rise time pulses.[3]

Measurement of the pulse shape using a frequency resolved optical gating system showed that the highest electron yield was obtained for pulses with a fast rise time, regardless of the chirp sign. [3,6] Modeling of the self-modulated and Raman forward scattering laser instabilities in the presence of laser chirp supports the experimental observation that laser pulse shape is much more important in practical parameter regimes than laser chirp. [7]

3.1.3. Observation of coherent THz radiation emitted via transition radiation from laser accelerated electron bunches crossing the plasma-vacuum boundary

For nearly a decade, the l'OASIS group has devoted significant effort to the development of advanced beam diagnostics that are capable of measuring the properties of electron beams in both transverse and longitudinal phase space. A detailed overview was written of the various diagnostic techniques that we have developed, and the physics behind them. [8] Some of the novel diagnostics discussed in the article have the potential to resolve fs-bunches.

Recently we have studied the generation of coherent radiation from the electron bunches as they exit the plasma, both as a radiation source and as a diagnostic for measuring the electron bunch properties. The interest in using these bunches for generation of coherent radiation is motivated by two components: (1) extremely dense, sub-ps electron bunches produced with a compact laser-plasma accelerator and (2) the production of coherent transition radiation by these bunches at the boundary between a plasma and vacuum. [9,10] Modeling of the performance of this source indicates that it has the potential for generating up to tens of mJ per pulse, which is several orders of magnitude beyond that of conventional THz radiation sources. Laser-triggered solid-state based sources of THz radiation have been developed that rely on switched photoconducting antennas (e.g., Ref. [11] and references therein) or optical rectification of femtosecond pulse trains. [12] Large aperture biased GaAs structures, operated at 1~kHz repetition rate, have produced on the order of 0.5~μJ/pulse. [13] Most other sources using either laser switched structures or optical rectification have operated at high frequency (10's of MHz) with μW--mW level average power. Our recent experiments have measured coherent radiation with energies near the 100 nJ/pulse level. The measured energy was limited primarily by the small collection angle (~ 100 mrad) and the small transverse size (~ 100 μm) of the plasma. [10] Modeling indicates that by increasing the collection angle, the plasma transverse size and the electron beam energy, energies as high as 100 μJ/pulse are achievable.

Measurements of the emitted radiation were conducted in several frequency ranges. A heterodyne detection system was used to measure radiation at 94.3 GHz and a bolometer covered the 0.3-30 THz range. The origin of the radiation emitted by the laser accelerated electrons was found to be consistent with a diffraction limited transition radiation process by the dense ultrashort electron bunches, when they exit the plasma into vacuum. [9,10] The radiated energy was found to scale quadratically with electron beam charge, consistent with a coherent emission process (see Figure 3). The polarization of the radiation was measured by placing a polarizing wire mesh in front of the bolometer, and found to be independent on rotation angle of the polarizer, consistent with radial polarization of transition radiation. The radiated energy was measured using two different collection angles and the results agreed reasonably well with theoretical predictions. We also fielded a bolometer and, with the use of a long pass filter, were able to obtain the first measurements of bunch duration of a laser accelerated electron bunch. The measurements were found to be consistent with an electron bunch duration of less than 50 fs and a plasma radius of 100 micron. [5]

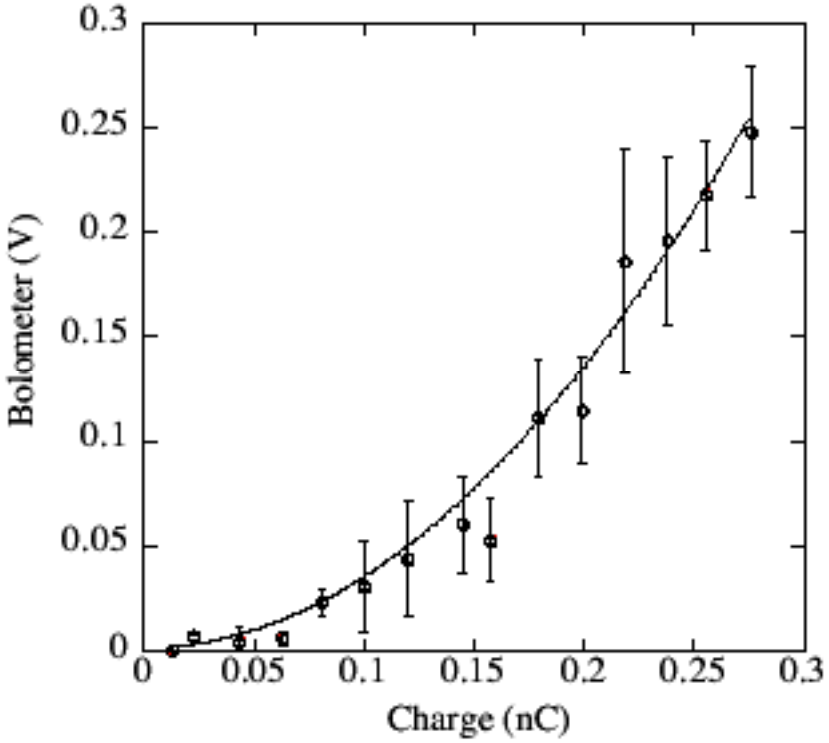

Figure 3: Bolometer voltage vs. charge per bunch for an 80-300 mrad collection half-angle. [5,9] Each dot represents an average of 50 experimental shots, with rms variation as error bar. The bolometer voltage is directly proportional to the collected energy. The solid line is a quadratic fit to the data, indicating coherence of the radiated signal.

3.1.4. Radio-isotope production using laser accelerated electron bunches

Experiments studying the production of radio-isotopes using laser driven accelerators have also being done at LBNL. In single beam experiments, isotopes were produced in several materials via (γ,n) reactions. [14] Bremsstrahlung radiation was produced by stopping the electron beams in a lead or tungsten plate. The gamma-rays then impinged on either a copper or Teflon target. Although most electrons had energies less than 5 MeV, a significant fraction of the electrons had energy above 15 MeV. Using on-line γ-ray and neutron detection, the accelerator was optimized and utilized for activation of Pb/Cu targets and W/Teflon. Several isotopes such as ^{62}Cu, ^{61}Cu were produced using (γ,n) reactions in ^{63}Cu and ^{11}C and ^{18}F was produced in the Teflon target. For the relatively short activation times, the accumulated activity was on the order of 1-10 μCi, consistent with simulation results from a nuclear physics Monte-Carlo code that used the measured electron energy distribution as input.

Methods for enhancing the activation yield have been studied theoretically and rely on post-acceleration of the electron beam produced in a single stage self-modulated laser wakefield accelerator, using a channel guided laser wakefield accelerator. [15] Such experiment is now possible using the recently implemented ignitor-heater system for producing preformed plasma channels (see Section 5).

3.1.5. Laser guiding in preformed plasma channels at relativistic intensities

To reach multi-GeV beam energies with laser driven accelerators will require laser guiding to extend the distance over which the large accelerating gradients can be

generated. Guiding concepts relying on the use of preformed channels are being studied by several groups around the world including the University of Maryland, University of Texas, UCLA, Naval Research Laboratory, Ecole Polytechnique, University of Tokyo and others. Some of the research is described in the contributions in this Newsletter by correspondents from those institutions. At LBNL, using the ignitor-heater concept [16], we have recently produced plasma channels and guided to our knowledge the highest peak power to-date in a preformed plasma channel. Pulses were guided over distances on the order of 2.5 –3 mm (15-20 Rayleigh ranges) with an output intensity exceeding $3x10^{18}$ W/cm^2. [17] Figure 4 shows the input mode profile and the exit mode profiles without and with guiding turned on.

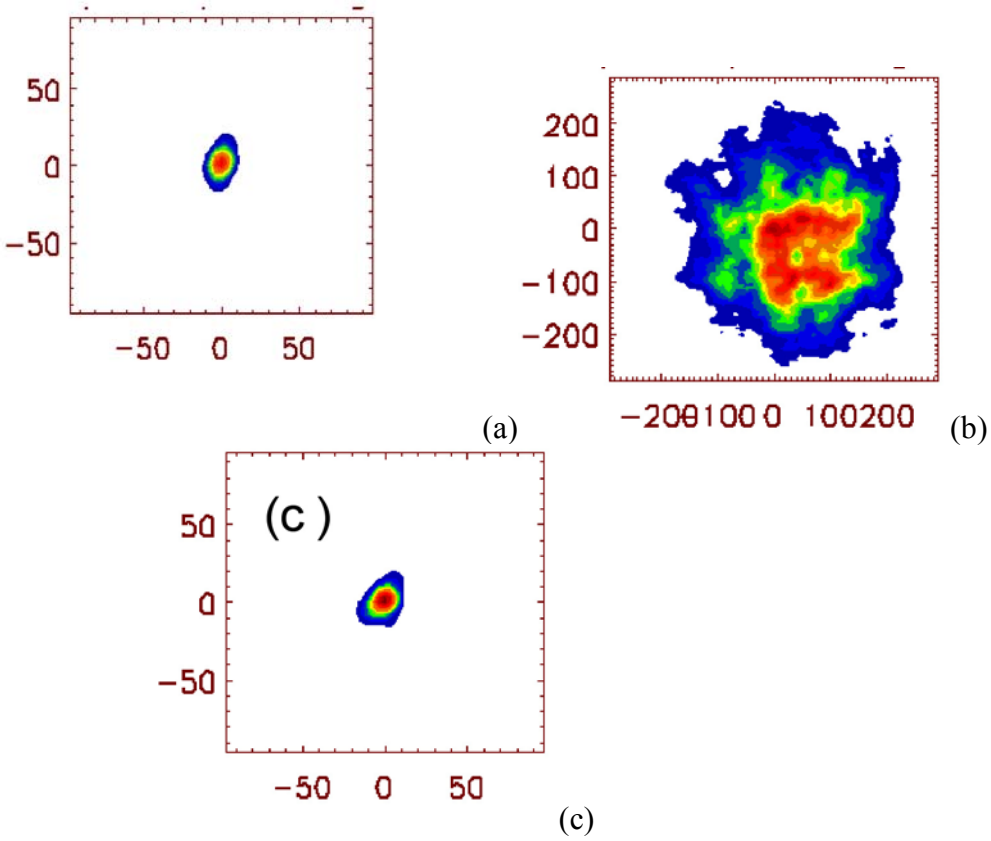

Figure 4: (a) Input mode and exit modes without (b) and with (c) a preformed plasma channel. The injected intensity was on the order of $7x10^{18}$ W/cm^2 and the exit intensity was > 10^{18} W/cm^2. The channel length was > 2.5 mm, equivalent to > 15 Rayleigh lengths[17] (Units in fingures are all in μm) .

At the present time, acceleration experiments are being carried out with these channels in an effort to increase the electron beam energy by extending the acceleration distance. Preliminary results from magnetic spectrometer measurements indicate that a substantial number of electrons has been accelerated to multi 10's of MeV's, consistent with the observed large increase in the neutron yield over previous single beam experiments.

3.1.6. Colliding pulse injection experiments

One of the most actively studied ways of reducing electron beam energy in laser accelerators is the use of laser triggered trapping techniques. [18-20] As a first step towards implementing the "colliding pulse" optical injection method, a second laser pulse

was injected into a plasma intersecting the driving laser pulse at an angle of 150˚. Preliminary results indicate that the electron yield is affected and detailed studies of the electron beam spectrum are in progress. The colliding pulse injection method is expected to produce low emittance (1 π mm-mrad), low energy spread (1%), 40 MeV femtosecond electron bunches containing $>10^7$ electrons per bunch. [21] Combining this injector with 5-10 cm long plasma channels will be attempted for a 1 GeV module using the new 100 TW, 10 Hz laser system (Fig. 5).

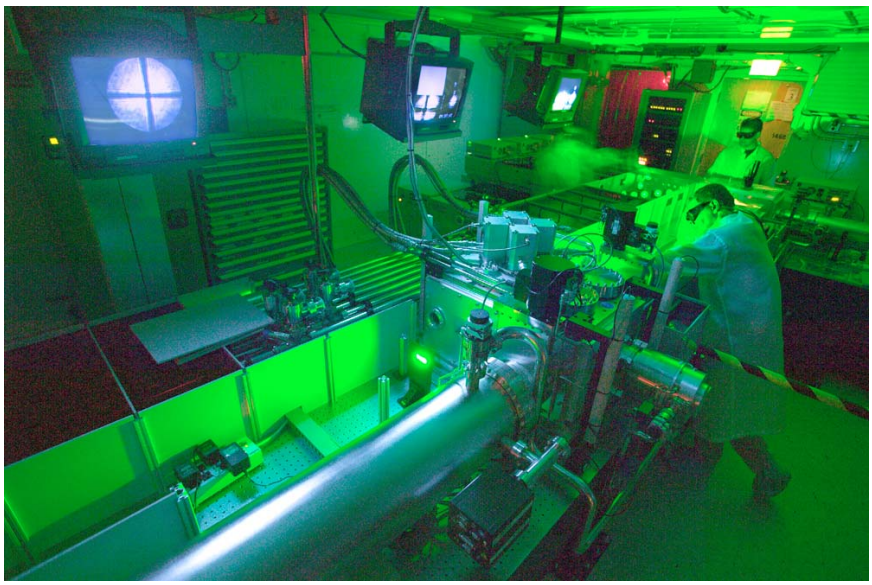

Figure 5: Photograph of the main amplifier for the 100 TW, 10 Hz upgrade of the Ti:sapphire laser system being commissioned at the l'OASIS laboratory. The green glow is from 532 nm radiation produced by the frequency doubled Nd:YAG pump lasers. The laser will be the main power source for the all-optical 1 GeV laser driven accelerator experiments at LBNL.

This work was done with support from the Department of Energy, High Energy Physics under contract DE-AC03-76SF0098. Support for C.G.R. Geddes, who is a graduate student on this project, from the Hertz Foundation is also acknowledged.

3.1.7. References

1. E.H. Esarey et al., IEEE Trans. Plasma Science 24, 252 (1996).
2. A. Modena et al., Nature **377**, 606 (1995); R. Wagner et al., Phys. Rev. Lett. **78**, 3125 (1997); A. Ting et al., Phys. Plasmas **4**, 1889 (1997); C. Gahn et al., Phys. Rev. Lett. **83**, 4772 (1999); X. Wang et al., Phys. Rev. Lett. **84**, 5324 (2000); M. I. K. Santala et al., Phys. Rev. Lett. **86**, 1227 (2001).
3. W. P. Leemans et al., Phys. Rev. Lett. **89**, 4802 (2002).
4. V. Malka et al., Science 298, 1596 (2002); K. Krushelnick, 2003, private communication.
5. W.P. Leemans et al., Phys. Plasmas, in print (2004).
6. C. Toth et al., Optics Letters **28**, 1823-5 (2003).
7. C.B. Schroeder et al., Phys. Plasmas **10**, 285-295 (2003).
8. P. Catravas et al., Phys. Plasmas **9**, 2428 (2002).
9. W. P. Leemans et al., Phys. Rev. Lett. **91**, 074802 (2003).
10. C.B. Schroeder et al., Phys. Rev. E **69**, 016501 (2004).

11. A. S. Weling et al., Appl. Phys. Lett. **64**, 137 (1994).
12. X.-C. Zhang et al., Appl. Phys. Lett. **56**, 1011 (1990).
13. E. Budiarto et al., IEEE J. Quantum Electron. **32**, 1839 (1996).
14. W.P. Leemans et al., Phys. Plasmas **8**, 2510 (2001)
15. A.J.W. Reitsma et al., Phys. Rev. Special Topics Accel. Beams ***5*,** 051302 (2002).
16. P. Volfbeyn et al., Phys. Plasmas **6**,2269-2277 (1999).
17. C.G.R. Geddes et al., in preparation.
18. D. Umstadter et al., Phys. Rev. Lett. **76**, 2073 (1996).
19. E. Esarey et al., Phys. Rev. Lett. **79**, 2682 (1997).
20. C.B. Schroeder et al., Phys. Rev. E **58**, 6037 (1999).
21. C. Moore et al., Phys. Plasmas **8**, 2481 (2001).

3.1.8. Current Staff of l'OASIS Group

- Leemans, W.P. Group Leader
- Esarey, E. Deputy Group Leader
- Toth, C. Staff Scientist
- Schroeder, C. Staff Scientist
- Nagler, B. Postdoc, Fulbright Fellow
- Saleh, N. Postdoc
- Shadwick, B.A. Scientist, part time

3.1.9. Current Graduate Students

- G. Fubiani, Ph.D., University of Paris, France, in progress
- C. G.R. Geddes, Ph.D., University of California, Berkeley, in progress.
- K. Nakamura, Ph.D., University of Tokyo, in progress
  J. van Tilborg, Ph.D., Technische Universiteit Eindhoven, the Netherlands, in progress.

3.1.10. Contact Information

Wim Leemans
Ernest Orlando Lawrence Berkeley National Laboratory
1 Cyclotron Road, MS 71-259
Berkeley, California 94720
PHONE: 510/486-7788
FAX: 510/486-7981
E-MAIL: wpleemans@lbl.gov
WEBSITE: http://bc1.lbl.gov/CBP_pages/LOASIS/

3.2. Basic Beam Physics in Plasma Wakefield Acceleration

Chan Joshi, *University of California, Los Angeles*

mail to:joshi@ee.ucla.edu

Plasma Wakefield Acceleration (PWFA)[1] is one of the most vigorously pursued advanced acceleration scheme at this time. In this scheme the high-gradient wakefield is driven by an intense, high-energy charged particle beam as it passes through the plasma.

In the case of an electron beam the space-charge of the bunch blows out the plasma electrons which rush back in and overshoot setting up a plasma oscillation (See Fig. 1). A second, appropriately phased accelerating beam, containing fewer particles than the drive beam, can now be accelerated by the wake. Both electron and positron beams can be used to drive plasma wakes. In the case of a positron beam the plasma electrons are "pulled in" instead of being expelled as in the case of an electron beam driver. The PWFA scheme is very attractive because of its potential to double the beam energy of a high energy accelerator beam in a single stage of acceleration that is only tens of meters long using existing state-of-the-art driver beams.

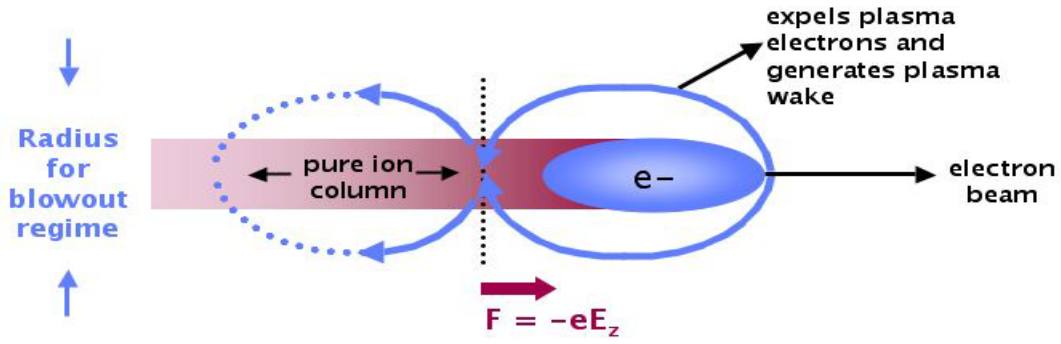

Figure 1. Physical principle of a Plasma Wakefield Accelerator.

Experimental research on PWFA has been going on at Argonne National Lab,[2] Fermi National Lab,[3] KEK (Japan)[4] and more recently at Brookhaven National Laboratory.[5] Using relatively low energy drive beams, researchers at these facilities were able to demonstrate proof-of-principle PWFA. In contrast, a collaboration of scientists from SLAC, USC and UCLA are systematically addressing the relevant physics issues in PWFA in order to realize a prototype of a meter-scale, high-gradient plasma wakefield acceleration stage.[6] In a series of experiments at the Final Focus Test Beam (FFTB) that use the 28.5 GeV electron and positron drive beams from the Stanford Linear Accelerator Center, these researchers have quantitatively elucidated basic beam physics phenomena that determine the transport of such beams through a meter-scale column of plasma and energy loss/gain, to/from the plasma wakefield.

Beam Transport Through Meter-Scale Plasma Columns

In this series of experiments (SLAC experiments E157, E162, E164 and 164X (approved)) the drive beam density typically exceeds the plasma density. Therefore, as the electron beam enters the plasma, the head of the beam blows out all the plasma electrons and produces a pure ion column. The ion column in turn exerts a significant focusing force on the bulk of the beam causing its transverse spot size to oscillate as the beam propagates through the plasma.[7] If a "matched " beam is injected into the plasma, i.e., if the emittance-driven beam expansion is exactly compensated by the ion column focusing force, the beam propagates without transverse size variations along the plasma. Both of these effects were clearly observable in SLAC experiments[8]. When the beam was viewed on a screen placed approximately 1 meter downstream from the plasma the spot size of an unmatched beam oscillated as the plasma density was increased (see Fig. 2(a)). In addition to these "betatron" oscillations, the center of mass of the beam can oscillate about its equilibrium position at exactly half of this frequency if the beam has a finite head-to-tail tilt.[9] Such beam tilts are produced by self-wakefield effects in the linac itself. These

oscillations were also observable in the experiments (see Fig. 2(b)). As individual beam particles oscillate they emit synchrotron radiation. At a plasma density of ~ 10^{14} electrons cm^{-3}, the synchrotron radiation is emitted in a relatively narrow cone of angles in the forward direction with photon energies of ~ 10 KeV.[10] (see Fig. 3). At plasma densities greater than $10^{16} e^{-} cm^{-3}$ a significant number of photons are expected to be emitted with energies greater than 10 MeV, well above the positron production threshold.

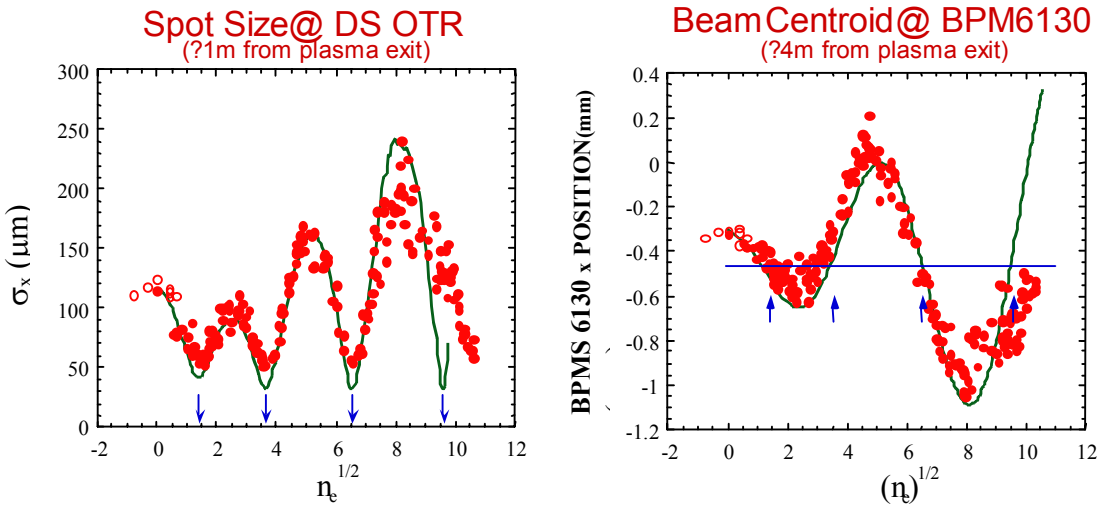

Figure 2. (a) The observed variation of the spot size σ_x of the beam, and (b) the oscillation of the beam centroid as measured by a beam position monitor (BPM) as a function of the square root of the plasma density. (Refs. 7 and 9). The dots are data and the continuous curves are theory.

In the case of a positron beam the plasma wakefield is more coherent (and therefore the acceleration is enhanced) if the drive beam is propagated in a plasma channel. A plasma channel has either no, or a very low density plasma inside the channel up to a few beam radii. Such meter long, weakly ionized plasma channels were created using photo-ionized plasmas. The channel was shown to retain its radial density depression for several hundred nanoseconds because plasma diffusion was strongly inhibited by electron-neutral collisions. The positron beam was shown to propagate more stably through such a channel compared to its propagation through a uniform plasma.[11]

Energy Exchange Between Beam Particles and Wakefield

As the drive beam expels the plasma electron it does work, and thus must lose energy. However, if the drive beam is sufficiently long, or the plasma density sufficiently high, the bulk of the particles lose energy while particles in the back of the beam can actually be accelerated as the expelled plasma electrons rush in and the longitudinal wakefield changes sign.

In the initial experiments performed at SLAC both the electron and positron drive bunches were approximately 4 ps long with a peak current of about 1kA. When such electron bunches were passed through a 1.4 m long lithium plasma of density ~ 1.5 x 10^{14} cm^{-3}, the center slice of the Gaussian beam was seen to lose ~ 150 MeV energy while particles in the back of the beam gained ~ 250 MeV.[8]

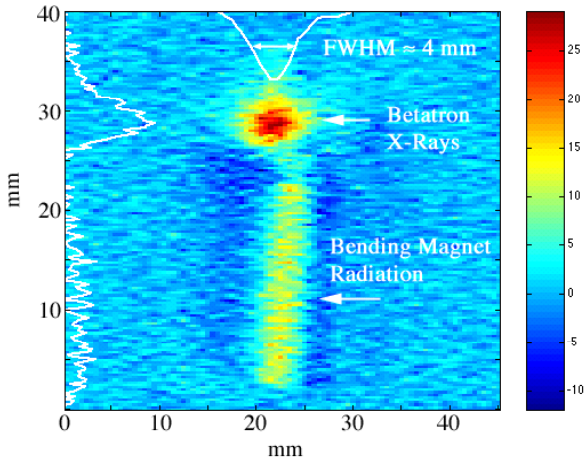

Figure 3. Emission of betatron x-rays from spot size oscillations of the beam.(Ref. 10)

For plasma waves that are not too large a plasma wakefield accelerates positrons in much the same way as it does electrons except, of course, that the positrons are carried along on the opposite phase of the plasma wave. For strongly driven plasma waves, however the wakes produced by an otherwise identical positron beam tend to be somewhat smaller than those produced by an electron beam because of phase-mixing of plasma electrons that are pulled in from different radii by the positron beam.

Figure 4 compares the energy change of the positron beam observed in SLAC experiments with simulation results. The bulk of the beam loses about 55 MeV energy while the particles in its tail gain a maximum energy of 80 MeV. The observed acceleration gradients were in excellent agreement with the predictions of plasma wakefield theory and self consistent 3D particle in cell simulations. These results represent the first high-gradient acceleration of positrons using collective plasma fields.[12]

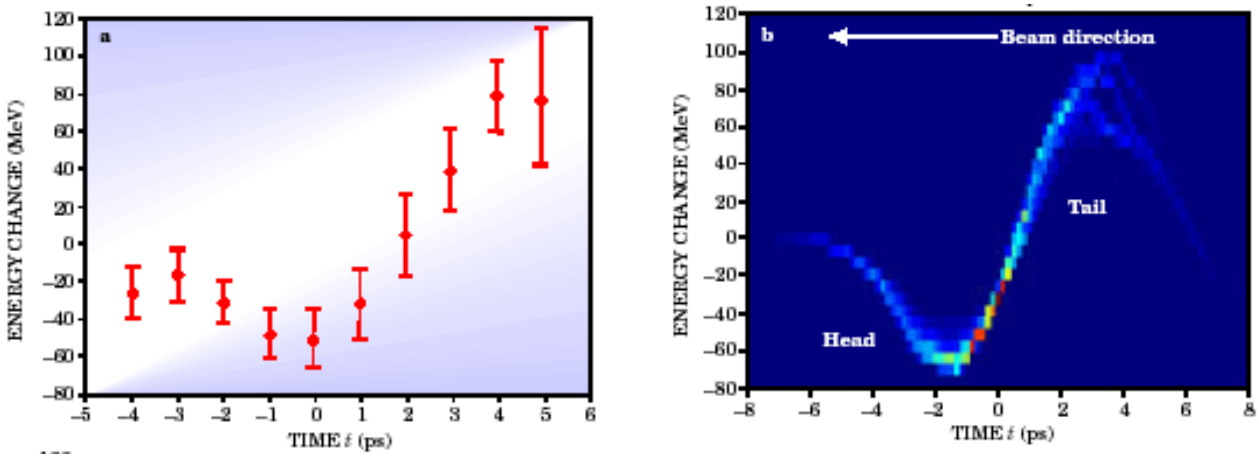

Figure 4. The experimentally measured and predicted energy change experienced by different time slices of a positron beam showing energy loss of the main body of the beam and energy gain in the "tail" slices of the beam (Ref. 12). The Gaussian beam is centered at t= 0.

Where is the research on PWFA headed? Encouraged by the qualitative and quantitative agreement between the predicted and observed transverse and longitudinal effects in beam-driven PWFA experiments thus far, the SLAC experiments are headed

towards the demonstration of even higher acceleration gradients and therefore energy gains for a given length of the plasma. It turns out that if the plasma density is optimized, the plasma wakefields scale as the inverse of the square of the drive bunch length. Simulations show that while a 700 μm bunch produces a useful gradient of 250 MeV/m, a 100 μm bunch increases this gradient dramatically to 10 GeV/m, comparable to what has been observed in laser-plasma acceleration experiments at plasma densities.

Fortunately, it is now possible to test out such scaling. The Sub Picosecond Pulse Source (SPPS) at SLAC is able to deliver electron bunches as short as 20 μm at the interaction point of the PWFA experiment. The transverse electric fields of such short bunches are large enough to field ionize the gas at the beam focus to produce a 100% ionized, perfectly homogeneous plasma, therefore diminishing the need for a preformed plasma. First two runs using sub 100 μm electron bunches have yielded extremely encouraging results which will be reported in a future ICFA newsletter.

For more information on laser and beam-driven plasma accelerator see the recent article, "Plasma Accelerators at the Energy Frontier and on Tabletops," by C. Joshi and T. Katsouleas in *Physics Today*, June (2003).

References

1. P. Chen et al., *Phys. Rev. Lett.* **54**, 693 (1989).
   J. Rosenzweig et al., *Phys. Rev. A*. **44**, R6189 (1993).
2. J. Rosenzweig et al., *Phys. Rev. Lett*. **61**, 98 (1988).
3. N. Barov et al., *Phys. Rev. Lett*. **80**, 81 (1995).
4. H. Nakanishi et al., *Phys. Rev. Lett*. **66**, 1870 (1990).
5. V. Yakimenko et al., *Phys. Rev. Lett*. **91**, 014802-1 (2003).
6. www.slac.stanford.edu/grp/arb/e164/
7. C. Clayton et al., *Phys. Rev. Lett*. **88**, 154801 (2002).
8. P. Muggli et al., *Phys. Rev. Lett*. (submitted).
9. C. Joshi et al., *Phys. Plasmas* **9**, 1845 (2002).
10. S. Wang et al., *Phys. Rev. Lett*. **88**, 135004 (2002).
11. K. Marsh et al., Proceedings of PAC Conference 2003, Portland, OR, May 2003.
12. B. Blue et al., *Phys. Rev. Lett*. **90**, 214801 (2003).

3.3. Advanced Accelerator research in the Accelerator Research Department A at SLAC

R. Ruth, SLAC
mail to: rruth@slac.stanford.edu

The Accelerator Research Department A at SLAC has worked on a wide variety of topics this past year. The work has three main thrusts: performance enhancement of current accelerators at SLAC such as PEP-II, research and design for near-future facilities such as NLC or upgrades to PEP-II, and research in fundamental aspects of accelerator and beam physics. Below we discuss some of the research which has a more fundamental character and also research which is directed towards advanced accelerator topics.

3.3.1. CSR instability in rings

The development of the Coherent Synchrotron Radiation (CSR) instability has been studied numerically [1]. It was shown that above a certain current threshold, which agrees fairly well with the linear theory, the nonlinear calculation gives a rapidly developing

instability leading to microstructures on the phase-space distribution and bunch profile. The instability quickly reaches a sort of "saturation" in which micro bunching largely washes out. The figure below shows the evolution of the distribution function.

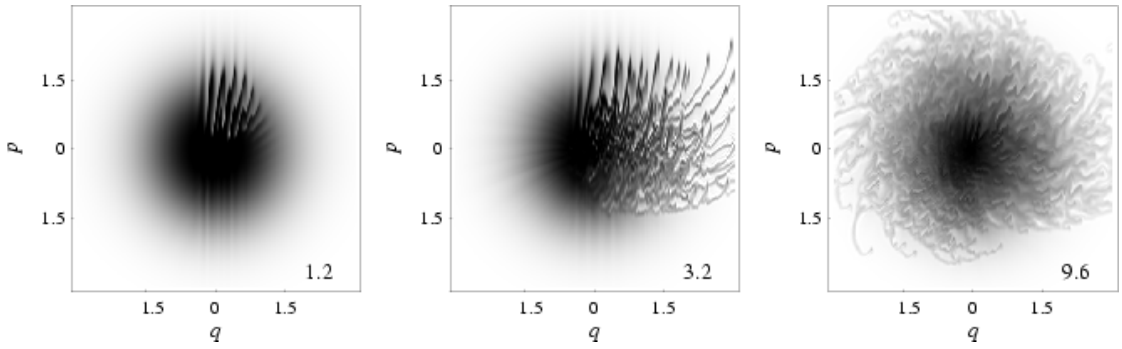

Fig. 1. Phase space of the beam showing development and saturation of the CSR instability. The horizontal axis is a dimensionless longitudinal coordinate, and the vertical axis is a dimensionless energy deviation.

The same computer model mentioned above, but augmented to include Fokker-Planck terms, accounts for the main features of the observations of recurrent short bursts of infrared radiation which have been observed at storage rings of several synchrotron light sources (SURF III, NSLS-VUV, MAXLAB, BESSY, ALS). More recently, the CSR instability was also studied for the NLC damping rings, where it can be caused by the radiation in the wigglers.

CSR instability for single modes was studied including effect of shielding caused by finite beam pipe aperture [2,3]. A system of equations for the beam-wave interaction was derived and its similarity to the 1D free-electron laser theory was demonstrated. In the linear regime, the growth rate of the instability was obtained and nonlinear evolution of the single-mode instability, both with and without synchrotron damping and quantum diffusion, was also studied.

3.3.2. Short X-ray pulses in LCLS

A proposal was made, with detailed calculations, to produce sub-femtosecond x-ray pulses with the LCLS FEL [4]. The idea involves the use of a thin slotted foil in a bunch compressor chicane to emittance-spoil all but a very narrow time-slice of the electron bunch. Detailed calculations, including the transition radiation wakefield of the foil and the FEL dynamics, were used to show that a 2-fs FWHM pulse width is immediately possible in the LCLS (see Fig. 2), with the further possibility of pushing this scheme into the sub-femtosecond range.

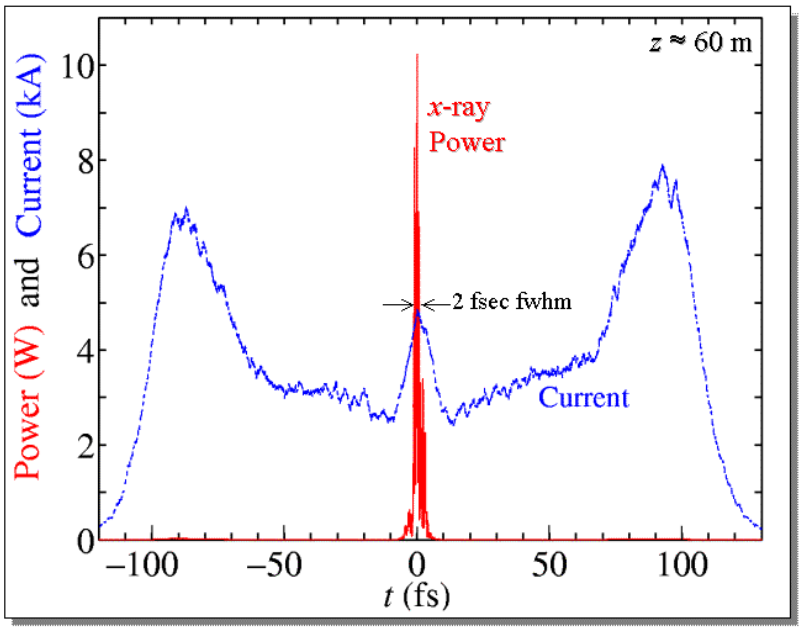

Fig. 2. Power (red) and current (blue) for LCLS beam with a thin slotted foil.

3.3.3. Cosmic Plasma Wakefield Acceleration

A new acceleration mechanism has been recently introduced by P. Chen, T. Tajima, and Y. Takahashi [5]. Ultrahigh energy cosmic rays (UHECR) with energies above the Greisen-Zatsepin-Kuzmin (GZK) limit (~5×10^{19} eV for protons originated beyond the local galaxy cluster) have been observed by several recent experiments. This posts an acute challenge to astrophysics. So far the theories that attempt to explain this phenomenon can be generally categorized into the "top-down" and the "bottom-up" scenarios. The top-down scenario assumes UHECR to be some unknown heavy particle. The drawback is that it relies on exotic physics beyond the standard model and the fine-tuning of particle lifetime. The bottom-up scenario, on the other hand, assumes that UHECRs are actually ordinary particles but are accelerated to extreme energies. In addition to the challenge of the GZK limit, it also lacks an efficient acceleration mechanism. The new mechanism that Chen et al. proposed is based on the plasma wakefields excited by the Alfven shocks in the relativistic plasma that is exploding from the epicenter of a gamma ray burst (GRB). In the example given by the authors, the acceleration gradient is ~10^{16} GeV/cm. With such high efficiency, super-GZK energy can be reached in the close vicinity of a GRB.

3.3.4. High Power RF

Recently 400 ns rf pulses of greater than 500 MW at 11.424 GHz were produced with an RF system designed to demonstrate technology capable of powering a TeV scale electron-positron linear collider [6,7]. This system included a novel approach to microwave component design. All the components are overmoded and most of them can handle more than one mode at the same time, i.e., multimode. This design philosophy is now extended to active and nonreciprocal components with the promise to push the power handling capabilities of these RF components orders of magnitude beyond the state of the art. Then, these components can be used to produce rf sources and active rf pulse

compression systems needed for economical and reliable operation of a future accelerators and colliders.

We also developed overmoded rf semiconductor switches [8]. The first of these devices is an active rf window operating at the TE_{01} mode in circular waveguide. This window comprises an array of 400 distributed PIN/NIP diodes. The device is shown in Figure 3. This window was tested up to 13 MW at X-band. This pushes the state of the art of semiconductor microwave switches few orders of magnitude. These concepts are now being extended to semiconductor rf sources to develop a spatially combined, in a overmoded waveguide, an array of rf sources or phase locked oscillators.

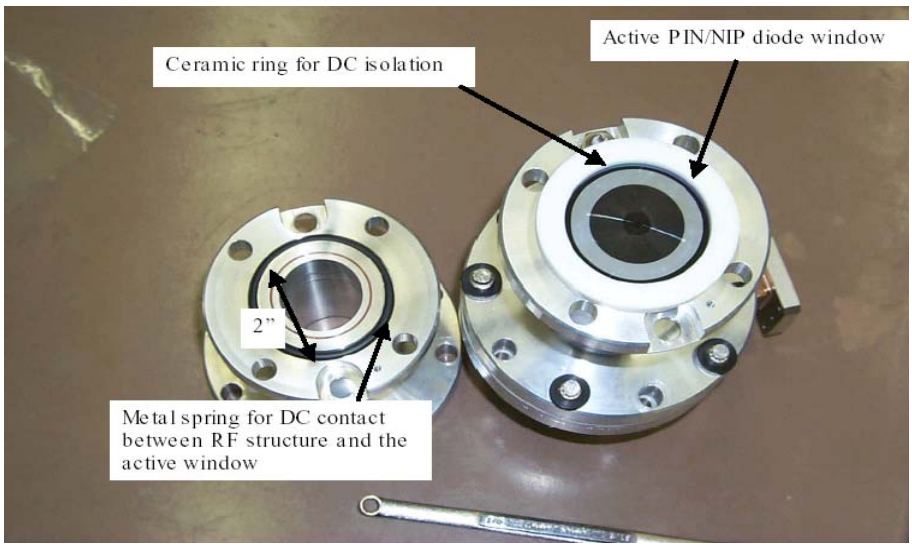

Figure 3. Active window/X-band switch.

3.3.5. X-Band Room Temperature Accelerator R&D

In recent two years, 28 structures with improved design and fabrication technologies have been tested at the Next Linear Collider Test Accelerator (NLCTA) with over 15,000 hours of high power operation logged. The main conclusion from this program is that low group velocity (3 to 4% c initially), 60 cm long, high phase advance (150 degrees), traveling-wave structures are the best candidates for the linear collider. Standing-wave cavities have also been tested, and could provide the design gradient, but they are less cost-effective, and wakefield damping would need to be developed for them. Fig. 4 below summarizes the performance of the candidate structures tested in 2003. It shows the breakdown rate versus unloaded gradient during operation at the nominal 400 ns pulse width at a repetition rate of 60 Hz. All of these structures have an acceptable average iris radius and dipole mode detuning. In addition, three of the structures (H60VG3-6C, H60VG3S18 and H60VG4S17-1) have slots (manifolds) in all or some of the cells to damp the long-range wakefield, consistent with GLC/NLC specifications.

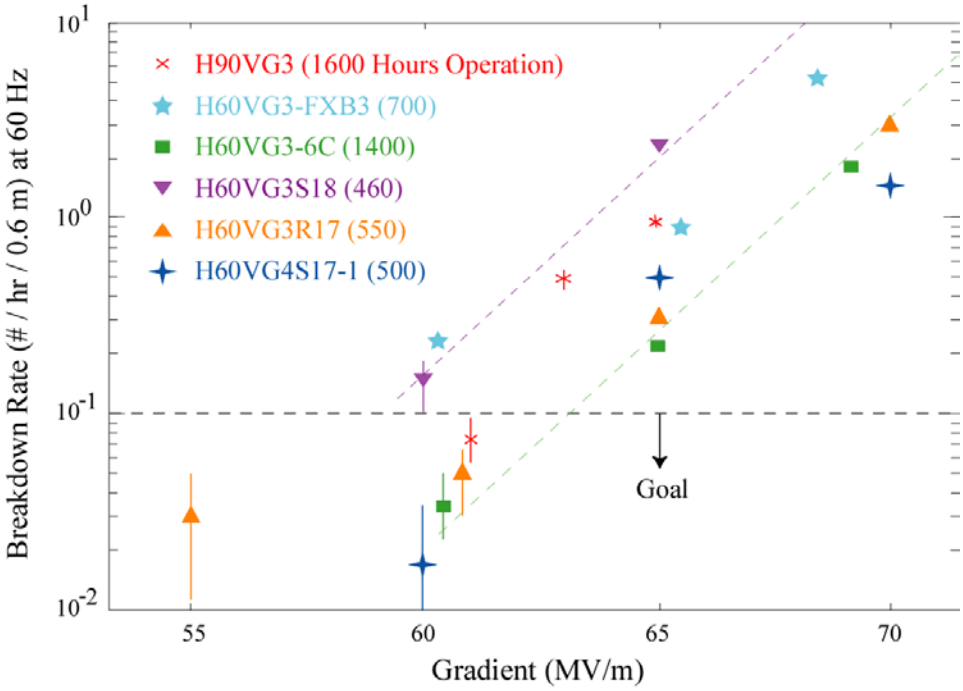

Fig. 4. Breakdown rate as a function of unloaded gradient for several recently tested structures.

3.3.6. **References**

[1] M. Venturini and R. Warnock . "Bursts of Coherent Synchrotron Radiation in Electron Storage Rings: A Dynamical Model", Phys. Rev. Lett. **89**, 224802 (2002).
[2] S. Heifets and G. Stupakov. "Single-mode coherent synchrotron radiation instability", Phys. Rev. ST Accel. Beams **6**, 064401 (2003)
[3] S. Heifets. "Single-mode coherent synchrotron radiation instability of a bunched beam**",** Phys. Rev. ST Accel. Beams **6**, 080701 (2003)
[4] P. Emma *et al*. "Femtosecond and sub-femtosecond x-ray pulses from a SASE-based free-electron laser", accepted for publication in Phys. Rev. Lett.
[5] P. Chen, T. Tajima, and Y. Takahashi. "Plasma Wakefield Acceleration for Ultrahigh-Energy Cosmic Rays", Phys. Rev. Lett., **89** , 161101 (2002)
[6] S. G. Tantawi and C. D. Nantista, "High Power Tests of a Multimode X-Band RF Distribution," Proceedings of Particle Accelerator Conference, 2003. pp. 482-486, June 2003
[7] S. Tantawi, "Overmoded high-power RF magnetic switches and circulators," Proceedings of Particle Accelerator Conference, 1216, **2** (2001).
[8] F. Tamura and S. G. Tantawi, "Development of high power X-band semiconductor microwave switch for pulse compression systems of future linear colliders," Phys. Rev. ST Accel. Beams **5**, 062001 (2002).

3.4. SLAC Accelerator Research Department B

R. Siemann, SLAC
mail to: siemann@slac.Stanford.edu

3.4.1. Overview

SLAC Accelerator Research Department B (ARDB) performs experimental research in high gradient acceleration. High gradient RF, laser driven structures and plasma based accelerators are explored. Much of the ARDB work is performed at SLAC facilities in collaboration with other principal investigators. Our collaborators in the ARDB research program and the ORION Center for Advanced Accelerator and Beam Physics Research are: Profs C. Joshi, W. Mori and J. Rosenzweig of UCLA, T. Katsouleas of USC, and R. Byer of Stanford.

3.4.2. Summary of Current Activities

Plasma Wakefield Acceleration (SLAC Experiments E157, E162, E164 and E164X)

These experiments are studies of the interactions of electron and positron beams with plasmas performed by a UCLA/USC/SLAC collaboration. E157 was the first of these experiments. It was followed by E162 and E164, which have completed data taking, and the program will continue with E164X. All of these experiments take place in the SLAC Final Focus Test Beam (FFTB) using 28.5 GeV electron or positron beams. The FFTB and high energy beams are unique aspects of these experiments. The incoming and outgoing beams are well-characterized with a variety of detectors.

E157 and E162 used a 1.4 m long lithium plasma, and together they gave the opportunity to study many aspects of the beam-plasma interaction at the scale of interest to a plasma accelerator. There were eight data taking runs extending through 2001, and data analysis has been the recent focus of these experiments. Recently published results include: a concept for a plasma-wakefield based energy doubler,[1] measurements of transverse focusing of electron beams,[2,3] X-ray production by electrons traversing the plasma,[4] an overview of the high energy density plasma science that has been in these experiments,[5] and transport and acceleration of positron beams[6,7]. Three graduate students (Brent Blue, UCLA, Seung Lee, USC, and Shoquin Wang, UCLA) received PhD degrees for their work on E157 and E162.

The next experiment in this series is E164, which completed data taking in November, 2003. The goal of E164 is to reach higher gradients by employing shorter bunches and higher density plasmas. The short, high current bunch, $1.5X10^{10}$ electrons in a 10 to 20 micron long bunch (!), is produced with a bunch compressor chicane in the SLAC linac. The plasma density must be increased to keep the plasma wavelength approximately the same as the bunch length. Data have been taken with lithium, hydrogen and xenon plasmas. Tunneling ionization of the plasma by the beam fields is routinely observed. The data from E164 are being analyzed at the present time. The experimental work will continue with experiment E164X that is tentatively scheduled to run in Spring 2004.

Laser Electron Acceleration Project (LEAP) and E163

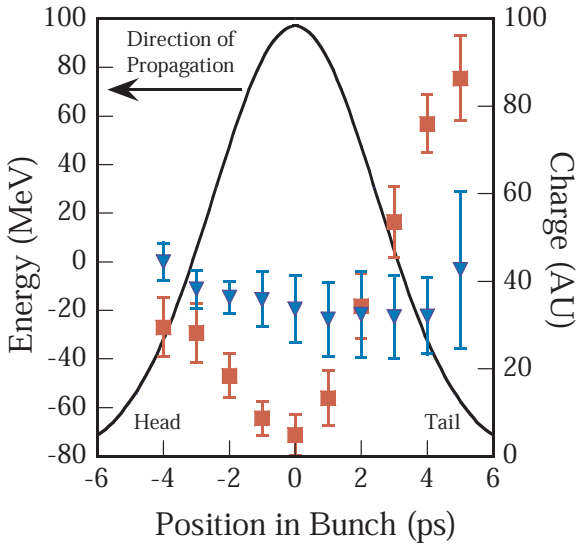

High gradient plasma acceleration of a positron beam (B. Blue et al, ref. [7]). With the plasma off (blue triangles) there is a slight head-tail energy chirp of 20 MeV. When the plasma is on (red squares), the front half of the beam loses energy driving the plasma wave, while the back half of the beam is accelerated by the plasma wave. The accelerating gradient is 56 MeV/m. The black line is the charge distribution within the bunch.

The Laser Electron Acceleration Project (LEAP) is a Stanford/SLAC experimental program that has the goal of building accelerators based on near IR lasers in the 1 to 2 micron wavelength range. There is an enormous commercial market for near-IR lasers from telecommunications and laser machining, and this market is producing rapid advances and significant cost reductions. The LEAP goal is to develop accelerator structures and acceleration mechanisms that will benefit from these developments.

The first stage of LEAP has been a proof-of-principle experiment located at the superconducting accelerator on the Stanford campus. There was a one-week long run in June 2002, and significant amounts of data were taken, but there was no convincing evidence of acceleration. However, we have learned a great deal about techniques and instrumentation for laser acceleration experiments, and Tomas Plettner, a Stanford graduate student, received his PhD degree for this work.

SLAC experiment E163 has been approved to provide the electron beam needed for long-term progress. E163 would continue the proof-of-principle studies and follow that with demonstration of optical bunching at 1 micron and acceleration using a lithographically fabricated multi-cell structure. E163 is presently under construction. It calls for modifications of the SLAC Next Linear Collider Test Accelerator (NLCTA), and the building of a shielded enclosure for performing experiments. The shielding enclosure has been design for a 60 MeV, 1 nC beam. It is located to the north of the NLCTA and has been completed recently. The LEAP apparatus will be moved from the Stanford campus to SLAC when appropriate. The major E163 technical system is a photoinjector with associated drive laser and RF system. All of these are well on the way to completion, and E163 data taking could begin within a year.

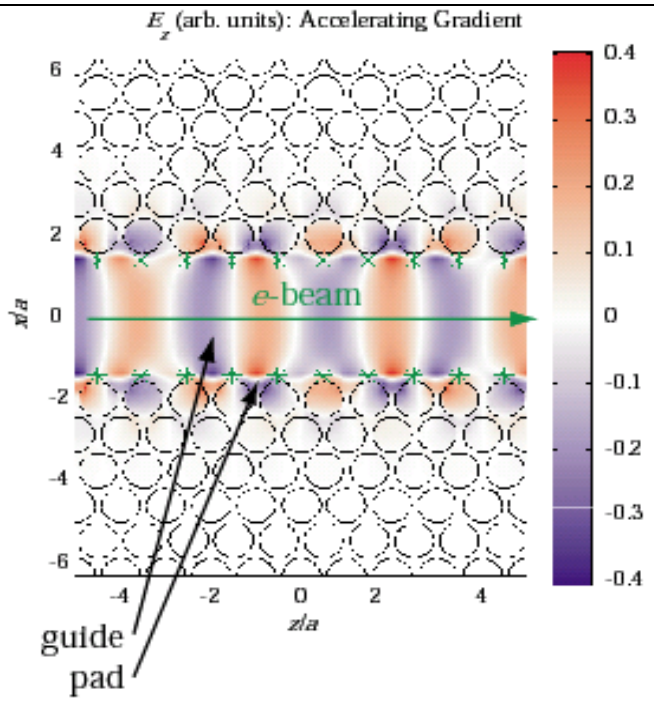

A photonic crystal accelerator structure geometry with a speed-of-light waveguide mode. (B. M. Cowan, ref. [10]) The circles delineate the vacuum holes, and the blue/red coloring denotes the accelerating *Ez* component. The asterisks show the damage sites, where the field magnitude in the dielectric is maximized.

There are important issues related to laser acceleration that can be addressed without an electron beam, and we continue to work on them. Recent activities included measurements of laser and radiation damage of materials,[8] Inverse Free Electron Laser bunching of beams, lithographic fabrication of structures, general considerations for laser driven accelerators, and photonic crystal accelerators. Work in many of these areas has been presented at conferences, and papers on photonic crystal optical fibers[9] and lithographically fabricated photonic crystals have been published.[10]

High Gradient RF Technology

This was the last year of activity in this area with the final analysis and publication of the results on surface pulsed heating of copper RF cavities.[11] The results are that damage was measured after 56 million pulses with a temperature rise of 120 K and after 86 million pulses with a temperature rise of 82 K. David Pritzkau received his PhD degree from Stanford and the 2003 APS Division of Physics of Beams PhD Prize for this work.[12]

The ORION Center for Advanced Accelerator and Beam Physics Research and the ORION Facility

Advanced accelerator research, with its goal of understanding the physics and developing the technologies for reaching higher energies, is essential for the future of particle physics. The ORION Center is a Stanford/UCLA/USC/SLAC collaboration devoted to advanced accelerator and beam physics research. A critical mass of researchers from diverse scientific backgrounds will be brought together with state-of-the-art beams,

apparatus and computing. The ORION Center holds the promise of significant advances through rapid assessment and development of new acceleration concepts.

ORION Center experiments will take place at the FFTB and the ORION Facility. The FFTB experiments will exploit the apparatus developed for E157, E162, etc. The ORION Facility is a proposed user-oriented facility for advanced accelerator research that will be based on the NLCTA. The facility will provide 60 MeV beams in a Low Energy Hall and nominal 350 MeV beams in a High Energy Hall. The E163 photoinjector is based on an ORION design, and it will serve the entire facility with modest upgrades. In addition, the E163 beam line will be the extraction line for the Low Energy Hall. Diagnostics and data acquisition systems developed for E157, etc and E163 will be available to researchers at the ORION Center.

3.4.3. Current ARDB Scientific Staff

Robert Siemann	Professor, SLAC and Stanford Applied Physics
Eric Colby	W. K. H. Panofsky Fellow
David Fryberger	SLAC Staff
Mark Hogan	SLAC Staff
Robert Noble	SLAC Staff
Dennis Palmer	SLAC Staff
James Spencer	SLAC Staff
Christopher Barnes	Graduate Student (Stanford)
Alex Butterwick	Graduate Student (Stanford)
Benjamin Cowan	Graduate Student (Stanford)
Atsushi Fukasawa	Graduate Student (Tokyo)
Mehdi Javenmard	Graduate Student (Stanford)
Devon Johnson	Graduate Student (UCLA)
Caolionn O'Connell	Graduate Student (Stanford)
Christopher Sears	Graduate Student (Stanford)
Ning Wu	Graduate Student (Stanford)

3.4.4. Publications & References

[1] S. Lee *et al*, "Energy Doubler For A Linear Collider", Physical Review Special Topics - Accelerators and Beams **5**, 011001 (2002).
[2] C. E. Clayton *et al,* "Transverse Envelope Dynamics Of A 28.5 Gev Electron Beam In A Long Plasma", Physical Review Letters **88**, 154801 (2002)
[3] C. O'Connell *et al*, "Dynamic Focusing Of An Electron Beam Through A Long Plasma", Physical Review Special Topics – Accelerators and Beams **5**, 1121301 (2002)
[4] Shouqin Wang *et al,* "X-Ray Emission From Betatron Motion In A Plasma Wiggler", Physical Review Letters **88**, 135004 (2002)
[5] C. Joshi *et al,* "High Energy Density Plasma Science With An Ultra-Relativistic Electron Beam", Physics of Plasmas **9**, 1845 (2002).
[6] M.J. Hogan *et* al, "Ultrarelativistic-Positron-Beam Transport through Meter-Scale Plasmas", Physical Review Letters **90**, 205002 (2003).
[7] B. E. Blue *et al*, "Plasma Wakefield Acceleration of an Intense Positron Beam" Physical Review Letters **90**, 214801 (2003)
[8] E. Colby *et al*, "Gamma Radiation Studies on Optical Materials", IEEE Trans. Nucl. Sci. (2002).

[9] Xintian Eddie Lin "Photonic band gap fiber accelerator" Physical Review Special Topics – Accelerators and Beams, **4**, 051301 (2001).
[10] Benjamin M. Cowan, "Two-dimensional photonic crystal accelerator structures", Physical Review Special Topics – Accelerators and Beams, **6**, 101301 (2003).

11 D. P. Pritzkau & R. H. Siemann, "Experimental Study of RF Pulsed Heating on Oxygen Free Electronic Copper", Physical Review Special Topics – Accelerators and Beams **5**, 112002 (2002)

[12] David Peace Pritzkau, "RF Pulsed Heating", PhD in Applied Physics from Stanford University. David is now a Senior Test Engineer at Big Bear Networks in Sunnyvale, CA.

3.5. Program for Plasma-Based Concepts for Future High Energy Accelerators

PI: Professor Thomas Katsouleas, University of Southern California
Co-PI: Dr. Patric Muggli, University of Southern California
mail to: katsoule@usc.edu

The USC program is focused on advancing plasma-based concepts for future high-energy accelerators. We are actively pursuing this goal through experiments, advanced computational modeling and theory.

3.5.1. Recent Accomplishments

Highlights of accomplishments in this period include:

- Performance of the E-162 Plasma Wakefield Accelerator Experiment at the Stanford Linear Accelerator Center.
- Development of the Plasma Afterburner concept for doubling the energy of a future linear collider.
- Development and application of advanced 3-D particle simulation tools (OSIRIS and QuickPIC) on high-performance platforms for modeling current plasma accelerator experiments with unscaled parameters and unprecedented fidelity, including self-consistent plasma ionization, beam and plasma imperfections, aperturing effects of the diagnostics, etc.
- Development of a novel circular accelerator simulation code exploiting the power of plasma wakefield algorithms to model the dynamics and stability of circulating beams in electron clouds.

The E-162 Plasma Wakefield Accelerator experiment was designed to demonstrate high-gradient electron and positron acceleration at energies of relevance to high-energy colliders and over meter length scales. This experiment has produced a wealth of spectacular results and physics milestones. As described in the references that follow, the collaboration between USC, UCLA and SLAC achieved a number of firsts: These include the acceleration of electrons in the tail of a 30 GeV SLAC bunch by up to 280 MeV over 1.4 meters of plasma. The experiment ran parasitically with PEP-II operation at SLAC. In this mode, the SLAC linac delivered stably $2x10^{10}$ electrons per bunch which was a factor of two lower than the original design. Consequently, the acceleration measured was lower than the design by a similar factor but in very good agreement with the simulations performed for the actually delivered beam parameters. The good agreement bodes well for the collaboration's next experiment – E-164. Preliminary simulations indicate that the

wakefield amplitude and acceleration gradient increase as the inverse square of the bunch length, and E-164 will test this scaling with bunch lengths 6 times shorter or more in upcoming runs in 2003-2004.

If plasma accelerators are to have an impact in future high energy physics colliders, they must address not only the need for high-gradients but also the need for high beam quality and the need to accelerate positrons as well as electrons. E-162 accomplished important firsts on both of these fronts. By designing the incoming beam optics to match the theoretical Twiss parameters associated with the plasma's strong transverse focusing fields, the first demonstration of matched beam propagation and acceleration were achieved. Such matching will be important to preserving beam emittance in future plasma accelerators such as an Afterburner in which the beam may propagate over a hundred betatron oscillations. The E-162 experiment also exploited the unique capability of the SLAC facility to deliver positron beams in order to perform the first plasma acceleration test of positrons. The results confirmed that the physics of positron acceleration and focusing is significantly different from that of electrons in the nonlinear regime, but showed excellent agreement with detailed PIC simulations (Fig. 1).

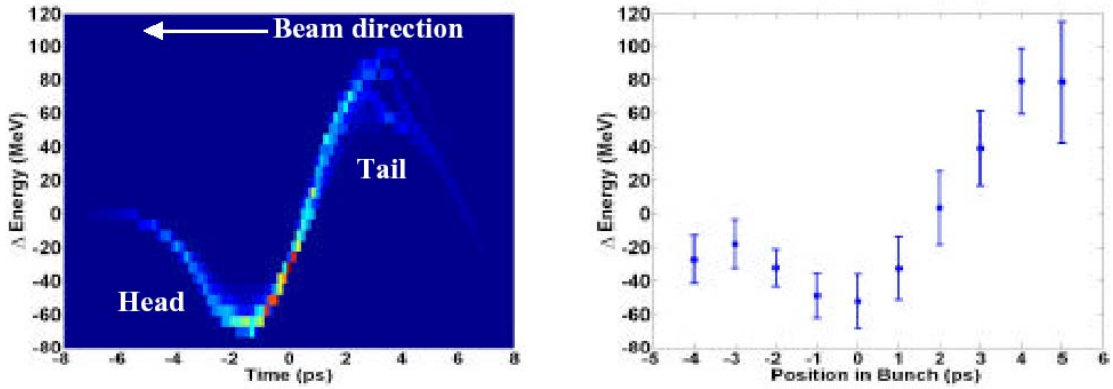

Figure 1 shows results of a 3-D OSIRIS simulation of the E-162 experiment (left) and the experimental data (right) for *positrons*. Plotted are the time-resolved energy loss and gain along the bunch. The tail was accelerated by 80 MeV in 1.4 meters**.**

The plasma afterburner is a concept for impacting the energy frontier with a plasma accelerator placed at the interaction point of a linear collider. The concept is described in the USC thesis of Ms. Seung Lee who graduated during this contract period. Ms. Lee used simulations to support key foundations of the afterburner such as the scaling of the wakefields with shortened bunch length well into the non-linear regime, the beam loading of a signficant number of particles (10^{10}) with modest energy spread, and the recovery of luminosity through plasma lensing. The interest in this original proposal has been spurred by experimental results on E-162 and elsewhere and is leading to work on a challenging but finite spectrum of remaining issues. Key among these are beam jitter and alignment tolerances, hosing instability limits and plasma source development.

The interaction between a positively charged high current beam with the low density electron cloud they create in circular accelerators has become a major concern in existing accelerators at high current and in the design of future circular accelerators (particularly LHC at CERN). Recently a meeting held at CERN under the title ECLOUD02 highlighted the fact that electron clouds lead to emittance blow-up and instability of beams in a number of accelerators world-wide, that the mechanisms of the e-cloud interaction are not

well understood and that predictive models are greatly needed. The challenge for computational modeling of e-clouds arises from the need to model beam propagation over hundreds of thousands of kilometers while resolving the self-consistent space charge fields of the cloud on cm scales. But just such a predictive model now appears possible feasible using high-performance parallel computing techniques and advanced algorithms developed for plasma wakefield studies.

A collaboration of the plasma wakefield accelerator groups at USC and UCLA has now adapted a code which they have been using for plasma based accelerators studies over the past decade, to the electron cloud problem (the electron cloud is after all a non neutral plasma problem). Their code, QuickPIC, is based on Viktor Decyk's (UCLA) Framework for developing parallel PIC codes. This includes highly optimized components and parallelization. In order to properly model the e-cloud problem, the capability of QuickPIC to model the cloud interaction needed to be combined with algorithms from the circular accelerator community to track particles in the external magnets and RF fields. Particularly synchrotron and betatron motions are added to the code and the chromaticity is also included to take care of the changes in the betatron frequency due to momentum spread of the beam. To this end, G. Rumolo from CERN visited USC for a month to collaborate on the code. An early milestone was reached recently: Using 16 processors at NERSC, the propagation of the beam through 50 turns (350 km) of the SPS at CERN was modeled. This is the relevant number of turns to begin to see the tune shift due to the cloud. Based on this preliminary work, it appears to be possible to develop a high-fidelity model capable of simulating hundreds or even a thousand turns in the near future. The goal is to develop predictive capability to ensure the performance of major upcoming facilities such as the LHC and SNS.

3.5.2. Publications

1. P. Muggli, S. Lee, T. Katsouleas, et al., "Refraction of a Particle Beam," NATURE **411**: 43 MAY 3 2001.
2. N. Spence, T. Katsouleas, P. Muggli, W. B. Mori, and R. Hemker, "Simulations of Cerenkov Wake Radiation Sources," Physics of Plasmas **8** (11) pp. 4995-5005 (2001).
3. S. Lee, T. Katsouleas, R. Hemker,E.S. Dodd, W.B. Mori, "Plasma-Wakefield Acceleration of a Positron Beam" PHYSICAL REVIEW E, 6404 (4): 5501-+ Part 2 OCT (2001).
4. P. Catravas, et al. "Measurements of Radiation Near an Atomic Spectral Line From the Interaction of a 30 GeV Electron Beam and a Long Plasma," art. no. 046502 PHYSICAL REVIEW E, 6404 (4): 6502-+ Part 2 OCT 2001.
5. P. Muggli, et al., "Collective Refraction of a Beam of Electrons at a Plasma-Gas Interface," PHYSICAL REVIEW SPECIAL TOPICS-ACCELERATORS AND BEAMS, 4 (9): U14-U16 SEP 2001.
6. J.R. Hoffman, P. Muggli, R. Liou, M. Gundersen, J. Yampolsky, T. Katsouleas, C. Joshi, W.B. Mori, "High Power Radiation From Ionization Fronts in a Static Electric Field in a Waveguide," JOURNAL OF APPLIED PHYSICS, 90 (3): 1115-1123 AUG 1 2001.
7. C. Ren, B.J. Duda, R.G. Hemker, W.B. Mori, T. Katsouleas, T.M. Antonsen, P. Mora, "Compressing and Focusing a Short Laser Pulse By a Thin Plasma Lens" - art. no. 026411, PHYSICAL REVIEW E, 6302 (2): 6411-+ Part 2 FEB 2001.
8. M. Conde and T. Katsouleas, "Summary Report: Working Group 5 on 'Electron Beam-Driven Plasma and Structure Based Acceleration Concepts'," in Adv. Accel. Concepts, AIP Conf. Proc. Vol. 569, P. Colestock and S. Kelley, Eds., pp. 61-64, AIP, NY (2001).
9. P. Muggli, et al., W.B. Mori, "Dynamics of 28.5 GeV Electron and Positron Beams in a Meter-Long Plasma," LASERS 2001 Conference Proceedings.

10. D.T. Palmer, et al., "ORION: an Advanced Accelerator Facility at SLAC," Proc. Of the 2001 Particle Accelerator Conference, IEEE, Part Vol. 3, pp. 2251-2253 Vol. 3 (2001).
11. P. Muggli, et al., "Status of the Plasma Wakefield Acceleration Experiment at the Stanford Linear Accelerator Center," Proc. Of the 2001 Particle Accelerator Conference, IEEE. Part Vol. 1, 2001, pp. 122-125 Vol. 1 (2001).
12. S. Wang, et al., "Observation of Spontaneous Emitted X-ray Betatron Radiation in Beam-Plasma Interactions," Proc. Of the 2001 Particle Accelerator Conference, IEEE, Part Vol. 5, pp. 3999-4001 Vol. 5 (2001)
13. P. Muggli et al., "Refraction of a Beam of Electrons at an Interface of Gas and Plasmas," Nature, Vol. 411, p. 43 (2001).
14. B. Blue et al., "Test of the Electron Hose Instability in the E157 Experiment," Proc. Of the 2001 Particle Accelerator Conference, IEEE, Part Vol. 5, pp. 4002-4004 (2001).
15. C. Huang, V. Decyk, S. Wang, E.S. Dodd, C. Ren, W.B. Mori, T. Katsouleas, and T. Antonsen, Jr., "QuickPIC: A Parallelized Quasi-Static PIC Code for Modeling Plasma Wakefield Acceleration, Proc. Of the 2001 Particle Accelerator Conf, IEEE, Vol. 5, pp. 4005-4007 (2001).
16. T. Katsouleas, A.Z. Ghalam, S. Lee, W.B. Mori, C. Huang, V. Decyk, and C. Ren, "Plasma Modeling of Wakefields in Electron Clouds," ECLOUD'02 Mini-Workshop on Electron-Cloud Simulations for Proton and Positron Beams (CERN 2002-001); CERN pp. 239-42, Geneva, Switzerland (2002).
17. F.S. Tsung, R.G. Hemker, C. Ren, W.B. Mori, L.O. Silva, and T. Katsouleas, "Generation of Ultra-Intense, Single-Cycle Laser Pulse using Photon Deceleration," Proc. of the Nat. Acad., Vol. 99, pp. 29-32 (2002).
18. S. Lee, T. Katsouleas, P. Muggli, W.B. Mori, C. Joshi, R. Hemker, E.S. Dodd, C.E. Clayton, K.A. Marsh, B. Blue, S. Wang, R. Assmann, F.J. Decker, M. Hogan, R. Iverson, and D. Walz, "Energy Doubler for a Linear Collider," Phy. Rev. Special Topics-Accelerators & Beams, Vol. 5, No. 1 (January 2002).
19. E.S. Dodd, R.G. Hemker, R.G, C.-K. Huang, S. Wang, C. Ren, W.B. Mori, S. Lee, and T. Katsouleas, "Hosing and Sloshing of Short-Pulse Ge-V-Class Wakefield Drivers," Phys. Rev. Lett., Vol. 88, No. 12, pp. 125001/1-4 (25 March 2002).
20. C.E. Clayton et al., "Transverse Envelope Dynamics of a 28.5-GeV Electron Beam in a Long Plasma," Phys. Rev. Lett., Vol. 88, No. 15 pp. 154801/1-4 (15 April 2002).
21. S. Wang et al., "X-ray Emission from Betatron Motion in a Plasma Wiggler," Phys. Rev. Lett., Vol. 88, No. 13, pp. 135004/1-4 (1 April 2002).
22. C. Joshi et al., "High Energy Density Plasma Science with an Ultrarelativistic Electron Beam," Physics of Plasmas, Vol. 9, No. 5, pp. 1845-1855 (May 2002).
23. M.J. Hogan et al., "Acceleration and Focusing of Electrons and Positrons using a 30 GeV Drive Beam," Advanced Accelerator Concepts, Tenth Workshop, eds. C. E. Clayton and P. Muggli, AIP Conf. Proc. No. 647, pp. 3-10 (2002).
24. S. Deng et al., "Modeling of Ionization Physics with the PIC Code OSIRIS," Advanced Accelerator Concepts, Tenth Workshop, eds. C. E. Clayton and P. Muggli, AIP Conf. Proc. No. 647, pp. 219-223 (2002).
25. A.Z. Ghalam, T. Katsouleas, S. Lee, W.B. Mori, C. Huang, V. Decyk, and C. Ren, "Simulation of Electron-Cloud Instability in Circular Accelerators using Plasma Models," Advanced Accelerator Concepts, Tenth Workshop, eds. C. E. Clayton and P. Muggli, AIP Conf. Proc. No. 647, pp. 224j-231 (2002).
26. J.H. Cooley, T.M. Antonsen Jr., C. Huang, V. Decyk, S. Wang, E.S. Dodd, C. Ren, W.B. Mori, and T. Katsouleas, "Further Developments for a Particle-in-Cell Code for Efficiently Modeling Wakefield Acceleration Schemes," Advanced Accelerator Concepts, Tenth Workshop, eds. C. E. Clayton and P. Muggli, AIP Conf. Proc. No. 647, pp. 232-239 (2002).
27. S. Deng et al., "3-D Simulation of Plasma Wakefield Acceleration with Non-Idealized Plasmas and Beams," Advanced Accelerator Concepts, Tenth Workshop, eds. C. E. Clayton and P. Muggli, AIP Conf. Proc. No. 647, pp. 592-599 (2002).
28. N. Yugami, T. Higashiguchi, H. Gao, S. Sakai, K. Takahashi, H. Ito, Y. Nishida, and T. Katsouleas, "Experimental Observation of Radiation from Cherenkov Wakes in a Magnetized Plasma," Phys. Rev. Lett. 89, 065003 (2002).

29. M. Gundersen, P.T. Vernier, L. Marcu, A. Li, X. Zhu, A. Ghalam, T. Katsouleas, C. Young, M. Behrend, and C. Craft, "Ultrashort Pulse Electroporation: Applications of High Pulsed Electric Fields to Induced Caspase Activation of Human Lymphocytes," Conference Record of the 25th International Power Modulator Conference and High Voltage Workshop, pp. 667-670 (2002)
30. C. O'Connell *et al.*, "Dynamic focusing of an electron beam through a long plasma," Phys. Rev. ST Accel. Beams **5**, 121301 (2002).
31. M. J. Hogan, C. E. Clayton, C. Huang, P. Muggli, S. Wang, B. E. Blue, D. Walz, K. A. Marsh, C. L. O'Connell, S. Lee, R. Iverson, F.-J. Decker, P. Raimondi, W. B. Mori, T. C. Katsouleas, C. Joshi, and R. H. Siemann, "Ultrarelativistic-Positron-Beam Transport through Meter-Scale Plasmas," Phys. Rev. Lett. **90**, 205002 (2003)
31. B. E. Blue *et al.* "Plasma-Wakefield Acceleration of an Intense Positron Beam," Phys. Rev. Lett. **90**, 214801 (2003)

Current Staff

- Dr. Thomas Katsouleas - PI
- Dr. Patrick Muggli - Assc. Rsh. Prof.
- Ms. Suzhi Deng – PhD Student
- Mr. Ali Ghalam – PhD Student
- Mr. Erdem Oz – PhD Student
- Mr. Jitendra Kulshreshtha – MS Student
- Mr. Reid Maeda - Undergraduate
- Mr. Bill Quillinan – Middle School Science Tchr.
- Mr. Paul Kim – HS Science Teacher

Past Students

1.	Dr. Seung Lee (PhD, 2001)	International Rectifier
2.	Dr. Jerry Hoffman (PhD, 2001)	Cymer Corp.

Thomas C. Katsouleas (PI)
University of Southern California, Electrical Engineering Department
Los Angeles, CA 90089-0271
PHONE: 213/740-0194
FAX: 213/740-8677
E-MAIL: katsoule@usc.edu
Website: http://www.usc.edu/dept/engineering/eleceng/plasma_accelerator/

3.6. Laser-Driven Accelerators and their Applications

Donald Umstadter

FOCUS Center, University of Michigan, Ann Arbor

3.6.1. Electron Acceleration

In recent years, there has been interest in an acceleration concept based focusing terawatt-power laser beams into plasma, setting up a fast (relativistic) wave (wakefield). If timed just right, electrons in the plasma can surf the plasma waves to high energies, as high as 100 MeV, in the distance of only a millimetre[1]. One problem with this concept is the mismatch between the electron source (sometimes an external photocathode, sometimes uncontrolled electrons from the plasma itself) and the plasma wave used for

acceleration. Thus, we have been investigating a new means of generating electrons in a controllable way, namely the use of a pair of laser beams which position, heat, and synchronize the insertion of electrons into the plasma wave[1]. This is predicted theoretically and numerically to result in a monoenergetic beam with femtosecond duration and extremely low transverse emittance[2]. Besides potential applications to particle physics, ultra-high-gradient acceleration is also expected to benefit other research on x-ray light sources, the production of medical radioisotopes and the ignition of thermonuclear fusion reactions.

One of the most important outcome of our research thus far was demonstration of the principle of optical control of laser accelerators, namely, that one laser pulse could modify the properties (e.g., emittance and electron number) of an electron beam accelerated by a separate but synchronized laser pulse[3][4][5][6][7]. While this was done with long duration laser pulses and thus did not result in a reduction of the energy spread, it did demonstrate that with the addition of a second pulse the energy of electrons could be increased and the beam emittance decreased.

We also studied the propagation of an intense (1×10^{19} W/cm^2) ultrashort (30-fs duration) laser pulse in plasma conditions that are similar to those that will be encountered in an injection experiment[8][9][10]. The plasma density was varied in such a way that the parameters of the interaction crossed for the first time the transition from the resonant to the self-modulated regime. In so doing, we found that under certain conditions, self-focusing into multiple filaments accompanies self-trapping and acceleration of electrons, both of which must be avoided if injection is to be successful. This same experiment demonstrated electron acceleration at a repetition rate of 10 Hz, which is an improvement of several orders-of-magnitude in the duty cycle of laser accelerators, bringing a practical injector closer to reality.

Another recent highlight from our research was that, using our new 30-fs 10-TW laser system, we accelerated with a laser accelerator an electron beam with a record low divergence (0.2 degrees). This is more than 100 times lower than the 30-degree divergence that was reported elsewhere using a laser with similar parameters[11]. Our previous measurements of surprisingly low transverse emittance beams (see Figure 1)[11] were recently explained theoretically[12].

Last, a method for the control of stimulated Raman scattering and hot electron production in short-pulse laser-plasma interactions was studied[11]. It relies on the use of a linear frequency chirp in non-bandwidth limited pulses. Theoretical calculations show that a 12% bandwidth will eliminate Raman forward scattering for a plasma density that is 1% of the critical density. The predicted changes to the growth rate are confirmed in two-dimensional particle-in-cell simulations.

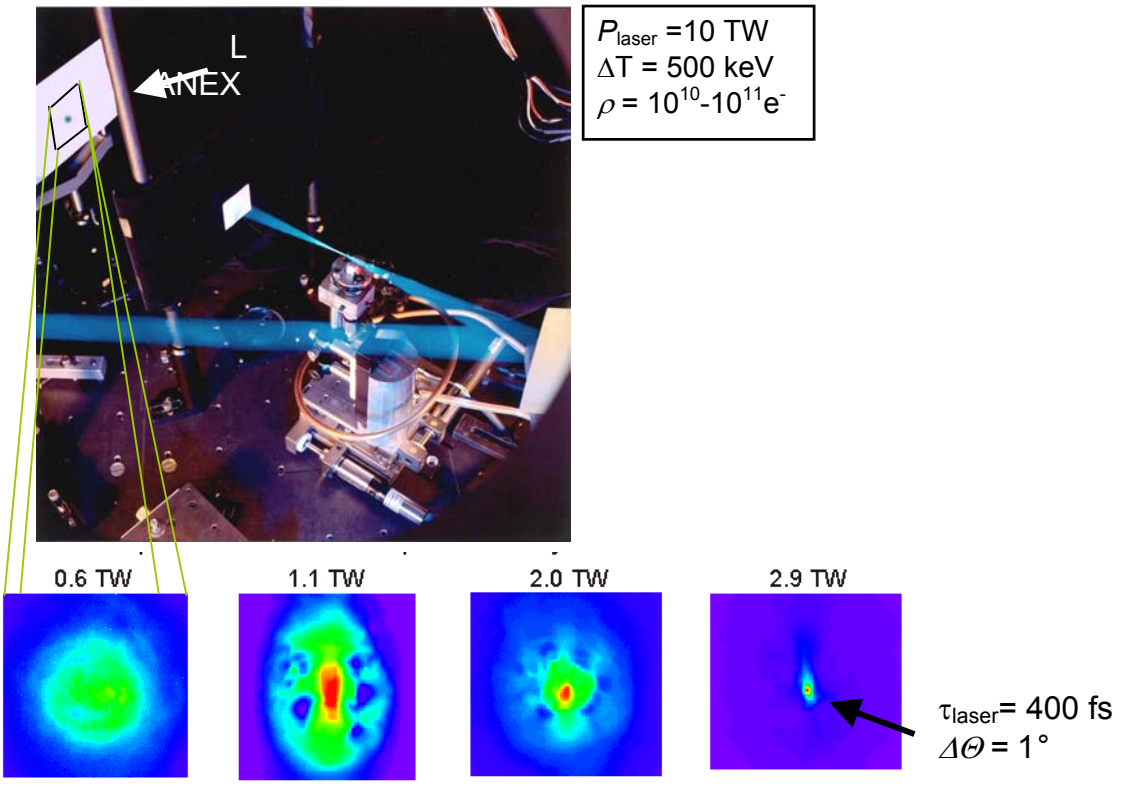

Figure 1. Top: Artistically enhanced photograph of the experimental apparatus used to accelerate and electron beam with a laser. Bottom: Spatial profiles of the electron beam (measured by imaging a LANEX screen to a CCD camera) at various laser powers.

3.6.2. Novel Compact X-Ray Sources from Nonlinear Thomson Scattering

The electron beams discussed above can form the basis of novel compact light sources, which are generally referred to as Thomson sources because they are based on the scattering of electrons with photons. In this case, a high-intensity laser beam is focused to overlap spatially and temporally with the laser-driven electron beam discussed above (as shown in

Figure 2). When compared with conventional light sources based on cm-wavelength magnetostatic wigglers and GeV-energy RF-accelerators, the electromagnetic wigglers of these all-optical-laser-based EUV sources have ten-thousand times shorter wavelength (micron-scale). Thus, the total length of the wiggler region is correspondingly smaller (only mm in length). Another consequence of this is that the frequency upshift required to reach a given output wavelength is also ten-thousand times smaller. Also, given that the required electron energy scales as the square root of the upshift, the required electron energy can be one-hundred-times lower (10-100 MeV). It follows from this, and the fact that the field gradients of these accelerators can be ten-thousand-times higher (1 GeV/cm), that the size of the accelerating region can in principle be a million times smaller (only mm in length). Besides its small size, this EUV source can produce femtosecond duration pulse and be synchronized with a relatively low jitter with another femtosecond light pulse having a different wavelength (by virtue of the possibility of deriving the two pulses from the same laser pulse); this is advantageous for the study of ultrafast pump-and-probe photo-initiated processes.

We have recently studied these incoherent Thomson sources both theoretically[15][16][17], as well as experimentally[18][19][20], Using a long pulse (400-fs) laser, collimated beams of third harmonic radiation[17] and even EUV-energy high-

order harmonics[18][19] were produced from Thomson scattering of a high intensity laser off of a co-propagating laser-accelerated relativistic electron beam. More recently, using a 30-fs, 30-TW laser located at, and in collaboration with colleagues at, the Laboratoire d'Optique Appliquee (LOA), in Palaiseau, France, a beam containing 5×10^9 keV-energy x-ray photons/shot (integrating over all angles) was produced[20] (see

Figure 2) by this same mechanism. Experiments are currently underway to conduct experiments on scattering from a counter-propagating electron beam. While not having the same ease of alignment as the co-propagating case (since the beams are automatically aligned in this case), it does have the advantage of producing a more energetic photons, by means of the Doppler upshift $\lambda= \lambda_L/4\gamma^2$. Theory shows that a 1-keV energy x-rays can be produced with only 10-MeV energy electrons. Recent analysis has discussed the critical role of the initial electron phase[16] and the optimal scattering conditions for this configuration[15][17].

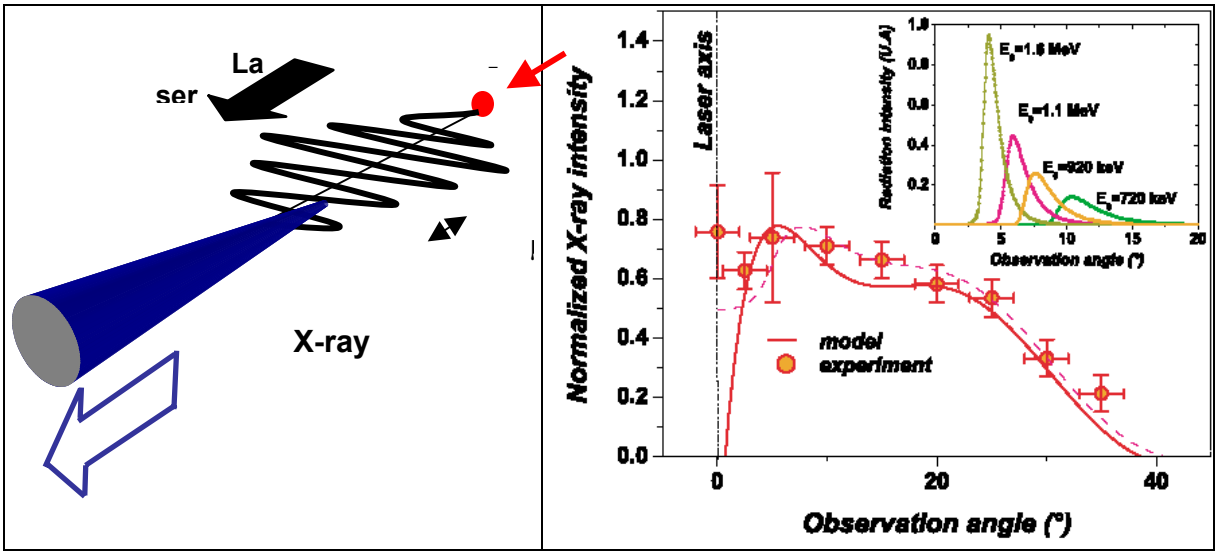

Figure 2. Left: Schematic diagram of Thomson scattering from a co-propagating laser-driven electron beam. Right: (from Ref. 19) Spatial distribution of the observed x-ray emission for a_0=5.6. The solid line (dotted line) is the numerical result obtained for a Gaussian electron distribution with a temperature of 0.9 MeV and without (with) 5° k spread. The inset shows the effect of the initial energy of monoenergetic electrons on the spatial distribution of the nonlinear Thomson scattering.

3.6.3. Ion Acceleration

The acceleration of protons to MeV energies by the interaction of relativistically laser pulse with a thin solid-density film was studied [21][22], as shown in \

Figure **3**. It was found that up 10^{10} protons, with energies up to 10 MeV, were accelerated in collimated beams (20° divergence angles). The laser parameters were as follows: l=1.053 mm, P < 12 TW, energy = 5 J, t = 400 fs, and I < 2x10^{19} W/cm^2. Deuterons were also accelerated to energies of about 2 MeV from a thin layer of deuterated polystyrene deposited on Mylar film[23] These high-energy deuterons were directed to the boron sample, where they produced atoms of positron active isotope ^{11}C from the reaction ^{10}B(d,n)^{11}C. The activation results suggest that deuterons were accelerated from the front surface of the target. Such short-lived isotopes have medical applications, as in the detection of cancer by means of positron-emission tomography.

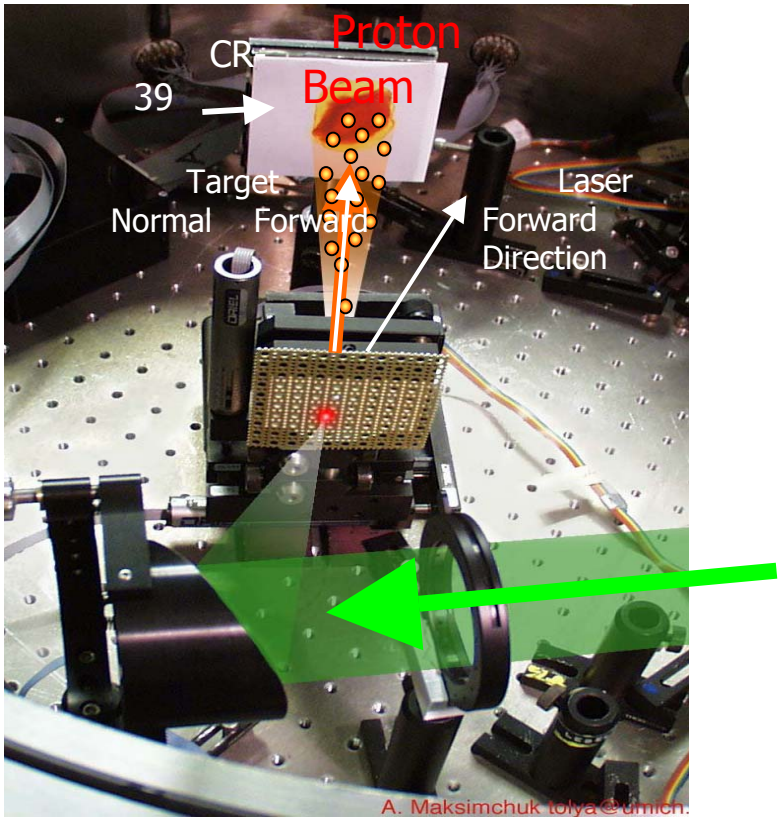

Figure 3. Artistically enhanced photograph of the experimental setup used to accelerate protons.

3.6.4. References

[1] D. Umstadter, "Relativistic laser-plasma interactions," Journal of Physics D (Applied Physics) 36, 151-65 (2003).

[2] D. Umstadter, J.K. Kim and E. Dodd, "Laser injection of ultrashort electron pulses into wakefield plasma waves," Phys.Rev.Lett. **76**, 2073-6 (1996).

[3] P. Zhang, N. Saleh, S. Chen, Z.M. Sheng and D. Umstadter, "An Optical Trap for Relativistic Plasma," *Phys. Plasmas* **10**, 2093 (2003).

[4] D. Umstadter, S. Banerjee, S. Chen, E. Dodd, K. Flippo, A. Maksimchuk, N. Saleh, A. Valenzuela, and P. Zhang, " Developments in relativistic nonlinear optics," AIP Conf. Proc. **611**, 95 (2002).

[5] N. Saleh, P. Han, C. Keppel, P. Gueye, V. Yanovsky, and D. Umstadter, "Status of the LILAC experiment," AIP Conf. Proc. **569**, 127 (2001).

[6] P. Zhang, N. Saleh, S. Chen, Z.M. Sheng and D. Umstadter, "Laser-energy transfer and enhancement of plasma waves and electron beams by interfering high-intensity laser pulses," Phys. Rev. Lett. **91**, 225001-1 (2003).

[7] N. Saleh, P. Zhang, S. Chen, C. Widjaja, W. Theobald, V. Yanovsky, and D. Umstadter, "Towards realizing optical injection of electrons in reasonantly excited plasma wakefields," submitted to PAC2003.

[8] X. Wang, N. Saleh, Mohan Krishnan, H. Wang, S. Backus, M. Murnane, H. Kapteyn, D. Umstadter, Q. Wang, and B. Shen, "Generation of mega-electron-volt electron beams by an ultrafast intense laser pulse," *J. Opt. Soc. Am. B* **20**, 132 (2003).

[9] X. Wang, M. Krishnan, N. Saleh, H. Wang and D. Umstadter, Phys. Rev.Lett. **84**, 5324 (2000).
[10] N. Saleh et al., "Low Divergence Laser-Plasma-Based Beams," PAC 2001, Proceeding of the 2001 Particle Accelerator Conference, Chicago, Illinois U.S.A., June 18-22, 2001, Editors, P. Lucas, S. Webber, (IEEE, New Jersey, 2001), p. 4029.
[11] V. Malka et al., Science **298**, 1596 (2002).
[12] S.-Y Chen et al., "Detailed dynamics of electron beams self-trapped and accelerated in a self-modulated laser wakefield," Phys Plasmas **6**, 4739-49 (1999).
[13] Chao et al., Physical Review, Special Topics in Accelerators and Beams, **6**, 024201 (2003).
[14] E. Dodd and D. Umstadter, "Coherent control of stimulated Raman scattering using chirped laser pulses," *Phys. Plasmas* **8**, 3531 (2001).

[15] F. He Y. Y. Lau, D. Umstadter, and R. Kowalczyk., "Backscattering of an intense laser beam by an electron," Phys.Rev.Lett. **90**, 055002-1 (2003).
[16] Fei He et al., "Phase dependence of Thomson scattering in an ultraintense laser field," Phys Plasmas **9**, 4325-9 (2002).
[17] Y.Y. Lau F. He, D. Umstadter, "Nonlinear Thomson scattering: a tutorial," Phys Plasmas **10**, 2155-62 (2003).
[18] S.-Y Chen et al., "Observation of phase-matched relativistic harmonic generation," Phys.Rev.Lett. **84**, 5528-31 (2000).
[19] S. Banerjee, A. R. Valenzuela, R. C. Shah, A. Maksimchuk, and D. Umstadter, "High-harmonic generation in plasmas from relativistic laser-electron scattering," Journal of the Optical Society of America B (Optical Physics) **20**, 182-90 (2003).
[20] K.Ta Phuoc et al., "X-ray radiation from nonlinear Thomson scattering of an intense femtosecond laser on relativistic electrons in a helium plasma," Phys.Rev.Lett. **91**, 195001-1 (2003).
[21] K. Flippo, A. Maksimchuk, S. Banerjee, K. Nash, V. Wong, T. Lin, K. Nemoto, V. Yu. Bychenkov, Y. Sentoku, G. Mourou, and D. Umstadter, "Study of Energetic Ion Generation from High-Intensity-Laser Dense-Plasma Interactions," AIP Conf. Proc. **647**, 255 (2002).
[22] K. Flippo, S. Banerjee, V. Yu. Bychenkov, S. Gu, A. Maksimchuk, G. Mourou, K. Nemoto, and D. Umstadter, "Laser acceleration of protons from thin film targets," AIP Conf. Proc. **569**, 553 (2001).
[23] K. Nemoto, A. Maksimchuk, S. Banerjee, K. Flippo, G. Mourou, D. Umstadter, V. Yu. Bychenkov, Appl. Phys. Letts. **78**, 595 (2001).

3.7. The Advanced Accelerator R&D Activities at Argonne

Wei Gai, Argonne National Laboratory
mail to: wg@hep.anl.gov

3.7.1. Introduction

The Advanced Accelerator R&D Group at Argonne National Laboratory (ANL) focuses on the physics and technology of advanced methods to accelerate charged particle beams with the potential to impact the world-wide, high-energy physics program. Experiments are carried out at the Argonne Wakefield Accelerator (AWA) facility [1], which was designed, constructed and operated by the group for the last 8 years.

The central focus of the program is the development of advanced acceleration concepts that are more efficient, compact, and inexpensive than present-day particle

accelerators. The major effort of the group is spent developing: (1) the electron beam-driven dielectric wakefield acceleration scheme; (2) the electron beam-driven plasma wakefield acceleration and focusing technology; (3) techniques to generate high-power rf using dielectric-lined waveguides or other types of slow wave structures; (4) enabling technologies for photocathode-based electron sources necessary to produce electron beams with the required characteristics for the all of the above; and (5) externally rf-driven dielectric-loaded structures.r

3.7.2. Historical Milestones

The Advanced Accelerator R&D Group has an impressive list of major accomplishments: the first ever demonstration of collinear wakefield acceleration in dielectric devices, plasmas, and disk-loaded structures; the first ever direct measurement of transverse wakefields in linac structures (including the NLC prototype design); generation of high-current beams unique among RF photocathode based linacs (for example, the group was the first to produce individual electron bunches with charge in excess of 100 nC); production and measurement of high, accelerating-gradients in both plasmas and dielectric structures; originated and demonstrated the principle of the wakefield step-up transformer using dielectrics. The AWA facility also serves as a general purpose resource for the high-energy physics community. A few notable examples of past collaborative efforts include: the Tesla Test Facility photoinjector test with FNAL; the non-linear plasma wakefield experiment with UCLA; coherent Cherenkov and transition radiation with JPL and UCLA; positron source measurements with APS; and laboratory astrophysics with the University of Hawaii. In the near-term, experiments have been planned for the AWA facility by DULY Research (high-frequency, high-power RF generation) and Euclid Concepts (advanced collinear wakefield dielectric acceleration). Several other institutions are currently developing plans for experiments to be performed at the AWA. This program has also served as a training ground for many Ph.D. thesis students.

3.7.3. Research Focus

A major portion of the group's effort is spent on the development of electron beam-driven wakefield acceleration schemes [2]. The term *wakefield* refers to the electromagnetic fields left behind a charged particle beam passing a discontinuity in a beamline. If this discontinuity happens to be a resonant device, like an iris-loaded or a dielectric-loaded structure, the beam will drive structure's accelerating modes that can then be used to accelerate a second beam. The fundamental concept of *electron beam-driven wakefield acceleration* is that a high-current, low energy electron beam can be used to accelerate a separate low-current electron beam to high energies. This concept may also be used as the basis of the *plasma wakefield accelerator*, where the electron beam is used to excite large amplitude electrostatic oscillations in plasma, which can be used to accelerate a second beam.

In addition to development of wakefield-based acceleration schemes, the group is also involved in the design and operation of novel photocathode sources [1]. The 1/2 cell AWA drive gun has produced unprecedented 100 nC and 30 ps electron beams. Based on our prior experience with high current photoinjectors, we have developed a third-generation, photocathode-based electron source capable of producing, for the same 100 nC-scale intensities, drive beams which are a factor of three shorter in duration and ten times smaller in emittance than the existing gun. The improvement in beam quality translates into significant increases in the performance level of our wakefield accelerator

devices and makes them comparable to, or exceeding, those of conventional, high-frequency structures.

The group also maintains productive collaborations with other institutions. We have proposed and developed a preliminary design of a facility for making high-precision wakefield measurements of NLC structures [3]. Working with S. H. Gold at Naval Research Laboratory (NRL) and R. Ruth's Department at SLAC, we are using the Magnicon Facility at NRL [4] to conduct high-power testing of externally driven, X-band traveling and standing wave dielectric accelerators [5].

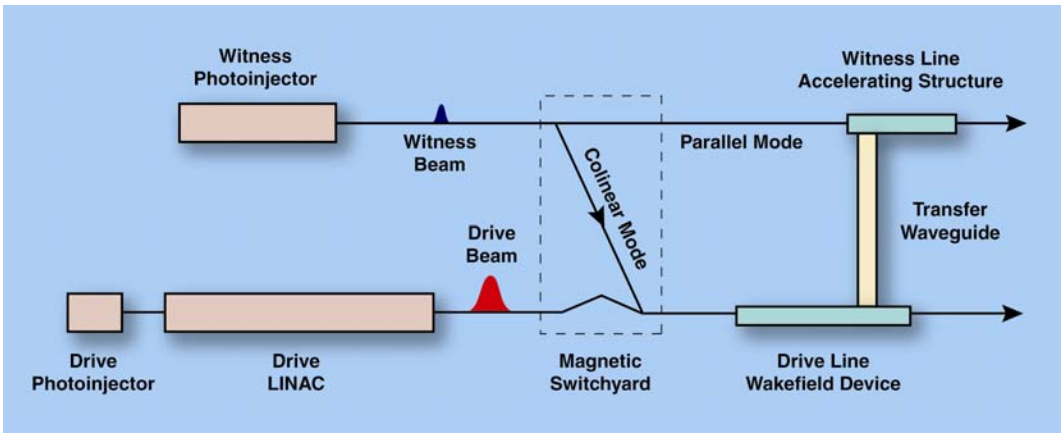

Figure 1. Block Diagram of the Argonne Wakefield Accelerator. A high-current 16 MeV drive beam is steered into the Wakefield Device. The low-current 4 MeV witness beam can be delivered to either of the devices.

3.7.4. The Argonne Wakefield Accelerator Facility

Commissioned in 1996, the AWA's present configuration (Fig. 1) includes a high-current 16 MeV drive line (drive photoinjector + linac) and a low-current 4 MeV witness photoinjector. (A photoinjector is a device where electrons are produced by a short UV laser pulse striking a photocathode located inside a rf accelerating cavity.) The AWA drive photoinjector produces a 100 nC beam pulse, an intensity two orders of magnitude greater than had been attained at the time it was turned on. While the drive beam is always delivered to the drive line wakefield device, the path of the witness beam depends on the mode of operation. When running in collinear mode the witness beam is magnetically steered into the drive line wakefield device. When running in parallel mode the witness beam is delivered into the witness line accelerating structure. And since both beams originate in photoinjectors, it is easy to vary the time separation between the beams by adjusting the optical path of one injector's laser input pulse with respect to the other.

3.7.5. Recent Research Highlights

1) ***New RF Photocathode Gun*** [1]. The new RF gun design was based on our experience with the original AWA drive gun --- which at present is the highest current photoinjector in existence. The new gun was commissioned (Fig. 2) and now operates at the design gradient of 80 MV/m while maintaining vacuum in the 10^{-9} Torr range under full RF power (adequate for the use of high QE photocathodes). During the commissioning period, numerous diagnostics such as emittance pepper pot plates, OTR screens, and Cherenkov radiators, were fabricated and installed in the beamline.

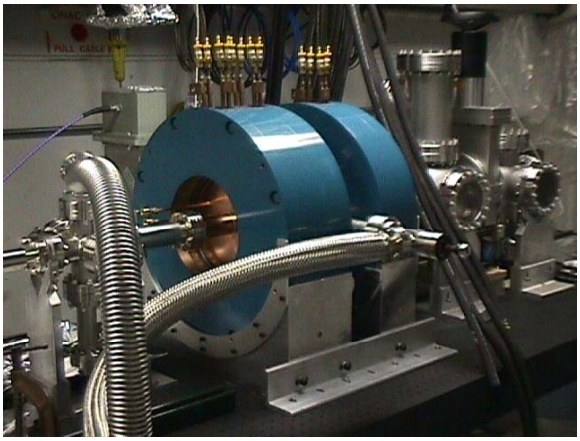

Figure 2. The new RF photocathode gun installed at the AWA during recent commissioning.

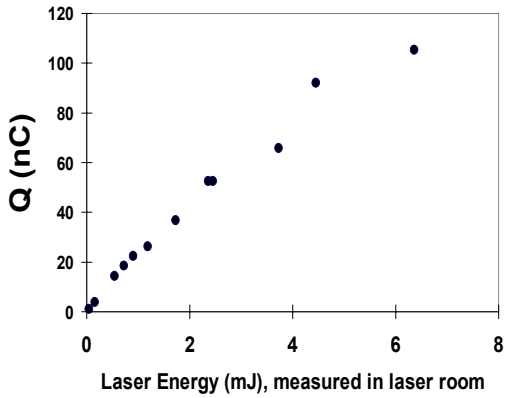

Figure 3. Measured electron beam at exit of the RF gun vs. the laser energy. More than 100 nC beam is generated and its bunch length are measured to be less than 10 ps FWHM.

Using the original Cu cathode, an electron beam was generated with charge ranging from 1 nC to 25 nC and a beam energy of 6 - 7 MeV. Initial beam characterization experiments indicate that the beam emittance is low, however, bunch length measurements using OTR foil proved to be difficult because the OTR light for 6 – 7 MeV beam proved too diffuse and difficult to collect. Thus, the OTR foil has been replaced with a quartz Cherenkov radiator. The original Cu cathode has been recently replaced with a Mg one. Due to the higher QE of Mg, the gun can now produce an electron beam charge of greater than 100 nC (Fig. 3). The electron bunch length of the Mg produced photoelectrons was measured using Cherenkov light emitted from electron beam by passing through a thin quartz plate. The bunch length is in a good agreement with the simulations and its FWHM has been measured to be less than 10 ps for beam up to 70 nC.

2) ***High Power test of the dielectric-loaded accelerator (DLA) at the NRL*** [5]. Due to arcing in the coupler observed during the first round of high power tests (2002) of the DLA structures at NRL [6], we re-examined the coupling scheme and designed a new modular coupling structure (Fig. 4). The modular approach has several advantages: it separates the coupler from the accelerator; the coupling does not depend on location of taper with respect to the aperture; the copper residue on outside of dielectric won't be harmful; larger coupling- aperture lowers the power density. We then fabricated a cold-test alumina-based structure and the results were in good agreement with the theory and simulation. Upon completion of a high-power modular structure, a second round of experiments was performed at NRL using the new modular alumina-based structure. The goals of this test were to confirm that the new RF coupling scheme would function at high power without breaking down and to test the high power

Figure 4. The modular dielectric-loaded accelerating structure installed at NRL.

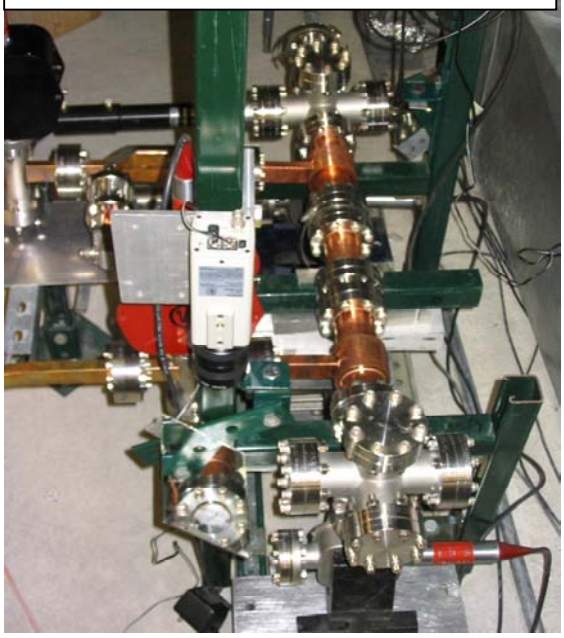

response of the alumina structure.

High Power tests were carried out in 2003 at NRL and went very well. From this run we have drawn the following conclusions: (1) the redesigned DLA structure has eliminated the coupler-arcing problem; (2) no dielectric breakdown was observed at an incident power of > 5 MW; however (3) SEE appears to be absorbing RF power and producing light emission. We are now investigating techniques (TiN coatings, different materials, magnetic field suppression, etc.) to reduce the SEE. For example, a program has been setup to investigate TiN coating on inner radius of the dielectric tubes and we are also constructing a new set of modular structures with a different dielectric material (MCT20) which may have a reduced sensitivity to SEE problems.

3) ***Compact Wakefield Measurement Facility*** [3]. We have investigated the high-brightness electron beam generation at the ANL and its application to a precision wakefield measurement system. Through collaborative work with Fermilab and ANL-APS, it became apparent to us that a compact high-brightness electron beam could be used for precision transverse wakefield measurements of linear collider structures. We have performed numerical simulations of a low charge 1 nC beam using the new AWA gun. Without any attempt at optimizing the hardware parameters (because the gun was already installed in place), we were able to achieve ~ 1 mm mrad transverse emittance and pulse length of 5 ps. These parameters are close to or better all existing RF photocathode guns. Detailed experimental beam characterization was begun in 2003 and will continue this year.

4) ***Other interesting beam physics studies***. Some of the projects carried out at the AWA are not directly related to advanced accelerator R&D, but impact the broader physics community. For example, in a recent collaboration, the high charge electron beam (100 nC) available at the AWA was used to help in the search for ultra high-energy cosmic rays. (greater than 10^19 eV). In this experiment, we conducted another round of coherent and incoherent RF signal generation using an intense electron beam passing through an air and some minerals. This study was for simulating the interaction between an ultra high energy cosmic ray and air and it is conducted by University of Hawaii and UCLA. Data were collected and is now being analyzed.

3.7.6. References

1. M. E. Conde, W. Gai, R. Konecny, X. Li, J.G. Power, P. Schoessow, and N. Barov, "*Generation and Acceleration of High Charge Short Electron Bunches*", Phys. Rev. ST Accel. Beams 1, 041302 (1998); or "*A New High Intensity Electron Beam for Wakefield Acceleration Studies*", Particle Accelerator Conference 2003 (PAC2003) , May 12-16, 2003 at Portland, Oregon

2. M. Rosing and W. Gai, "Longitudinal- and transverse- wake-field effects in dielectric structures", Phys. Rev. D **42**, 1829 (1990).

3. J. G. Power, W. Gai, J. Lewellen, S. Milton, K.J. Kim, J. Simpson, H. Wang, D. Finley, H. Carter, *"A Compact Wakefield Measurement Facility,"* Particle Accelerator Conference 2003 (PAC2003) , May 12-16, 2003 at Portland, Oregon (ANL-HEP-CP-03-44)

4. S.H. Gold et al., in Advanced Accelerator Concepts, AIP Conference Proceedings 647, pp. 439–447 (2002).

5. J. G. Power, W. Gai, C. Jing, R. Konecny, W. Liu *ANL* , A.K. Kinkead *LET Corporation*, S.H. Gold *Naval Research Laboratory, "High Power Testing of X-Band*

Dielectric-Loaded Accelerating Structures," *PAC2003,* May 12-16, 2003, Portland, Oregon (ANL-HEP-CP-03-43)
6. J.G. Power, W. Gai, C. Jing, R. Konecny, S.H. Gold. and A.K. Kinkead, "High Power Testing of ANL X-Band Dielectric-Loaded Accelerating Structures", in *Advanced Accelerator Concepts*, AIP Conference Proceedings 647, edited by Christopher E. Clayton and Patrick Muggli, New York: American Institute of Physics, 2002, pp 556-564.

3.8. Intense Laser Pulse Guiding in Preformed Plasma Waveguides

M. C. Downer**,** Department of Physics, University of Texas at Austin,

Austin, TX 78712, USA

mail to: downer@physics.utexas.edu

3.8.1. Abstract

Preformed plasma waveguides capable of controllably guiding relativistically intense femtosecond laser pulses over multiple Rayleigh lengths without optical distortion are essential to developing GeV-scale laser wakefield accelerators (LWFAs). We present recent experimental results showing guiding of pulses at intensities above 10^{17} W/cm^2. Pump-probe experiments further characterize guided pulse propagation, and provide tools for characterizing channeled LWFAs. Particle-in-cell simulations of a Raman-seeded channeled LWFA are presented.

3.8.2. Introduction

Preformed plasma channels provide damage-resistant wave-guides for intense laser pulses that can extend the length of a plasma accelerator stage from one diffraction-limited Rayleigh length (typically $z_R \sim 10^{-2}$ cm) to tens or hundreds of z_R. They can potentially improve current laser accelerator performance in several ways [1]. First, they can increase maximum particle energy from the MeV to the GeV range. Secondly, they can improve the accelerator's stability, efficiency and average current. This is because un-channeled accelerators (*e.g.* the much-studied self-modulated LWFA [2]) rely on rapid growth of high-density plasma waves driven at extremely high laser intensity, at the cost of unstable laser-plasma interaction and low laser pulse repetition rate. A guiding channel enables LWFAs that operate in a stable, linear regime of laser-plasma interaction that requires less energetic driving pulses. Finally, laser accelerators in preformed channels will have longer plasma wavelength than un-channeled laser accelerators. Consequently, they provide better opportunity for phased injection, and thus lower energy spread, than current high-density laser accelerators.

Single pulses with peak intensity $I_{guided} > 10^{17}$ *W/cm*^{2} have been guided through plasma channels generated by two main methods. One type is formed inside solid capillaries (*e.g.* by ablating the inner wall [3] or by thermally inducing density gradients in a gas-filled interior [4]). Such channels tend to support modes with radii in the range $20 < w_0 < 40\ \mu m$, are usually limited to low repetition rates (< 1 *Hz*), and require replacement of the capillary after a finite number of shots. A second type of channel, developed by Milchberg *et al.* [5], is formed by cylindrical shock waves emanating from the line-focus of a laser in a gas backfill or jet [5,6]. These channels tend to support smaller modes ($w_0 < 10\ \mu m$), can operate at higher repetition rates and are indefinitely replenishable. $I_{guided} \approx 10^{18}$ *W/cm*^{2} is needed to produce high-amplitude channeled LWFAs.

3.8.3. Intense pulse guiding through fully-ionized helium channels

We have achieved distortion-free guiding of single 80 fs, 800 nm pulses over $60z_R$ ($1.5\ cm$) at $I_{guided} \approx 2 \times 10^{17}\ W/cm^2$ in a fully-ionized channel of the Milchberg type formed in a He backfill [7]. Although channels form more easily in higher Z gases, the guided pulse typically suffers distortions at $I_{guided} > 10^{16}\ W/cm^2$ as a result of ionizing residual incompletely ionized cores. By using He, we were able to form fully ionized channels, thus minimizing distortions and enabling higher I_{guided}. Channels were created by sending $400\ ps$, $1\ J$ Nd:YAG laser pulses through the flat base of a conical axicon lens into a $400\ Torr$ He backfill (Fig. 1a, left). Fig. 1a shows fluorescence from the resulting 1-cm-long line focus, which ionizes and heats the gas, driving a cylindrical shockwave radially outward. The expanding He channel profile was probed transversely by shearing interferometry at several time delays $0 < T \leq 6\ ns$ following the arrival of the channel forming pulse (Fig. 1b, top). The interferograms show initial (*i.e.* $T \approx 0.2\ ns$) electron density of $n_e = 3 \times 10^{19}\ cm^{-3}$, consistent with full ionization. By $T \approx 3\ ns$, axial electron density drops to $5 \times 10^{18}\ cm^{-3}$; simultaneously an image of the guided pulse profile exiting the channel (Fig. 1b, bottom row) shows an optimized TEM_{00} mode with radius $w_0 = 8\ \mu m$, and 50% energy throughput (excluding the halo evident in Fig. 1b), corresponding to $I_{guided} \approx 2 \times 10^{17}\ W/cm^2$. No distortion of the pump spectrum is observed under this condition (Fig. 1c). We are currently repeating these experiments with more powerful fs input pulses and differentially-pumped channel entrance and exit regions in an effort to guide fully relativistic intensities ($I_{guided} \approx 10^{18}\ W/cm^2$) without distortion.

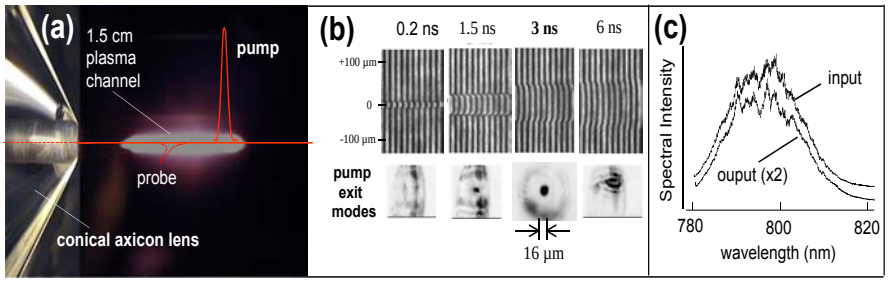

Fig. 1 - (a) Photograph of conical axicon lens (left) and fluorescence from line focus of channel-forming laser pulse. Orthogonally-polarized pump and probe pulses are focused by a parabolic mirror through an axial hole in the conical lens into the channel entrance. (b) Characterization of He plasma channels and guided pump pulses. Top row: transverse Mach-Zehnder interferograms of the expanding channel at 4 time delays after line focus of the channel-forming pulse. Bottom row: Mode images of the exiting pump pulses. (c) Spatially integrated spectra of the input and output pump pulses at $I_{guided} = 2 \times 10^{17}\ W/cm^2$, $T = 3$ ns.

3.8.4. Femtosecond pump-probe study of preformed plasma channels

Femtosecond pump-probe experiments will be essential for characterizing LWFA inside plasma waveguides. In particular, double-probe frequency-domain interferometry (FDI), which has been widely used to characterize un-channeled laser-plasma accelerators [8-10], and photon acceleration [11], in which a trailing probe pulse blue-shifts in frequency at locations in a plasma wave where electrons accelerate, are well suited for plasma channel diagnostics because of their high sensitivity and their ability to yield fs-time- and μm-space-resolved data in both multi- and single-shot configurations.

To adapt these techniques to channels, we performed a preliminary pump-probe study with pump intensity $I_{guided} \approx 2 \times 10^{17}$ W/cm^2 in the He channel [12]. Probe pulses ($I_{probe} \approx 10^{14}$ W/cm^2) were split from the pump, passed through a variable time delay Δt, rotated in polarization by 90°, then recombined with the pump at a thin film polarizer. An f/10 off-axis parabolic mirror focused the co-propagating, orthogonally-polarized pump and probe pulses to the channel entrance. Pump and probe pulses of the same wavelength were used to ensure that they traversed the channel with identical group velocities (Fig. 1a). A polarization analyzer isolated the probe pulse before the detector. To implement FDI, an additional "reference" pulse is needed to interfere with the probe. However, because of the difficulty of coupling multiple pulses into the small core of a plasma fiber, we instead used a depolarized component of the pump pulse as a "built-in" reference pulse. This component can be created intentionally by rotating the incident pump polarization slightly, or advantage can be taken of the natural pump depolarization inherent in its interaction with the channel. Light exiting the channel was imaged with 100× magnification onto the entrance slit of an imaging spectrometer. A two-dimensional CCD recorded single-shot probe (+ pump leakage) spectra with ~1 μm spatial resolution along the dimension parallel to the slit (Fig. 2a).

Fig. 2b shows representative results. Except for $\Delta t \approx 0$ (middle panel), FDI fringes of period proportional to Δt^{-1} are clearly visible along the wavelength (horizontal) axes. Moreover, the fringes show a distinct spatial tilt, that reverses sign on going from Δt = +700 fs (top row) to Δt = -700 fs (bottom row). Such tilts signify an asymmetric phase front on one of the interfering pulses that was not present before it was injected into the channel. In the present case, the weak depolarized component of the pump pulse develops an asymmetric mode structure $E_{depol} \propto x\ exp(-x^2)$ that accounts for the measured fringe tilt. Calculated interferograms, shown on the right, based on a model of pump depolarization, indeed reproduce the main observed features. Quantitative analysis showed that most of the depolarization originates not in the main channel, but in short transitional regions near the entrance where the channel is denser and narrower [12]. In future experiments, the same technique will be used to measure non-Gaussian phase structure imposed on the probe pulse by its interaction with channeled wakefields.

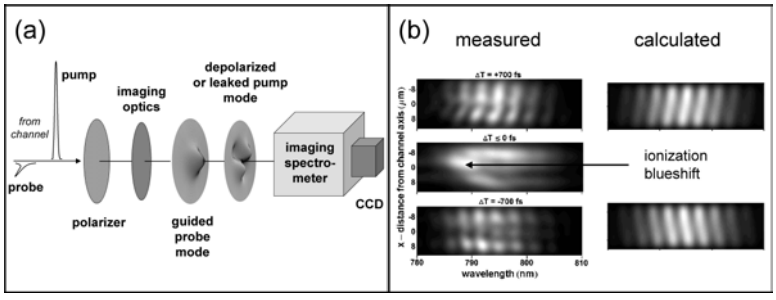

Fig. 2 - (a) Experimental configuration for fs-time-resolved, μm-space-resolved pump-probe measurements of plasma channel using frequency-domain interferometry. (b) Typical single-shot FDI results at three pump-probe time delays (ΔT = + 700, ~ -50 and -700 fs). Fringe tilt at 700 fs signifies an asymmetric phase distortion imposed on one of the pulses as a result of its interaction with the channel - in this case, on the pump, because of depolarization, in agreement with calculation. The same technique can measure phase distortions on probe caused by channeled wakefields. The weak ionization blueshift seen at $\Delta T \approx$ -50 fs characterizes residual un-ionized gas.

At $\Delta t \approx 0$ (middle panel in Fig. 2b), FDI fringes were absent, but a blue-shift of the spectrum of the channeled probe pulses was observed near the center $(x \approx 0)$ of the guided mode, even though no blue-shift was detected in the transmitted pump pulses (see Fig. 1c). This blue-shift is caused by pump ionization of residual un-ionized gas (< 1% of plasma density). However, at $I_{guided} \approx 10^{17}$ W/cm^2 the He ionization front occurs so far in the leading edge of the pump pulse that it shifts only an unobservable fraction of its energy. The peak of the probe pulse, on the other hand, can be timed to "ride" the ionization front, thereby causing a large fraction of its energy to shift. Thus the blue-shift of an appropriately timed probe pulse more sensitively characterizes residual ionization than the transmitted pump spectrum alone. In future experiments, probe blue-shifts will be used to characterize the accelerating gradients of channeled wakefields by photon acceleration.

3.8.5. Simulation of channeled Raman-seeded wakefield accelerator

Most simulations of channeled LWFA have concentrated on the "resonant" LWFA, for which the duration τ of the driving laser pulse is approximately equal to a period ω_p^{-1} of the plasma wave [1]. With resonant LWFA, high amplitude wakefields (~ *1 GV/cm*) can be generated in a stable, linear regime of laser-plasma interaction over a dephasing length of ~ *1cm*, in principle enabling single-stage acceleration to *1 GeV*. However, channeled resonant LWFA requires terawatt laser pulses of $\tau \leq 20$ *fs* duration because channel generation becomes increasingly difficult at densities below $n_e \approx 10^{19}$ cm^{-3}. Moreover, charged particles must be injected externally into the accelerator.

As a complementary approach that may be useful for low energy applications such as radiation oncology and isotope production, we are investigating Raman-seeded (RS) LWFA [13]. In RS-LWFA a weak seed pulse with frequency $\omega_{seed} \approx \omega - \omega_p$ co-propagates inside the envelope of the strong driving pulse with frequency ω. As in self-modulated LWFA, the pulse durations significantly exceed a plasma period ($\tau >> \omega_p^{-1}$), so RS-LWFA is compatible with plasma densities $n_e \sim 10^{19}$ cm^{-3} present in many types of plasma channels. However, in sharp contrast to self-modulated LWFA, the seed enables the plasma wave to grow to large amplitude in a controlled manner even with driving pulses of sub-relativistic intensity (*i.e.* normalized vector potential $a_0 < 1$). Moreover, with a guiding channel, driving pulses below the threshold of the relativistic self-focusing instability can be used [13]. Such pulses can be generated at repetition rates approaching *1 KHz*. Thus RS-LWFA can potentially produce much larger average currents than self-modulated LWFA.

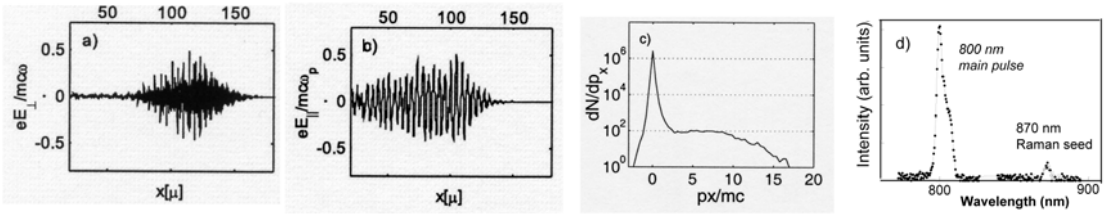

Fig. 3 - 2D PIC simulations of Raman-seeded LWFA in a preformed plasma channel. Longitudinal profile of the electric field of a) laser pulse and b) wakefield after $2.5z_R$; c) momentum distribution of electrons picked up and accelerated by wakefield; d) experimental spectrum of 800 nm main pulse and 870 nm Raman shifted pulse generated by stimulated Raman scattering in barium nitrate.

Fig. 3 illustrates the result of a 2D particle-in-cell simulation of channeled RS-LWFA based on the VORPAL code [14]. A driving pulse with a peak field of only a_0 =

0.35 --- nearly one order of magnitude weaker than typical driving fields for self-modulated LWFA --- was injected into a channel with a seed pulse ($a_{oseed}/a_o = 0.1$) co-propagating in its leading edge. Fig. 3a shows the total laser field at 2.5 z_R into the channel. The pulse has developed a strong, uniform modulation. Moreover, its transverse structure (not shown) is well preserved because transverse self-modulation and filamentation are greatly suppressed in the absence of relativistic self-focusing. Fig. 3b shows the corresponding channeled wakefield. It has high amplitude, but does not break. Figs. 3c shows the energy distribution of the electron bunch of *0.33 nC* generated in a well collimated beam by the seeded pulse in the channel. Fig. 3d shows the power spectra of the main pulse and Raman-shifted seed pulse that we are using in our laboratory to investigate the RS-LWFA.

3.8.6. Conclusion

Preformed plasma channels capable of guiding relativistically intense laser pulses over more than *1 cm* have been demonstrated in several laboratories. Pump-probe techniques for characterizing channeled LWFAs have been developed. Such channels promise to improve laser-plasma accelerators in several ways, including extending single-stage acceleration to GeV energy, and enabling stable, controlled generation of high-gradient wakefields at repetition rates up to *1 kHz*.

3.8.7. References

1. R. Hubbard *et al*., "Simulation and design of stable channel-guided laser wakefield accelerators," *Phys. Rev. E* **63**, 036502 (2001).
2. S. P. Le Blanc *et al*., "Temporal characterization of a self-modulated laser wakefield," *Phys. Rev. Lett.* **77**, 5381 (1996).
3. Y. Ehrlich *et al*., "Guiding of high intensity laser pulses in straight and curved plasma channel experiments," *Phys. Rev. Lett.* **77**, 4186 (1996).
4. A. Butler *et al*., "Guiding of high-intensity laser pulses with a hydrogen-filled capillary discharge waveguide," *Phys. Rev. Lett.* **89**, 185003 (2002).
5. C. G. Durfee *et al*., "Development of plasma waveguide for high-intensity laser pulses," *Phys. Rev. E* **51**, 2368 (1995).
6. P. Volfbeyn *et al*., "Guiding of laser pulses in plasma channels created by the ignitor-heater technique," *Phys. Plasmas* **6**, 2296 (1999).
7. E. W. Gaul *et al*., "Production and characterization of a fully ionized He plasma channel," *Appl. Phys. Lett.* **77**, 4112 (2000).
8. C. W. Siders *et al.*, "Laser wakefield excitation and measurement by femtosecond longitudinal interferometry," *Phys. Rev. Lett.* **76**, 3570 (1996).
9. J. R. Marques *et al*., "Laser wakefield experimental study of nonlinear radial electron oscillations," *Phys. Plasmas* **5**, 1162 (1998).
10. H. Kotaki *et al*., "Direct measurement of coherent ultrahigh wakefields excited by intense ultrashort laser pulses in a gas-jet plasma," *Phys. Plasmas* **9**, 1392 (2002).
11. S. C. Wilks *et al*., "Photon accelerator," *Phys. Rev. Lett.* **62**, 2600 (1989).
12. R. Zgadzaj *et al*., "Femtosecond pump-probe study of preformed plasma channels," submitted to *J. Opt. Soc. Am. B* (2004).
13. M. Fomytskyi *et al*., "Raman-seeded laser wakefield acceleration," submitted to *Phys. Plasmas* (2004).
14. Nieter and J. R. Cary, "VORPAL: a versatile plasma simulation code," *J. Comp. Phys*., in press (2004).

3.9. Acitivity at ICR, Kyoto University

A. Noda, Institute of Chemical Research (ICR), Kyoto University, Japan
mail to: noda@kyticr.kuicr.kyoto-u.ac.jp

At Institute for Chemical Research (ICR), Kyoto University, activities of the group belonging to the graduate course of Department of Physics, Faculty of Science have been shifted to accelerator and beam physics from nuclear physics after the shutdown of the old cyclotron in 1985. Utilizing 7 MeV proton linac consisting of RFQ and Alvarez type cavities of 433 MHz and100 MeV electron linac with disc-loaded type S-band acceleration tubes and 300 MeV electron storage ring, KSR, various researches have been pursued [1]. KSR is also utilized as a stretcher of the electron beam from the linac with combined use of the third order resonance and RF-Knockout method, which provided the electron beam duration from 0.1 sec to several hundreds seconds with the duty factor larger than 90% [2].

3.9.1. Laser produced Ion Beam as the Injection Beam for Cancer Therapy Synchrotron

Recently, downsizing of an accelerator utilizing the advanced technology such as high-power short-pulse laser has become one of the major research scopes of the facility A high power laser is known to produce high energy electron and ion beams by its very high electromagnetic field when it is focused into a very high power density higher than 10^{18} W/cm^2. By collaboration with JAERI, Kansai Research Establishment, National Institute of Radiological Sciences, University of Tokyo and Hiroshima University, it has been shown that the proton production from a thin (5μm) foil target can be explained by under dense plasma model for the case accompanied with pre-pulse [3].

The energy spectrum of the produced ions has no peak and the intensity of the produced ions decreases exponentially according to the increase of the energy. Phase rotation of laser produced ions with use of an RF electric field synchronized to the pulse laser is proposed in order to improve this situation [4]. A λ/4 RF cavity with double gaps of the same frequency as the source laser is utilized for this purpose. By this scheme, we aim at the reduction of energy spread from ±5% to ±1% as illustrated in Fig.1 without significant beam loss. Another one order of magnitude reduction in energy spread is required for efficient acceleration by a synchrotron, which is attained by the electron cooling.

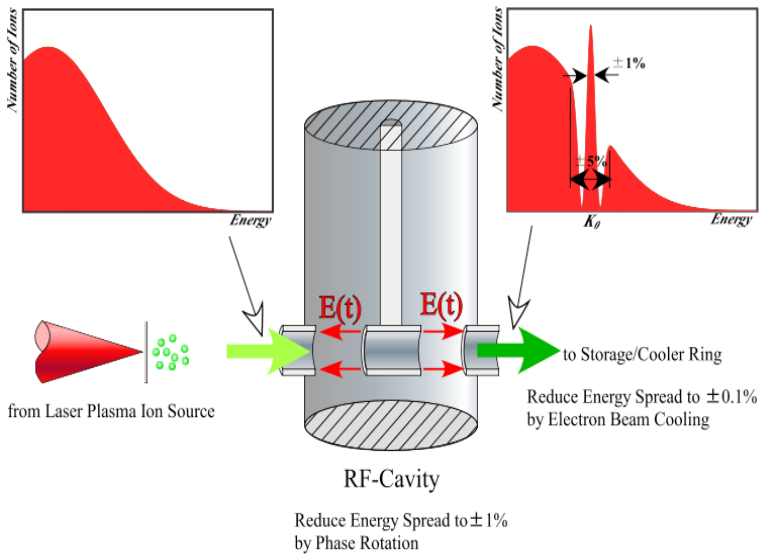

Fig.1. Principle of Phase Rotation of Laser-produced Ions

3.9.2. Electron Cooling of Hot Ion Beam

Electron cooling has so far been considered to be only suitable to cool down rather mild beam to much colder temperature, because of the steep relative velocity dependence of its cooling force, $\mathbf{F_e}$, given by

$$\mathbf{F_e}(\mathbf{v_i}') = -\frac{4\pi n_e Z^2 e^4}{(4\pi\varepsilon_0)^2 m_e} \int L_C(u) f(\mathbf{v_e})$$

where $\mathbf{u}=\mathbf{v_i}-\mathbf{v_e}$ is ion velocity

difference, $L_C(u)=\log(b_{max}/b_{min})$ is the Coulomb logarithm, n_e is the electron density and $f(v_e)$ is the normalized velocity distribution of the electron beam. By sweeping the ion energy with use of an induction accelerator, the ion beam is pushed rapidly to the optimal velocity range of the cooling force as shown in Fig. 2 (a) and damping rate of the longitudinal velocity spread is increased Application of induction acceleration, however, shifts the stable point and acceleration voltage has a threshold, above which the stable point will be lost.

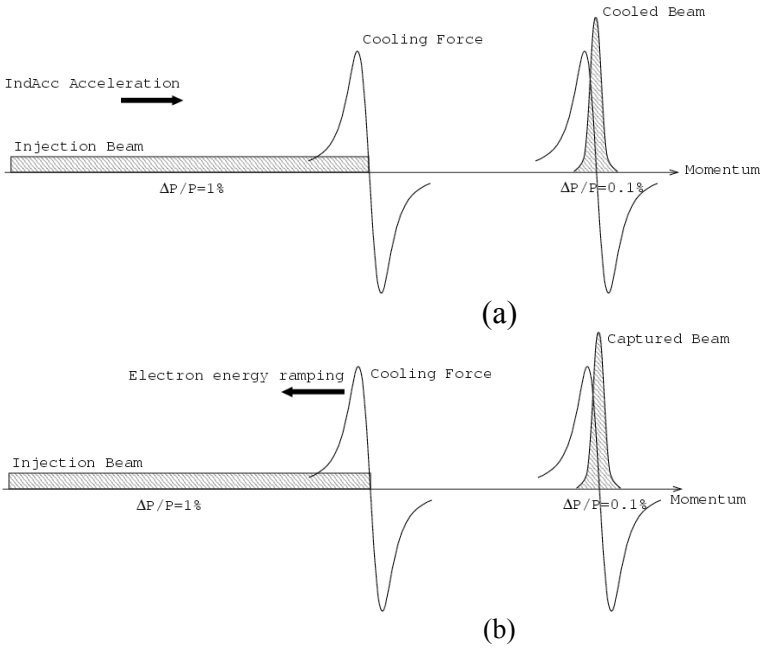

Fig.2 Schemes of electron cooling of hot ion beam, (a) ion energy sweep with use of induction accelerator, (b) electron energy sweep by ramping the high voltage to accelerate the electron.

The proof of principle experiment of the above scheme was made using TSR at Max-Planck-Institut für Kernphysik, Heidelberg. The time needed to shift $^{12}C^{6+}$ beam with the kinetic energy of 73.3 MeV from –1 % less momentum to the central one by an electron beam cooling with electron density of 2.4×10^{7}cm^{-3} was reduced from 2.8 s with no induction voltage to 0.65 s with the induction voltage of 0.4 V. The opposite scheme to sweep the electron energy keeping the ion energy at the same value (Fig.2 (b)) was also experimentally tested at TSR and the cooling time needed was found to be reduced to 0.35 s for small transverse emittance beam [5].

3.9.3. New Cooler Ring for Beam Physics, S-LSR

In the space charge dominant regime, the stability of the ion beam envelope strongly depends on the phase advance per cell both in storage rings and linacs. The new cooler ring, S-LSR has 6 superperiods and the phase advance less than 90˚ in both horizontal and vertical directions [6]. It has two kinds of cooling devices, the electron cooler and the laser cooling system to reach ultra-cold beam temperature. In order to enable the research related to beam crystallization, S-LSR is designed to satisfy the "maintenance condition", which requires (1) beam energy is below transition energy and (2) the phase advance per cell is lower than 127˚. In order to avoid the effect of shear

force, the possibility to compensate the dispersion in deflecting section by superposing the radial electric field with the vertical magnetic field is also experimentally to be studied [7].

The circumference of S-LSR is 22.557m and the average radius is 3.59 m. The bending radius is 1.05m and the maximum magnetic rigidity is 1 Tm. The engineering features are high precision of the magnet fabrications, stable power supplies, good alignments and good vacuum conditions. The 6 bending magnets and the 12 quadrupole magnets have already been fabricated precisely from the block iron. The deviation of BL product and the filed uniformity are better than 10^{-4}. The injector of the high intensity proton beam to S-LSR is an RF linac, which consists of 2 MeV RFQ and 7 MeV DTL. The heavy ion injector is a 35 keV sputter ion source, CHORDIS.

Short bunch formation with use of the electron cooler is one of the major research scopes of S-LSR [8] Research capability of pulse radiolysis with ion beams will be provided by adding fast extraction channel to S-LSR, which is expected to be applicable also for possible “crystalline beam”.

3.9.4. Super-Strong Permanent Magnet as Final Focus Quad for Linear Collider

High magnetic field generation as high as 4.45T has been demonstrated without superconducting technology. High magnetic flux density is usually generated by Halbach’s configuration [9], which consists only permanent magnet materials. The higher magnetic flux density is achieved by the modified Halbach’s configuration, which introduces saturated iron poles to the original configuration to enhance the magnetic field strength [10 ,11 ,12]. The magnetic flux density is expected to become higher when we cool down it further. When the same technique is applied to a permanent magnet quadrupole (PMQ), it can generate a higher magnetic field gradient than a plain electromagnet. This feature may have advantage in the linear collider since it needs rather stronger magnetic field gradient [13].

The fabricated PMQ was designed so that it demonstrates the highest field gradient at a given bore radius. The inner and outer diameter are ø14 mm and ø100 mm, respectively. It is segmented into 12 trapezoidal sections and inner parts of four of them are replaced by soft iron material. The outer diameter of the SUS case is ø130 mm, which can leave a space for outgoing beam after the interaction point assuming that the crossing angle of the two colliding beams is set to 0.02 radian and that the distance between the interaction point and the edge of the quadrupole is 3.5m. The total length of the quadrupole magnet is 10cmwhile that of the iron poles is 9cm. Both ends of the iron poles are capped by extra permanent magnet pieces, which push the flux in and reduces the fringing field. The field gradient with this configuration is calculated as 0.3T/mm [[14,15]]. The measurement of the magnet is performed at SLAC [16] using a rotating coil. Figure 3 shows the assembled PMQ and the measurement setup. The measured integrated field gradient was 28.5 [T] while the calculated value was 29.7 [T]. About 5% difference seems reasonable according to our experience.

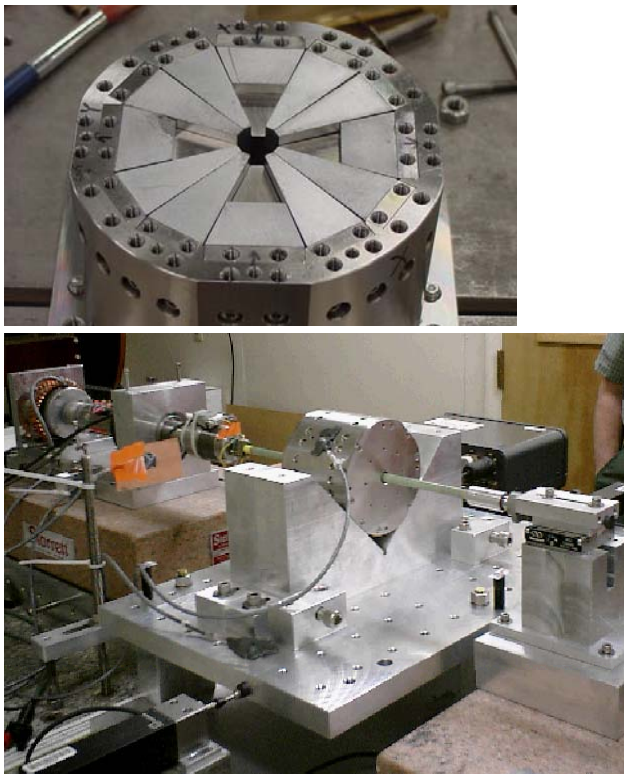

Fig. 3 The assembled PMQ (top) and the measurement setup (bottom). The endplate is removed to show the magnet in the top figure.

Because a temperature coefficient of the magnet material is not small (~0.1%/°C), we are testing a compensation method using high temperature coefficient material MS-1, which has been long used to stabilize magnetic field strength of permanent magnets. Another advantage of the introduction of the saturated iron is that the temperature coefficient of the soft iron is much less than the permanent magnet material and thus the resulted temperature coefficient becomes slightly smaller. The preliminary results seem promising.

In order to use such permanent magnets in a beam line, we need a capability to adjust the strength. Although rotations of one or more PMQ's in a set of PMQ's have been used for such purposes, it introduces skew components, which should be strongly avoided in this application. A rotation of a quadrupole with just 90°, however, changes only its sign (like a switch) and no skew component arises. When a PMQ is longitudinally sliced in binary power way, for example, to have 1, 2, 4, 8cm in length, the rotational switching of the sliced magnets can change its strength in equal steps. Beam optics simulations showed that about 1% resolution (step size) is enough for this device [17] and thus smallest piece of PMQ becomes 1cm in length when the total length is 2m. One weak point of such a scheme is that the movement of the magnetic center caused by the mechanical adjustment of the strength. In order to increase a tolerance in a rotation mechanism, we introduce a nested double ring structure, where an inner ring is fixed, while sliced outer rings can be flipped independently. The tolerances of the outer ring increase about 30 times. [18] The design and the fabrication of such a system is underway. Delivery of this system is expected in this fiscal year.

3.9.5. References

[1].Dewa H, Ao H, Kihara T, Tonguu H, Shirai T, Okamoto H, Iwashita Y, Fujita H, Kakigi S, Noda A, Inoue M, Longitudinal Beam Emittance Monitor for 433 MHz Proton Linac Review of Scientific Instruments 67 No.9, 3085-3091 (1996).

[2] Sugimura T, Morita A, Tongu H, Shirai T, Iwashita Y, Noda A, A Pulse Stretcher by Slow Extraction Utilizing the Third-Order Resonance with the RF Knockout Method JPN. J. Appl. Phys. 41, 2276-2284 (2002)

[3] K. Matsukado, T. Esirkepov, K. Kinoshita, H. Daido,T. Utsumi, Z. Li, A. Fukumi, Y. Hayashi, S. Orimo, M. Nishiuchi, S. V. Bulanov, T. Tajima, A. Noda, Y. Iwashita, T. Shirai, T. Takeuchi, S. Nakamura, A. Yamazaki, M. Ikegami, T. Mihara, A. Morita, M. Uesaka, K. Yoshii, T. Watanabe, T. Hosokai, A. Zhidkov, A. Ogata, Y. Wada, and T.

Kubota," Energetic Protons from a Few-Micron Metallic Foil Evaporated by an Intense Laser Pulse", Phys. Rev. Lett. **91** (2003) 215001.
[4] Noda A, Fadil H, Iwashita Y, Morita A, Nakamura S, Shirai T, Tongu H, Yamazaki A,Daido H,Hayashi Y, Kato Y, Orimo S, Yamakawa K, Beutelspacher M, Grieser M, Li Z, Matsukado K, Noda K, "on Production with a High-Power Short-Pulse Laser for Application to Cancer Therapy", Proc. of the 8th European Particle Accelerator Conf. EPAC 2002 Paris, France. , 2748-2750 (2002).
[5]H. Fadil, A. Noda, T. Shirai, K. Noda, T. Furukawa, M. Beutelspacher, M. Grieser, "Electron cooling of longitudinally hot ion beams", Nucl. Instr. and Meth in Phys. Res. A, in print (2003).
[6] Shirai T, Fadil H, Ikegami M, Iwashita Y, Noda A, Tongu H, Yamazaki A, Okabe K, Okamoto H, Yuri Y, Morita A, Grieser M," Design of New Compact Cooler Ring for Crystalline Beams", Proc. of the 8th European Particle Accelerator Conf. EPAC 2002 Paris, France. , 623-625 (2002).
[7] Masahiro Ikegami, Manfred Grieser and Akira Noda, "Heavy ion storage ring without momentum dispersion", Phys. Rev. ST-AB, submitted.
[9] Noda K, Furukawa T, Honma T, Muramatsu M, Shibuya S, Takada E, Yamada S, Iwashima T, Ogawa H, Takubo T, Uchiyama H, Fadil H, Noda A, Shirai T, Syresin E.M, Maeda K, Nagafuchi T, "Electron Cooling Experiment at HIMAC Synchrotron", Proc. of the 8th European Particle Accelerator Conf. EPAC 2002 Paris, France. , 1380-1382 (2002).
[10] K.Halbach, IEEE, Trans., NS26(1979),3882, NIM,169(1989) 1, NIM,187(1981) 109, NIM,198(1982) 213.
10. CERN Courier, "Magnet becomes more compact", volume 41,number 7,september 2001, page 9.
[11] M. Kumada, T. Fujisawa, Y. Hirao, M. Endo, M. Aoki, T. Kohda, Y. Iwashita, Bolshakova, R. Holyaka, "Development of a Model 4 Tesla Dipole Magnet", pac2001, June, 18-22, 2001, Chicago.
[12] M. Kumada, T. Fujisawa, Y. Hirao, M. Endo, M. Aoki, T. Kohda, Y. Iwashita, Bolshakova, R. Holyaka, "Development of high field permanent magnets", IEEE Trans. on Applied superconductivity, MT17, 9/24-28,2001,Geneve.
[13] http://lcdev.kek.jp/
[14] Y. Iwashita, M. Kumada, "Permanent Magnet Quadrupole Lens with Variable Strength", Proc. Nanobeam, Lausanne, Switzerland, 2-6 Sept. 2002, CERN Proc.2003-001, p.153.
[15] Y. Iwashita, T. Mihara, E. Antokin, M. Kumada, M. Aoki, "Permanent Magnet Quadrupole For Final Focus For Linear Collider", PAC03, MAY, 12-16,2003,Oregon
[16] C.E. Rago, C.M. Spencer, Z. Wolf, "High Reliability Prototype Quadrupole for the Next Linear Collider", IEEE Transaction on Applied superconductivity, MT17, 9/24-28,2001,Geneve.
[17] http://acfahep.kek.jp/subg/ir/minutes.html
[18] T. Mihara, Y. Iwashita, M. Kumada, A. Evgeny and C. Spencer: "Development of a Final Focus Quadrupole for Linear Collider" IEEE Transaction on Applied superconductivity, MT18, Morioka, 2003.

3.10. Improving the quality of energetic electron beams produced by Laser Wake Field Acceleration

P. Tomassini. M. Galimberti, A. Giulietti, D. Giulietti*, L.A. Gizzi, L. Labate†
Intense Laser Irradiation Laboratory - IPCF, Area della Ricerca CNR, Via Moruzzi 1, 56124 Pisa, Italy

mail to : tomassini@ipcf.cnr.it
WWW: ILIL.ipcf.cnr.it

F. Pegoraro
Dipartimento di Fisica Univ. di Pisa and I.N.F.M Unita' di Pisa, 56124 Pisa, Italy

*also at Dipartimento di Fisica, Universita; di Pisa and INFN, Sezione di Pisa (Italy)
†also at Dipartimento di Fisica, Universita' di Bologna (Italy)

Laser Wake Field Acceleration (LWFA) of relativistic electron bunches is a promising method to produce a large amount of energetic particles with a table-top equipment. To date, the quality of the electron beams produced with the widely used scheme employing a gas-jet system and a single femtoscond laser pulse is very poor, the energy spread being of the order of 100% and the angular divergence usually exceeding several degrees. The Intense Laser Irradiation Laboratory (ILIL, IPCF-CNR) in Pisa, Italy, is currently deeply involved, both on the experimental and theoretical sides, in studies devoted to increase the beam quality of the LWFA produced electron beams. Here we report on the two parallel activities of ILIL in this field. The first achieved its main results started with an experiment held at the LOA facility, based on LWFA in preformed plasmas obtained with the exploding foils technique and demonstrating the production of a relativistic electron bunch with a record value of angular divergence (less than one degree) but still with a large energy spread. The second activity is presently at the theoretical/numerical stage and is aimed to produce electron bunches with both small transverse and longitudinal emittances by taking advantage of the partial nonlinear, longitudinal wave-breaking of the Langmuir wave behind the pulse crossing a sharp density downramp. In this way a large amount of electrons can be injected in a controlled way in the accelerating region of the wake. PIC simulations (3D in the fields and 2D in the coordinates) demonstrate that, once concurring trapping phenomena are inhibited, extremely low values of the beam energy spread and divergence can be obtained.

Short scale-length prefomed plasmas (SSPP) are currently easily produced with the exploding-foils technique [2] in which a foil target of thickness ranging from a fraction of micrometer to few micrometers is exploded by an heating pulse before the arrival of the intense femtosecond pulse, thus producing a fully ionized hot plasma. The use of SSPP as a medium for LWFA experiments has several advantages among the classical scheme gas-jet + laser-pulse, the most relevant being the possibility to study the interaction of a laser pulse with a plasma having scale-lengths comparable with the Langmuir wavelength λ_p. Futhermore, the pulse interacts with an already fully ionized medium, whose electron density map can be accurately estimated [3,4,5]. Finally, diffraction effects on the pulse can be neglected since the longitudinal size of the plasma is usually lower than the focused pulse Reyleigh length. Drawbacks are, however, the intrinsic difficulty of making high repetition-rate experiments, the reproducibility of the single shots results and, of course, the small extension of the acceleration length which limits the energy of the produced bunches to tens of MeV's.

In the above mentioned experiment at the Laboratoire d'Optique Appliquee (LOA) near Paris, France, the SSPP was produced using the nanosecond Amplified Spontaneous Emission (ASE) associated to the $35fs$, $1J$ Ti:Sa laser pulse, which was focused in a $6\mu m$ spot on the target foil [1]. A detailed mapping of the $3D$ preformed plasma density profile was obtained by using both a Nomarski interferometer and advanced numerical analysis methods [3,4,5]. The produced electron bunch was characterized by using either a standard magnetic spectrometer or the novel spectrometer SHEEBA [6,7], having also an angular resolution. The SHEEBA spectrometer consisting of a stack of radiochromic films, which change their optical density according to energy locally released by the beam. With the help of an Monte Carlo based analysis code, an accurate angular and spectral distribution of the single-shot produced electron bunches was obtained. The results show that, with a suitable set of the foil and pulse parameters, energetic bunches composed by an ultrarelativistic and collimated component (energy up to $40MeV$ and divergence less than one degree) and a less energetic ring-like component, are produced by means of the LWFA process. In Fig. 1 an example of the sequence of the images of the released energy in each foil of the stack in SHEEBA is reported.

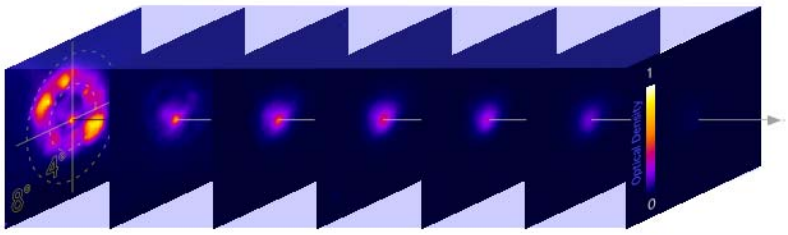

Figure 1: Example of the sequence of patterns prduced by the electrons on the layers in the SHEEBA spectrometer. Electrons are coming from the left and the layer number is increasing on the right. The ring-like and less energetic (few hundreds keV's) component is stopped by the first layer. The more energetic component has an angular divergence less than one degree. The increasing of the central spot size on the layer number is mainly due to the multiple scattering of the electrons by the foils.

We stress, however, that even if the produced electron bunches have a very low angular divergence (to our knowledge, the lowest obtained so far), the energy spectral width is of the order of 100%, i.e. as large as that usually gas-jet systems.

To reach the goal of the production of highly collimated and monochromatic electron beams, an efficient method to control the self-injection of the electrons in the accelerating region is needed. Several mechanisms have been proposed and are currently subject of active studies [8,9,10,11,12]. Among these, controlled injection with partial

longitudinal breaking of the Langmuir wave after a density downramp [11,12], is the mechanism which uses only one laser pulse.

A joint research programme involving the ILIL group, the Physics Department of the University of Pisa, I.N.F.N and I.N.F.M has been recently started, aiming the optimization of the controlled injection by a sharp density downramp method. The first step of the programme was devoted to extend the original results of S. Bulanov et al. [11] in a multidimensional geometry, seeking the occurrence of competitive trapping processes which could degrade the final electron beam quality. The first numerical results of such a collaborations are encouraging [13,14,15]: in an 'ideal' plasma profile consisting of two perfectly flat plateaux, we found a regime in which all the trapping mechanisms except the nonlinear wavebreaking at the transition are inhibited, with the final production of a $10MeV$ bunch with about 5% energy spread and angular divergence about five degrees. The preformed plasma density profile is chosen in order to enable the partial breaking of the wake behind the laser pulse, with a scalelength of the density transition L much smaller than the Langmuir wave number λ_p (sharp density transition). We used a fully relativistic PIC code developed by H. Ruhl [18], which runs on a *SP*4 system at CINECA, Italy [19]. Fig 2 shows the main results of the simulation. The laser pulse propagates along the z direction and it is polarized along y, has a wavelength λ_l=1μm, a duration τ_{FWHM}=17fs full width at half maximum and a waist w_0=20μm. The preformed plasma has longitudinal density profile presenting two contiguous plateaux with a transition having scalelength L=2μm located at z=50μm. The electronic density of the first plateau (region I), where a regular wake develops, and the second plateau (region II) where the trapped particles are accelerated are $n_e^{\ I} = 2.1 \bullet 10^{19} cm^{-3}$ and $n_e^{\ II} = 1.1 \bullet 10^{19} cm^{-3}$, respectively. The laser pulse peak intensity was $I = 2.5 \bullet 10^{18} W/cm^2$, corresponding to a normalized pulse amplitude $a_0 \cong 1.3$. The value of the peak intensity was chosen in order to suppress the trasverse wave breaking process, which can be responsible for the uncontrolled injection of particles and the degradation of the wake field quality.

At the final simulation time the wake is still regular far beyond the pulse, even if an inverted curvature of the constant-phase lines due to beam loading developed (Fig. 2-a and c). The trapped bunch is well localized in the phase-space plot, both longitudinally and transversally and the final energy spectrum consists of a narrow peak with energy spread $\Delta E / E \approx 5\%$ full width at half maximum and a background containing a second bunch with a lower energy and beam quality, which can be easily separated from the first one.

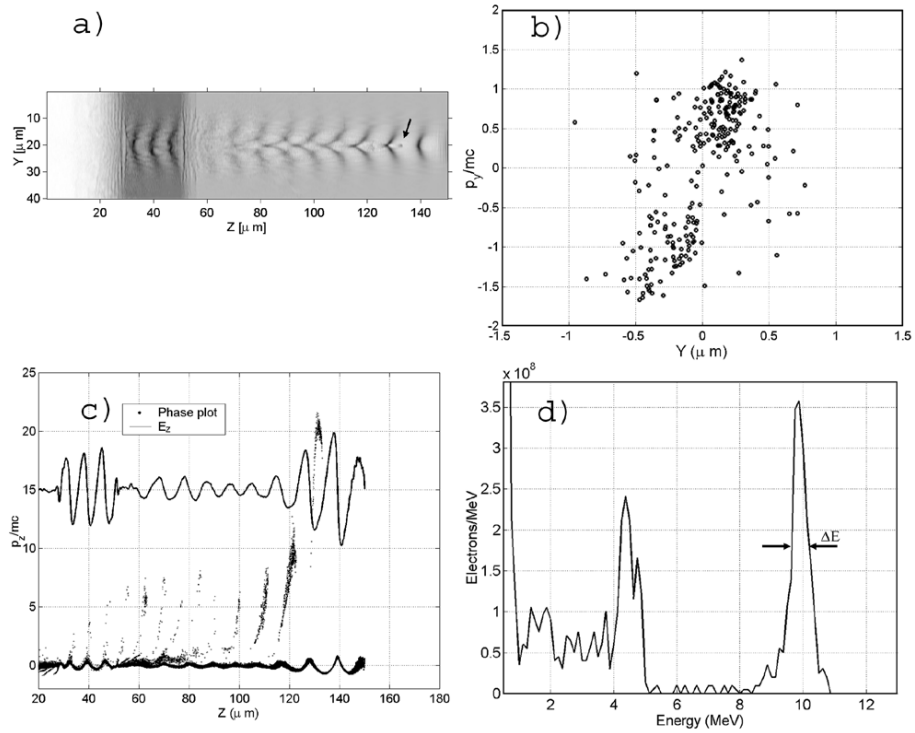

Figure 2: Final simulation time. a) Electron density. The arrow indicates the electron bunch. b) Transverse (y-p_y) phase-space plot of the bunch. c) Line-out on axis of the Longitudinal phase-space plot (single points) and line-out of the longitudinal electric field. Almost all the particles of the bunch are in a region in which the accelerating force is maximum. d) Energy spectrum of the particles accelerated with energy E>0.5MeV.

We stress that remarkable low values of both the normalized *rms* transverse $\varepsilon_n^{\perp} \cong 0.1 mm \cdot mrad$ and longitudinal $\varepsilon_n^{\parallel} \cong 2 mm \cdot keV$ beam emittances can be obtained.

The generation of a plasma with the required tailored plasma density profile is, to date, a challenge. Recently, Hosokai *et al.* [16] have employed a gas-jet system and produced a density transition by inducing in the plasma a shock wave produced by the laser pulse ASE. They demonstrated the trapping and acceleration of electron bunches with low angular divergence, but still having a large energy spread. Another possible method to produce a plasma with an electronic density presenting a sharp downramp employes a couple of plastic thin foils, which are exploded by the irradiation with a heating laser pulse before the arrival of the femtosecond main pulse. In order to test this last scheme with 2D hydrodynamical simulations, we considered an heating pulse of duration 3ns, peak intensity $1 \circ 10^{14} \Omega / \chi \mu^2$, wavelength 0.8μ$m$ and focal spot of about 10μm, counter-propagating with respect to the main pulse. The two parallel plastic foils are placed about 200μm far away and have different thickness (0.1μm and 0.2μm). The simulation of the foils irradiation and plasma formation has been performed with the hydrodynamic eulerian code POLLUX [17] in 2D with azimuthal symmetry. 1.5ns after the arrival of the heating peak pulse, the plasma electron density shows two plateaux separated by a very short scalelength transition (L≈5μm), which is probably the effect of a shock caused by the collision between the expanding plasma regions of the rear side of the first foil and the front side of the second foil. The radial density profile is flat within a radius exceeding 30μm. As a result, a long acceleration region (about 500μm) with a good flatness of the electron density, as well a density transition with a short scalelength, are obtained. The value of the electron density in the accelerating region is optimum for a laser pulse of a duration not exceeding $\tau \cong \lambda_p / c \cong 35 fs$, being c=0.3 μm/fs the light speed.

3.10.1. Acknowledgments

Authors are indebted with H.Ruhl for providing the Particle In Cell code. The PIC simulations have been performed with the support from CINECA High Performance Computing and from INFM Parallel Computing Initiative. Fruitful discussions with S.V. Bulanov were also greatly appreciated.

3.10.2. References

[1] D. Giulietti, M. Galimberti, A. Giulietti, L.A. Gizzi, P. Tomassini, M. Borghesi *et al.*, Phys. Plasmas **9**, 3655-3659 (2002).
[2] L.A. Gizzi *et al.*, Phys. Rev. Lett. **76**, 2278 (1996).
[3] P. Tomassini, *et al.*, Applied Optics. **40** 35 (2001).
[4] P. Tomassini and A. Giulietti, Opt. Comm. **199**, pp 143-148 (2001).
[5] P. Tomassini *et al.*, Laser and Particle Beams **20**, 195-199 (2002).
[6] M. Galimberti, " Electron trapping and acceleration by relativistic laser interactions with underdense plasmas", Ph.D. thesis, Universita' di Pisa (2003); avaible at http: //ILIL.ipcf.cnr.it
[7] M. Galimberti, "SHEEBA: a Spatial High Energy Electron Beam Analyzer", in preparation.
[8] D. Umstadter *et al.*, Phys. Rev. Lett **76**, 2073 (1996).
[9] E. Esarey *et al.*, Phys. Rev. Lett **79** 2682 (1997).
[10]H. Kotaki *et al.*, *submitted to* Phys. Plasmas (2003); ICFA-Workshop 2003, Portovenere (Italy), 9/28-10/3. http: //www.ipcf.cnr.it/plasma_accelerators/.
[11] S.V. Bulanov *et al.*, Phys. Rev. E **58**, R5257.
[12] H. Suk *et al.*, Phys. Lett. **A 316** 233-237 (2003).
[13] P. Tomassini *et al.*, Phys. Rev. ST-AB **6**, 121301 (2003).
[14] P. Tomassini *et al.*, ICFA-Workshop 2003, Portovenere (Italy), 9/28-10/3. http: //www.ipcf.cnr.it/plasma_accelerators/.
[15] P. Tomassini *et al.*, submitted to Laser and Particle Beams.
[16] T. Hosokai *et al.*, Phys. Rev. **E 67**, 036407 (2003). (1997).
[17] G.J Pert, Journal Comp. Physics **43**, 111-117 (1981).
[18] H. Ruhl, *Collective Super-Intense Laser Plasma Interaction*, Als habilitationsschrift dem Fachbereich Physik, Univ. of Darmstadt, 2000.
[19] High Performance Systems Division of CINECA,
http: //www.cineca.it/HPSystems/.

3.11. The TU-Eindhoven high-brightness program

Marnix van der Wiel, Eindhoven University of Technology

At Eindhoven University of Technology, the effort on high-brightness electron guns is focused on two goals: injection into a laser wakefield accelerator and conversion of electron bunch energy into coherent transition radiation in the THz-range. The latter is a new subject introduced recently by staff member Jom Luiten. Both goals require bunch lengths in the sub-100 fs range, from a compact gun.

3.11.1. RF photogun and LWFA

As a first step towards such extremely short bunches, we made a number of innovations to the BNL/UCLA/SLAC photogun. Our 2.5-cell version of this gun is now fully operational (Thesis F.B.Kiewiet, TU-Eindhoven, 1 December 2003, ISBN 90–386–1815–8). Using 30 fs UV-pulses, the gun produces 100 pC bunches at bunch lengths around 1 ps and emittance of order 1μm.rad. Our GPT-simulations (postdoc Bas van der Geer) show that at bunch charges of 5-10 pC, bunch lengths of order 50 fs can be expected. Our short-term goal is to inject such bunches into a 100-fs period plasma wave, driven by a 1 TW-laser in a Hooker-type capillary discharge channel. This would lead to a first demonstration of "controlled" wakefield acceleration, i.e. a bunch shorter than the plasma wavelength is accelerated to tens of MeV with final energy spread well below 100%.

3.11.2. High-gradient pulsed-DC fields

In order to further reduce the bunch length, we have been working for some time towards applying to the photocathode a short-pulsed DC gradient which far exceeds the gradient achievable with RF. A laser-triggered 2 MV, 1 ns pulser, delivered in rudimentary state by the NIEFFA Institute, St. Petersburg, has been upgraded by PhD-student Dmitry Vyuga and is currently capable of producing hundreds of reproducible shots per day. The pulser is now coupled to a small diode-gun (3 mm gap) with an electron beam line including a magnetic spectrometer. The latest result is a measurement of 4 MeV electron bunches, produced by field emission from the cathode during the few-hundred ps top of the high-voltage pulse. This confirms our expectation that doubling of the 2 MV-pulse occurs on the cathode, since it forms an open end to the transmission line. This exciting result, which is based on a 1.3 GV/m gradient, is an important step towards a breakthrough in achievable brightness in photoemitted bunches.

3.11.3. Synchronisation

Before we can start testing photoemission from the pulsed-DC gun, however, the problem of synchronization of the 2 MV-pulse with the Ti-sapphire laser producing the 30 fs UV-pulse, has to be addressed. The jitter of the 2-MV pulse with respect to the trigger laser, presently a 5-ns Nd-YAG laser, is of order 5 ns.

We are engaged in improving the synchronization to less than the 1-ns width of the 2-MV pulse, by using part of the Ti-sapphire output (uncompressed, i.e. at 200 ps) to provide the trigger pulse for the spark gap. This should enable experiments in which photoemitted bunches in the 50-100 fs range can be characterized. For the longer term, we plan to achieve even better control of the 2-MV pulse, the target being risetime and jitter in the 10-ps range. To this end, staff member Seth Brussaard and PhD student Jimi Hendriks are running separate triggering experiments, in which a spark gap, integrated in a co-axial transmission line, is triggered by a cylindrically-focussed TW laser. Current experiments involving 10 kV voltages switched by 40-GW laser pulses, look very promising for achieving the extreme target values. This may eventually open the way to both time-focussing of the bunches and even to multistage acceleration at ≥ 1 GV/m gradients, allowing absolute record brightness.

3.12. Measurements of a Higher-Order Mode Vacuum Photoinjector Cold Test Cell

John W. Lewellen[†,§], John Power[‡], John Noonan[†], Oliver Schmidt[†]
[†]Advanced Photon Source, Argonne National Laboratory
[‡]Argonne Wakefield Accelerator, Argonne National Laboratory
9700 S. Cass Ave, Argonne, IL 60439 USA

[§] Corresponding author
401/B2190 9700 S. Cass Ave.
Argonne, IL 60439 ABÎMA
mail to :lewellen@aps.anl.gov

Typical photoinjected radiofrequency electron guns rely on closely coupled rf cavities to provide initial acceleration and emittance damping of a high-brightness electron beam. These gun designs, while generally successful, are complex to build and are prone to a number of operational problems. These include difficulties in cooling the intercell coupling iris, stored energy limitations for long-pulse operation, frequency pulling due to the strong coupling, and changes to the cell-to-cell rf field balance as a result of small changes to the gun geometry, e.g., cathode replacement. A single higher-order-mode (HOM) rf cavity can be constructed to generate fields appropriate for the generation of a high-brightness electron beam. These designs offer very stable rf field configurations, store more energy, and have no internal structures to pose cooling or arcing problems; however, these benefits come at the expense of higher rf power requirements per unit accelerating gradient than conventional designs. The lack of internal structure renders these designs extremely easy to fabricate, and promises simplified cooling for high-duty-factor operation.

We present the results of mode and beadpull measurements on a higher-order-mode cavity, for both the accelerating mode and other neighboring modes of interest. The calculated axial fields are presented along with the results of simulated beadpull measurements, and we present an approximation for using the standard cylindrical-cavity resonant frequency calculation with these types of cavities.

3.12.1. Introduction

Photocathode rf electron guns, also known as photoinjectors, are generally seen as good candidates for producing high-quality electron beams suitable for use in the next generation of linear colliders and linac-based light sources. The typical photoinjector gun, such as the SLAC/BNL/UCLA 1.6-cell design [1], consists of two resonant cavities operating in a π-mode, has been scaled from L-band (1.3 GHz) [2] to 17 GHz [3], and is in use at many facilities around the world. Typical variations include the addition of a third full-length rf cavity for additional energy gain. A drift distance, usually on the order of 1 m, separates the electron gun itself from a booster linac section. A solenoid magnet either surrounding a portion of the gun, or immediately following it, provides required focusing and allows for emittance growth compensation [4].

The basic 1.6-cell photoinjector design generates reasonably bright electron beams, however there are some features that can impact its successful operation. The field balance between the cells, for instance, is very sensitive to the individual cell tuning, and the iris separating the cells can represent a challenge for high-field, long-pulse, or high-repetition-rate operation. Also, the iris separating the cells presents a challenge to high-

gradient operation, limiting the acceleration that can be applied to the electron beam as it leaves the cathode.

A photoinjector built using a single higher-order-mode (HOM) rf cavity as the gun can address some of these limitations. Specifically, a "vacuum HOM"-based gun can consist of a single cavity with no internal structures such as irises, eliminating cell-to-cell coupling concerns and all issues associated with intercell irises within the cavity. Simulations indicate that a vacuum HOM-based photoinjector, properly constructed, offers potential beam performance approximately equal to that of the typical 1.6-cell design [5]; additional work to be published in the Proceedings of the LINAC 2002 conference].

A cold-test cavity of a single-cell $TM_{0,1,1}$-mode photoinjector has been constructed at the Advanced Photon Source; this paper reports on the initial measurements on the cold-test cavity. These include simulated vs. actual beadpull measurements on the three lowest transverse-magnetic (TM) modes, measurement of some transverse-electric (TE) modes, and the measured validity of approximated mode resonant frequencies in the modified HOM-type cavity.

3.12.2. Test Cell Geometry

The geometry of the test cell is shown in Figure 1. This is different than the geometry described in [5]. The test cell described in this paper is equivalent to a standard SLAC/BNL/UCLA 1.6-cell S-band gun in terms of effective number of cells and device length. Beam dynamics calculations have been performed on this gun and find it to be approximately equal to the standard 1.6-cell gun design in terms of obtainable emittance. Details of the simulation, and more specific comparisons to the traditional designs, are beyond the scope of this paper but are intended for a future publication.

The test cell features an outer wall that has a truncated conic portion, as well as a cylindrical portion. These features, plus the addition of a beam-exit port at one end of the cell, preclude the direct use of the analytic "pillbox" cavity mode calculations. (It has been suggested [6] that an exact solution for a truncated cone could be found using spherical harmonics. This is true; however, given the actual geometry, it would still be only an approximation. As will be shown, the use of the pillbox cavity results represent an adequate starting point for modeling when the taper angle is small.)

A stainless steel cold test model was constructed in three sections: a cathode plate, a cell body shell, and a nose cone plate. Measurements were made with a loop coupler mounted in the side wall of the cell body. To simplify construction, the nose cone plate uses two conic sections to approximate a rounded nosecone geometry. This does not result in a significant variation of the on-axis fields inside the gun proper. In all beadpull simulations, and resonant frequency and axial field calculations, the test cell geometry was used, as opposed to a geometry with rounded nosecones at the exit port.

3.12.3. Resonant Mode Frequencies

The measured frequencies of the the cavity modes are presented in Table 1, along with the results from several simulation codes, and an approximation to the simulation results generated via the pillbox-cavity formulas. Mode identifications are also given. The initial cavity simulations were performed with the code SUPERFISH [7], which solves for axisymmetric modes (m=0) only, and URMEL [8], which can find modes with azimuthal dependence.

The resonant frequencies of the TM (transverse-magnetic) and TE (transverse-electric) modes in a true pillbox cavity are given by [9]

$$f^{TM}_{m,n,p} = \frac{c}{2\pi}\cdot\sqrt{\left(\frac{x_{m,n}}{R_{cav}}\right)^2+\left(\frac{p\pi}{L_{cav}}\right)^2}, \quad f^{TE}_{m,n,p} = \frac{c}{2\pi}\cdot\sqrt{\left(\frac{x'_{m,n}}{R_{cav}}\right)^2+\left(\frac{p\pi}{L_{cav}}\right)^2}, \qquad (1)$$

where m, n, and p are integers specifying the azimuthal, radial, and longitudinal dependence of the field, respectively, R_{cav} is the cavity radius, L_{cav} is the cavity length, $x_{m,n}$ is the n^{th} root of the $J_m(x)$ Bessel function of the first kind of order m, and $x'_{m,n}$ is the n^{th} root of the $J'_m(x)$ derivative of the same. For any given pillbox cavity, therefore, the only free parameters for setting the mode frequencies are R_{cav} and (in the case where $p > 0$) L_{cav}. The HOM cavity geometry is not pillbox due to the taper and the beam exit port; we find, however, that for the lower-frequency modes, the pillbox-frequency equations can be used to find reasonable approximations to the true frequencies.

To generate the approximation, SUPERFISH is first used to find the resonant frequencies of the TM_{010}, TM_{011}, and TM_{012} modes. Then, an rms minimization is performed on L_{cav} and R_{cav} to minimize the difference between the SUPERFISH-calculated frequencies and those given by Eq. (1). Twice the weighting was given to the accelerating $TM_{0,1,1}$ mode in the minimization.

Strictly speaking, the resonant modes of the HOM cavity are neither truly TE nor TM. Based on the appearance of the modes, an argument can be made that a given mode is "TE-like" or "TM-like" in terms of overall field pattern; but the distinction can become blurred, especially at higher mode numbers. Thus the mode identifications are provided as a means to help visualize the mode patterns, rather than as a rigorous identification.

3.12.4. Beadpull Measurements

3.12.4.1.Simulation

Simply comparing the results of a beadpull measurement to the calculated on-axis field profile of a cavity can be misleading due to the bead's finite size and geometry. To help eliminate some of the uncertainties, therefore, SUPERFISH was used to simulate the passage of the bead through the cavity. The result is a calculation of frequency shift vs. bead position, just as one would measure in a beadpull experiment. Both the SUPERFISH output and the measured data can then be processed in an identical fashion and compared directly. The propagation of the bead through the cavity was performed with a general-purpose simulation code sequencer program, **sequence**, written at Argonne National Laboratory. A sample SUPERFISH input "template" is shown in Figure 2. The input deck, as written, allows for a hollow bead, and also allows for increased model mesh density in the vicinity of the bead. SUPERFISH can perform a simulated beadpull only for axisymmetric modes. URMEL, however, did not provide for a sufficiently fine mesh in the vicinity of the bead to the order of accuracy we wished to achieve, therefore nonaxisymmetric mode beadpulls were not simulated.

3.12.4.2.Measurement

Beadpulls were performed on the $TM_{0,1,0}$, $TM_{0,1,1}$, $TM_{0,1,2}$, and $TE_{1,1,1}$ modes. The TM modes were measured with a hollow needle bead, with a length of 8.61 mm, inner diameter 0.508 mm, and outer diameter 0.914 mm. The outer diameter is small enough to allow the bead to pass through the small aperture in the cathode plane. A washer was used to measure the TE mode, as the needle bead outer radius was too small to significantly perturb the off-axis fields, and was also used to measure the TM_{011} mode. The washer had a length of 0.5 mm, an inner radius of 3.43 mm, and an outer radius of 8.02 mm. Both the washer and needle were made of stainless steel and were carried through the cavity on

nylon fishing line. The washer was fitted with an interior plastic bushing to keep it centered on the line; pulling the bushing alone through the cavity did not result in an observable frequency shift. During the actual bead pulls, the bead was typically advanced in 1 – 5 mm increments, with larger shifts in regions of more constant fields. Error in position is taken to be +/- 0.1 mm. The frequency was measured three times at each location. Each bead pull, in total, was done by hand and took on the order of one hour.

The average field $<E_z(z)>$ at each location can be determined via the standard method based on Slater's perturbation theorem [10], which in the absence of a magnetic field (accurate to a reasonable approximation for the on-axis accelerating mode) can be reduced to:

$$|E_z(z)| \cong \alpha\sqrt{f_o - f(z)}\,, \tag{2}$$

where α is a scaling factor, f(z) is the frequency measured at location z, and f_o is the unperturbed frequency. For the needle bead, since the needle can be pulled completely through the cavity, f_o can be written as a function of position,

$$f_o \approx f_{start} + \frac{z - z_{start}}{z_{end} - z_{start}} \cdot (f_{end} - f_{start}), \tag{3}$$

where z_{start} and z_{end} are the bead starting and ending positions, respectively, and should be outside of the cavity volume, and f_{start} and f_{end} are the resonant frequencies measured at z_{start} and z_{end}, respectively. This baseline subtraction helps take into account average temperature variation and calibration drift over the course of the measurement; in general, however, the difference between f_{start} and f_{end} was small enough so as to make this a trivial correction. For the washer beads, the washer could not be completely removed from the cavity at both ends; in this case, f_o was determined from the unperturbed frequency with the bead outside the exit port.

The error in field measurement at each point is calculated via

$$\sigma_E \cong \frac{\left(\delta f + \frac{1}{2}\sigma_f(z)\right)}{\sqrt{f_o - f(z)}}\,, \tag{4}$$

where δf is the frequency resolution of the network analyser, and σ_f is the standard deviation of the three frequency measurements. From this, one would expect to see larger relative errors at smaller on-axis fields, since at those locations the denominator will tend towards zero.

3.12.5. Discussion of Results

In general, as seen in Table 1, both URMEL and SUPERFISH calculated the resonant modes to within reasonable tolerances. The pillbox approximation, as expected, often diverges from the actual mode frequencies by nontrivial amounts, particularly as the mode frequency increases. The main purpose of the approximation, however, is to help ensure that there are no "missed" modes in the vicinity of the accelerating mode, from either an unresolved resonance or a numerical degeneracy in URMEL. Alternately, the technique should prove useful if one does not happen to have access to URMEL or to another code that can calculate nonaxisymmetric modes. For this purpose, the approximation is adequate, and in fact the agreement is, on occasion, good to higher frequencies and to TE modes.

Comparisons of measured and simulated bead pulls with calculated on-axis field profiles are shown in Figures 3 through 6, for the TM-like modes mentioned above. In

these plots, the data points with error bars are experimental data, processed as described in Eqs. (2) – (4). The solid lines show the simulated beadpull data, with frequency offsets computed via SUPERFISH and then processed as described above (but without error bars). The dashed line is on-axis electric field strength as a function of position, as calculated via SUPERFISH. In general, the agreement between simulated and measured beadpulls is acceptable; as expected from Eq. (4), larger error bars occur at smaller measured field strengths. It is interesting to note that the results of both the measured and simulated beadpull measurements do not match the calculated on-axis field profile. This is due to the finite length of the bead. Given that the simulated beadpull measurement provides such a consistently good match to the actual measurement, however, one may say with confidence that the calculated on-axis field is indeed correct. In Figure 5 the washer, rather than the needle, was used to map the TM_{011} mode. Again, the measured and simulated beadpull data agree reasonably well with each other, and also with the calculated on-axis field in high-field regions. It does not accurately resolve the zero crossing at about z=3.2 cm, even though the washer is longitudinally much smaller than the needle, because of the radial extent of the washer. The radial electric field $E_r \sim r \cdot dE_z/dz$; therefore at the zero-crossing E_r can become substantial due to the large longitudinal gradient of the longitudinal field. The comparatively large radius of the disk results in an integration of E_r as well as E_z, blurring the measurement.

Finally, Figure 7 presents the result of a washer beadpull for the TE_{111} mode, along with an URMEL calculation of the on-axis radial field strength. (This is a dipole mode.) As mentioned, a simulated washer pull was not performed for this mode.

3.12.6. Conclusions and Future Plans

The measured resonant frequencies and beadpulls for the higher-order mode cold-test cavity prototype agree very well with both URMEL and SUPERFISH simulations. This increases confidence in electron beam dynamics simulations based on SUPERFISH-generated field maps of the higher-order-mode cavity. The higher-order-mode test cell, as predicted, shows excellent mode separation between the accelerating mode and next-nearest modes. Finally, an approximation to the resonant frequencies of non-TM_0 modes, based on the results of SUPERFISH simulation of TM_0 modes, was generated. While this is clearly only an approximation, it is accurate enough to predict the absence of troublesome modes in the vicinity of the desired accelerating mode.

As of the time of this writing, work has commenced on a copper prototype. This initial version is intended not only to allow the exploration of coupling techniques, but also initial high-power testing and beam generation. Cold-test studies are anticipated to begin within three months of the start of the design process.

3.12.7. Acknowledgements

The authors wish to thank Stephen V. Milton and Wei Gai for support, discussion, and encouragement, and Louis Emery for help with URMEL.

3.12.8. References

[1] D.T. Palmer et al., "Microwave measurements of the BNL/SLAC/UCLA 1.6 cell photocathode RF gun," presented at the 16th IEEE Particle Accelerator Conference (PAC 95) and International Conference on High Energy Accelerators (IUPAP), Dallas, Texas, 1-5 May 1995.

[2] E. Colby et al., "Design and construction of high brightness rf photoinjectors for TESLA," presented at the 16th IEEE Particle Accelerator Conference (PAC 95) and

International Conference on High Energy Accelerators (IUPAP), Dallas, Texas, 1-5 May 1995.
[3] S. Trotz et al., "Experimental operation of a 17 GHz photocathode rf gun," presented at the 17th IEEE Particle Accelerator Conference, Vancouver, B.C., Canada, 12-16 May 1997.
[4] K.-J. Kim, Nucl. Instrum. Methods Phys. Res. A**250**, 396 (1986).
[5] John W. Lewellen, "Higher-order mode RF guns," Phys. Rev. ST Accel. Beams **4**, 040101 (Issue 4 – April 2001).
[6] James Rosenzweig, UCLA, private communication.
[7] James H. Billen and Lloyd M. Young, "Poisson Superfish," Los Alamos document LA-UR-96-1834 (October 27, 1998).
[8] U. Lauströer, U. van Rienen and T. Weiland, "URMEL and URMEL-T User Guide (Modal Analysis of Cylindrically Symmetric Cavities; Evaluation of RF-Fields in Waveguides)," DESY-M-87-03, February 1987.
[9] J.D. Jackson, *Classical Electrodynamics*, 2nd Ed., p. 355. (Wiley, New York, 1975.)
[10] L.C. Maier and J.C. Slater, "Field strength measurements in resonant cavities," J. Appl. Phys. **23**, 68-77 (1952).

Table 1: Measured, calculated, and approximated frequencies of the various resonant modes in the cavity. All frequencies are given in MHz.

Measured Frequency	URMEL Calculation	SUPERFISH Calculation	Mode Assignment	Pillbox Approx. Frequency	Approx. Frequency Error
2032	2031	2032	TM 0,1,0	2122	90
2449	2445		TE 1,1,1	2497	48
2849	2854	2855	TM 0,1,1	2846	-3
3200	3198		TM 1,1,0	3381	181
3218	3227		TE 2,1,1	3295	77
3782	3794*		TM 1,1,1	3877	91
3790					
4040	4056		TE 3,1,1	4164	124
4121	4127		TE 1,1,2	4127	6
4243	4241		TM 2,1,1	4912	669
4320	4324	4329	TM 0,1,2	4346	26
4563	4559	4564	TM 0,2,0	4870	307
4590	4595		TE 2,1,2	4653	63
4882	4899*		TE 1,2,2	6043	1161
4897					
4943	4947		TM 2,1,2	5910	967

*Mode appears to be split due to the presence of the probe

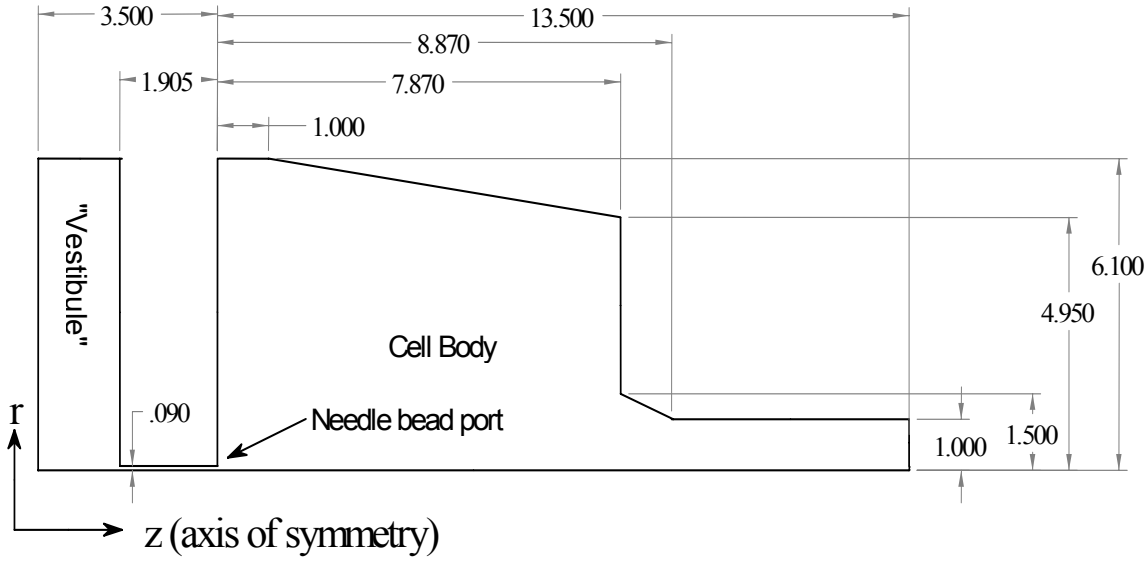

Figure 1: Cold-test cell geometry. All units are in cm.

Figure 2. Sample input file for beadpull simulation.

```
HOM gun v0.5
;0,1,1 mode (no azimuthal, one radial zeros, one longitudinal node)
;Created: 02/12/2000 Lewellen
; cold test model
; file modified for beadpull measurement simulation

&reg kprob=1,
freq=resFreq,
icylin=1,
xmin=-3.5, xmax=13.5,
ymax=6.1,
xreg1=xProbeStart, kreg1=xCountStart,
xreg2=xProbeEnd, kreg2=xCountEnd,
kmax=xTotalCount,
yreg1=yProbeEnd, lreg1=yCountEnd,
lmax=yTotalCount,
xdri=0.0, ydri=6.1 &
&po x=-3.5, y=0 &
&po x=-3.5, y=6.1 &
&po x=-1.905, y=6.1 &
&po x=-1.905, y=0.09 &
&po x=0, y=0.09 &
&po x=0, y=2.5 &
&po x=0.,y=6.1 &
&po x=1, y=6.1 &
&po x=7.87, y=4.95 &
&po x=7.87, y=1.5 &
&po x=8.87, y=1.0 &
;&po nt=2, x0=8.87, y0=2.0, radius=1, theta=270 &
&po x=13.5, y=1.0 &
&po x=13.5, y=0 &
&po x=-3.5,y=0 &

; define the bead below
&reg mat=0 &
&po x=beadStart, y=beadInnerRad &
&po x=beadStart, y=beadOuterRad &
&po x=beadEnd, y=beadOuterRad &
&po x=beadEnd, y=beadInnerRad &
&po x=beadStart, y=beadInnerRad &
```

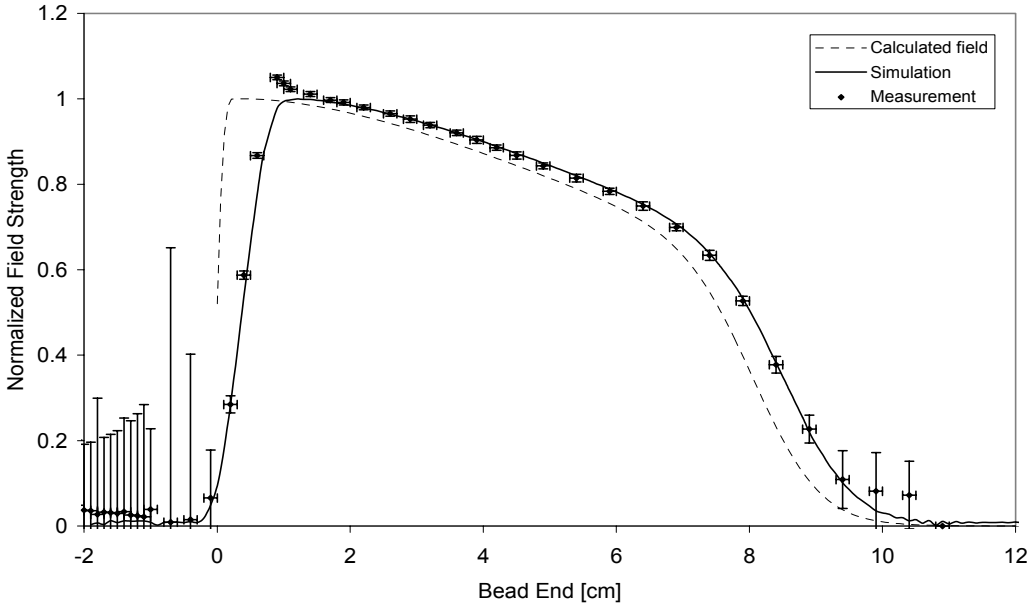

Figure 3: Measured and simulated beadpull, needle bead, TM_{010} mode.

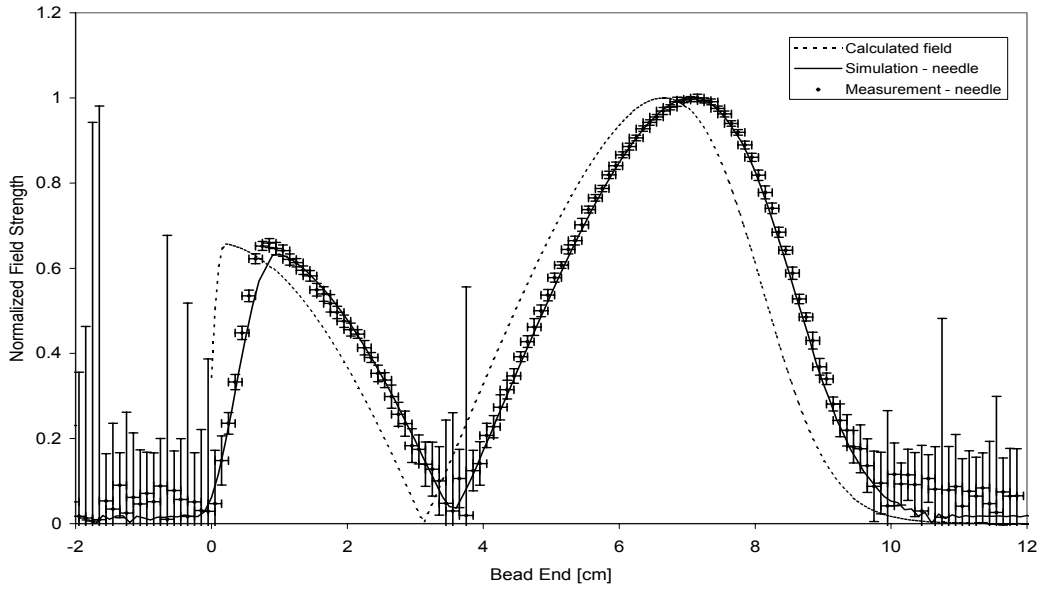

Figure 4: Measured and simulated beadpull, needle bead, TM_{011} mode.

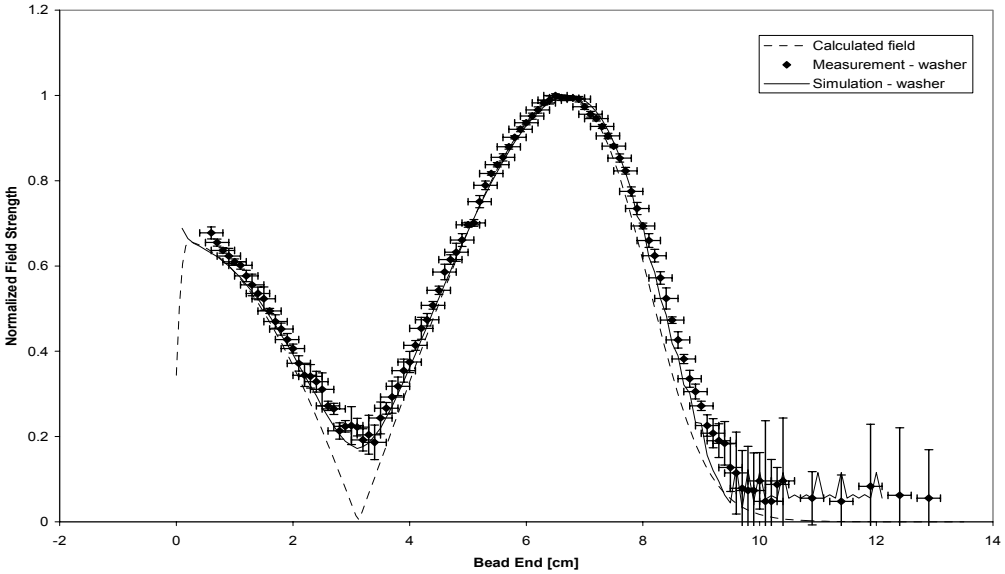

Figure 5: Measured and simulated beadpull, washer bead, TM_{011} mode.

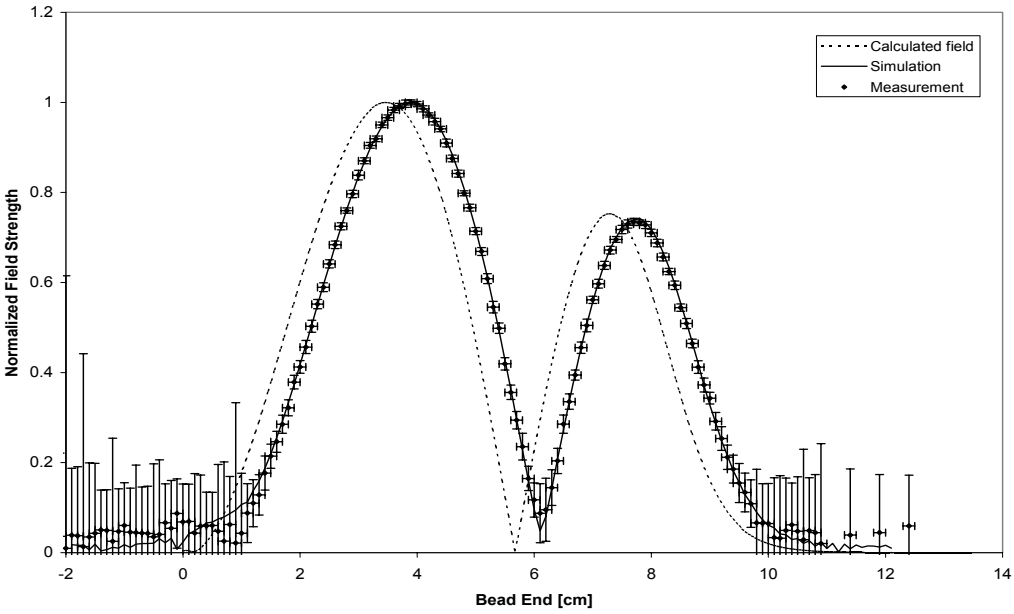

Figure 6: Measured and simulated beadpull, needle bead, TM_{012} mode.

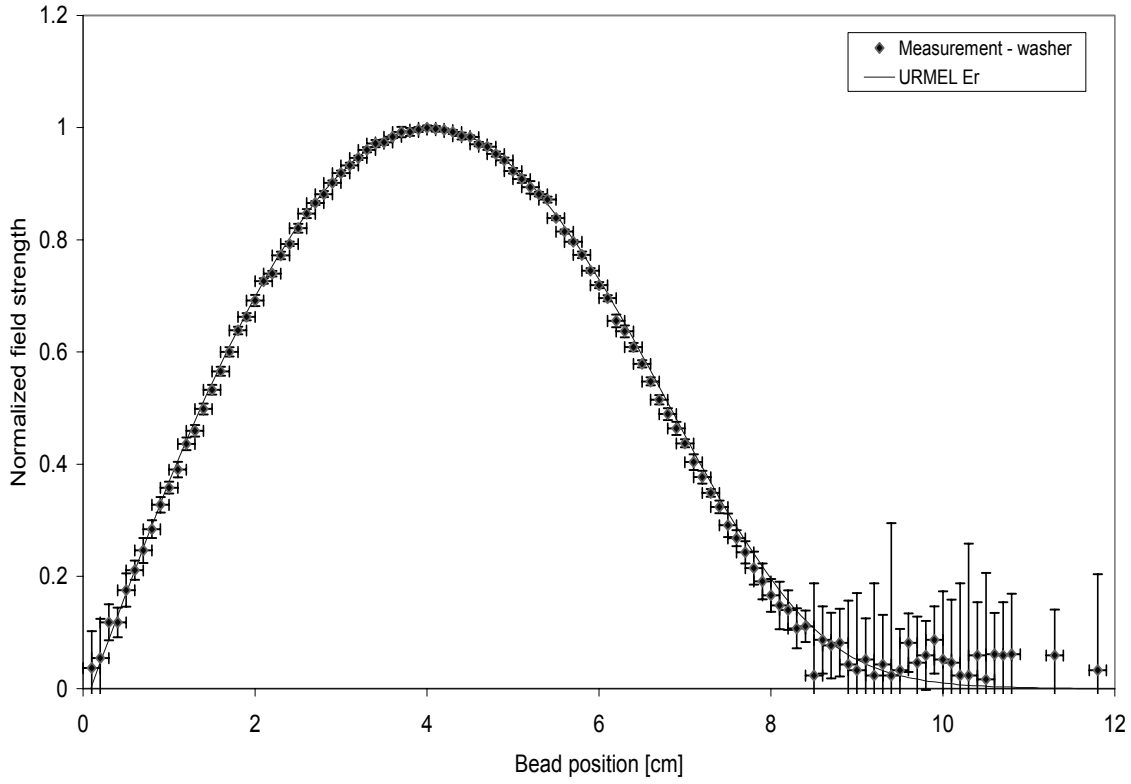

Figure 7: Measured beadpull, washer bead, TE_{111} mode, with URMEL-calculated field.

3.13. STRONG-FIELD SCIENCE AND TECHNOLOGY AT ADVANCED PHOTON RESEARCH CENTER, JAERI

H. Daido
[1]Advanced Photon Research Center, Kansai Research Establishment
Japan Atomic Energy Research Institute
mail to:daido@apr.jaeri.go.jp

Recently, ultra-high intensity short pulse lasers have been applied to the fields of hard x-ray generation and high energy particle generation [1,2]. The essence of the laser-produced plasma is that a high intensity laser can feed its ultra-high energy density into the matter via the ponderomotive heating of electrons. Then the electron energy is transferred into the atoms and ions, which include excitation, ionization by collisions. The electron energy is also converted into energetic ion energy by electro-static potential driven by electron ejection from a plasma. Subsequently, high flux few tens of MeV x-ray can drive nuclear reactions, which open up the new fields of plasma physics and applications. The ultra-high intensity short pulse lasers will also contribute to the cancer therapy as a source of energetic particle source. We are now characterized laser-driven ion source [3] in collaboration with several domestic Institutes and Universities. The basic laser-plasma interaction study with a practical point of view opens up the new attractive fields not only the practical applications but also new aspects of the basic sciences such as control of a high temperature and high-density relativistic plasma. The high intensity physics experiments of this project are schematically shown in Fig. 1.

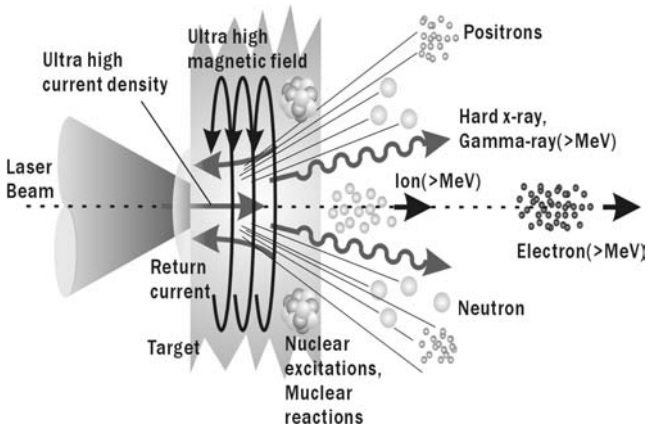

Fig. 1 Schematic diagram of the ultra-intense laser-matter interaction.

For the cancer treatment, desired properties of an ion source for patients are listed as follows;
(1) 10^9 heavy ions per second, $10^{10\text{-}11}$ protons per second,
(2) the particle energy of ~100 MeV/nucleon for a carbon ion and the total energy of >1GeV are necessary. At present, a carbon ion source for cancer treatment is too expensive to be built in a medium size hospital. To reduce the size of the machine, we are developing the compact therapy machine as shown in Fig. 2. At the injector the ions in the co-axial direction of the laser illumination are most useful to be transferred into the next beam cooling and acceleration stages. The issues to be studied are listed below.

1st: Efficient conversion of laser energy into the energetic electrons, which are created via relativistic laser-plasma interactions. We are very much interested in the high-energy tail of the electron distribution functions which may be play significant role to accelerate ions.

2nd: Efficient generation of energetic ions via the electrostatic potential driven by the energetic electrons. We will measure the energy distribution as well as angular distribution. The important issue for this purpose is how many ions at the specific energy with the desired energy band and desired solid angle for next stage device.

3rd: Mechanism of the ion acceleration influenced by ionization time, especially for the heavy ions such as carbon ions. The charge to mass ratio of the ions is very important parameter for the heavy ion accelerator. We have to investigate ionization processes by laser field.

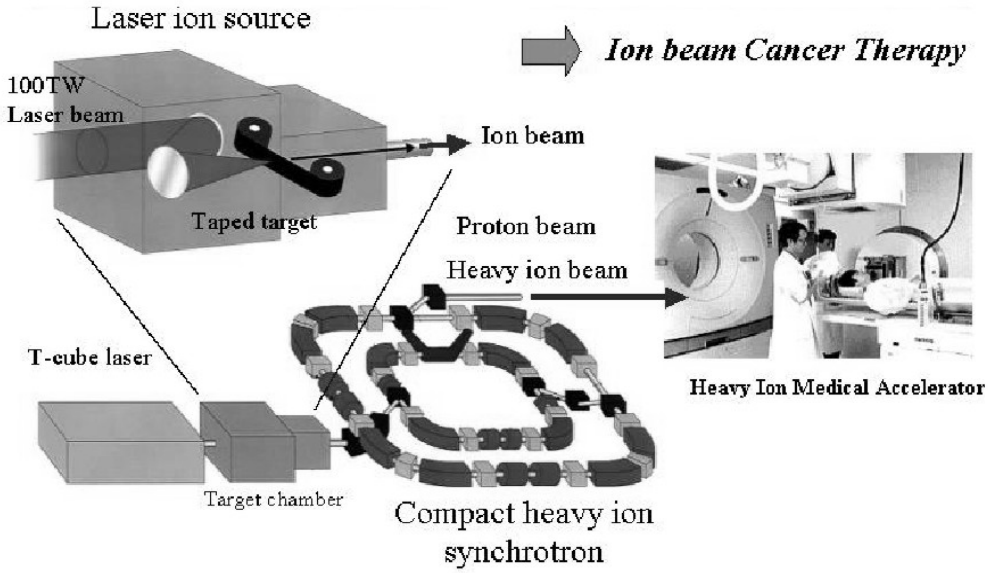

Figure 2. Schematic diagram of the ion acceleration project for cancer therapy. The laser driven ion source as an injector of the accelerator is found in the figure.

4th: Get rid of hydrogen contamination from the surface of the laser irradiated target surface. Hydrogen atoms are easily ionized and its charge to mass ratio is high. Therefore most of the laser energy goes into the proton acceleration rather than higher atomic number ions. Removal of hydrogen contamination is very important subject for the energetic heavy ion production. On the other hand, if we need energetic protons, we have to maximize the proton contamination on the surface of the metal foils.

5th: Transport of the energetic ions from the laser driven ion source to the vacuum. The charge neutralization in a bunch of the energetic ions is very important for long scale propagation.

6th: Large scale particle simulation contributes to make the guide-line of the experiment.

We have performed ion generation experiments here at the Advanced Photon Research Center. The unique mechanism described in the ref.3 will be further investigated experimentally as well as computationally. The schematic diagram of the laboratory for high energy ion generation and the photo of the vacuum chamber can be seen in Fig. 3 and 4.

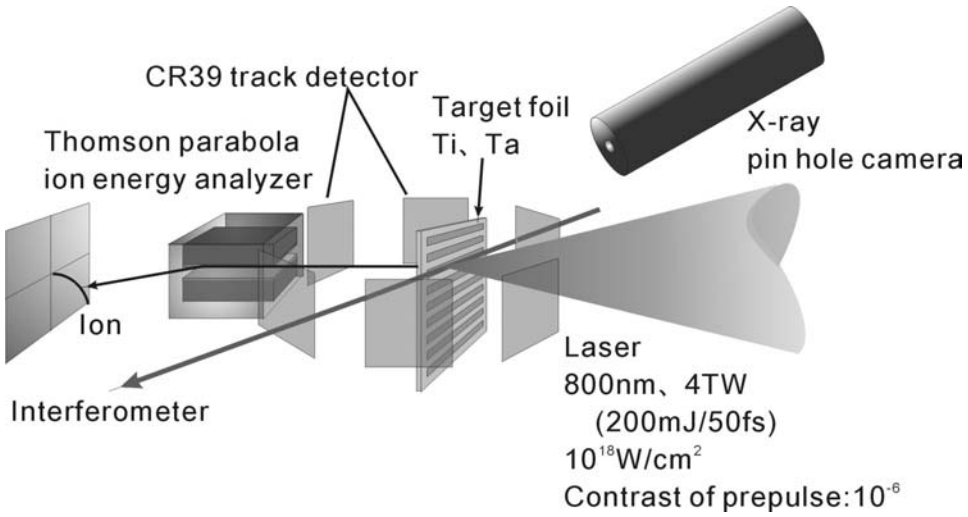

Fig. 3 The schematic diagram of the laboratory for high energy ion generation.

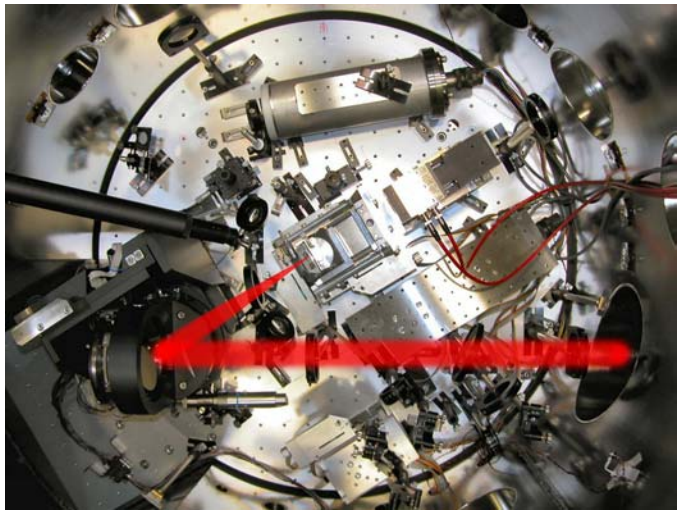

Fig. 4 Photo of the vacuum chamber for high energy ion generation.

References

[1] C. J. Joshi and P. B. Corkum, "Interaction of ultra-intense laser light with matter," *Physics Today*, pp. 36-43 January (1995).
[2] D. Umstadter, "Review of physics and applications of relativistic plasmas driven by ultra-intense lasers," *Physics of Plasmas* **8**, pp.1774-1785 (2001).
[3] K. Matsukado, T. Zh. Esirkepov, H. Daido, T. Utsumi, Z. Li, A. Fukumi, Y. Hayashi, S. Orimo, M. Nishiuchi, S. Bulanov, A. Noda, Y. Iwashita, T. Shirai, T. Takeuchi, S. Nakamura, A. Yamazaki, M. Ikegami, T. Mihara, A. Morita, M. Uesaka, K. Yoshii, T. Watanabe, K. Kinoshita, T. Hosokai, A. Zhidkov, A. Ogata, Y. Wada, T. Kubota, Phys. Rev. Lett. 91 p.215001 (2003).

Publication list

[1] K. Matsukado, K. Kinoshita, Z. Li, H. Daido, Y. Hayashi, S. Orimo, M. Uesaka, K. Yoshii, T. Watanabe, T. Hosokai, A. Zhidkov, A. Noda, Y. Iwashita, T. Shirai, S.

Nakamura, A. Yamazaki, A. Morita, A. Ogata, Y. Wada, T. Kubota, F. Soga, S. Yamada, “Ion Generation via Interaction between Intense Ultra-short Laser Pulse and Solid Target for Application to Cancer Therapy,” Proceedings of ADVANCED ACCELERATOR CONCEPTS: Tenth Workshop Mandalay Beach, California USA, 22-28 June 2002, pp. 265-268.

[2] K. Matsukado, Z. Li, H. Daido, Y. Hayashi, S. Orimo, M. Uesaka, K. Yoshii, T. Watanabe, T. Hosokai, K. Kinoshita, A. Zhidkov, A. Noda, Y. Iwashita, T. Shirai, S. Nakamura, A. Yamazaki, A. Morita, A.Ogata, Y. Wada, T. Kubota, F. Soga, S. Yamada, “Laser Driven High Energy Ion Generation for a Compact Cancer Therapy Accelerator,” ECLIM2002, Moscow Russia, 7-11, Oct, 2002.

[3] K. Matsukado, H. Daido, Z. Li, A. Fukumi, T. Takeuchi, Y. Hayashi, S. Orimo, S. V. Bulanov, M. Uesaka, K. Yoshii, T. Watanabe, T. Hosokai, K. Kinoshita, A. Zhidkov, A. Noda, Y. Iwashita, T. Shirai, S. Nakamura, A. Yamazaki, A. Morita, A. Ogata, Y. Wada, T. Kubota, F. Soga, S. Yamada, E. Timur, K. Nishihara, “High Energy Ion Generation from Laser Plasma for a Compact Cancer Therapy Accelerator,” APLS2002, Senri life Science center Osaka, Japan, 17－20, Oct.2002.

[4] T Zh. Esirkepov, S. V. Bulanov, K. Nishihara, T. Tajima, F. Pegoraro, V. S. Khoroshkov, K. Mima, H. Daido, Y. Kato, Y. Kitagawa, K. Nagai, ande S. Sakabe, “Proposed Double-Layer Target for the Generation of High-Quality Laser-Acelerated Ion Beams,” Phys. Rev. Lett. **89**, 175003 (2002).

[5] A. Zhidokov, M. Uesaka, A. Sasaki and H. Daido, “Ion Acceleration in a Solitary Wave by an Intense Picosecond Laser Pulse,” Phys. Rev. Lett. **89**, 215002 (2002).

[6] A. Fukumi, H. Daido, K. Matsukado, Z. Li, Y. Hayashi, S. Orimo, M. Nishiuchi, A. Sagisaka, K. Ogura, M. Mori, K. Takagaki, T. Tajima, T. Utsumi, S. Bulanov, T. Esirkepov, M. Uesaka, K. Yoshii, T. Watanabe, T. Hosokai, K. Kinoshita, A. Zhidkov, A. Noda, Y. Iwashita, T. Shirai, T. Takeuchi, S. Nakamura, A. Yamazaki, M. Ikegami, T. Mihara, A. Ogata, Y. Wada, T. Kubota, A. Morita, “Development of Laser-Driven Ion Source for Compact Cancer Therapy Accelerator,” Laser Beam Interactions, St Catherine's College, Oxford, England, 7-11, Jul. 2003.

[7] S. Nakamura et. al. “Phase Rotation Scheme of the Laser-Produced Ion Beam,” Laser Beam Interactions (St Catherine's College, Oxford, England, 2003/7/7-11).

[8] High energy particles generated by the interaction between fs-laser and metal target

[9]Y. Hayashi et al. Workshop on Laser and Plasma Accelerators, Portovenere (La Spezia), Italy September 29-October 3, 2003.

[10] A. Sagisaka et. al. Topical meeting Applications of High Field and Short Wavelength Sources X, October 12-15, 2003, Biarritz, France, K. Matsukado, T. Zh. Esirkepov, H. Daido, T. Utsumi, Z. Li, A. Fukumi, Y. Hayashi, S. Orimo, M. Nishiuchi, S. Bulanov, A. Noda, Y. Iwashita, T. Shirai, T. Takeuchi, S. Nakamura, A. Yamazaki, M. Ikegami, T. Mihara, A. Morita, M. Uesaka, K. Yoshii, T. Watanabe, K. Kinoshita, T. Hosokai, A. Zhidkov, A. Ogata, Y. Wada, T. Kubota, “Characterization of preformed plasmas for ultra-short high-intensity laser-plasma interactions,” Phys. Rev. Lett. 91 p.215001 (2003).

3.14. ICFA Report from Korea

H. Suk, Center for Advanced Accelerators, KERI, Korea

mail to: hysuk@keri.re.kr

3.14.1. Activities at Center for Advanced Accelerators, KERI

The KERI group was founded just two years ago and most scientists in the group do not have previous experience in laser-based accelerators, but we have made a rapid progress.

In 2003 we installed the Ti:sapphire/Nd:glass laser system at KERI, which can deliver 2 TW (1.4 J/700 fs). It consists of an Nd:glass oscillator with a pulse duration of 200 fs, Ti:sapphire regenerative amplifier, and three stage Nd:glass amplifier. The overall picture of the laboratory is shown in Fig. 1 and the laser-plasma interaction chamber is shown in Fig. 2. In the beginning the laser system had some problems, but eventually we fixed all bugs. Now it works stably and the laser beam profile is very good. We are going to use the laser system for several advanced-accelerator experiments. The SM-LWFA is obviously simplest, so we started from the SM-LWFA experiment to acquire some experience in laser-based acceleration and to test several developed diagnostic tolls. Very recently (in December) we could successfully generate lots of high energy electrons from the SM-LWFA. The emitted beam image from a Lanex film was so bright that we could not believe it in the beginning (see Fig. 3). Now detailed measurements of several beam and plasma parameters are under way, and the result will be reported later. After the SM-LWFA experiment is finished, we are going to move ahead for other planned experiments. One of them is the Thomson-backscattering experiment using collision of a laser beam and high-energy electrons from the laser accelerator. In this case we do not need a high energy accelerator. This experiment could be done at KERI or somewhere else. We will decide where to do it soon.

In addition to experiments, the KERI group did extensive theoretical/simulation studies. The major tools for simulation are PIC codes including the X-OOPIC and OSIRIS codes. For simulations we developed a Linux-based computer cluster consisting of 12 Pentium-IV PCs and the OSIRIS code was successfully implemented in collaboration with the UCLA group led by Warren Mori. The Linux-based computer cluster was proved to be a cheap, but powerful tool for massive parallel computing.

Fig. 1. Overall picture of the laboratory at Center for Advanced Accelerators, KERI.

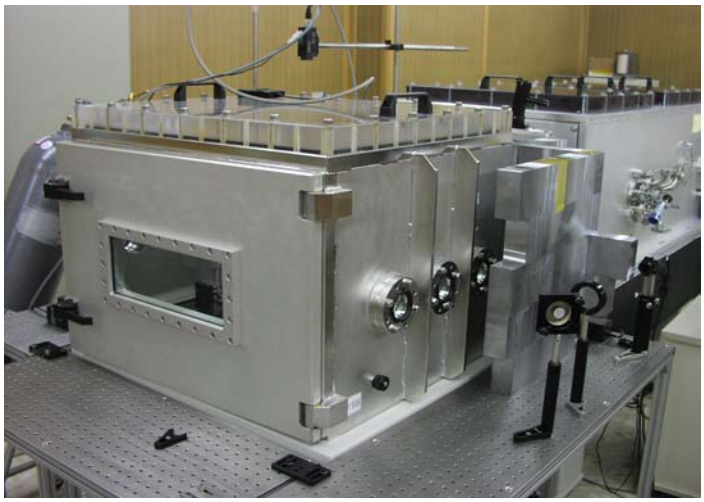

Fig. 2. Laser-plasma interaction chamber.

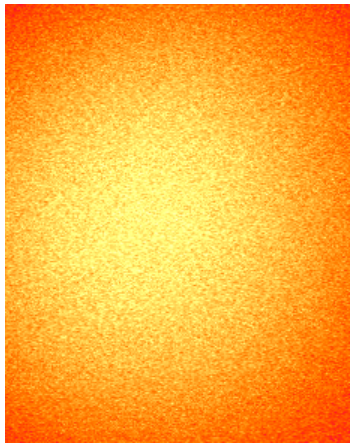

Fig. 3. Electron beam image from a Lanex film.

3.14.2. Activities at Advanced Photon Research Institute, K-JIST

K-JIST is a research-oriented graduate school and APRI (Advanced Photon Research Institute) is located on the campus of K-JIST. This year APRI, whose director is Prof. Jongmin Lee, launched a big laser project. It is to build a 500 TW Ti:sapphire laser at APRI over the next 6 years. The project was approved by the Korean government and it started officially this summer. The project aims to promote research in various fields of femto-science (see Fig. 4). One of them is the particle acceleration using the high power laser and the KERI group is one of main users in this field. APRI is going to provide a 20 TW laser beam in the summer of 2004 and the KERI group will use it for various experiments for electron and ion acceleration. Progress at APRI will be reported in the future.

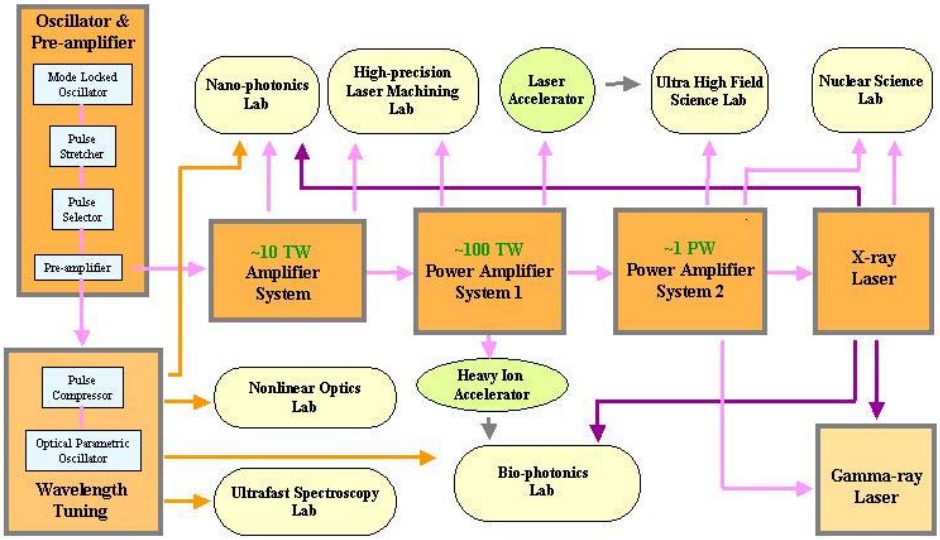

Fig. 4. Schematic of the planned 500 TW laser system at APRI.

3.14.3. Publications

1. J. U. Kim, C. Kim, G. H. Kim, H. J. Lee, and H. Suk, "Characteristics of Laser-Produced Plasmas in a Gas Filled Chamber and in a Gas Jet by Using a Long Pulse Laser," Journal.Applied Physics 94, 5497 (2003).
2. N. Hafz, H. Lee, G. H. Kim, and H. Suk, "Ultrashort X-ray source based on the nonlinear Thomson scattering of femtosecond lasers from plasma-accelerated electron beams," IEEE Trans. Plasma Sci. 31 (6) (December issue of 2003).
3. H. Suk, C. Kim, G. H. Kim, J. U. Kim, I. S. Ko, and H. J. Lee, "Energy enhancement in the self-injected laser wakefield acceleration using tapered plasma densities, Applied Physics Letters A 316, 233 (2003).

4. J. Kim, H. J. Lee, H. Suk, and I. S. Ko, "Characteristics of pulse compression in laser pulse amplification by stimulated Raman backscattering," Physics Letters A 314, 464 (2003).

4. Recent Doctoral Theses

4.1. Dynamics of the storage ring Free Electron Laser : theoretical and experimental study of two SRFELs in Europe

Cyrille Tomas
mail to: cyrille.thomas@diamond.ac.uk

Affiliation: DIAMOND Light Source

Title: Dynamics of the storage ring Free Electron Laser : theoretical and experimental study of two SRFELs in Europe

Name: Cyrille Tomas

Graduation date: 27 May, 2003
Supervisor1: M. E. Couprie
Supervisor2: M. Van der Wiel

Abstract:

The purpose of the present work is to study the dynamics of the storage ring free electron laser in the UV-VUV wavelength range and in the presence of the microwave instability. In practice, this instability is always present during the operation of a free electron laser in a storage ring, and it may degrade the performance of the laser. In order to investigate the behaviour of this complex system, we used a dual approach, in which theoretical results have been compared with measurements performed on two storage ring free electron lasers, at Super ACO (France) and at ELETTRA (Italy). As a first theoretical step, we analyzed a simple model which describes qualitatively the behaviour of the storage ring free electron laser only, including the effects due to the microwave instability. In order to get more quantitative predictions, which can not be obtained from the simple model, we developed a 1-dimensional numerical code for the evolution of the laser electric field along the optical cavity axis. The code was validated by the comparison with experimental measurements performed at Super ACO and at ELETTRA. The experimental approach has also been done in two steps. The first step was to characterize the electron beam behaviour in the storage ring without the free electron laser. This has only been done at Super ACO. We measured the beam characteristics (electron distribution, beam energy spread, etc.) for the free electron laser operation, and we characterized two effects of the wake-field on the electron beam. The first effect is the so-called potential well distortion, which only modifies the beam properties, leaving the beam stable. The second effect induces instabilities in the beam, in particular the microwave instability, with on average an enhancement of energy spread and a proportional bunch lengthening. Next, we characterized the laser behaviour, measured the laser pulse properties (pulse duration, average power, etc.) under detuning conditions, and deduced from measurements the parameters of the dynamical system, such as the gain at start-up, the cavity loss, etc.

The main conclusion of the present work is that the microwave instability can seriously degrade the performance of the storage ring free electron laser. For any design of such a system, one has to make sure that the impedance of the storage ring, which scales the strength of the microwave instability, is as low as possible. The laser is in competition with the instability, and is able to damp it in a range of current determined by the gain of

the free electron laser, the optical cavity loss and the microwave instability strength. At higher current the laser is unstable, or simply, it may be switched or by the microwave instability. The numerical code we developed has been used to simulate successfully the behaviour of two different storage ring free electron lasers. It can be used reliably as a tool for the design of new storage ring free electron lasers.

5. Workshop and Conference Reports

5.1. Report on the Workshop on "e+e- in the 1-2 GeV range: Physics and Accelerator Prospects"

C. Biscari and F. Bossi
LNF, INFN, Frascati, Italy
mail to: caterina.biscari@lnf.infn.it
fabio.bossi@lnf.infn.it

The Workshop on "e+e- in the 1-2 GeV range: Physics and Accelerator Prospects" was held from 10-13 September 2003 at Alghero, Sardinia. It was also sponsoured as an ICFA Beam Dynamics Panel Miniworkshop, by the working group on High Luminosity e+e- colliders.

Participation was shared between Experimental and Theoretical Physics and Accelerator Physics, attending the two different working groups on the Physics case in the range of c.o.m energy between 1 and 2 GeV and the luminosities issues at these energies.

Physics topics under discussion included:

- Prospects for kaon physics and tests of fundamental symmetries through rare kaon decays; here the impact of a future very high luminosity Φ-factory was extensively discussed also in relation with present and future fixed-target experiments.
- Low energy spectroscopy and baryon form factors. In this field, a new e+e- collider with a luminosity in the range of $10^{32}cm^{-2}sec^{-1}$ at these energies would greatly improve the present experimental accuracy.
- Hypernuclear spectroscopy. The recent start of data taking of the FINUDA experiment at DAΦNE is bringing a completely new experience and fresh data in this field. If operations prove successful as hoped, there will be the strong case for increasing the luminosity of the machine up to $10^{34}cm^{-2}sec^{-1}$ to start looking systematically for neutron rich hypernuclei, and to study hypernuclear transitions with the emission of hard photons. This program is complementary to that of the JPARC facility, under construction in JAPAN.

The accelerator group was attended in majority by the DAΦNE community, and participants from the other lepton factories were also present.

Status reports on existing and in construction factories in the low energy regime were reported: the Beijing τ-charm, the Novosibirsk VEPP-2000, the CESR-c evolution and DAΦNE.

It was stressed in all of them the importance of the energy scaling of many aspects of the accelerator, essentially all phenomena dominated by the synchrotron radiation and the impedance, and their impact on the beam-beam interaction.

The round-beam collisions in VEPP-2000 are expected for the end of next year. This collider, the first one built on the principle of colliding round beams, will show the feasibility of very high beam-beam tune shifts.

The τ -charm in Beijing is based on the explotation of the present BEPC ring, which is used also for synchrotron radiation experiments, plus the construction of a second ring. Double symmetric rings, with one Interaction Region and multibunch flat beams is the design basis for the factory. It is already in the construction stage and the first beam is foreseen for the 2007, when CESR-c will be shutdown. CESR-c, which is running now at lower energy, has installed wigglers to increase the radiation damping and a new Interaction Region. The physics program will have a continuation between the two τ-charm factories.

DAΦNE is now running for the third experiment, FINUDA; at the workshop the modifications done to the ring in order to install the experiment, plus the shimming of the wiggler poles in order to optimize the sextupolar components and the dynamic aperture were presented.

The original physics program of DAΦNE should be completed in 2-3 years and it was discussed which future is expected for the collider. Two possibilities are envisaged: transform the collider in a light –quark factory doubling its energy or upgrade it to a super-regime factory with luminosity of at least $10^{34}cm^{-2}sec^{-1}$. This second possibility, much more appealing for its challenge and interest was strongly discussed.

The increase of energy needs upgrades of some of the present systems: essentially the dipoles, the Interaction Region and the injection. All the other systems, rf, feedback, vacuum, quadrupoles, sextupoles, correction coils, diagnostics, are already dimensioned for the higher energy. The requested luminosity is of the order of the luminosity already achieved in DAΦNE at the lowest energy, and the value of 10^{32} $cm^{-2}sec^{-1}$ can be obtained with currents of the order of 0.5 A per beam.

The dipole preliminary designs, fitting the present vacuum chambers, were presented.

Two possibilities are being considered for the injection: a Linac upgrade to 1 GeV for on-energy injection, or ramping of the collider. The first one has the advantage of optimizing the average luminosity but is more expensive.

The IR design, based on the principles of the present DAΦNE ones, could use superconducting quadrupoles very similar to those presented by the CESR group.

The DAΦNE group has presented some different options for the very high luminosity regime at the Φ-energy. One is based on the explotation of collisions of higher energy rings with a very large crossing angle, with the advantage of simplifying all the single ring challenges for low-energy/high-currents regimes. The design of a specific detector for the boosted production of collisions presents some disadvantages with respect to the non-boosted case, and since the luminosity reachable with this scheme is also affected by the geometrical reduction due to the crossing angle, the idea has not been further investigated.

The second option, on which a preliminary conceptual design was presented, is based on the strong rf focusing principle, very high radiation emission and negative momentum compaction ring configuration.

The strong rf focusing is a modulation of the bunch length along the ring, with a very large longitudinal phase advance, corresponding to synchrotron tune near the half integer. The minimum of the bunch length occurs at the IP, while the maximum occurs at the rf cavity position. Such a scheme needs a large absolute value of the momentum compaction and a high rf voltage.

The high radiation emission is obtained with a lattice based on positive and negative dipoles cells, similar to the All-Wiggler-Machine, in which the damping time is of the order of few msec, about a factor 5 less than the present DAΦNE one. The dispersion self solution oscillates around zero and in each dipole has the sign opposite to the bending angle and has a high value, so that its contribution to the momentum compaction is always negative and high. The advantages of the negative momentum compaction regime, like shorter bunches, and more regular bunch shape are also included in the design.

An rf system at 500 MHz, with voltage of the order of 10 MV, for a 100m long ring, and momentum compaction near -0.2, will give bunch lengthes at the IP near 2 mm.

The Interaction Region fitting the existing KLOE detector, is based on low-beta quadrupoles very close to the Interaction Point, to focus the vertical beta to the millimeter values.

Considerations on beam lifetime, background, and dynamic aperture are in the preliminary stage. A design for the normal conducting dipoles at 1.8T were presented.

A preliminary configuration of the feedback system in the regime of very high synchrotron frequency, based on GPboards, was also presented by the PEP-II participants.

The collider layout fits the existing DAΦNE hall and could utilize all existing infrastructures and sub-systems. An upgrade of the injection system allowing continuous injection has been deined, in order to increase the average luminosity considering the few minutes lifetime that are foreseen at the very high luminosity regime.

5.2. Beam-Beam'03 Workshop Summary

Wolfram Fischer[†]
mail to: Wolfram.Fischer@bnl.gov
Tanaji Sen[‡]
mail to: tsen@fnal.gov

[†]Brookhaven National Laboratory, Upton, New York 11973
[‡]Fermi National Accelerator Laboratory, Batavia, Illinois 60510

5.2.1. Abstract

This paper summarizes the presentations and discussions of the Beam-Beam'03 workshop, held in Montauk, Long Island, from May 19 to 23, 2003. Presentations and discussions focused on halo generation from beam-beam interactions; beam-beam limits, especially coherent limits and their effects on existing and future hadron colliders; beam-beam compensation techniques, particularly for long-range interactions; and beam-beam study tools in theory, simulation, and experiment.

5.2.2. Introduction

The Beam-Beam'03 workshop was held in Montauk, Long Island, from May 19 to 23, 2003. It was attended by 15 participants from 9 institutions. Beam-Beam'03 was held in conjunction with the 29th ICFA Advanced Beam Dynamics Workshop HALO'03. Part of the program, registration, abstract submission, and proceedings were shared with HALO'03.

The workshop concentrated on beam-beam effects in circular colliders, with emphasis on hadron colliders, and followed earlier workshops on this subject[1][2]. After a plenary talk on halo formation due to the beam-beam interaction, three main topics were discussed:

1. Beam-beam limits, especially coherent limits and their effects on existing and future hadron colliders.

2. Beam-beam compensation techniques, particularly for long-range interactions.

3. Beam-beam study tools, in theory, simulation, and experiment.

In the following we summarize the presentations and discussions for each of these topics.

5.2.3. Beam-beam Halo Formation

F. Zimmermann, CERN, summarized the measurements, simulations, and analytical models for the halo formation due to beam-beam interactions for both lepton and hadron colliders. In lepton colliders, two beam-beam limits are observed: the first limit restricts the beam-beam parameter ξ, the second limit is due to the formation of transverse tails (Seeman, 1983). Tails in lepton colliders reach a 'steady state' due to radiation damping. They cause experimental background, reduce the beam lifetime, and often limit the luminosity. Dramatic increases of both core and tails were observed with increasing beam currents. With no radiation damping in hadron colliders, the betatron amplitudes of particles in the tails are not reduced. Tails not only cause background, they can damage collimators and quench a superconducting machine.

A number of mechanisms for halo generation were considered in the past, among them beam-beam bremsstrahlung (Burkhardt et al., 1997), stochastic diffusion (Cornelis, 1993), Arnold diffusion (Chirikov, 1979), resonance trapping (Chao, Month, 1974), phase convection (Gerasimov, 1990),resonance streaming (Tennyson, 1980), and modulational diffusion (Chirikov, 1979). Transverse tails were most often measured with the help of collimators. In LEP, beam-beam bremsstrahlung was found to be the dominant tail generating process. Halo generation in lepton colliders was studied with a number of computer codes. Self-generated boundary conditions were proposed by Irwin in 1989, and subsequently implemented in two codes. In addition, macro particle and PIC codes were developed. Typically 10^7 to 10^9 particle turns are tracked, and a good predictive power of these codes has been demonstrated. Diffusive rates with beam-beam interactions in HERA and RHIC show similar values. However, the Tevatron in Run II and the LHC enter a new regime where long-range collisions dominate. These have caused fast beam losses in simulations and they may ensure that no tails develop. Various tools are available to manipulate tails. Matched beam sizes, centered collisions, zero crossing angles and optimized tunes (with tolerances of approximately 0.001) were shown to be beneficial. Octupoles were used in VEPP-4, VEPP-2M, and DAΦNE.

Table 1: Comparison of maximum beam-beam parameters in hadron colliders[3]-[6]. Note that machine configurations change over time and that parameters in routine operation may be different.

Quantity	**ISR**	**SPS**	**Tevatron Run II (design)**	**HERA p**	**RHIC p 2003**	**LHC (design)**
Bunches per beam	coasting	3	36	174	55	2808
Experiments (head-on interactions)	6	2	2	2	4	4
Long-range interactions	…	4	70	—	2	120
Beam-beam parameter per IP ξ	0.001	0.009	0.01	0.007	0.004	0.003
Total beam-beam tune-spread ΔQ_{bb}, max	0.008	0.028	0.024	0.0014	0.015	0.010

5.2.4. Beam-beam Limits

In circular colliders the beam-beam interaction is one of the most limiting effects. The maximum beam-beam parameters achieved in hadron colliders are shown in Table 1. A table comparing lepton colliders can be found in elsewhere[7].

Y. Alexahin, FNAL, reviewed the theory and observations of coherent beam-beam effects. The eigenmodes of coherent dipole oscillations can be found by solving the Vlasov equation in first order perturbation theory. At intensity ratios greater than 0.6, the discrete π-mode lies outside the continuous spectrum and therefore may not be Landau damped. Multi-bunch modes with 36×36 bunches in the Tevatron were considered. The tune spread induced by the head-on and long-range interactions is large enough to damp the multi bunch modes provided the tunes of both beams are the same. If the anti-proton tunes are lower than the proton tunes, the coherent modes shift by less than the incoherent tunes and may not be damped. A number of mechanisms were proposed to suppress the π-mode: a split of bare lattice tunes (A. Hoffman), redistribution of phase advances between interaction points (A. Temnykh, J. Welch), different integer parts of tunes in separate rings (W. Herr), and long bunches (due to the overlapping of synchrotron sidebands). During discussions, Alexahin suggested separating "collective" from "coherent", the former applying to purely intensity dependent phenomena, the latter applying to phenomena where particle phases are correlated. L. Jin, University of Kansas, showed a case of collective instability in HERA. When the e^+-beam approached a fourth order resonance, a 30% emittance growth was observed in the proton beam. This observation could be well reproduced in a simulation. Later he discussed the importance of tune spread to the collective beam-beam instability. W. Fischer, BNL, gave a presentation of strong-strong and other beam-beam observations in RHIC. With the current bunch spacing, bunches in RHIC experience only two long-range interactions. It is intended to accommodate a total tune spread as large as has been achieved in the past. Furthermore, RHIC is the first bunched beam hadron collider in which strong-strong effects are observed. Beam-beam generated σ- and π-modes were seen with a frequency difference that matches expectations from calculations[8]. The coherent modes observed could be suppressed by separating the tunes of the two rings. This may not be sufficient if the beam-beam parameter is doubled and the triplets are better corrected, leaving the beam-beam interaction as the dominant source of transverse nonlinearities. In two talks the performance of the B-factories were reviewed. W. Kozanecki, CEA-Saclay/SLAC, showed the recent performance of the SLAC B-factory. A strong interplay between electron cloud and beam-beam effects is observed. With changing parameters along the bunch train, luminosity and background optimization relies on a delicate balance between currents, tunes, beam-beam, and e-cloud parameters.

Long-range interactions have an observable negative impact on the luminosity. As of May 2003, the tunes were moved closer to the half integer and were found to improve machine performance. Beam-beam simulations show encouraging agreement with experiments although not all relevant phenomena were included. The beam-beam parameters (ξ_x,ξ_y) achieved in the LER and HER respectively are (0.065,0.048) and (0.075,0.060), the luminosity reached $6\times10^{33}cm^{-2}s^{-1}$. K. Ohmi, KEK, reported on the experience with finite crossing angles at KEKB. With a crossing angle of 2×11mrad a luminosity of $1\times10^{34}cm^{-2}s^{-1}$ was achieved. No problems were encountered with the crossing angle up to a beam-beam parameter of $\xi\approx0.05$. The beam-beam parameters (ξ_x,ξ_y) achieved in the LER and HER respectively are (0.097,0.066) and (0.067,0.050). Electron cloud effects in the positron ring (LER) are mitigated (both in KEKB and PEP II) by wrapping Solenoidal coils around most of the machine. As in PEP II, a day-by-day fine-tuning of the machine parameters is required to maintain the highest luminosities. Simulations helped with the choice of the tuning parameters. The use of crossing angles and long bunches is also under consideration for hadron colliders[9]. W. Fischer showed an example of a possible luminosity increase at the incoherent beam-beam limit with six superbunches in RHIC. Assuming that the incoherent tune shift is the limiting effect, and neglecting a number of other effects, a luminosity increase of about two orders of magnitude was estimated. T. Sen, FNAL, reviewed the theory and observations of beam-beam interactions in the Tevatron. One of the key observations is that a small tune footprint by itself does not guarantee good beam lifetime. At injection, the long-range beam-beam interactions (which create a small tune footprint) limit the anti-proton beam lifetime to 1-5 hours compared to 25 hours without the beam-beam interactions. No significant effect on the protons is seen. On the ramp, about 10% of the anti-protons are lost and the observed anti-proton emittance growth is suspected to be caused by beam-beam. During the beta-squeeze, anti-proton losses are low while proton losses are occasionally high enough to cause quenches. At collision, beam lifetimes are mainly determined by the p-pbar interactions at the detectors. Bunch dependent emittance growth of anti-protons due to beam-beam effects at collision is sometimes observed. This can usually be corrected by a change of tune. Changes to the helices, realignment of the Tevatron, cleaner IR optics, different bunch patterns and active beam-beam compensation are among the several methods under development to mitigate the effects of the beam-beam interactions. B. Erdelyi, FNAL, compared simulations with experimental studies in the Tevatron. Until the recent commissioning of the vertical dampers, the vertical chromaticity was set to a high value to keep the protons stable at injection energy. This however leads to a low anti-proton lifetime and the emittance was found to decrease initially before reaching a constant value. From these observations, the dynamic aperture of anti-protons could be measured and was found to be in good agreement with the simulation results. At collision, lifetimes observed at different tunes were compared with dynamic aperture calculations at these tunes and found to be in qualitative agreement. W. Fischer showed how the beam-beam interaction and unequal rf frequencies can generate tune modulation. This effect leads to a reduction of the beam lifetime in RHIC when the rf frequencies of the two rings are not locked, a situation typically encountered during the RHIC energy ramp.

5.2.5. Beam-beam Compensation

Two approaches are currently pursued to compensate the long-range beam-beam interactions: electric wires and electron lenses. Attempts to compensate the direct space charge forces through four-beam schemes were not successful in the past, but are under investigation again. Also under investigation is the compensation of the beam-beam

multipole effect with magnets. A short summary of earlier compensation schemes can be found elsewhere[10].

5.2.6. Wire Compensation at the SPS

The idea of compensating the long-range beam-beam interactions by the magnetic field of a current carrying wire was proposed for the LHC by Koutchouk. In the LHC the long-range interactions are clustered around each IP and occur at nearly the same betatron phase. Simulations showed that two wires placed around each IP reduced the tune footprints and increased the diffusive dynamic aperture by about (1-2)σ.

F. Zimmermann reported on recent experiments performed at the SPS to observe the effects of a single wire on a beam. A 1m long wire supported on a rigid structure and carrying 267 A of current was placed in the vacuum chamber. Water flow through the hollow wire was required for cooling. Orbit bumps were used to change the transverse separation of the beam and the wire. Beam lifetime dropped and background rates increased at separations smaller than 9σ - close to the predictions from simulations. Orbit distortions and tune shifts due to the wire were also close to predictions. Diffusion rates could not however be measured.

These initial observations are indeed encouraging and suggest that the idea is worth pursuing. The next critical step is to demonstrate that the wire can compensate the effect of another field on the beam. The plan in the next stage of the experiment is to install two wires in the SPS. The second wire will be powered to cancel the effect of the first wire on the beam. If the experiment succeeds, the wire compensation idea will likely be pursued seriously not only for the LHC but also for the Tevatron and future hadron colliders.

5.2.7. Multiple Wires and Modeling for the Tevatron

The wire compensation principle is also being tested at the Tevatron. The long-range interactions occur at different phases all around the ring and both beams traverse the same beam pipe. This necessarily makes the application of the wire compensation more complicated. One advantage is that the wire needs to operate only in a DC mode since the average effect on all bunches needs to be compensated.

B. Erdelyi discussed a fast and accurate model of the field of a finite length wire that allows misalignments and is now implemented in the codes COSY Infinity and SixTrack. First simulation results at injection energy with four wires placed in the Tevatron are encouraging. The maximum current required in each wire is estimated to be 232 Amps, a value close to the current used in the SPS measurements. At suitably chosen distances and angles of the wire relative to the anti-proton beam, the resonance structure excited by the wires resembles that generated by the long-range interactions. However the resonance structure depends sensitively on the placement of the wires suggesting a more robust compensation is necessary. One possibility is to place several wires in a cylindrical cage at each location. Initial investigations of the multiple-wire scenario show that the nonlinear components of the field created can be chosen with greater flexibility. Nevertheless, several issues with the wire compensation principle in the Tevatron need to be resolved before it can proceed to an experimental test.

5.2.8. TEL Results

V. Shiltsev (FNAL) reported on the status of the beam-beam compensation at the Tevatron with an electron lens. The Tevatron electron lens (TEL) was designed to counteract mainly the effects of the tune spreads between anti-proton bunches and the large tune footprint due to the beam-beam interactions at top energy. Initial observations showed

that the tune shift due to the electron beam was as expected but the action of the lens usually worsened the lifetime. Unexpectedly the TEL found use as a resonant kicker in clearing the DC beam that circulates in the machine. Recently the situation improved, when the electron gun that generated a uniform rectangular profile, was replaced by a gun that generates a smooth Gaussian profile. At good working points the electron lens preserves the beam lifetime. During stores the TEL has occasionally been used in an attempt to reduce emittance growth of selected anti-proton bunches. A recent attempt was successful but two other attempts had no influence or slightly negative effects. Several upgrades are planned to improve the performance of the lens - perhaps the most important will be reducing the orbit jitter of the electron beam.

5.2.9. Multipole Compensation

J. Shi, University of Kansas, proposed a method for compensating the nonlinearities of the beam-beam interactions with multipoles. This is achieved by minimizing the coefficients in a Taylor map of the nonlinear fields order by order. It was applied to a model of the LHC using either correctors locally in the IR sections or distributed globally in the arcs. It was demonstrated that the tune footprint could be reduced and the dynamic aperture increased using only up to third and fourth order nonlinearities of the map. The sensitivity of this compensation to lattice and orbit errors was not addressed.

5.2.10. Four Beam Bompensation

K. Ohmi reported on a new simulation study of the four beam neutralization scheme as a possible luminosity upgrade for KEKB. This scheme where beam-beam forces are canceled by virtue of no net charge at the collision points was first tried at DCI (Orsay) in the 1980s but did not succeed because of coherent instabilities. The DCI performance was compared with simulations earlier [11]. Two schemes were investigated in the present study. One scheme uses the present KEKB rings for two beams and two external beams are provided by linacs. In the other scheme two additional rings are built to have four circulating beams. Active feedback systems to damp the coherent dipole motion were included. However both schemes are plagued by higher order coherent and incoherent motion and the available tune space is very limited.

5.2.11. Beam-beam Study Tools

J. Ellison, University of New Mexico, showed averaging techniques in the weak-strong case with only head-on interactions, pointing to areas of high and low stability of particle motion in the tune plane. Averaged Hamiltonians were derived to describe motion in the vicinity of two low order resonances: the 4th order resonance $2\nu_x+2\ \nu_y= p$ and the linear coupling resonance $\nu_x - \nu_y = 0$. The conjecture is that motion is generically chaotic in this neighborhood. He also presented a new model for the two degrees of freedom collective beam-beam interaction. J. Rogers, Cornell University, reviewed beam-beam simulation methods for lepton machines. A key motivation for the simulations is to understand whether coherent or incoherent motion or some combination of the two is responsible for the two beam-beam limits observed in e^+-e^- machines. Weak-strong simulation methods require tricks to follow particle distributions long enough to calculate lifetimes, typically of the order of an hour or 10^9 turns. These include the leapfrog method of Irwin (1989) and inclusion of scattering processes by Kim and Hirata (1998). Weak-strong simulations have proven useful for accelerator design, the choice of operating parameters, and the investigation of beam halos (second beam-beam limit). Self-consistent strong-strong simulations are necessary to understand coherent effects but at present are

able to follow particle distributions only for several damping times. Each e^+-e^- collider has developed its own PIC style code. These include CESR: Krishnagopal and Siemann (1996), Anderson (1999); PEPII: Cai et al. (2001); KEKB: Ohmi (2000). The luminosities calculated from these codes for their respective machines are found to be within 10% of observed luminosities when the machine is well tuned. A comparison of these codes is desirable. J. Shi reviewed the simulations for hadron machines. Strong-strong methods currently employed include the soft Gaussian approximation, direct multi-particle tracking, Particles-In-Cell (PIC), Hybrid Fast Multipole Method (HFMM), and canonical perturbation theory for solving the Vlasov equation. It is important to check that convergence is achieved with respect to simulation parameters such as the number of macro-particles and the grid-size.Currently only fast processes (within ~10^6 turns) can be analyzed. Slow particle loss, emittance growth and the formation of tails cannot be predicted with confidence. Using a PIC style code, he reported chaotic motions of the centroid in a model of the LHC at ten times the design value of the beam-beam parameter. This is an interesting prediction but observation of this phenomenon may be unlikely in the near future. J. Qiang, LBNL, discussed the computational challenges in modeling beam-beam and space charge simulations. These include efficient Poisson solvers on parallel computers, large particle numbers, long tracking times, and stable direct solvers. He also discussed a parallel computational tool for strong-strong and weak-strong beam-beam modeling. The code is based on shifted Green functions and models efficiently the long-range parasitic collisions. The code was used to investigate the emittance growth caused by modulated transverse offsets in RHIC and the LHC. For the Tevatron, the anti-proton lifetime at injection has been simulated. The calculated lifetime is of the order of a few hours (close to observations) when the physical aperture chosen is small enough.

A. Sobol, University of New Mexico, presented numerical calculations of the phase space density for the strong-strong beam-beam interaction that addressed the problem of storing a large amount of data into a computers cache. Weak-strong simulation tools are useful standard tools for both lepton and hadron colliders. But while strong-strong simulations have gained predictive power for lepton colliders, their use for hadron colliders so far is limited. This should only encourage further development of codes and new methods such as the direct integration of the non-linear Vlasov equation. In a discussion with the HALO diagnostics groups it was pointed out that for operational observations of the beam-beam effect, it would be desirable to have most beam quantities available on a bunch-by-bunch basis. Due to abort or other gaps in the bunch fill patterns, parameters such as closed orbit, tune, linear coupling, chromaticity and emittance vary from one bunch to another. Currently, bunch-by-bunch coupling, chromaticity and emittance measurements are not easily available.

5.2.12. Conclusions

While there are a number of beam-beam phenomena, in both lepton and hadron colliders, that are not completely understood, the three major questions currently relevant to collider operation may be the following.

1. Are coherent modes dangerous in hadron colliders?

   They could be if the modes are outside the incoherent tune spread. However the spectrum of these modes and their relationship to the incoherent spectra depends on several factors including the intensity ratio of the beams, long-range interactions, synchrotron tune, chromaticity, tune splits etc. Until now the presence of these beam-beam driven modes has not limited the operation of any collider - either lepton or hadron. Damping mechanisms, e.g. changing the tune split or an increase in

chromaticity, seem to be available to render these modes innocuous. That may change in the future so theoretical and experimental studies of these modes need to be vigorously pursued.

2. Can beam-beam compensations techniques be made to work?

This is being actively studied experimentally and theoretically at the Tevatron, and at the SPS for application in the LHC. Both the electron lens and wires may be used in the Tevatron. The lens would be used to reduce the tune shifts between bunches and the wires to reduce the average effect of the long-range interactions on all bunches. The accelerator physics challenges are many: ensuring the proton beam is not affected, and coherent instabilities are not excited, to name a few.

3. What can analysis and simulations predict in hadron machines?

Solutions of the linearized Vlasov equation with beam-beam interactions have been successfully used to predict the frequencies of π-modes. Analytically it would be desirable to develop a weakly nonlinear theory that exhibits coupling of the modes and perhaps other features. Numerical tools to analyze the nonlinear Vlasov equation also need to be developed. Lifetime simulations for the Tevatron at injection energy are now yielding results, of the order of an hour, close to observations. Longer lifetimes are at present out of reach. Further improvements in the modeling and the use of the latest advances in computing technology are greatly needed to run both weak-strong and strong-strong simulations for the time scales of interest.

5.2.13. References

[1]. J. Poole and F. Zimmermann (editors), "Proceedings of the workshop on beam-beam effects in large hadron colliders - LHC99", Geneva, Switzerland, CERN-SL-99-039 AP (1999).

[2]. T. Sen and M. Xiao (editors), "Proceedings of a workshop on beam-beam effects in circular colliders", Fermilab, FERMILAB-Conf-01/390-T (2001).

[3]. W. Schnell, "Report on the ISR", proceedings of the 1975 Particle Accelerator Conference, Washington D.C. (1975).

[4]. W. Herr, "Beam-beam issues in the LHC and relevant experience from the SPS proton antiproton collider and LEP", proceedings of the Workshop on Beam-beam Effects in Circular Colliders, Fermilab, FERMILAB-Conf-01/390-T (2001).

[5]. M. Bieler et al., "Recent and past experiences with beam-beam effects at HERA", proceeding of the Workshop on Beam-beam Effects in Large Hadron Colliders - LHC99, Geneva, CERN-SL-99-039 AP (1999).

[6]. The LHC Study Group, "The Large Hadron Collider conceptual design", CERN/AC/95-05 (LHC) (1995).

[7]. J.T. Seeman, "Luminosity and the beam-beam interaction", Joint US-CERN-Japan-Russia Accelerator School on High Quality Beams, St. Petersburg and Moscow, Russia, AIP Conference Proceedings, Vol. 592, Melville, New York (2001).

[8]. K. Yokoya and H. Koiso, "Tune shift of coherent beam-beam oscillations", Part. Accel. Vol. 27, pp. 181-186 (1990).

[9]. K. Takayama, J. Kishiro, M. Sakuda, Y. Shimosaki, and M. Wake, "Superbunch hadron colliders", Phys. Rev. Lett. Vol. 88 No. 14 (2002).

[10]. S. Peggs, "Beam-beam compensation schemes", in "Handbook of accelerator physics and engineering" edited b A.W. Chao and M. Tigner, World Scientific (1999).

[11]. B. Podobedov and R.H. Siemann, "Coherent beam-beam interaction with four colliding beams", Phys. Rev. E **52** No 3, pp 3066 (1995).

5.3. Summary of workshop on beam halo dynamics, diagnostics, and collimation (HALO'03)

Contact: Jie Wei, Collider-Accelerator Department,
Brookhaven National Laboratory, USA
mail to: jwei@bnl.gov

Co-authors: Ingo Hofmann (GSI), Alexei Fedotov (BNL), Pete Cameron (BNL), Kay Wittenburg (DESY), Nikolai Mokhov (FNAL), and Angelika Drees (BNL)

The 29th ICFA Advanced Beam Dynamics Workshop on Beam Halo Dynamics, Diagnostics, and Collimation, in conjunction with the 3rd Workshop on Beam-Beam Interactions, was held during the week of May 19 – 23, 2003, at Gurney's Inn at the eastern end of Long Island, New York. The Brookhaven National Laboratory, the Brookhaven Science Associates, the Spallation Neutron Source Project, and the US Department of Energy sponsored the workshop.

Beam halo is a performance-limiting factor to modern particle accelerators. Impact of beam halo challenges the design and operations of high-intensity, high-brightness, and high-energy accelerators: ISIS operating at the Rutherford-Appleton Laboratory, the Spallation Neutron Source (SNS) and the Japan Proton Accelerator Research Complex (J-PARK) presently under construction, various proton drivers, the Relativistic Heavy Ion Collider (RHIC), the Fermilab Tevatron, the Large Hadron Collider (LHC), and the proposed lepton linear colliders and proton drivers. Although progress has been made in recent years, physical understanding of halo dynamics is still far from comprehensive, and experimental benchmarking is just beginning. State-of-the-art techniques are required for the detection and diagnosis of the formation and development of beam halo, and technically demanding design and material selection are needed for the scraping and collimation systems. It has become urgently important to bring together theoretical and experimental physicists and engineers, with expertise on beam dynamics, diagnostics, and collimation design working on both linear and circular accelerators, for focused discussions and investigation of the subject. The HALO'03 workshop was intended to provide such a platform for experts from the fields of accelerator physics, diagnostics, engineering and material science.

The goal of the workshop was achieved by the effective planning and leadership of the working-group chairs, a close interaction between various working groups, and an active participation of our colleagues. There were 94 participants from laboratories and universities in Asia, Europe, and America, and 88 invited and contributed presentations. Each working day starts with a plenary session consisting of plenary talks and working-group progress report followed by parallel sessions consisting of parallel talks and organized discussions. Joint sessions were arranged among each of the three HALO'03 working groups and the Beam-Beam'03 working group.

We would like to thank the local organizing committee, the program committee, the international advisory committee, John Jowett and the ICFA committee for their planning and organization of the workshop. In particular, we would like to thank our working-group chairs for their devotion and leadership, to thank Pam Manning for her coordination for more than a year before, during, and after the workshop, and to thank the participants for

meeting the challenge of an unconventional workshop that bring together scientists of typically non-overlapping fields into close interaction. The working-group chairs were:

HALO dynamics:	Ingo Hofmann (GSI) and Alexei Fedotov (BNL)
HALO diagnostics:	Pete Cameron (BNL) and Kay Wittenburg (DESY)
HALO collimation:	Nikolai Mokhov (FNAL) and Angelika Drees (BNL)
Beam-Beam:	Wolfram Fischer (BNL) and Tanagi Sen (FNAL)

Viewgraphs of all presentations is available on the web site:
www.sns.bnl.gov/halo03

5.3.1. Summary of the Beam Halo Dynamics Working Group

5.3.1.1. Topics of discussion

1. Mechanisms of halo formation
2. Analytic developments and theories
3. Observation from existing machines
4. Measurement

5.3.1.2.How complete is our understanding of halo?

A good deal of contributions to this working group has explicitly or implicitly addressed the mechanism of halo production, and the diversity of phenomena encountered in simulation work, as well as the few experiments on halo presented at the workshop. In spite of the practical importance of halo, with its impact on machine design and protection as well as diagnostic, the imbalance between the relatively large number of theoretical-numerical studies presented over the years on the hand, and the scarcity of experimental data on the other hand is still striking.

In the joint discussion with the diagnostics working group the need was emphasized to understand better the actual mechanism of halo formation, and to have some kind of "definition of a halo", either by the geometrical characteristics, or by the nature of mechanism. From the discussions during the working group meetings the latter appeared to be the more unambiguous choice. Nonetheless it was suggested as sometimes useful to also bring into the discussion geometrical features of halo, like "whatever exceeds a Gaussian" or "whatever is beyond 3σ".

Resonant halo

Here, the idea is that particles are pushed out of the core – which may have a uniform or Gaussian profile or anything in between – by a resonantly acting force. This force is in most a periodic or nearly periodic one. In principle, the origin of the force may be from the coherent motion of the beam itself (dipole, envelope, etc.), or from a driving lattice harmonic term; combinations of various contributions are also possible.

1. Coherent motion of beam core. The "energy" for driving particles into a halo stems from a periodic core coherent oscillation, which gets damped by "pumping" energy into single particles provided that their oscillation frequencies match the core frequency. Several possibilities exist:

- *envelope mismatch* (parametric 2:1 halo), as the most well-known case reflected in the experimental papers by T. Wangler and N. Pichoff. Both succeeded to relate the observed rms emittance growth to the imposed initial mismatch strength. In this context it was brought to the attention of the working group that halo properties in the context of strong space charge where measured at LBL for heavy ion fusion beam transport already in 1985 by M. Tiefenbach et al. Promising first results of the University of Maryland (UMER) Ring have demonstrated flexibility and unique diagnostics possibilities.
- *mismatch by dipole offset* (commonly understood as coherent oscillation) was shown for the SNS ring to be a potential candidate of significant halo, which in turn is damping the coherent motion (V. Danilov); more study is needed including full impedances and distributions other than Lorentzian.
- *error driven envelope mismatch*, where random lattice errors drive the envelope mismatch, although the role of resonant behavior is not quite clear; evidence for halo formation was given by F. Gerigk (CERN sc p-Linac study), while P. Ostroumov (sc Linac for the RIA project) found that such errors can be kept sufficiently low by a proper design.
- *anisotropy effects*, where the papers by J.-M. Lagniel, J. Qiang and D. Jeon suggest that the expected emittance exchange should not lead to any significant halo.

2. Lattice harmonics as driving source. In circular accelerators lattice errors may have a resonant effect on halo formation by driving single particles as well as coherent modes.

- Measurements at the KEK synchrotron (S. Igarashi et al.) during few ms of foil stripping injection exhibit shoulders, which are identified by simulation as a result of fourth order space charge resonance. S. Machida's talk discusses loss in 3D bunch simulations with yet unclear origin.
- An experiment at the CERN-PS on a 1.2 s long injection flat-top using a strong octupole has been simulated in 3D bunches over 10^6 turns (tune modulation by space charge and synchrotron motion causing island trapping) with good agreement (G. Franchetti et al.).
- In the discussion the role of tune modulation studied earlier (in the 1970's) for beam cleaning was pointed out (see note by A. Chao); islands moving in and out as a result of the tune modulation by whatever reason (like chromaticity in the earlier work) lead to trapping of particles.
- Related to the CERN octupole experiment coherent modes were shown (in 2D) to be practically damped for Gaussian beams in contrast with KV or waterbag beams (I. Hofmann et al.), which simplifies the picture as one of single particle crossing.

Non-resonant halo

Several papers discussed halo, which was not related to resonant motion.

- Halo by intrabeam scattering – in practice relevant to rings only – was considered by N. Pichoff as well as by G. Turchetti et al. with respect to numerical noise in linacs.
- Also, halos due to H-stripping or due to interaction with the residual gas (talk by

W. Weng) were addressed.

Machine specific halos

The working group discussed the following cases of halo for specific machines, which were not part of the above groups.

- For LANSCE, by far the largest measured contribution to emittance growth was reported to be a result of strong rf bunching mismatch.
- In both the SNS and J-PARC MEBT lines "spherical aberration" (octupolar force from space charge or RF leading to S-shaped emittance projections) are believed to cause the measured halo profiles (simulations carried out by D. Jeon and M. Ikegami).

5.3.1.3. What determines the size of halo?

For the parametric 2:1 halo, the 10^{-4} level of beam intensity is shifted from the 3σ level of the matched beam to typically 5 – 7 σ for a mismatch as large as 30%. F. Gerigk suggested a similar number for lattice error driven halo, but more work needs to be done in this context.

In the KEK experiment the effect was mainly found in the development of shoulders caused by resonance islands pushed away from the core during stacking – in principle, no upper bound to the halo size.

In the CERN PS-experiment the halo size is also predicted to be unbounded for working points sufficiently close to the resonance condition, which is confirmed by the observed beam loss.

5.3.1.4. Dominant mechanisms of halo generation

In linacs, the following conclusions can be attempted:

- • Initial mismatch from poor matching between sections -in principle it can be kept low if sufficient diagnostics is available.
- • Are random errors (gradients, misalignment etc.) large enough to justify worries about a sizeable halo? Clearly more systematic work is needed here, which should also address sufficiently large error sets. For rings, the picture is somewhat different:
- • Initial mismatch halo (parametric resonance) may be observable for poorly matched bunch transfer, but it should be possible to minimize this effect.
- • The effect of nonlinear resonances is suggested to depend on the time scale (1 ms vs. 100-1000 ms); experiments and simulations should be extended to a larger range of parameters. Systematic comparison of codes and experiments is needed.

In summary, for lattice error driven halos in linacs as well as for nonlinear resonance driven halos in rings work is just at the beginning. Significantly more efforts are needed in both experiments and interpreting simulations

5.3.2. Summary of the Beam Halo Diagnostics Working Group

5.3.2.1. Introduction

The plenary presentation on Halo Diagnostics (T. Shea) offered the participants several different approaches to organizing their thinking on this diverse and complex

subject. In terms of the fundamental goal of understanding halo, the involvement of diagnostics was considered in analytical approaches, in simulations, and in experiments. In terms of the priority given to diagnostics, the range goes from purpose built experiments, to dedicated beam experiments at user facilities, to measurements parasitic to normal operations. In terms of challenges, the task begins with a simple definition of halo, requires clear specification of diagnostics requirements as a variety of next generation machines take shape, confronts the dynamic range and sensitivity problems, and finally addresses two omnipresent challenges to the diagnostics specialist – cost, and building trust in the measurements. With the above considerations in mind, and after a survey of the current state of the art, goals for the workshop were presented.

As the working group efforts got underway, it became clear that even at this workshop a general definition of "Beam Halo" could not be given, because of the very different requirements in different machines, and because of the differing perspectives of instrumentation specialists and accelerator physicists. Definitions were offered both from a geometric perspective (point of departure of beam from Gaussian profile, portion of the density distribution beyond n sigma,…) and from the perspective of the formation mechanism (space charge halo, parametric resonance halo,…). From the Diagnostics point of view, one thing is certainly clear – by definition halo is low density and therefore difficult to measure, due to both low count rates in the tails and the large dynamic range (it is desirable to measure the profile of the core 'simultaneous' with the tails).

At this workshop diagnostics were approximately separated into two subgroups – diagnostics for halo measurement, and diagnostics for halo prevention. Diagnostics for halo measurement presented at this workshop include wire scanners (both solid and laser wires), scrapers, the ionization profile monitor, and (for measurement of longitudinal halo) kickers with gated detectors. Presented diagnostics for halo prevention include electron cloud monitors, instability monitors, the quadrupole moment monitor, energy analyzers, tune monitors, and the AC dipole. The above two categories are somewhat artificial – it is straightforward to imagine using halo measurement in conjunction with machine tuning as a halo prevention diagnostic, though somewhat more difficult to imagine using the diagnostics in the halo prevention group for halo measurement. In the following, short summaries of the presented devices and their results will be given. The halo measurement devices are summarized in a table.

5.3.2.2. Halo measurement

Many of the contributions presented refinements to conventional wire scanners to permit tail measurements. Several schemes were described to achieve the required large dynamic range.

In an extracted beamline at the PSR (R. Macek), detection of secondary emission currents from 100μSiC wires led to a dynamic range up to 10^{6}. The emphasis was on noise suppression, which was achieved by locating the electronics on the beamline, minimizing integration time, limiting bandwidth, performing background subtraction, and auto-zeroing leakage currents and offset voltages. A logarithmic amplifier was used to make possible the required dynamic range with 12 bit digitizers. Measured profiles were approximately Gaussian to almost 10^{-4}, with broad shoulders beyond that. The demarcation between the central Gaussian and the shoulders was strikingly clean and abrupt. The mechanism of halo production is not understood. Future plans include adding a –5 KV bias to the wire to minimize electron cloud effects in the measurement.

At LEDA (D. Gilpatrick) a combination of a 33 μcarbon wire for core measurements and a 1.5mm thick graphite scraper for the tails are mounted on a single

scanning actuator, and make possible a 10^{5} dynamic range. Detection was by measurement of secondary emission current for the wire and stopped protons for the scraper. Considerable effort was given to determining optimum bias for both wire (-12V) and scraper (+25V). Scraper insertion was limited to about 2σ by beam heating. The differentiated scraper data was merged with the wire data on-line. Measured profiles appeared to have three distinct regions – a sharp peak extending to ~10^{-1}, a broader approximately Gaussian shape extending to 10^{-3}, and broad shoulders beyond that. The mechanism of formation of this structure was not explained.

Both counting and secondary emission techniques were used with good agreement in the slow extracted beam at the AGS (D. Gassner). In the counting measurement, three-fold coincidence horizontal and vertical scintillator telescopes effectively minimized background. Acceptance was about 10^{-4} steradian. The scattering targets were 2.5mm diameter tungsten rods. Singles peak rates of ~5M/sec were a factor of 10 below saturation level. Dynamic range was 10^{-2} to 10^{-3} for secondary emission and 10^{-3} to 10^{-4} for counting. The purpose of this installation was to diagnose emittance growth during slow extraction from the AGS. Measurements showed an asymmetric halo. The problem was solved by positioning the extraction kicker and ejection septum further from the beam, causing the slow extracted beam to spend less time in the fringe fields of the AGS main magnets. The wire scanner was then de-commissioned.

Counting techniques were also used with a 7μwire at HERA (K. Wittenburg). The very clean background conditions at HERA led to a dynamic range of >10^{8}, using the fast scan technique in the beam core and a very slow scan in the beam tail. The efficiency (counts per proton intersecting the wire) was about 10^{-7}. Measurements clearly showed the effectiveness of the scraper in removing beam tails.

Scintillation counting techniques were supplemented by local silicon detectors as well as the experiment detectors in the HERA-B experiment (K. Wittenburg), which uses an internal target inserted into the halo of the beam. Detection efficiency was (remarkably) greater than 50%. The large bandwidth of the counting method permitted beam-in-gap measurements between the ~10MHz bunches. With improved machine performance beam halo practically vanished, a circumstance that made it necessary to artificially generate halo without disturbing the core by means of tune modulation together with beam-beam interaction (C. Montag). With this forced diffusion it was possible to stabilize interactions at the desired rate. It was also shown that the core of the beam and the luminosity at the colliding experiments were not deteriorated by this method, a result of possible significance for the PLL tune measurements mentioned in the next section.

A new readout scheme for wire scanners was successfully tested in Yerevan (reported by K. Wittenburg), where the change of the natural oscillation frequency caused by the heating of the 90μberyllium-bronze wire was detected. Temperature resolution of this method is of the order of 10^{-4} C. Beams with intensities down to 3.4nA were successfully scanned, which shows the very high sensitivity of this technique. The authors expect a dynamic range of up to 10^{7}. Concern was expressed about the effect of ohmic heating of the wire by the beam fields. A vibrating wire scanner has been installed at PETRA at DESY, and is waiting for beam.

In an effort where the focus was not so much on dynamic range as the measurement of fast profile changes, counting techniques were utilized in the fast (20 m/s) 7μcarbon flying wire at KEK (S. Igarashi). The flying wire was used to measure the beam profile during injection with the goal of minimizing losses. A series of profiles were acquired by

changing the trigger setting in 0.2ms increments (each scan needs 4ms). Full beam profiles with good time resolution were assembled by reconstructing the data from successively injected pulses at different sweep trigger settings/wire positions but at the same time after injection. Tune and intensity dependent profile modulations were observed, and were attributed to the space charge driven fourth order resonance. There was good qualitative agreement between measurements and simulations.

Proof-of-principle for a laser wire scanner for the SNS linac was demonstrated at Brookhaven, with further development work and installation taking place at Oak Ridge (S. Assadi). Short (~10ns) pulses from a 1032nm Nd-YAG laser strip electrons from the H-minus beam particles. In the Brookhaven prototype profile measurements were accomplished by using differential current measurements to observe the resulting current notch. The sensitivity of the laser wire at Oak Ridge was improved by collecting and measuring the stripped electrons, allowing a dynamic range of up to 10^4. The laser wire method permits measurement of full power beam during normal operations without burning wires, and reduces the danger of expensive contamination of RF cavities in the superconducting portion of the linac.

The RHIC ionization profile monitors (R. Connolly) have been steadily and significantly improved since prototype testing in a transfer line in 1996, and since the acquisition of the first single bunch turn-by-turn injection profiles in the RHIC ring in 1999 (which clearly showed quadrupole oscillations due to injection mismatch). Modifications include improved RF shielding to minimize coupling to beam fields, improved detector geometry to minimize sensitivity to radiation from beam losses, improved geometry of adjacent electric and magnetic fields to prevent migration of non-signal electrons into the detector, improved sweep field geometry and higher sweep voltage to minimize measured profile sensitivity to sweep voltage, and the addition of electron sources to permit calibration. The resulting background reduction has made it possible to begin to probe into the beam tails. A dynamic range approaching 10^3 has been achieved. A similar (but considerably larger) version of this IPM will be built for the SNS Ring.

To meet the stringent 10^{-4} loss requirement of the SNS (losses due to beam-in-gap are estimated to be second only to those due to space charge driven halo), longitudinal halo measurement in the SNS Ring (D. Gassner) will be accomplished by a beam-in-gap kicker driving the gap beam onto a scraper, with detection by a fast gated micro-channel plate. In addition, this system will accomplish gap cleaning before extraction, with the scraper retracted and the gap beam landing in the collimators. Without the kicker, the scraper and data acquisition system will also be used for transverse halo measurements.

Table 1. Presented instruments for beam profile measurements, their dynamic range and operational status.

Machine	Type	Signal	Dynamic range	Status
LEDA (LANL) (6.7MeV p)	Scanner+ Scraper	SEM	10^5-10^6	Working in control-system
AGS slow extraction line (2GeV p)	Scanning Target	Counting mode + SEM	10^4-10^5 10^2-10^3	De-commissioned
PSR extraction line (LANL) (800MeV p)	Wire Scanner with thin wire	SEM Log amp	10^6	In regular operation
SNS LINAC (2.5MeV to 1GeV H)	Laserwire scanner	Photo-neutralization electron detection	10^3-10^4	In operation
DESY HERA (40 – 920GeV p)	Wire Scanner with thin wire	Counting mode	10^7-10^8	In operation, Reado prototype
Yerevan (20 MeV e) DESY PETRA (40GeV p)	Wire Scanner with thin wire	Vibrating wire; natural frequency	10^6-10^7	Preliminarytests; More tests planed
KEK PS (12GeV p)	Wire Scanner with thin wire	Scintillators	~10^3	In operation
RHIC (polarized p, ions)	IPM	Current	10^2-10^3	In operation

5.3.2.3.Halo prevention

The summary of the Beam Dynamics working group in these proceedings separates halo formation mechanisms into the categories of 'non-resonant' and 'resonant'. The diagnostics presentations for non-resonant mechanisms addressed tools for the observation and analysis of instabilities. The presentations for resonant mechanisms dwelt primarily upon measurement of tune-related parameters.

An overall view of instabilities in both time and frequency domains (M. Blaskiewicz) presented data showing recent measurement of the head-tail instability in RHIC as well as the electron cloud instability in both the AGS Booster and the LANL PSR. The usefulness of principal component analysis in understanding this data was demonstrated. In the effort to understand the conditions for onset of instability, data was presented showing the measurement of longitudinal impedance in RHIC from Schottky spectra. The agreement between theory and measurement in this data was remarkably good. Particularly interesting in this presentation was the observation of long-lived (~1hr) longitudinal 'hot spots' (solitons?) in the proton beam at store in RHIC, and their possible role in triggering instabilities during acceleration. These hot spots were not observed with gold beams, probably as a result of the damping/diffusion effect of IBS.

The electron cloud instability results from a form of multipacting driven by time gradients of the beam space charge field in the longitudinal tail of the bunch. Different instruments were developed and studied at the PSR (R. Macek) for the measurement of electron cloud parameters. Historically, the presence of electron cloud was observed from

pressure rise due to multipacting electrons causing desorption at the beampipe wall, and looking at ion pump currents with sufficient bandwidth provided early time domain information. Early studies of direct electrons utilized simple biased electrodes to collect electrons. Data from these electrons was often puzzling and difficult to interpret, particularly the copious presence of electrons at the wall in bending dipoles in the plane normal to the dipole field (the IPM has clearly demonstrated the practical efficiency of magnetic field in confining electron trajectories). This motivated the development of the Retarding Field Analyzer (RFA), where the presence of a repeller grid permits measurement of the electron energy spectrum at the beam pipe wall. The 80MHz bandwidth of the RFA makes possible detailed study of the time evolution of the electron cloud, and clearly shows the 'trailing edge multipactor' behavior. This multipactor is seeded by electrons released from the beam space charge potential well at the tail of the bunch. A key factor in buildup of the instability is how many seed electrons survive the gap to be captured by the following bunch. To this end, an Electron Sweeping Detector (ESD) was developed. The ESD is basically an RFA with the added capability of applying a fast high voltage (~1KV) pulse at the beginning of the following bunch. Successful measurements were made of surviving electrons.

In an application of similar techniques to the longitudinal, a high-resolution retarding field energy analyzer (Y. Zou) was developed at UMER (a 10keV, 100mA, electron accelerator) to study the mechanism of beam energy spread and its evolution in the electron beam. Detailed analysis of the device parameters had led to an energy resolution of better than 2eV. First experimental results show excellent agreement between the experiments and the theory (Boersch effect and longitudinal-longitudinal effect). More experiments and further improvements are in preparation.

In the case of resonant mechanisms of halo formation, measurement of tune-related parameters (coherent tune, incoherent tune, beam-beam tune shift, coupling, chromaticity, non-linear tune spread, tune shift due to electron cloud,…) is essential. The application of Phase-locked Loop (PLL) and Schottky techniques to these measurements in RHIC was presented (P. Cameron), as well as plans for utilizing these methods in the SNS Ring. Concern was expressed by Professor Hoffman regarding the reliability of these methods in space-charge dominated beams, and this subject is under investigation. PLL data was also presented showing lock to the large amplitude oscillations of beam in islands of the 2/9 resonance in RHIC, data which might be used in resonance compensation. Preliminary data from a resonant quadrupole monitor was presented, in which the quadruple mode was resonated to improve sensitivity and diminish the dynamic range problem characteristic of this type monitor.

The techniques of electron cooling and stochastic cooling are complementary – electron cooling effectively cools the beam core, whereas stochastic cooling is efficient on the beam tails. In the case of Optical Stochastic Cooling (OSC), undulator magnets would be used for both the pickup and the kicker, and cooling time is power limited rather than bandwidth limited (V. Yakimenko). Present plans on the path to eventual OSC in RHIC include summer 2003 testing of an optical parametric amplifier, in which a frequency doubled CO2 laser pumps a nonlinear crystal to amplify the signal (ultimately from the undulator pickup). Gains of over 100dB are anticipated. Pickup and kicker should be installed in regions of non-zero dispersion to permit simultaneous longitudinal and transverse cooling. In the case of halo cooling, the power limitation can be overcome by adjusting timing of the pump laser to apply power predominantly to the longitudinal beam tails, reducing the practical cooling time from ~1hr for the entire beam to ~<1min for the beam tails. A concern is the requirement for an isochronous lattice between pickup and kicker, the requirement being a few microns (~10^{-14} sec) at the 12 micron cooling

wavelength.

With the AC Dipole (M. Bai), adiabatic turn on and off of a 1m long 0.01T kicker driving the beam at a frequency close to the betatron tune permits excitation of large amplitude coherent oscillations without measurable emittance growth. Data was presented showing 2mm p-p coherent oscillations in RHIC. Measurements accomplished to date include beta functions, phase advance, and linear coupling. By driving the beam at the spin tune rather than the betatron tune, this kicker is also used as a spin flipper for the polarized beam program. Possible applications of this method to halo measurements are under study.

RHIC boasts an active and well-organized Beam Experiments program focused on improvements in machine performance. Essentially all experiments in this program have direct bearing on halo formation. In a summary of beam experiments results (F. Pilat), data was presented on measurements of dynamic aperture, diffusion coefficients (both at injection and store), beam transfer functions in the 4-8GHz range (in preparation for initial stochastic cooling efforts in 2004), IR triplet nonlinearities and corrections, beam-beam tune shift vs. crossing angle, nonlinear chromaticity, resonance compensation, and pressure rise/electron cloud. Plans for 2004 include addressing the requirements for luminosity increases and RHIC upgrade plans, improved machine modeling, and increased collaboration with FNAL and CERN.

5.3.2.4. Conclusion

Wire scanners and scrapers define the state of the art in halo measurements, with high sensitivity and huge dynamic range. With the variable-delay trigger method, and given the possibility of repeated replication of beam conditions, wire scanners can measure fast profile changes. With continuous steady improvements, the IPM is starting to make contributions to halo measurement, including fast profile changes without the requirement of repeated replication of beam conditions. Beyond these bread-and-butter tools, there are evolving a variety of nice (and sometimes even fancy) instruments to measure the parameters which may drive beam tails.

A difficult challenge posed by the accelerator physicists is the turn-by-turn (or better yet, bunch-by-bunch) measurement of beam parameters, both in static and ramped machines.

5.3.3. Summary of the Beam Halo Collimation Working Group

5.3.3.1. Introduction

The creation of beam halo and corresponding beam loss is unavoidable at any accelerator. The consequences to the machine and detector components can range from minor to severe. An accidental beam loss can cause catastrophic damage to the complex equipment. Only with a very efficient beam collimation system can one reduce uncontrolled beam losses in the machine to an allowable level. This Working Group overviewed and discussed the status of the collimation system developments, design and performance in three machine categories: high-power proton machines, hadron colliders and *e*+*e*- linear colliders.

5.3.3.2.High-power proton machines

In his plenary talk, J. Wei (BNL) overviewed the collimation issues at high-power proton accelerators. He demonstrated a vitality of collimation for a Megawatt beam machines to minimize uncontrolled beam loss. Using the Spallation Neutron Source as an example, he described guiding principles, beam cleaning strategies and collimator design and handling issues. Based on the experience at the existing machines, he concluded that

two-stage collimation in both transverse and longitudinal directions is essential in achieving a high efficiency. Cleaning of electron cloud and suppression of electron generation are important aspects in the design of new rings.

C. Warsop (RAL) described an approach to beam loss control at the ISIS synchrotron. Collimation is done by betatron and momentum collectors (graphite-copper-graphite devices 5 to 30 cm long) to shave off 2 kW halo out of a 240 kW 800-MeV beam. The system is instrumented with 40 BLMs. A halo growth rate is 10 μm per turn. Simulations and measurements on beam loss are in a good agreement. The plans exist for further upgrades.

E. Prebys (FNAL) presented a well-designed two-stage collimation system for the Fermilab 8-GeV Booster to be installed in the tunnel this fall. It consists of two scattering foils followed by three integrated collimator-shielding modules about $1\times1\times1\text{m}^3$ each, well controlled and instrumented. The system will be intercepting up to 1 to 2 kW halo out of a 64-kW beam, providing $\leq$ 0.1-1 W/m beam loss rates in the rest of the ring. Prompt radiation, sump water activation, residual dose and dose to sensitive components are within the stringent regulatory limits.

N. Nakao (KEK) described results of the MARS14 collimation and shielding studies for the 3-GeV ring of the J-PARC project. He impressed the audience by the MARS model built for the entire ring with all machine and tunnel components, shielding and soil, almost 10^5 elements total. A 4-kW collimation system and sophisticated shielding designed with this model, will provide prompt and residual radiation levels within the regulatory limits.

The SNS collimation system design, shielding and handling were reviewed in great detail by N. Simos (BNL), H. Ludewig (BNL) and G. Murdoch (ORNL). The system will be intercepting 2 kW on each of the seven collimators, providing less than 1 W/m beam loss rate in the ring. Impressive ANSYS analysis and experiment were performed on thermo-mechanical response of the critical components to beam accidents. Estimates of dose and residual activity in collimation region were done via MCNPX-CINDER90-ORIGEN-MCNP chain of the computational codes. A thorough consideration was given to mechanical engineering design of collimators and their windows, collimator removal procedure, fast disconnects, remote vacuum clamps etc. A very complex cooling system raised some questions.

In all the machines considered, collimators take about 2 kW of beam power, resulting in a very similar scope and level of radiation, cooling, thermal, mechanical, engineering and handling problems. It was recognized that dry runs are very useful, such as collimator removal procedure etc. Although the codes used for the collimator and shielding design are quite reliable, benchmarking of residual dose predictions would be useful (contribution of low-energy neutrons, borated water in the SNS collimators etc.).

5.3.3.3.hadron colliders

In his plenary talk, N. Mokhov (FNAL) described principles and realization of a reliable beam collimation system required to sustain favorable background conditions in the collider detectors, provide quench stability of superconducting magnets, minimize irradiation of hadron collider equipment, maintain operational reliability over the life of the machine, and reduce the impact of radiation on personnel and the environment. He discussed sources, beam loss and scraping rates at hadron colliders and approach to design of an optimal two-stage collimation system, the Tevatron and HERA collimator performance, needs for a multi-component approach to collimation at LHC, and possible ways to improve collimation efficiency such as use of a bent crystal.

D. Still (FNAL) presented results on the Tevatron Collider Run II collimation

system performance. The proton and antiproton halo removal is done by 12 L-shape collimators catching about 0.4% of intensity for each beam. The flexible system is programmable, well-controlled and instrumented with motion based on BLM feedback. It is efficient and handled automatically at the beginning of every store.

R. Schmidt and J.B. Jeanneret (CERN) described Beam loss scenarios and strategies for machine protection and on-going work on collimation at the LHC. A BPM system will be used as a protection system for collimators. BPMs will catch beam motion (both planes) and give a warning to dump the beam before damage can happen. BLMs are not reliable enough at low halo level. Two serious issues were discovered recently in their studies: impedance created by collimators and baseline materials won't withstand a misbehaved beam. The studies are underway to solve these problems. I. Rakhno (FNAL) presented a sophisticated movable collimator system designed on a basis of thorough MARS calculations to protect the LHC machine and collider detectors at an unsynchronized beam abort. D. Kaltchev (TRIUMPH) showed results on the LHC collimator performance as calculated with three different codes.

A. Drees (BNL) described collimation experience at RHIC. Background conditions were more challenging in the last two runs than before (horizontal crossing angles (dAu), the ramping and squeezing scheme (pp)). Experimental background could be reduced with the primary collimators alone but not to a tolerable level at all experiments at the same time. Additional secondary collimators will be installed for the next run.

R. Fliller (BNL) described first results on crystal collimation of relativistic heavy ion beam. A fraction of the beam deflected by a bent crystal ended up at a secondary collimator. The result of studies was that at the present location, ion and proton beam channeling could be observed but crystal contribution to collimation efficiency is negligible. The crystal will be removed and replaced by a standard primary collimator.

M. Kostin (FNAL) discussed simulation aspects of beam collimation and their remedies in the MARS14 code.

5.3.3.4. e+e- *Linear colliders*

In his plenary talk, T. Raubenheimer (SLAC) discussed *e*+*e*-linear collider halo and collimation issues.

W. Kozanecki (Saclay) presented detector background requirements at *e*+*e*-linear colliders. He analyzed contributions of different source mechanisms to the background rates in major detector components (silicon vertex detector, calorimeter and muon system) and discussed possible shielding strategies.

A. Seryi (SLAC) described a novel approach to collimation via nonlinear optics with focusing using an octupole doublet folding in position tails. This provides no beam outside a certain sigma (beam size).

A. Seryi (SLAC) presented results of detailed analysis of collimation system performance for NLC, TESLA and CLIC under the same 0.1% beam loss scenario. It was shown that the current collimation schemes in the beam delivery systems perform well at the NLC and CLIC while there is some problem at TESLA. The work is in progress to fix this problem.

F. Zimmerman (CERN) described collimation for CLIC. CLIC has crossing angles, conflicting requirements and only one-stage momentum collimators. The collimation depth is $\pm 10\sigma x$, $\pm 80\sigma y$ and $\pm 1.5\%$ in momentum. Laser wire signals are dominated by particle losses. He discussed possible blow-up of a vertical beam size for collimator survival and a non-linear collimation system.

T. Markiewicz (SLAC) presented results of the GEANT3 simulation of the NLC collimation, featuring rescattering, energy deposition, synchrotron radiation and energy

cutoffs, a house-made interface between MAD and GEANT. He showed difficulties and possible solutions in dealing with Bethe-Heitler muons. The MUCARLO code was used for tracking and transport of 50-GeV muons. Their fluxes at the detector are reduced by betatron and momentum collimation, and additionally by a 9-m steel shielding wall magnetized with "donuts" (tunnel magnetized spoilers). He also highlighted novel technologies with renewable and consumable collimators. Consumable collimators: rotating wheel concept or tape collimators, wheel prototype not as good as requirements (yet) but encouraging, Renewable spoilers: liquid metal, Tin and Molybdenum.

H. Schlarb (SLAC) described design and performance of the TESLA Test Facility (TTF) collimation system. Purpose is undulator protection (damage of NdFeB permanent magnet), dark current from RF of same magnitude, collimation uses two spoilers and three absorbers.

P. Tennenbaum (SLAC) gave an excellent overview of the collimator wakefield problem. Two effects contribute: resistive wall (the non-zero resistivity of the the wall adds a kick) and geometric wall (the change in cross section adds a kick). Results from a wakefield test box: (i) measured/predicted (MAFIA) agreed quite well but disagreed with calculations; (ii) resistivity (copper vs. graphite) agrees with calculations.

Linear collider collimation challenges include small beam size, high repetion rate and high beam power. Detector specifications are vital to finalize collimation system design goals. Two major components to deal with: muons and sunchrotron radiation. A careful layout of beam delivery systems is necessary. Two novel technologies look promising: octupole halo folding and renew-able/consumable collimators.

5.4. Workshop on BEPCII Interaction Region

J.Q. Wang, IHEP, Beijing, P.R. China mail to: wangjq@ihep.ac.cn

From Jan. 12 to 16, the Workshop on BEPCII Interaction Region was held in the Institute of High Energy Physics (IHEP, Beijing, P.R. China). BEPCII is the upgrade project of the Beijing Electron Positron Collider (BEPC), adopting the two-ring scheme to reach the luminosity of $10^{33}cm^{-2}s^{-1}$ for τ-charm physics study. It was approved by the government in the end of last year and has started officially. Compared to other machines, such as B-factories, DAΦNE, BEPCII has the similarly ambitious parameters and extreme engineering complexity, particularly, due to the more constraint on the space available, the IR design of BEPCII is of more challenge. Thus this workshop was suggested by the International Machine Advice Committee (IMAC) on the BEPCII to review and optimize the design of IR. More than 60 participants attended the workshop, among them 16 experts are from aboard, including 6 from KEK, 3 from DESY, 2 from BNL, 2 from SLAC, 1 from CESR, 1 from INF and 1 from IHI company. After the first day of plenary session with presentations of IR design of BEPCII and relevant machines such as KEKB, PEPII, CESRc, DAΦNE and HERA-upgrade, the workshop is divided into 4 working groups with experts to discuss in detail on each subject as: group 1 on optics, instrumentation & control, commission; group 2 on background issues; group on superconducting & special magnets; group 4 on mechanical issues. With intense discussion among the participants, a very detailed review of the BEPCII IR design and comparison with similar system at other accelerators was made and a large number of detail issues were revealed for future improvement, particularly the experiences from the existing machines are beneficial. To investigate the feasibility of the installation of IR components, a mockup of the BEPCII IR was made and the demonstration gave deep impression on the experts. On the aspect of

beam physics issue in IR, emphasis were given to the beam-beam effect due to the large crossing angle with the relatively high synchrotron tune, and the analysis tool of IR parameters such as the coupling, orbit, beam size and so on. These issues seem common for high luminosities colliders, thus arose intense exchange of ideas and experiences. As summarized by Dr. Ferdinand Willeke, the co-chairman of the workshop " Very detailed discussions have been taken place which have potential to trigger further improvements of the design…the difficulties and iterations of the various designs have been openly revealed and there is hope that some of the mistakes made elsewhere can be avoided at BEPCII" and "a lot interesting technical information has been exchanged which makes the meeting scientifically and technically worthwhile for all participants".

For detailed information and the presentations on the workshop, please refer to http://www.ihep.ac.cn/english/WORKSHOP/index-031126.html

6. Forthcoming Beam Dynamics Events

6.1. The 33rd ICFA Advanced Beam Dynamics Workshop on High Intensity and High Brightness Hadron Beams "HB2004"

The 33rd ICFA Advanced Beam Dynamics Workshop will take place from October 18 to 22, 2004 in Bensheim (near Darmstadt), Germany. With the theme *"High Intensity and High Brightness Hadron Beams"* this workshop is a follow-up of the very successful 20th ICFA Advanced Beam Dynamics Workshop held at Fermilab April 8-12, 2002. Topics include accelerator and beam physics issues associated with high intensity and/or high brightness, technical system designs, reviews of existing machines and overviews of planned projects for protons and ions.

The location is the conference center in the old town of Bensheim, a romantic place with medieval charm situated between Darmstadt and Heidelberg.

The workshop is co-sponsored by GSI Darmstadt and CEA France. For further information please contact:

Ingo Hofmann, workshop co-chairman, GSI Darmstadt, +496159712409,

mail to: i.hofmann@gsi.de

Jean-Michel Lagniel, workshop co-chairman, CEA, +33169265249,
mail to: jean-michel.lagniel@cea.fr

Further details will soon be added to our conference webpage:
http://www.gsi.de/ICFA-HB2004

7. Announcements of the Beam Dynamics Panel

7.1. ICFA Beam Dynamics Newsletter

7.1.1. Aim of the Newsletter

The ICFA Beam Dynamics Newsletter is intended as a channel for describing unsolved problems and highlighting important ongoing works, and not as a substitute for journal articles and conference proceedings which usually describe completed work. It is published by the ICFA Beam Dynamics Panel, one of whose missions is to encourage international collaboration in beam dynamics.

Normally it is published every April, August and December. The deadlines are 15 March, 15 July and 15 November, respectively.

7.1.2. Categories of Articles

The categories of articles in the newsletter are the following:

1. Announcements from the panel.
2. Reports of Beam Dynamics Activity of a group.
3. Reports on workshops, meetings and other events related to Beam Dynamics.
4. Announcements of future Beam Dynamics-related international workshops and meetings.
5. Those who want to use newsletter to announce their workshops are welcome to do so. Articles should typically fit within half a page and include descriptions of the subject, date, place, Web site and other contact information.
6. Review of Beam Dynamics Problems: this is a place to bring attention to unsolved problems and should not be used to report completed work. Clear and short highlights on the problem are encouraged.
7. Letters to the editor: a forum open to everyone. Anybody can express his/her opinion on the beam dynamics and related activities, by sending it to one of the editors. The editors reserve the right to reject contributions they judge to be inappropriate, although they have rarely had cause to do so.
8. Editorial.

The editors may request an article following a recommendation by panel members. However anyone who wishes to submit an article is strongly encouraged to contact any Beam Dynamics Panel member before starting to write.

7.1.3. How to Prepare a Manuscript

Before starting to write, authors should download *the latest* model article file, in Microsoft Word format, from the Beam Dynamics Panel home page

http://wwwslap.cern.ch/icfa/

It will be much easier to guarantee acceptance of the article if the latest model is used and the instructions included in it are respected. These model files and instructions are expected to evolve with time so please make sure always to use the latest versions.

The final Microsoft Word file should be sent to one of the editors, preferably the issue editor, by email.

The editors regret that LaTeX files can no longer be accepted: a majority of contributors now prefer Word and we simply do not have the resources to make the conversions that would be needed. Contributions received in LaTeX will now be returned to the authors for re-formatting.

In cases where an article is composed entirely of straightforward prose (no equations, figures, tables, special symbols, etc.) contributions received in the form of plain text files may be accepted at the discretion of the issue editor.

Each article should include the title, authors' names, affiliations and e-mail addresses.

7.1.4. Distribution

A complete archive of issues of this newsletter from 1995 to the latest issue is available at

http://wwwslap.cern.ch/icfa/

This is now intended as the primary method of distribution of the newsletter.

Readers are encouraged to sign-up for to electronic mailing list to ensure that they will hear immediately when a new issue is published.

The Panel's Web site provides access to the Newsletters, information about Future and Past Workshops, and other information useful to accelerator physicists. There are links to pages of information of local interest for each of the three ICFA areas.

Printed copies of the ICFA Beam Dynamics Newsletters are also distributed (generally some time after the Web edition appears) through the following distributors:

Weiren Chou	chou@fnal.gov	North and South Americas
Helmut Mais	mais@mail.desy.de	Europe* and Africa
Susumu Kamada	Susumu.Kamada@kek.jp	Asia** and Pacific

* Including former Soviet Union.

** For Mainland China, Chuang Zhang (zhangc@bepc3.ihep.ac.cn) takes care of the distribution with Ms. Su Ping, Secretariat of PASC, P.O.Box 918, Beijing 100039, China.

To keep costs down (remember that the Panel has no budget of its own) readers are encouraged to use the Web as much as possible. In particular, if you receive a paper copy that you no longer require, please inform the appropriate distributor.

7.1.5. Regular Correspondents

The Beam Dynamics Newsletter particularly encourages contributions from smaller institutions and countries where the accelerator physics community is small. Since it is impossible for the editors and panel members to survey all beam dynamics activity world-wide, we have some *Regular Correspondents*. They are expected to find interesting activities and appropriate persons to report them and/or report them by themselves. We hope that we will have a "compact and complete" list covering all over the world eventually. The present *Regular Correspondents* are as follows

Liu Lin	liu@ns.lnls.br	LNLS Brazil
S. Krishnagopal	skrishna@cat.ernet.in	CAT India
Ian C. Hsu	ichsu@ins.nthu.edu.tw	SRRC Taiwan

We are calling for more volunteers as *Regular Correspondents*.

7.2. ICFA Beam Dynamics Panel Members

Caterina Biscari	caterina.biscari@lnf.infn.it	LNF-INFN, Via E. Fermi 40, Frascati, Italy
Swapan Chattopadhyay	swapan@jlab.org	Jefferson Lab, 12000 Jefferson Avenue, Newport News, VA 23606, USA
Pisin Chen	chen@slac.stanford.edu	SLAC, P.O. Box 4349, MS26, Stanford, CA 94309, USA
Weiren Chou	chou@fnal.gov	FERMILAB, MS 220, P.O.Box 500, Batavia, IL60510, USA
Yoshihiro Funakoshi	yoshihiro.funakoshi@kek.jp	KEK, Oho, Tsukuba, IBARAKI 305-0801, Japan.
Jie Gao	gao@lal.in2p3.fr	Laboratoire de L'Accélérateur Linéaire, B.P. 34, 91898, Orsay cedex, France
Sergei Ivanov	ivanov_s@mx.ihep.su	Institute for High Energy Physics, Protvino, Moscow Region, 142281 Russia
John M. Jowett (Chairman)	John.Jowett@cern.ch	CERN, CH-1211 Geneva 23, Switzerland
Kwang-Je Kim	kwangje@aps.anl.gov	Argonne Nat. Lab., Advanced Photon Source, Accelerator Systems Division, 9700 S. Cass Avenue, Bldg 401/C4265, Argonne, IL 60439, USA
Alessandra Lombardi	Alessandra.Lombardi@cern.ch	CERN, CH-1211 Geneva 23, Switzerland
Helmut Mais	mais@mail.desy.de	DESY, Notkestrasse, 85 D-2000, Hamburg 52, Germany
David Rice	dhr1@cornell.edu	Cornell University, 271 Wilson Lab, Ithaca, NY 14853-8001, USA
Yuri Shatunov	Yu.M.Shatunov@inp.nsk.su	Acad. Lavrentiev prospect 11, 630090 Novosibirsk, Russia
Junji Urakawa	junji.urakawa@kek.jp	KEK, Oho, Tsukuba, IBARAKI 305-0801, Japan.
Jie Wei	wei1@bnl.gov	BNL, Bldg. 911, Upton, NY 11973- 5000, USA
JiuQing Wang	wangjq@mail.ihep.ac.cn	IHEP,CAS,BEPCNational Laboratory, P.O. Box 918, 9-1, Beijing 100039, China

The views expressed in this newsletter do not necessarily coincide with those of the editors. The individual authors are responsible for their text.